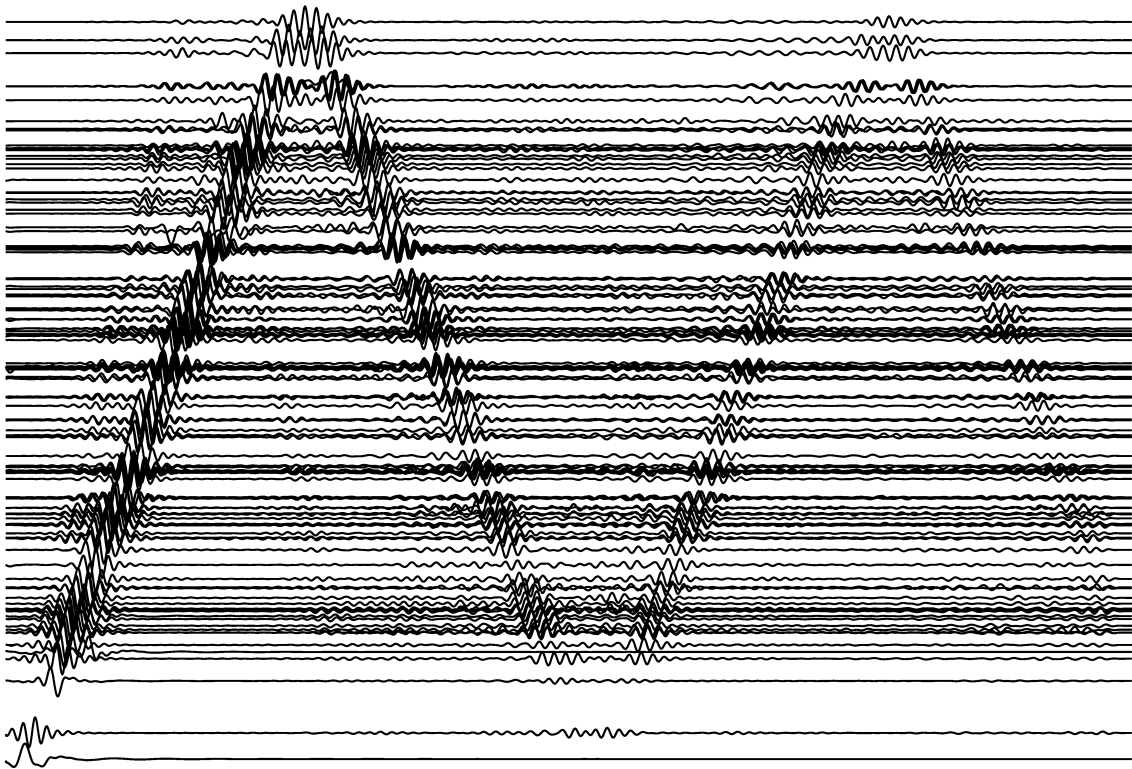# A theory of seismic wave propagations

—To decipher seismic waveforms—

Kiwamu Nishida

December 14, 2023

Contents

Introduction

Chapter 1

There are many different fields of research in this world. When we learn about a new research area, what is the best part? Of course, there is no right answer to this question. However, if I were to venture a guess, I would say that the new perspective changes the way we see the world before. For example, let us say you learn about geology. You will understand that you will be able to read the history of millions of years from geological clues in a field that you have never seen before. You will realize that observing phenomena is not simple, and what you can decipher depends on your understanding. In fact, the act of **observation** is not so simple and in itself reflects how the observer understands the phenomenon with a model. This lecture covered a branch of geophysics. How does geophysics expand our horizons?

Physics is the study of symmetry and universality. In geophysics, we observe some geophysical data about the Earth and read information from it. Symmetry and universality are very important criteria for interpreting a phenomenon. Consider a situation where the data seem to be too complex. Even in such a case, once we recognize the governing process, previously unseen symmetries may unexpectedly emerge. If you understand how to manage to understand them, such symmetry may often appear sparkling like a kaleidoscope. But if you do not understand the background theory, they just look like a mess.

Let us imagine a scene where the wind makes waves on the surface of a river. If you have a background in the physics of water waves, you can see the dispersion of the waves and observe how they change depending on the depth of the water. If there is a current in the river, you can also observe the effect of the current. Suppose that there is a duck swimming in the river (Fig. 1.1). First of all, you would notice that the duck is swimming faster than the speed of the wave, so it is creating a shock wave. You may also notice that the group velocity behind the duck differs from the phase velocity. Then you also notice the angle made by the wedge-shaped wave behind the duck. Thus, if you have a background in physics, you will be able to decipher some of the information about the wind and water depth. The purpose of this lecture is to learn such a physical background to interpret wave information.

In this chapter, I will first explain what seismology deals with and then discuss the importance of understanding seismic wave propagation in this context. This is followed by an overview of what is covered in seismic wave theory.

Fig. 1.1   Waves made by ducks. Such waves are generally called wake waves, and the ripples are described by the Kelvin pattern.

§1.1 How to interpret waveforms of recorded seismograms

In this section, we review briefly the basics of seismic wave propagation.

Seismology[note 1)] does not cover research on earthquakes but also seismic wave propagations of the Earth generally. Roughly speaking, we can categorize research areas of seismology into two. The former is how geophysical phenomena excite seismic waves. From the observed seismic records, seismologists infer the physical processes such as earthquakes, volcanic activities, and land slides[note 2)]. The latter one is a seismic exploration of the Earth's interior.

When we observe a natural phenomenon, we assume a model implicitly. For example, most seismologists had been interested in "earthquake" data. Of course, "earthquake" itself as faulting is an important topic, and the "earthquake" also illuminate Earth's interior. Seismologists, therefore, recognized seismic wave field excited by an "earthquake" as a signal,

---

[note 1)] The term of "seismology" originated from ancient Greek ($\sigma\epsilon\iota\sigma\mu\acute{o}\varsigma$ (seismós, "earthquake") and $\lambda o\gamma\acute{\iota}\alpha$ (-logía, "study of").

[note 2)] Of course, other approaches such as geology and geochemistry are also crucial for understanding earthquakes and volcanic activities.

whereas they recognized seismic wave field excited by other phenomena –including ocean swell, human activities, and so on– as noise. In spite of the explicit or implicit model, we call a phenomenon, which is described by the model, a signal, and vice versa. "Noise" for somebody could be a "signal" for others.
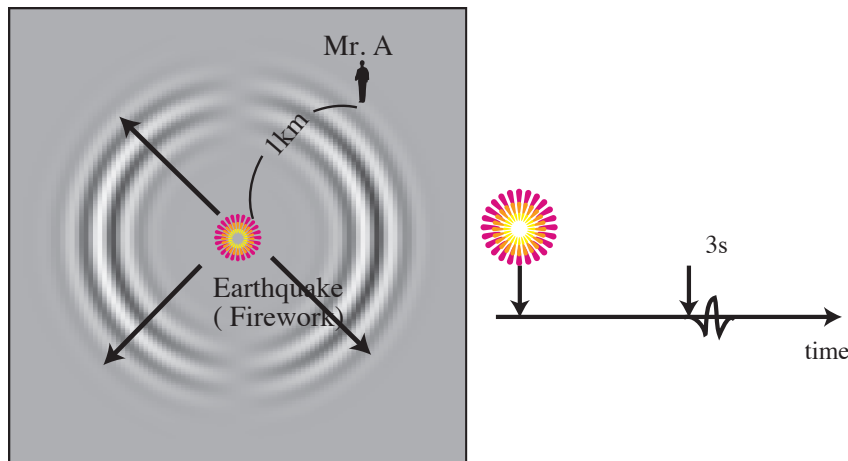
Fig. 1.2   Schematic figure of seismic wave field at an instance excited by an earthquake. We can see the concentric shape, which shows the propagation.

Here we consider a simple example. When we enjoyed fireworks on a summer night, we realized the lag time between the light and the sound. The lag is originated from the difference in propagation speeds between light and sound (Figure 1.2). This situation is similar to the seismic wave field of P- and S- waves: P- wave corresponds to light, and S-wave corresponds to sound. One can infer the distance between the observer and the firework by the lag. This principle is similar to locating a hypocenter of an earthquake from seismic data. When we know the distance in advance, we can infer sound velocity from the measured lag time, as in the seismic exploration of the Earth's interior.

For seismological investigations, the theoretical background of seismic wave propagation is indispensable. In this lecture, I introduce a framework for how we interpret seismic wavefields. note 3).

Last ten years, numerical methods for calculating seismic wavefields in a 3-D heterogeneous medium have become popular. They a feasible for estimating the 3-D seismic velocity structure and understanding the source processed of earthquakes. For interpreting the calculated seismic wave field, the background of seismic wave propagation based on physics and analytic representation is important.

---

note 3) Research on seismic wave propagation had been developed as an application of applied mathematics. For example, Jeffreys, who is famous for reference 1-D structure (Jeffreys and Bullen), is also known as a great applied mathematician (e.g. WKBJ approximation and Bayesian statistics.). Although a classic textbook of seismology focuses on techniques using complex analysis, this lecture emphasizes a more intuitive manner.

§1.2 Outline of this lecture

In this lecture, first, let us review a brief summary of governing equations of elastic media. Next, I introduce Green's function for understanding wave propagations in an infinite medium. Then, I will explain the representation theorem as a generalization of the Huygens principle. They give us a framework for understanding wave propagation.

As a first step for understanding wave propagations in a realistic medium, let us review the effects of a free surface. Reflections and refractions are keys to understanding. In general, a propagation problem in a semi-infinite medium is known as Lamb's problem. Under some situations, analytic formulations are obtained. Rayleigh wave is originated effects of the free surface.

Next, let us consider wave propagations in a two-layer medium. For understanding, reflections, and refractions on the inside boundary are given. Based on the framework with knowledge of the reflections and refractions, let us interpret wave propagation of the direct wave, head wave, and reflection wave in a two-layer medium. Love waves can exist in a two-layer medium, although they can't in a semi-infinite medium.

The last chapter describes ray theory, which is a framework for interpreting wave propagations in a multi-layer medium. The theory originated from optics, and the mathematical and physical treatments were already established firmly.

§1.2 Textbook

Dahlen and Tromp (1998)[2] and Aki and Richards (2009)[1] are standard textbooks in the area of seismic wave propagations. The mathematical approaches in an intuitive manner are given in Snieder and Wijk (2015).[3] Saito (2009)[4] is also a good textbook in this area but in Japanese.

§1.3 Bibliography

[1] K. Aki and P.G. Richards. *Quantitative Seismology*. Univ Science Books, 2nd edition, 2009.

[2] F.A. Dahlen and J. Tromp. *Theoretical Global Seismology*. Princeton University Press, Princeton, 1998.

[3] Roel Snieder and Kasper van Wijk. *A Guided Tour of Mathematical Methods for the Physical Sciences*. Cambridge University Press, 3 edition, 2015.

[4] 斎藤正徳. 地震波動論. 東京大学出版会, 2009.

Equations for the elastic Earth

<div align="right">Chapter 2</div>

In this chapter, I summarize governing equations of an elastic medium. For further understanding, please read Theoretical global seismology.[1]

§2.1 Lagrangian and Eulerian variables

Here we consider that a particle at x in a continuum at time 0. [note 1] move with time as $r(x, t)$. A Lagrangian variable describes a quantity with time by the initial location of x, and an Eulerian variable describes a quantity with time by a fixed frame as $r(r, t)$. An Eulerian quantity q^E can be related to the Lagrange quantity q^L as,

$$q^L(x, t) = q^E(r(x, t), t). \tag{2.1}$$

Time derivatives of the equation lead to

$$\partial_t q^L = \partial_t q^E + u^E \cdot \nabla_r q^E \equiv D_t q^E, \tag{2.2}$$

where u^E is Euler velocity. Material derivative D_t represents the Lagrangian time derivative of a particle in the Eulerian form. Later, ∂_t is an abbreviation of $\frac{\partial}{\partial t}$. A substitution of $r(x, t)$ to equation 3.2 as an Eulerian variable shows that equation 3.1 is equivalent to equation 3.2.

$$E \partial_t u^L = \partial_t u^E + u^E \cdot \nabla_r u^E \equiv D_t q^E, \tag{2.3}$$

When we consider seismic records, the Lagrangian description is more natural because the seismometer is pinned at a surface point.

Later we consider an infinitesimal deformation in a framework of linear elasticity. Let us consider small deformation s as,

$$r(x, t) = x + s(x, t). \tag{2.4}$$

---

note 1) A bold symbol like x show a vector in this textbook.

$$q^E(r, t) = q^0(r) + q^{E1}(r, t),$$
$$q^L(x, t) = q^0(x) + q^{L1}(x, t). \tag{2.5}$$

Because s is small, the perturbations e of Eulerian variable $q^{E1} and Lagrangian one q^{L1}$ can be written by,

$$q^{E1}(r, t) = q^{E1}(x, t), q^{L1}(x, t) = q^{L1}(r, t). \tag{2.6}$$

We note that the perturbations do not depend on x, r.

Next, let us consider a relation between an Eulerian preterition q^{E1} and a Lagrangian one q^{L1}. When we consider first-order perturbation q^{L1} can be written by[note 2)]

$$q^{L1}(x, t) = q^{E1}(r, t) + s \cdot \nabla_r q^0. \tag{2.7}$$

This equation is the integration of material derivatives. In a framework of linear elasticity, because we can neglect the second term of the right-hand side, we do not need to distinguish Eulerian from Lagrangian. However, because stress and density have initial values (∇q^0), the spatial derivatives cause the discrepancy between the Eulerian and Lagrangian. When we must consider initial stress (e.g. hydrostatic pressure owing to gravity), we must need attention to the difference between the descriptions. In §7.1, we will take such an example.

§2.2 Strain

In order to measure the deformation of an elastic body, let us trace two particles (r, $r + dr$). At $t = 0$, they are located at x, $x + dx$. dr can be related to dx as,

$$dr = \nabla_x r \cdot dx = (I + \nabla_x s) \cdot dx. \tag{2.8}$$

The change of the distance between the particles is estimated to be

$$|dr|^2 - |dx|^2 = 2(dx \cdot E^L \cdot dx). \tag{2.9}$$

Here E^L is Green-Lagrange strain defined by

$$E^L \equiv \frac{1}{2}[\nabla s + (\nabla s)^T - (\nabla s)^T \nabla s] = \frac{1}{2}\left(\frac{\partial s_j}{\partial x_i} + \frac{\partial s_i}{\partial x_j} + \frac{\partial s_l}{\partial x_i}\frac{\partial s_l}{\partial x_j}\right). \tag{2.10}$$

When s is enough small to neglect the second-order term, the stress can be simplified as,

$$E^L = \frac{1}{2}[\nabla s + (\nabla s)^T] = \frac{1}{2}\left(\frac{\partial s_j}{\partial x_i} + \frac{\partial s_i}{\partial x_j}\right) \tag{2.11}$$

Here, following Einstein's summation convention, we calculate the summation of the term over all the values of the index. Although strain tensor E^L is a Lagrangian variable, we do not need it from Eulerian strain when the infinitesimal deformation. The strain tensor has 6 independent components because of the symmetry.

---

note 2) See §3.2 of Dahlen and Tromp (1998)[1] in details.

> **Problem 2.1**
>
> Calculate the strain tensor up to the first order when considering a rigid rotation with an infinitesimal angle in 2-D. You can find second-order terms, although rigid rotation should not cause strain from a physical point of view. Next, show Green-Lagrange strain of an infinitesimal rigid rotation vanishes completely.

2.2.1 Strain in an arbitrary coordinate

Here we consider linear strain in an arbitrary coordinate. A displacement vector s can be represented by orthogonal unit vectors as

$$s = \sum_j s_j \hat{x}_j. \tag{2.12}$$

The gradient of the vector is written by

$$\nabla \equiv \hat{x}_i \frac{\partial}{\partial x_i}. \tag{2.13}$$

The insertion of the definition of s leads to the following equation:

$$\nabla s = \sum_i \hat{x}_i \frac{\partial s}{\partial x_i} = \sum_i \hat{x}_i \left[\sum_j \frac{\partial s_j}{\partial x_i} \hat{x}_j + \sum_j s_j \frac{\partial \hat{x}_j}{\partial x_i} \right]. \tag{2.14}$$

The second order tensor E can be represented by basis vectors and the corresponding components as

$$E = \sum_{ij} T_{ij} \hat{x}_i \hat{x}_j. \tag{2.15}$$

The complication originates from the partial derivatives of the basis vectors.

Strain in a cylindrical coordinate (r, φ, z)

Here we consider strain in a cylindrical coordinate (r, φ, z). Partial derivatives of the unit vector $\hat{r}$ are given by, $\hat{r}, \hat{\varphi}, \hat{z}$ です。

$$\frac{\partial \hat{r}}{\partial r} = 0, \qquad \frac{\partial \hat{r}}{\partial \varphi} = \hat{\varphi}, \qquad \frac{\partial \hat{r}}{\partial z} = 0$$

$$\frac{\partial \hat{\varphi}}{\partial r} = 0, \qquad \frac{\partial \hat{\varphi}}{\partial \varphi} = -\hat{r}, \qquad \frac{\partial \hat{\varphi}}{\partial z} = 0$$

$$\frac{\partial \hat{z}}{\partial r} = 0, \qquad \frac{\partial \hat{z}}{\partial \varphi} = 0, \qquad \frac{\partial \hat{z}}{\partial z} = 0. \tag{2.16}$$

The definition of the strain with the above equations leads to the following representation of the corresponding components as:

$$E_{rr} = \frac{\partial s_r}{\partial r}, E_{\varphi\varphi} = \frac{1}{r}\frac{\partial s_\varphi}{\partial \varphi} + \frac{s_r}{r}, E_{zz} = \frac{\partial s_z}{\partial z}$$

$$2E_{\varphi z} = \frac{\partial s_z}{\partial \varphi} + \frac{\partial s_\varphi}{\partial z}, E_{zr} = \frac{\partial s_r}{\partial z} + \frac{\partial s_z}{\partial r}, \tag{2.17}$$

$$2E_{r\varphi} = r\frac{\partial}{\partial r}\left(\frac{s_\varphi}{r}\right) + \frac{1}{r}\frac{\partial s_r}{\partial \varphi}.$$

Problem 2.2

Derive the strain in a cylindrical coordinate shown above.

Strain in a spherical coordinate (r, θ, φ)

Here only the results are shown as,

$$E_{rr} = \frac{\partial s_r}{\partial r}, E_{\theta\theta} = \frac{1}{r}\frac{\partial s_\theta}{\partial \theta} + \frac{s_r}{r}, E_{\varphi\varphi} = \frac{1}{r\sin\theta}\left(\frac{\partial s_\varphi}{\partial \varphi} + s_\theta\cos\theta\right) + \frac{s_r}{r}$$

$$2E_{\theta\varphi} = \frac{1}{r}\frac{\partial s_\varphi}{\partial \theta} + \frac{1}{r\sin\theta}\left(\frac{\partial s_\theta}{\partial \varphi} - s_\varphi\cos\theta\right), 2E_{\varphi r} = \frac{1}{r\sin\theta}\frac{\partial s_r}{\partial \varphi} + r\frac{\partial}{\partial r}\left(\frac{s_\varphi}{r}\right) \quad (2.18)$$

$$2E_{r\theta} = r\frac{\partial}{\partial r}\left(\frac{s_\theta}{r}\right) + \frac{1}{r}\frac{\partial s_r}{\partial \theta}.$$

§2.3 Stress and traction

$\hat{n}$

$d\Sigma$

Let us consider a small surface $d\Sigma$ in a continuum with the normal vector $\hat{n}$. Traction is defined by force f per unit area acting on $d\Sigma$. The traction is parallel to the normal vector $\hat{n}$, and the positive sign is defined by force from the positive side according to the normal vector to the negative side. Stress $T^{E\text{ note 3)}}$ is defined by
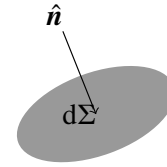
$$f = d\Sigma\hat{n} \cdot T^E. \quad (2.19)$$

Traction f_{12} of medium 1 from medium 2 is f_{21}.

§2.4 Conservation of angular momentum

Conservation of angular momentum requires that the stress tensor is symmetric as $T_{ij} = T_{ji}$.
note 4) as : $T_{ij} = T_{ji}$
This symmetry is held without microscopic spin interaction.[2]

---

note 3) This stress is Cauchy stress in a precise manner. There are two other definitions (see Dahlen and Tromp 1998 in details).

note 4) This symmetry is derived from the equilibrium of the moment of an infinitesimal volume.

> **Problem 2.3**
>
> Let us consider angular momentum along the z axis of an infinitesimal cube with a side of ϵ. Show $T_{xy} = T_{yx}$ from the conservation of angular momentum in cases:
>
> 1. T_{xy} and T_{yx} are constant, and other T_{ij} are zero.
> 2. (Optional)
>
> $$T_{xy}(\boldsymbol{x}) = \qquad T_{xy}(\boldsymbol{x}_0) + T_{xy}, x(\boldsymbol{x}_0)\delta x + T_{xy}, y(\boldsymbol{x}_0)\delta y, \qquad (2.20)$$
> $$T_{yx}(\boldsymbol{x}) = \qquad T_{yx}(\boldsymbol{x}_0) + T_{yx}, x(\boldsymbol{x}_0)\delta x + T_{yx}, y(\boldsymbol{x}_0)\delta y, \qquad (2.21)$$
>
> and other $T_{ij} = 0$.
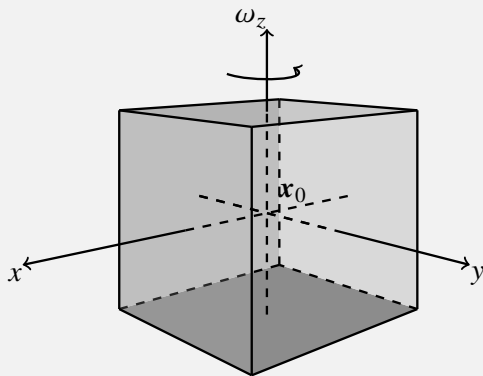
§2.5 Conservation of mass

Let us consider governing equations conservation of mass first. This equation becomes important for buoyancy force.

In general, conservation of mass can be written as,

$$\partial_t \rho^E = -\nabla \cdot (\rho^E \boldsymbol{u}^E), \qquad (2.22)$$

where $\boldsymbol{u}^E$ is Eulerian particle velocity.

Here we consider the first-order perturbation of the density as

$$\rho^E = \rho^0 + \rho^{E1}. \qquad (2.23)$$

Time integration of the first order perturbation leads to

$$\rho^{E1} = -\nabla \cdot (\rho_0 \boldsymbol{s}). \qquad (2.24)$$

The right-hand term represents the divergence of the mass flux, whereas the left one does the change of the mass. On the other hand, the Lagrangian form can be written by

$$\rho^{L1} = -\rho_0 \nabla \cdot (\boldsymbol{s}). \qquad (2.25)$$

Because we focused on a particle, the right-hand side shows corresponding expansion or deflation.

We note the discrepancy that the Lagrangian density perturbation ρ^{L1} is $\rho^{L1} = -\rho_0 \nabla \cdot \boldsymbol{s}$. If $\nabla \rho_0$ is 0, they are the same. However, they are different in general. When the wavelength of a seismic wave is much smaller than the typical scale of density change, we can neglect the difference.

§2.6 Equation of motions: conservation of momentum

Let us consider a temporal change a volume V^t.

$$\frac{d}{dt}\int_{V^t}\rho^E \boldsymbol{u}^E dV^t = \mathcal{F}, \tag{2.26}$$

The external force $\boldsymbol{F}$ can be written by surface force acting on ∂V^t and body force acting throughout the volume, such as gravity and electromagnetic force as

$$\mathcal{F} = \mathcal{F}_s + \mathcal{F}_b = \int_{\partial V^t}(\hat{\boldsymbol{n}}^t \cdot \boldsymbol{T}^E)d\Sigma^t + \int_{V^t}\rho^E \boldsymbol{g}^E dV^t. \tag{2.27}$$
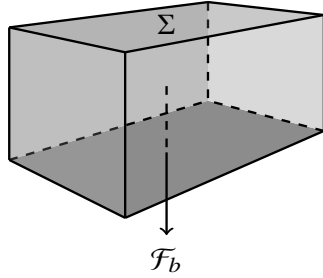
With a help of Gauss's divergence theorem, they can be written by

$$\rho^E D_t \boldsymbol{u}^E = \nabla_{\boldsymbol{r}} \cdot \boldsymbol{T}^E - \rho^E \nabla \phi^{E1}. \tag{2.28}$$

If we can neglect initial stress up to the first order, it can be simplified as

$$\rho_0 \partial_t^2 \boldsymbol{s} = \nabla \cdot \boldsymbol{T}^{E1}. \tag{2.29}$$

When we consider hydrostatic pressure, the equation of motions up to the first order can be written as

$$\rho_0 \partial_t^2 \boldsymbol{s} = \nabla \cdot \boldsymbol{T}^E - \rho^E \nabla \phi^E, \tag{2.30}$$

where ϕ^E is gravity potential [note 5)]. When we consider gravity, we must consider hydrostatic pressure, which sustains the gravity force. Deviatoric stress T^{E1} from the hydrostatic pressure can be written by,

$$T_{ij}^E = -p^0 \delta_{ij} + T_{ij}^{E1}. \tag{2.31}$$

Because the hydrostatic pressure sustains the gravity force, the pressure should satisfy the relation as,

$$\nabla p^0 = -\rho_0 \nabla \phi^0. \tag{2.32}$$

They lead to

$$\rho_0 \partial_t^2 \boldsymbol{s} = \nabla \cdot \boldsymbol{T}^{E1} - \nabla[\rho^0 \boldsymbol{s} \cdot \nabla \phi^0] - \rho^0 \nabla \phi^{E1} - \rho^{E1} \nabla \phi^0. \tag{2.33}$$

[note 5)] Here we consider gravity, but we neglect perturbation of gravity (an effect of self-gravitation). This approximation is known as the Cowling approximation in the field of astrophysics. In particular, this approximation is effective for a stratified atmosphere. The effect of self-gravitation becomes important in a period longer than 3000 s as described later.

§2.7 Conservation of energy

Total energy (kinetic energy + elastic energy) U, and energy flux K can be written by

$$U = \frac{1}{2} \left[\rho_0 \partial_t s \cdot \partial_t s + \sum_{ij} E_{ij} T_{ij} \right], \tag{2.34}$$

$$K = -T \cdot \partial_t s. \tag{2.35}$$

Conservation of energy can be written as,

$$\partial_t U + \nabla \cdot K = 0. \tag{2.36}$$

Elastic energy W can be defined by

$$W = \frac{1}{2} \sum_{ij} E_{ij} T_{ij}. \tag{2.37}$$

Stress can be represented by the spatial gradient of W as

$$T_{ij} = \frac{\partial W}{\partial E_{ij}}. \tag{2.38}$$

We will discuss the condition for the existence of elastic energy W as a potential energy below. Work per unit volume δR done by the internal stress T_{ij} can be given[3] by

$$\delta R = -T_{ij} \delta E_{ij}. \tag{2.39}$$

For deformation from $E = 0$ to $E = \Delta E$ of a given infinitesimal volume, the corresponding work ΔR by the internal stress is given by

$$\Delta R = -\int_0^{\Delta E} \sum_{ij} T_{ij} dE_{ij}, \tag{2.40}$$

which depends on the history of the deformation. Then we deform it again from $E = \Delta E$ to $E = 0$. Elastic deformation requires $\Delta R = 0$ because the internal stress should be conservative. The conservative property requires the following condition

$$\frac{\partial T_{ij}}{\partial E_{kl}} = \frac{\partial T_{kl}}{\partial E_{ij}}. \tag{2.41}$$

In the 2-D case (in this case, the number of the independent stress/strain components is 3), this condition can be interpreted as vortex-free (Problem 2.6). Consequently, the elastic energy W can be interpreted as a scalar potential.

Problem 2.4

Derive

$$dR = -T_{ij} dE_{ij}. \tag{2.42}$$

(Hint: Estimate work done by the internal force $F_j = \partial_i T_{ij}$.)

Problem 2.5

(1)

Let us consider works for two different deformation paths for a simple 2-D case. A rectangular area is deformed according to the strain of $E_{xx} = \Delta E_{xx}$, $E_{yy} = \Delta E_{yy}$ with two different paths: (i) first deform the area with ΔE_{yy}, then deform it with ΔE_{xx}. (ii) First deform it with ΔE_{xx}, then deform it with ΔE_{yy} as shown in Figure 2.1. Estimate works of $\Delta R^{(i)}$ and $\Delta R^{(ii)}$ for the cases (i) and (ii), respectively.
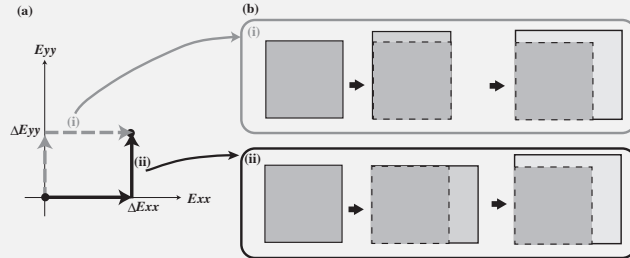
Fig. 2.1

When the stress satisfies the condition of a conservative force, $\Delta R^{(i)} = \Delta R^{(ii)}$ is required. Show the following condition of elastic modulus, which satisfies the above requirement.

$$C_{ijkl} = C_{klij}, \tag{2.43}$$

Problem 2.6

In order to understand the relation (equation 2.41):

$$\frac{\partial T_{ij}}{\partial E_{kl}} = \frac{\partial T_{kl}}{\partial E_{ij}}, \tag{2.44}$$

let us consider the 2-D case (3 independent variables of stress/strain components). Derive the condition for the case that works δR, which is work done by the internal stress, does not depend on deformation paths.

This condition guarantees that the spatial gradient of a scalar potential W can represent stress T. Thus elastic energy W can be interpreted as the scalar potential for stress $\mathbf{T}$.

§2.8 Constitution equation: Hooke's law

To determine elastic deformation, we must know the constitutional relation between stress T^{L1} and strain E_{L1}. For understanding the deformation of an arbitrary volume, Lagrangian description is essential. First, we do not take care of the difference between Lagrangian and Eulerian without considering initial stress. For a linear elastic medium, a relation between stress and strain can be represented by Hook's law as

$$T_{ij} = C_{ijkl}E_{kl}, \tag{2.45}$$

where C_{ijkl} is elastic tensor with 81 components. The symmetry of stress and strain tensor leads to the symmetry of C_{ijkl} as $C_{ijkl} = C_{jikl}, C_{ijkl} = C_{ijlk}$. 1st law of thermodynamics requires $C_{ijkl} = C_{klij}$[note 6]。 As a result, the elastic tensor has 21 independent components.

When an elastic medium is isotropic, the elastic tensor can be simplified using Lamé constants λ, μ as,

$$C_{ijkl} = \lambda\delta_{ij}\delta_{kl} + \mu(\delta_{ik}\delta_{jl} + \delta_{il}\delta_{jk}). \tag{2.46}$$

Here we derive Hooke's law for the isotropic medium explicitly for further sections.

$$
\begin{aligned}
T_{xx} &= (\lambda + 2\mu)E_{xx} + \lambda(E_{yy} + E_{zz}), & T_{xy} &= 2\mu E_{xy}, & E_{xz} &= 2\mu E_{xz} \\
T_{yy} &= (\lambda + 2\mu)E_{yy} + \lambda(E_{xx} + E_{zz}), & T_{yz} &= 2\mu E_{yz} \\
T_{zz} &= (\lambda + 2\mu)E_{zz} + \lambda(E_{xx} + E_{yy}).
\end{aligned}
\tag{2.47}
$$

The are several different definitions of the elastic constant, although they are identical in theory. Young modulus E and Poisson's ratio ν are also major, and they can be related to Lamé's constant as

$$E = \frac{\mu(3\lambda + 2\mu)}{\lambda + \mu}, \nu = \frac{\lambda}{2(\lambda + \mu)}. \tag{2.48}$$

Here we consider the effects of hydrostatic pressure on elastic medium. In the deep Earth, the hydrostatic pressure reaches several hundred GPa, the initial pressure is not negligible in some cases. In order to trace the temporal change of an infinitesimal volume V^t, the variables are described by Lagrangian as,

$$p^L = p_0 + p^{L1}. \tag{2.49}$$

The constitutional relation can be written by

$$p^{L1} = -\lambda(\boldsymbol{x})\nabla \cdot \boldsymbol{s}. \tag{2.50}$$

Eulerian equation of motions can be written by

$$p^{E1} = \boldsymbol{s} \cdot \nabla p_0 - p^{L1}. \tag{2.51}$$

The initial hydrostatic pressure p_0 should meet the following condition,

$$\nabla p_0 + \rho_0\boldsymbol{g} = 0. \tag{2.52}$$

[note 6] See a textbook of continuum mechanics in details.

With the conservation of mass, we obtain the following equation,

$$\rho_0 \partial_t^2 s = \nabla p^{L1} + \rho_0 [(\nabla \cdot s)g - \nabla(s \cdot g)]. \tag{2.53}$$

With wrong descriptions by a mixture between Eulerian or Lagrangian, the buoyancy term disappear. When we consider buoyancy owing to gravity, we must take care of the difference between Eulerian and Lagrangian descriptions.

2.8.1 A microscopic model for Hook's law

For a better understanding of P- and S-wave propagation in an elastic medium, let us consider a simple mass-spring model. In particular, for S-wave propagation, "cross spring" is important.

2.8.2 1-D case

Restoring force (stress) against stress in an elastic medium causes seismic wave propagations. First, let us consider a 1-D case for simplicity. Figure 2.2 shows such an example that masses (mass m) are connected by springs (spring constant k).
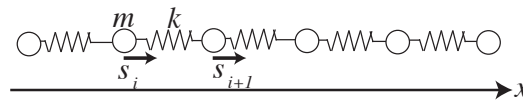
Fig. 2.2   A 1-D mass-spring model.

The equation of motions can be written by

$$m\frac{\partial^2 s}{\partial t^2} = k(s_{i+1} - 2s_i + s_{i-1}). \tag{2.54}$$

The right-hand term is the second-order finite difference of s. If the spatial interval of mass Δx is small enough, in the limit of a continuum, the equation becomes a wave equation as,

$$\frac{m}{\Delta x}\frac{\partial^2 s}{\partial t^2} = (k\Delta x)\frac{\partial^2 s}{\partial x^2}, \tag{2.55}$$

where $m/\Delta x$ represents the density ρ, and $k\Delta x$ represents the elastic modulus κ. Here κ satisfies the relation $\kappa = \rho c^2$ between ρ and the wave speed c. The wave equation can be rewritten by

$$\rho\frac{\partial^2 s}{\partial t^2} = \kappa\frac{\partial^2 s}{\partial x^2}. \tag{2.56}$$

Since strain E is given by $E = \frac{\partial s}{\partial x}$, the stress T is written by $T = \kappa E$. Therefore, the wave equation

$$\rho\frac{\partial^2 s}{\partial t^2} = \frac{\partial T}{\partial x} \tag{2.57}$$

can be interpreted by the equation of motions of the elastic body. Because the direction of particle motions coincides with the propagation direction, in this case, the wave corresponds to a P wave. Details will be explained in the next chapter.

2.8.3 2-D case: P and S waves

The P wave propagates faster than the S wave. The travel time difference is crucial for locating a hypocenter of an earthquake (e.g. Omori formula[note 7]). An early warning system of a large earthquake forecasts the arrival of the large S wave using the faster P wave arrivals. Why is the P wave faster than the S wave?

Let us consider a thought experiment described by Figure 2.3.

---

note 7) You can find the paper[4] at http://hdl.handle.net/2261/32677.

(1) 弾性体を液体に浸し圧力 p をかける

p

(2) 圧力の結果縮む

(3)P 波と対応させるため、減圧している部分と交互に並べる。層の間にズレが生じる。

P 波の伝播方向

(4) 境界を貼り付けると、ズレを解消するために shear の力がかかる。その分かたくなる。
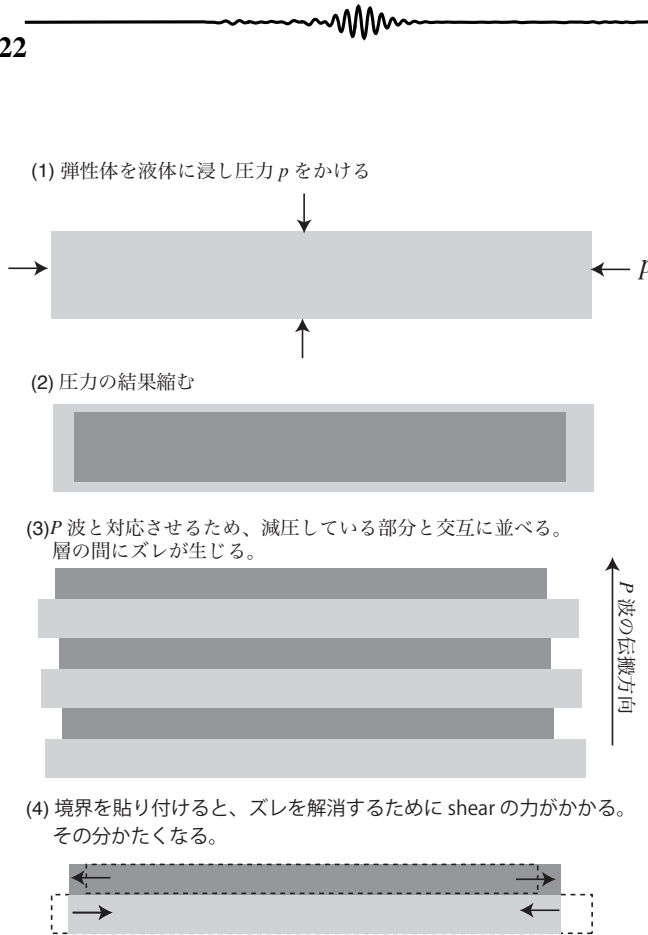
Fig. 2.3   Deformation of the medium associated with P-wave propagation.

1. Put pressure on the surface of a thin sheet.
2. The thin sheet shrinks.
3. Align compressed thin sheets and decompressed thin sheets alternatively. The decompression of a thin sheet causes the expansion as shown in this figure.
4. The thin sheets must be welded. To fit the boundaries, the thin sheets are accompanied by shear deformation. To keep the boundary of thin sheets, P waves require shear deformation. The deformation of the P wave in an elastic medium is composed of volumetric deformation and shear deformation, which corresponds to the S wave. As a result, the P wave is faster than the S wave.

Let us extend the 1-D mass-spring model to a 2-D one. "Cross-springs" are crucial for representing S-wave propagation in a 2-D case. Here we consider a simple model as shown in Figure 2.4.

First, let us consider a pain wave propagation of the S wave in the y direction. The displacement does not depend on x. The ith mass is moved with displacement s_{xi} in the x direction. The spring shown by the thick line in the Figure exerts restoring force T^S to the mass m. T^S can be written as,

平面波の伝播方向

$$T_i^S = \frac{1}{2}k(s_{x,i+1} - s_{x,i}). \tag{2.58}$$
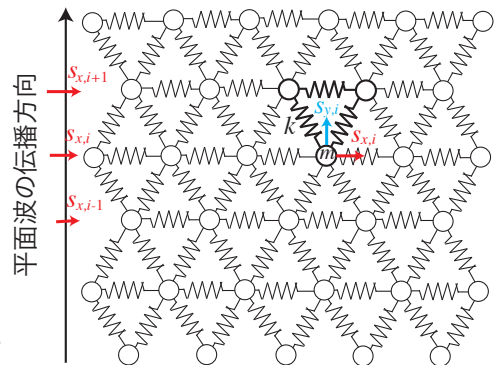
Fig. 2.4   A 2-D mass-spring model.

Because the lower spring also exerts restoring force to the mass, the total restoring force is $T_i^S - T_{i-1}^S$. Then we obtain a discretized wave equation.

Next, let us consider P-wave propagation. The displacement does not depend on x. The ith mass is moved with displacement s_{yi} in the y direction. The spring shown by the thick line in the Figure exerts restoring force T^P to the mass m. T^P in the x direction can be written as,

$$T_i^P = \frac{3}{2}k(s_{y,i+1} - s_{y,i}). \tag{2.59}$$

The total restoring force is $T_i^P - T_{i-1}^P$. A comparison of equation 2.59 with equation 2.58 shows that the restoring force of the P wave is stronger than that of the S wave. This leads to faster P-wave propagation than S-wave one.

Last, the relation of the mass-spring model to the Lamé constant is clarified as follows. A model depicted in Figure 2.4 leads to $\lambda = \mu = \sqrt{3}/4k$. In the case, S-wave β speed is determined by rigidity μ and density ρ, whereas P-wave velocity Vp) is related to both λ and μ as,

$$\alpha = \sqrt{\frac{\lambda + 2\mu}{\rho}}$$

$$\beta = \sqrt{\frac{\mu}{\rho}}. \tag{2.60}$$

For P-wave propagation, λ represents restoring force related to fluid pressure, whereas μ represents restoring force to suppress tangential motions.

Problem 2.7

Derive equation 2.58 and equation 2.59.
Hint: Because we consider a plain wave, relative motions depending on x are negligible. For a simple mode shown in Figure 2.5, calculate restoring force to displacement s_x and s_y.
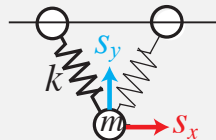
Fig. 2.5   A simplified model.

§2.9 Boundary conditions

When we solve equations of motion, the boundary conditions are indispensable. Lagrangian description of the boundary conditions is natural. However, we do not take care of the difference when we do not consider initial stress.

2.9.1 Solid-solid boundaries such as Moho and 660 km discontinuity
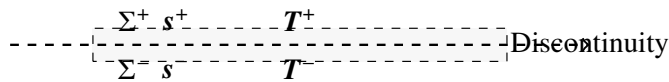
Fig. 2.6   Schematic figure of a plane Σ^+ and Σ^-.

Let us consider plane Σ^+ and Σ^- surrounding the boundary. The equilibrium of force and the continuity of the displacement s lead to the following boundary conditions:

Continuity of displacement : $[s]_-^+ = 0$.
Continuity of traction: $[T^{L1} \cdot \hat{n}]_-^+ = 0$.

2.9.2 Solid-fluid boundaries such as ocean floor and core-mantle boundary

For solid-fluid boundaries, free slip condition in the horizontal direction is important. The discontinuous property of displacement causes trapped modes along the boundary as explained in later sections[note 8].

Continuity of displacement: $[s \cdot \hat{n}]_-^+ = 0$. Horizontal slip to discontinuity is allowed.
Continuity of traction : $[T^{L1} \cdot \hat{n}]_-^+ = \hat{n} \cdot [\hat{n} \cdot T^{L1} \cdot \hat{n}]_-^+ = 0$. Note that shear stress in the fluid
   vanishes.

2.9.3 Continuity of gravity potential for all boundaries

$[\phi^{E1}]_-^+ = 0$
$[n \cdot \nabla \phi^{E1} + 4\pi G \rho^0 n \cdot s]_-^+ = 0$

---

note 8) When we need to consider hydrostatic pressure or initial stress, we must take care about the contribution
   [Dahlen and Tromp, 1998].[1]

§2.10 Comparison with terms of the equation of motions

Let us estimate the order of each term of the equation of motions for $u = e^{i(kx-\omega t)}$, where ω is angular frequency, and k is wavenumber.

Inertia: $\rho\partial^2 s$		$-\rho\omega^2 s$
Elasticity: $\nabla \cdot T$		$k^2\kappa s$
Gravity:		$\rho k s g$

Table 2.1   Estimation of each term of the equation of motions.

Here g is gravity acceleration, κ is a typical elastic constant (ρseismic-wave velocity^2). A comparison between the gravity term and the elasticity term is given by,

$$\frac{\text{Gravity}}{\text{Elasticity}} \sim \frac{\rho g}{k\kappa}. \tag{2.61}$$

$$T \sim \frac{2\pi\text{seismic-wave velocity}}{g} \sim 3000s \tag{2.62}$$

The period corresponds to the gravest mode of the Earth. We do not need to consider the gravity term in a period shorter than 100 s. For infra-gravity waves in the atmosphere, because the sound velocity is 340 m/s, the gravity term becomes comparable to the compressibility term for a period longer than 200 s.

At periods longer than 1000 s, Coriolis force originating from Earth's rotation is not negligible. In such a case, seismic wave velocity depends on the propagation direction[note 9]. Figure 2.7 shows the splitting of resonant peaks of $_0S_2$ due to Coriolis force during when 2004 Sumatra–Andaman earthquake. The directivity breaks the reciprocity of elastic Green's function, which is explained in the following chapter (see Dahlen and Tromp 1998 for details). Read Snieder *et al.* (2016)[5] for details of the Coriolis effects.

> **Problem 2.8**
>
> Based on a comparison of the Coriolis term and elastic restoration force, estimate the period at which the Coriolis force becomes significant.

[note 9] An example of the 1960 great Chilean earthquake can be found in The Feynman lectures on physics `http://www.feynmanlectures.caltech.edu/I_51.html`. We can imagine the atmosphere of Caltech in 1960'
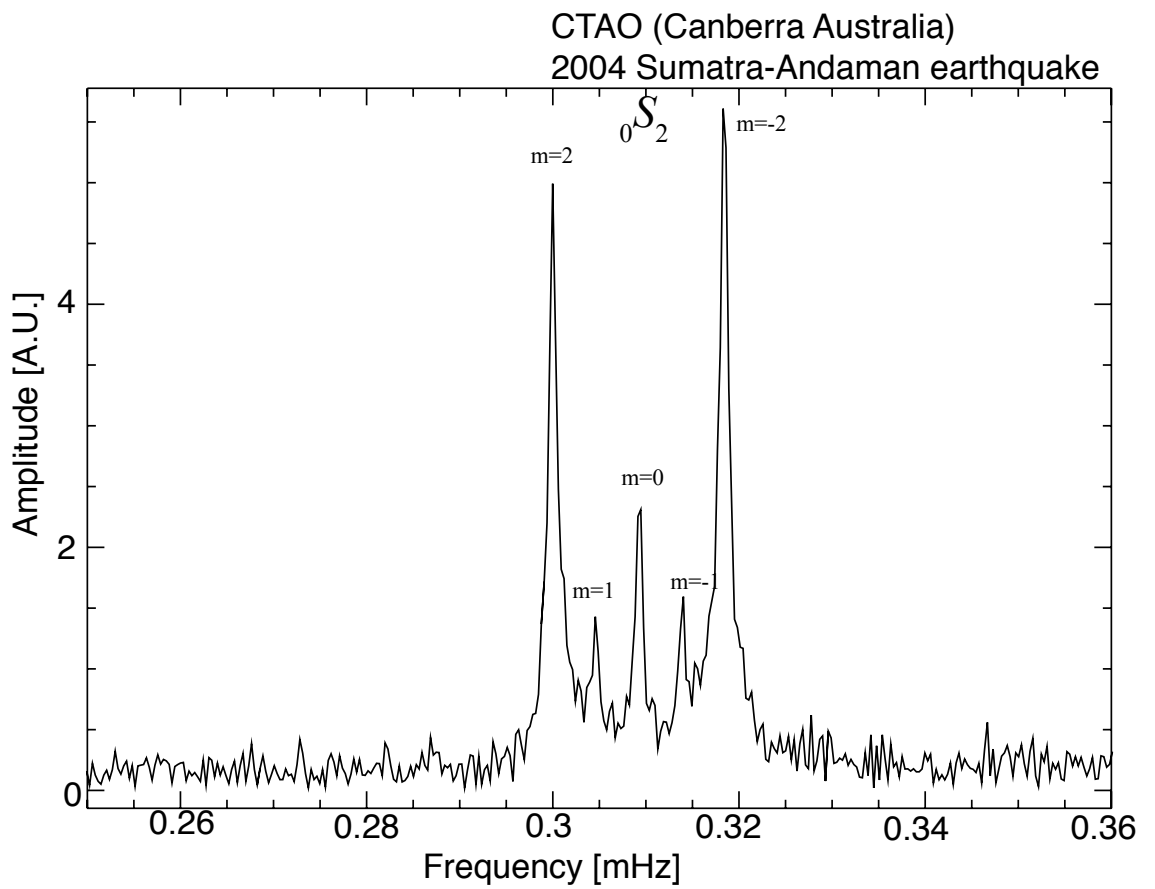
Fig. 2.7 Coriolis splitting of the resonant peak of $_0S_2$ when the great Sumatra-Andaman earthquake in 2004.

§2.11 Bibliography

[1] F.A. Dahlen and J. Tromp. *Theoretical Global Seismology*. Princeton University Press, Princeton, 1998.

[2] D. Kobayashi, T. Yoshikawa, M. Matsuo, R. Iguchi, S. Maekawa, E. Saitoh, and Y. Nozaki. Spin current generation using a surface acoustic wave generated via spin-rotation coupling. *Phys. Rev. Lett.*, Vol. 119, p. 077202, Aug 2017.

[3] L.D. Landau, E.M. Lifshitz, A.M. Kosevich, J.B. Sykes, L.P. Pitaevskii, and W.H. Reid. *Theory of Elasticity*. Course of theoretical physics. Elsevier Science, 1986.

[4] F. Omori. On the relation between the duration of the preliminary tremor and the epicentral distance for near earthquakes. *Bulletin of the Imperial Earthquake Investigation Committee*, Vol. 9, No. 1, pp. 33–39, mar 1918.

[5] Roel Snieder, Christoph Sens-Schönfelder, Elmer Ruigrok, and Katsuhiko Shiomi. Seismic shear waves as Foucault pendulum. *Geophys. Res. Lett.*, Vol. 43, No. 6, pp. 2576–2581, mar 2016.

Green's function and representation theorem

Green's function is useful when considering seismic wavefield excited by an event. This chapter explains a framework for interpreting seismic wavefields excited by various events, such as earthquakes and volcanic eruptions, using the representation theorem, which can be regarded as a natural extension of Huygens's principle. First, an acoustic (scalar) wave treatment is explained, then an elastic (vector) wave treatment is explained briefly.

§3.1 A solution of the wave equation in 1-D medium

First, let us consider the simplest case of a wave equation: 1-D wave equation. Here we consider acoustic wave propagations. The elastic constant κ and density ρ are homogeneous for simplicity. Pressure fluctuation p satisfies the following wave equation:

$$\frac{1}{\alpha^2} \frac{\partial^2 p(x,t)}{\partial t^2} - \frac{\partial^2 p}{\partial x^2} = 0, \tag{3.1}$$

where α is sound speed given by $\alpha = \sqrt{\kappa/\rho}$.

For understanding, the wave equation is mapped into the time-frequency domain by Fourier transform. The Fourier component $P(k, \omega)$ of the pressure fluctuation becomes a function of wavenumber k and the angular frequency ω as:

$$\left(\frac{\omega^2}{\alpha^2} - k^2 \right) P(k, \omega) = 0. \tag{3.2}$$

Thus P must satisfy a dispersion relation $\omega^2/\alpha^2 - k^2 = 0$. Here we consider one Fourier component $P(k, \omega)e^{i(\omega t + kx)}$. Because the dispersion relation leads to $k = \pm \omega/\alpha$, the The Fourier component can be rewritten as $P(k, \omega)e^{i(\omega(t \pm x/\alpha))}$, which represents the propagation toward the positive and negative directions of the x axis, respectively.

d'Alembert solution

Let us evaluate the behaviors of the solution more mathematically. With changes of variables; $\xi = x - \alpha t$, $\eta = x + \alpha t$, the solution of the 1-D wave equation can be represented by the arbitrary function ϕ and ψ as,

$$p(x, t) = \phi(x - \alpha t) + \psi(x + \alpha t). \tag{3.3}$$

The first term of the right-hand side represents the propagation toward the positive direction along the x axis, whereas the second term represents that toward the negative one.

Initial value problem

Let us consider how to solve the problem for the initial value at $t = 0$ given by

$$p(x, 0) = p_0(x), \tag{3.4}$$

$$\left.\frac{\partial p}{\partial t}\right|_{t=0} = q_0(x). \tag{3.5}$$

By comparing the initial value with the d'Alembert solution as

$$p_0 = \phi(x, 0) + \psi(x, 0) \tag{3.6}$$

$$q_0 = -\alpha \left(\frac{\partial \phi}{\partial t} - \frac{\partial \psi}{\partial t}\right). \tag{3.7}$$

Integrating equation 3.7 leads to the solution of ϕ と ψ. By the insertion of ϕ and ψ, we obtain the solution $p(x, t)$ as,

$$p(x, t) = \frac{1}{2} \left[p_0(x - \alpha t) + p_0(x + \alpha t)\right] + \int_{x-\alpha t}^{x+\alpha t} q_0(x')dx'. \tag{3.8}$$

Problem 3.1

1. Derive equation 3.3.
2. When p meets the initial condition at $t = 0$ given by

$$p(x, 0) = e^{-\frac{x^2}{\sigma^2}} \tag{3.9}$$

$$\frac{\partial p(x, 0)}{\partial x} = 0 \tag{3.10}$$

solve and plot the solution.
3. When p meets the initial condition at $t = 0$ given by

$$p(x, 0) = 0, \tag{3.11}$$

$$\left.\frac{\partial p(x, t)}{\partial t}\right|_{t=0} = e^{-\frac{x^2}{\sigma^2}}, \tag{3.12}$$

solve and plot the solution.

§3.2 Acoustic Green's function

An external force can represent the excited waves when considering seismic waves caused by geophysical phenomena such as earthquakes and volcanoes. In this case, we can evaluate the excited wave motion by considering the impulse response (Green's function) to the external force and by convolving the spatiotemporal distribution of the external force. This section first shows the features of Green's function.

First, let us consider acoustic wave propagation for essential understanding. Equation of motions and Hook's law ($\kappa \nabla \cdot s = -p$) lead to a wave equation concerning pressure perturbation $p(x, t)$ as,

$$-\nabla \cdot \frac{\nabla p(x, t)}{\rho_0(x)} + \frac{1}{\kappa(x)} \frac{\partial^2 p(x, t)}{\partial t^2} = -\nabla \cdot \left(\frac{f(x, t)}{\rho_0(x)} \right). \tag{3.13}$$

Here we consider a Green's function $g(x, t; \xi, \tau)$, which is an impulse response for impulsive force $\delta(x - \xi)\delta(t - \tau)$[note 1)] as

$$-\nabla \cdot \frac{\nabla g(x, t; \xi, \tau)}{\rho_0(x)} + \frac{1}{\kappa(x)} \frac{\partial^2 g(x, t; \xi, \tau)}{\partial t^2} = -\delta(x - \xi)\delta(t - \tau). \tag{3.14}$$

Problem 3.2

Explain physical meaning of the external force term $-\delta(x - \xi)$ of equation 3.14 (divergence of the particle velocity $\nabla \cdot v$).

If the boundary condition is time-independent, the Green's function exhibits time invariance as,

$$g(x, t; \xi, \tau) = g(x, t - \tau; \xi, 0). \tag{3.15}$$

Therefore, the time difference $t - \tau$ is enough variable to represent this problem.

Pressure field $p(x, t)$ can be represented by superposition of Green's function ($g(x, t - \tau; \xi, 0)$) as

$$p(x, t) = \int_V g(x, t; \xi, \tau) - \nabla \cdot \left(\frac{f}{\rho_0} \right) . dV(\xi) d\tau. \tag{3.16}$$

---

note 1)

$$f(0) = \int f(x) \delta(x) dx.$$

Therefore note that the dimension of the delta function is 1/m.

Next, the representation of the equation in frequency domain is considered. $P(\omega, \boldsymbol{x})$ shows Fourier transform of pressure p, and ω is angular frequency[note 2]

We do not consider hydrostatic pressure here.

$$\nabla \cdot \frac{\nabla P(\boldsymbol{x}, \omega)}{\rho_0(\boldsymbol{x})} + \frac{\omega^2}{\kappa(\boldsymbol{x})} P(\boldsymbol{x}, \omega) = F(\boldsymbol{x}, \omega), \qquad (3.17)$$

where F is Fourier transform of external force term $\nabla \cdot \left(\frac{f(\boldsymbol{x}, t)}{\rho_0(\boldsymbol{x})} \right)$.

Green's function in frequency domain satisfies the following equation,

$$\nabla \cdot \frac{\nabla G(\boldsymbol{x}, \xi, \omega)}{\rho_0(\boldsymbol{x})} + \frac{\omega^2}{\kappa(\boldsymbol{x})} G(\boldsymbol{x}, \xi, \omega) = \delta(\boldsymbol{x} - \xi), \qquad (3.18)$$

where $G(\boldsymbol{x}, \xi, \omega)$ is Green's function in frequency domain. Then, pressure field P excited by an arbitrary force distribution F can be represented by a convolution between Green's functions and the force distribution as,

$$P = \int_V G(\boldsymbol{x}, \xi, \omega) F(\xi, \omega) dV(\xi). \qquad (3.19)$$

§3.3 Green's function in an infinite homogeneous medium

To understand the behaviors of Green's function, this section explains the explicit representation of Green's function. First, let us summarize the basics of the wave equation.

3.3.1 1-D wave equation

Let us consider a 1-D wave equation. This solution can be recognized as plane wave propagation in a 3-D medium.

d'Alembert solution

With changes of variables $\xi = t - \alpha x$, and $\eta = t + \alpha x$, a solution of a 1-D wave equation can be written as

$$p(z, t) = p_0(t - z/\alpha) + p_1(t + z/\alpha), \qquad (3.20)$$

where f and g are arbitrary functions. The first term of the right-hand side represents the wave propagation toward the positive direction of the z axis, and the second term represents the negative direction.

[note 2] Take care about definitions of the sign and the normalization of the Fourier transform because the definition depends on the field. Fourier transform $\mathcal{F}$ and inverse Fourier transform $\mathcal{F}^{-1}$ are defined as

$$U(\omega) = \mathcal{F}(u) \equiv \int_{-\infty}^{\infty} u(t) e^{-i\omega t} dt,$$

$$u(t) = \mathcal{F}^{-1}(U) \equiv \frac{1}{2\pi} \int_{-\infty}^{\infty} U(f) e^{i\omega t} d\omega.$$

Details of the definition in this text are shown in the appendix 3.B.

3.3.2 Derivations of Green's function in a 1-D medium

For an infinite homogeneous medium, equation 3.18 can be simplified as,

$$\frac{1}{\rho_0}\frac{\partial^2 G^{1D}}{\partial z^2} + \frac{\omega^2}{\kappa}G^{1D} = \delta(z). \tag{3.21}$$

Problem 3.3

1. Solve the equation except for $z = 0$.
2. At $z = 0$, the equation is singular because of the delta function. Integrate equation 3.21 in a rage of $-\epsilon/2 <= z <= \epsilon/2$). Then derive the following equation,

$$\left[\frac{\partial G^{1D}}{\partial z}\right]_{-\epsilon/2}^{+\epsilon/2} = \rho_0. \tag{3.22}$$

   Note that integration of Green's function in the infinitesimal range is negligible from equation 3.19.
3. By continuation of the two solutions at $z = 0$, derive the following result of 1-D Green's function as,

$$G^{1D}(z, \omega) = \frac{\rho_0 i}{2k}e^{-ik|z|}. \tag{3.23}$$

4. Inverse Fourier transform of G^{1D} show

$$g^{1D}(z, t) = \begin{cases} 0 & t < |z|/\alpha \\ -\frac{\alpha}{2}\rho_0 & t >= |z|/\alpha. \end{cases} \tag{3.24}$$

5. Problem 3.1 (3) gave the initial velocity at $t = 0$. Compare the solution to the above solution of this problem, and interpret the physical relation.

3.3.3 Derivations of Green's function in a 2-D medium

Here we consider a cylindrical coordinate (r, ϕ) with origin at $\boldsymbol{xi}$.

$$\frac{1}{\rho_0}\frac{1}{r}\frac{\partial}{\partial r}\left(r\frac{\partial G^{2D}}{\partial r}\right) + \frac{\omega^2}{\kappa}G^{2D} = \delta(\boldsymbol{x} - \boldsymbol{x}_0). \tag{3.25}$$

1. Except for $r = 0$, a solution of equation 3.25 can be represented by superposition of 0th order Bessel function of the first kind $J_0(r)$ and 0th order Neumann function $N_0(r)$.
2. At $r = 0$, the equation is singular. Then integrate equation 3.25 at an infinitesimal circular area (C) at around the origin. Using Gauss's divergence theorem, show

$$\int_C \frac{\partial G^{2D}}{\partial r}dl = \rho_0. \tag{3.26}$$

3. By continuation of the two solutions at the origin $r = 0$ derive the following result of 2-D Green's function as

$$G^{2D} = -i\frac{\rho_0}{4}H_0^{(2)}(kr). \tag{3.27}$$
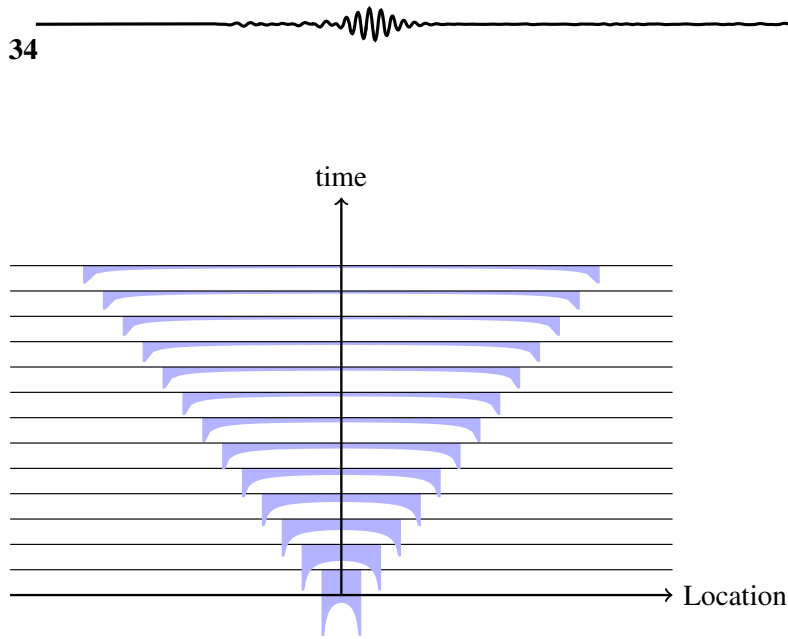
Fig. 3.1   Propagation of 2-D Green's function.

Here $H_0^{(2)}$ is Hankel's function of the second kind.

4. In the time domain, the corresponding Green's function can be written by,

$$g^{2D}(r,t) = -\frac{\rho_0}{2\pi} \frac{H(t-r/\alpha)}{\sqrt{t^2 - r^2/\alpha^2}}, \tag{3.28}$$

where H is the Heaviside step function.

Problem 3.4

1. Show that Hankel function of the first kind can be approximated by a cylindrical wave in far field.
2. Interpret distance dependence of the amplitude based on the conservation of energy.
3. Show the amplitude of 2D Green's function in time domain (equation 3.28) is proportional to $1/\sqrt{r}$ if the distance r is enough long.

3.3.4 Green's function of a 3-D medium

This subsection explains Green's function in a 3-D medium, which describes 3-D wave propagation for the forcing $\delta(\boldsymbol{x})\delta(t)$.

$$-\frac{1}{\rho_0}\frac{1}{r^2}\frac{\partial}{\partial r}\left(r^2\frac{\partial g^{3D}}{\partial r}\right) + \frac{1}{\kappa}g^{3D}\frac{\partial^2}{\partial t^2} = -\delta(\boldsymbol{x})\delta(t) \tag{3.29}$$

To consider the amplitude, first, let us consider the d'Alembert solution[note 3)]. With a change

---

[note 3)] In general, behaviors of solution of wave equations in even dimensions are quite different from those in odd dimensions. The former is localized close to the wavefront and lasts for a long time.

of the variable as $p = \bar{p}/r$, the solution is given by,

$$p = \frac{p_0(t - r/\alpha)}{r} + \frac{p_1(t + r/\alpha)}{r}, \tag{3.30}$$

which represents spherical waves outward and inward. The amplitude decays with $1/r$. The distance-dependent is also given by energy conservation on the expanding (or shrinking) wavefront.

Green's function in a 3-D medium is given by

$$g^{3D}(r, t) = -\frac{\rho_0}{4\pi} \frac{\delta(t - r/\alpha)}{r}. \tag{3.31}$$

See Problem 3.5 for the derivation.

Problem 3.5

Here we consider a spherical coordinate (r, θ, ϕ) with origin at $\boldsymbol{\xi}$.

$$\frac{1}{\rho_0} \frac{1}{r^2} \frac{\partial}{\partial r}\left(r^2 \frac{\partial G^{3D}}{\partial r}\right) + \frac{\omega^2}{\kappa} G^{3D} = \delta(\boldsymbol{x} - \boldsymbol{\xi}) \tag{3.32}$$

1. With a change of variable as $G^{3D} = \bar{G}/r$, rewrite the above equation.
2. Solve the equation except $r = 0$.
3. At $r = 0$, the solution is singular. Integrate equation 3.18 within an infinitesimal sphere. Then show the following equation

$$\int_\Sigma \frac{\partial G^{3D}}{\partial r} d\Sigma = \rho_0, \tag{3.33}$$

   using Gauss's divergence theorem.
4. By continuation of the two solutions at the origin $r = 0$ derive the following result of 3-D Green's function as,

$$G^{3D} = -\frac{\rho_0}{4\pi} \frac{e^{-ikr}}{r} \tag{3.34}$$

5. Calculate inverse Fourier transform the above equation.

> **Problem 3.6**
>
> 1. The pressure response for forcing $f(x) = \delta(z)$ in a 3-D medium can be interpreted by 1-D Green's function. Based on this fact, show the relation between 1-D Green's function and 3-D Green's function.
> 2. Equation 3.28 shows 2-D Green's function does not go zero after the arrival of the wavefront. Derive 2-D Green's function from the 3-D Green's function based on 3-D Green's function with a line source given by $\delta(r)$.

§3.4 Green's function in a homogeneous elastic medium

Let us consider the equation of motions

$$\rho \frac{\partial^2}{\partial t^2} s_i = \frac{\partial}{\partial x_j} T_{ij} + f_i. \tag{3.35}$$

Here we neglect self-gravitation and initial stress.

For an **isotropic and homogeneous elastic body**, the equation can be simplified as,

$$
\begin{aligned}
\rho \partial_t^2 s \quad &= (\lambda + \mu)\nabla(\nabla \cdot s) \quad + \mu \nabla^2 s \qquad\quad + f \\
&= \underbrace{(\lambda + 2\mu)\nabla(\nabla \cdot s)}_{Pwave} \quad \underbrace{- \mu(\nabla \times \nabla \times s)}_{Swave} \quad + f
\end{aligned}
\tag{3.36}
$$

The first term of the right-hand side represents the P wave with volumetric changes, whereas the second one represents the S wave with shear deformation. Later we consider a homogeneous and isotropic medium

3.4.1 Elastic potential: Separation between P save and S wave

In order to clarify the perspective, displacement s is written by scalar potential ϕ[note 4)] and vector potential ψ using Helmholtz's theorem as

$$s = \nabla \phi + \nabla \times \psi. \tag{3.37}$$

I note that vector potential ψ has ambiguity for the choice of the reference. Vector potential $\psi' \equiv \psi + \nabla \chi$ leads to $\nabla \times \psi' = \nabla \times \psi$. For static magnetic field, we choose a vector potential as $\nabla \cdot \psi$ in general. In the case of an electromagnetic field, vector potential is related to the scalar potential for each other, whereas, in the case of elastic deformation, they are independent, as shown in later sections. In the case of an elastic wave field, we can separate the P wave and S wave without the choice of a reference of vector potential as $\nabla \times \psi = 0$. For example, for a stratified medium described in later chapters, a form of vector potential as $\nabla \times (\psi + \nabla \times \chi)$ becomes convenient because the two terms (ϕ and χ) represent horizontally polarized S waves (SH) and vertically polarized S waves (SV), respectively.[5)]

Insertion of equation 3.37 into equation 3.36 leads to

$$
\begin{cases}
\nabla^2 \left(\rho \dfrac{\partial^2 \phi}{\partial t^2} - (\lambda + 2\mu)\nabla^2 \phi \right) = \nabla \cdot f \\[4mm]
\nabla \times \nabla \times \left(\rho \dfrac{\partial^2 \psi}{\partial t^2} + \mu \nabla \times \nabla \times \psi \right) = \nabla \times f
\end{cases}
\tag{3.38}
$$

where α is P-wave velocity and β is S-wave velocity ($\lambda + 2\mu = \rho\alpha^2$, $\mu = \rho\beta^2$).

---

note 4) Based on the definition, the scalar potential ϕ can be related to pressure $p = -\rho\alpha^2\nabla^2\phi$.

A formula of vector analysis of

$$\nabla \times \nabla \times \boldsymbol{\psi} = \nabla(\nabla \cdot \boldsymbol{\psi}) - \nabla^2 \boldsymbol{\psi} \tag{3.39}$$

and $\nabla \times [\nabla(\nabla \cdot \boldsymbol{\psi})] = 0$ lead to

$$\nabla \times \nabla \times \left(\rho \frac{\partial^2 \boldsymbol{\psi}}{\partial t^2} - \mu \nabla^2 \boldsymbol{\psi} \right) = \nabla \times \boldsymbol{f}. \tag{3.40}$$

Similarly, the Helmholtz decomposition of $\boldsymbol{f}$ is given by

$$\boldsymbol{f} = \nabla \Phi + \nabla \times \boldsymbol{\Psi} \tag{3.41}$$

Thus, to satisfy the equation of motions,

$$\begin{cases} \rho \dfrac{\partial^2 \phi}{\partial t^2} - (\lambda + 2\mu)\nabla^2 \phi = \Phi \\[2mm] \rho \dfrac{\partial^2 \boldsymbol{\psi}}{\partial t^2} - \mu \nabla^2 \boldsymbol{\psi} = \boldsymbol{\Psi} \end{cases} \tag{3.42}$$

is sufficient [note 5]. These equations correspond to wave equations of P-wave and S-wave, respectively.

[note 5] There are also terms for translational motion and rigid body rotation (see Problem 3.7) as solutions, but they can be dropped because they violate the infinitesimal assumption.

Problem 3.7

Let us consider the equation:

$$\nabla^2 \left(\frac{1}{\alpha^2} \frac{\partial^2 \phi}{\partial t^2} - \nabla^2 \phi \right) = 0 \qquad (3.43)$$

1. Estimate ϕ_0, which satisfies $\nabla^2 \phi_0(x, t) = 0$.
2. Show that $\phi + \phi_0$ also satisfies equation 3.43.
3. Show that ϕ_0 represents a translational motion when ϕ_0 satisfies equation 3.36.
4. Let us consider the same discussion for the vector potential ψ_0 given by

$$\psi_0 = \begin{pmatrix} 0 & r_{xy} & r_{xz} \\ -r_{xy} & 0 & r_{yz} \\ -r_{xz} & -r_{yz} & 0 \end{pmatrix} \begin{pmatrix} x \\ y \\ z \end{pmatrix}, \qquad (3.44)$$

which represents a rigid rotation. Based on the discussion for scalar potential, the vector potential satisfies the governing equation. In this text, we drop the effects because they are not first-order variables.

3.4.2 Green's function for an explosive source

In general, an excitation problem in an elastic medium by a force is complicated. In order to understand the important concept of "near field" and "far field", let us consider an excitation problem of elastic waves by an explosion source, which can be described by only a scalar potential. This simple example could be helpful for understanding elastic wave propagation.

First, let us consider Green's function G^ϕ for scalar potential ϕ. For an impulsive pressure $\delta(t)$, the Green's function is given by

$$\frac{\partial^2 G^\phi(x,t;\xi,\tau)}{\partial t^2} - \frac{1}{\alpha^2}\nabla^2 G^\phi = \delta(x-\xi)\delta(t-\tau) \tag{3.45}$$

$$G^\phi(x,t;\xi,\tau) = \frac{1}{4\pi\rho\alpha^2 \mid x-\xi \mid}\delta\left(t-\tau-\frac{\mid x-\xi \mid}{\alpha}\right) \tag{3.46}$$

Near field term and far-field term for a point explosive source

First, let us consider a response for a point explosive source for simplicity. Within an infinitesimal sphere with radius Δr at the origin suddenly increase the pressure Δp at $t = 0$ as,

$$p^{\text{source}}(\xi,\tau) = \Delta p(1 - H(r - \Delta r))H(\tau), \tag{3.47}$$

where $H(t)$ is Heaviside function[note 6]. The minus sign originated from the difference between pressure and stress tensor. Because an explosive source cannot cause shear deformation in a homogeneous medium, we consider only scalar potential ϕ here. ϕ can be given by convolution between the Green's function and the source term p^{source} as

$$\phi = \int_{-\infty}^{\infty} G^\phi(x,t,\xi,\tau)p^{\text{source}}(\xi,\tau)dV(\xi)d\tau$$

$$= -\frac{\Delta p\Delta r^3}{3\rho\alpha^2}\frac{H\left(t-\frac{r}{\alpha}\right)}{r}. \tag{3.48}$$
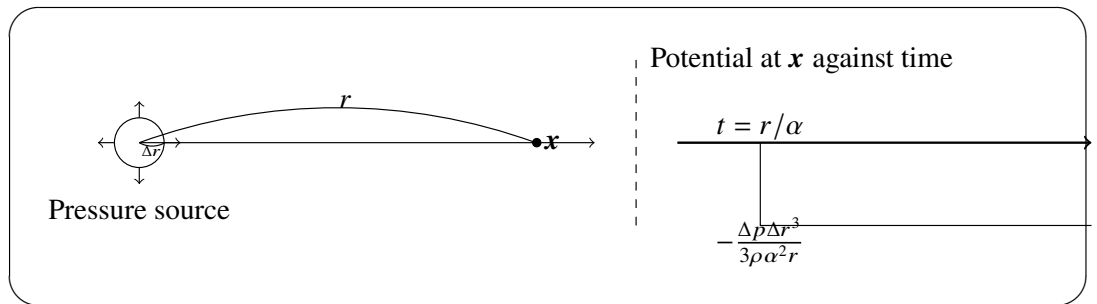
Fig. 3.2 Schematic figure of the deformation by the explosive source.

The displacement s can be represented by gradient of the scalar potential ϕ as

$$s_r = \frac{\Delta p\Delta r^3}{3\rho\alpha^2}\left(\underbrace{\frac{H(t-r/\alpha)}{r^2}}_{\text{Near field term}} + \underbrace{\frac{\delta(t-r/\alpha)}{\alpha r}}_{\text{far field term}}\right). \tag{3.49}$$

[note 6] $H(t) = 1, t \geq 0, H(t) = 0, t < 0$

The displacement of the near field term can be interpreted as static deformation by the incremental pressure at a point. For $t = \infty$ equation 3.45 can be simplified as,

$$\nabla^2 G^\phi = -\alpha^2 \delta(\boldsymbol{x} - \boldsymbol{\xi}). \tag{3.50}$$

The form of this equation is equivalent to a static electric field by a point charge.

The far-field term represents a propagation of the delta function. The amplitude decreases with distance $\sim 1/r$. This result means that net energy flux on a given sphere is constant ($4\pi r^2 (r^{-1})^2$ is constant) against the propagation distance. This result originated from energy conservation owing to the wave propagation.

vspace3cm

> **Problem 3.8**
>
> 1. Derive equation 3.48.
> 2. Derive equation 3.49, and plot the near field term and the far field term.

3.4.3 Green's function of a homogeneous medium for impulsive force: a general case

Green's function is feasible for estimating an elastic response by a general forcing. Let us consider Green's function for an impulsive force $X_0(t)\delta(t)$ in the x direction,

$$\frac{\partial^2}{\partial t^2} \boldsymbol{G} = \alpha^2 \nabla(\nabla \cdot \boldsymbol{G}) - \beta^2 (\nabla \times \nabla \times \boldsymbol{G}) + [\delta(\boldsymbol{x})X_0(t), 0, 0] \tag{3.51}$$

The external force can also be represented by scalar potential Φ and vector potential $\boldsymbol{\Psi}$ based on Helmholtz theorem as,

$$[\delta(\boldsymbol{x})X_0(t), 0, 0] = \nabla\Phi + \nabla \times \boldsymbol{\Psi}. \tag{3.52}$$

div of the both sides of the equation leads to

$$\nabla^2 \Phi = X_0(t) \frac{\partial \delta(\boldsymbol{x})}{\partial x}. \tag{3.53}$$

Here we consider the Green's function (equation 3.3.4) satisfies the following equation:

$$\nabla^2 \left(-\frac{1}{4\pi} \frac{1}{|\boldsymbol{x}|} \right) = \delta(\boldsymbol{x}). \tag{3.54}$$

The comparison leads to [note 7],

$$\Phi = -\frac{X_0(t)}{4\pi} \frac{\partial}{\partial x} \frac{1}{|\boldsymbol{x}|}$$

$$\boldsymbol{\Psi} = \frac{X_0(t)}{4\pi} \left(0, \frac{\partial}{\partial z} \frac{1}{|\boldsymbol{x}|}, -\frac{\partial}{\partial y} \frac{1}{|\boldsymbol{x}|} \right). \tag{3.55}$$

[note 7] see Aki and Richards[1] in details.

G can be also represented by a superposition of scalar potential ϕ and vector potential ψ based on Helmholtz theorem as,

$$G = \nabla\phi + \nabla \times \psi. \tag{3.56}$$

Each potential satisfies the wave equation. For example, the scalar potential satisfies the following equation,

$$\frac{\partial^2 \phi}{\partial t^2} = \alpha^2 \nabla^2 \phi + \Phi. \tag{3.57}$$

ϕ can be given by convolution between the scalar Green's function in the 3-D medium and the forcing term Φ (see the first section of this chapter).

The scalar potential can be written by a convolution between the scalar Green's function and Φ as

$$\phi(\boldsymbol{x}, t) = -\frac{1}{(4\pi)^2 \rho \alpha^2} \int_V X_0 \left(t - \frac{|\boldsymbol{x} - \boldsymbol{x}_0|}{\alpha} \right) \frac{1}{|\boldsymbol{x} - \boldsymbol{x}_0|} \frac{\partial}{\partial x_0} \frac{1}{|\boldsymbol{x}_0|} dV_0. \tag{3.58}$$

A change of variables of $|\boldsymbol{x} - \boldsymbol{\xi}| = \alpha\tau$ leads to the following equation:

$$\phi(\boldsymbol{x}, t) = -\frac{1}{(4\pi)^2 \rho \alpha^2} \int_0^\infty \frac{X_0(t - \tau)}{\tau} \left(\iint_S \frac{\partial}{\partial \xi_0} \frac{1}{|\boldsymbol{\xi}|} dS \right) d\tau. \tag{3.59}$$

Here we focus on the integral $\iint dS$. The circle in Figure 3.3 represents a spherical shell with the radius $\alpha\tau$. The surface integral of a potential $1/r$ leads to an analogy to a problem of gravity potential. If the mass is the uniform distribution on a closed shell, the term represents the spatial gradient of the potential along x direction at the origin $\boldsymbol{O}$ (i.e., it corresponds to x component of gravity). Based on the analogy for a problem of gravity, when the point $\boldsymbol{O}$ is inside the shell, the gravity is 0. On the other hand, when it is outside the shell, the mass is concentrated at the center $\boldsymbol{x}$ virtually. This result leads to the following form:

Fig. 3.3 Coordinate for evaluation the potential ϕ.

$$\phi(\boldsymbol{x}, t) = -\frac{1}{4\pi\rho} \left(\frac{\partial}{\partial x} \frac{1}{r} \right) \int_0^{r/\alpha} \tau X_0(t - \tau) d\tau. \tag{3.60}$$

The vector potential is also written similarly. With some calculations, we obtain the potentials as,

$$\begin{cases} \phi(\boldsymbol{x}, t) = -\dfrac{1}{4\pi\rho} \left(\dfrac{\partial}{\partial x} \dfrac{1}{r} \right) \displaystyle\int_0^{r/\alpha} \tau X_0(t - \tau) d\tau \\[4mm] \psi(\boldsymbol{x}, t) = \dfrac{1}{4\pi\rho} \left(0, \dfrac{\partial}{\partial z} \dfrac{1}{r}, -\dfrac{\partial}{\partial y} \dfrac{1}{r} \right) \displaystyle\int_0^{r/\beta} \tau X_0(t - \tau) d\tau. \end{cases} \tag{3.61}$$

By substituting the scalar and vector potentials into $\boldsymbol{s} = \nabla\phi + \nabla \times \psi$, we obtain the following

expression:

$$
s_i(\boldsymbol{x}, t) = \frac{1}{4\pi\rho} \left(\frac{\partial}{\partial x_i \partial x} \frac{1}{r} \right) \int_{r/\alpha}^{r/\beta} \tau X_0(t - \tau) d\tau
$$

$$
+ \frac{1}{4\pi\rho\alpha^2 r} \left(\frac{\partial r}{\partial x_i} \frac{\partial r}{\partial x} \right) X_0 \left(t - \frac{r}{\alpha} \right)
$$

$$
+ \frac{1}{4\pi\rho\beta^2 r} \left(\delta_{i1} - \frac{\partial r}{\partial x_i} \frac{\partial r}{\partial x} \right) X_0 \left(t - \frac{r}{\beta} \right). \tag{3.62}
$$

The first term represents a near field, the second represents a far field of the P wave, and the third represents a far field of the S wave.

Now let us consider the near and far field terms in more detail. We can determine whether we are near or far based on two timescales: the characteristic time of $X(t)$, and the P-S travel time difference $r/\beta - r/\alpha$. From a simple calculation (see Problem 3.9), when the characteristic time of $X(t)$ is sufficiently smaller than the P-S travel time difference, the second and third terms are proportional to $1/r$, and the first term is proportional to r^{-2}. The first term is negligible at an enough distant point, whereas it represents the static displacement corresponding to the crustal movement at a near-source point. On the other hand, if $X(t)$ is sufficiently longer than the P-S travel time difference, all terms are proportional to $1/r$, and all terms become important. The details will be explained in the next chapter. Still, the actual earthquake is a bit more complicated, and there are intermediate terms in addition to the far and near terms, which can be understood using Green's function derived in this section.

Problem 3.9

1. In a case of $X(t) = \delta(t)$, evaluate the near field term (the first term of the right-hand side of equation 3.62.
2. In a case of $X(t) = H(t)$, evaluate the near field term (the first term of the right-hand side of equation 3.62. Here H is the Heaviside step function.

Problem 3.10

1. When r is large enough, the far-field term of Green's function proportional to $1/r$ (the second term of equation 3.62) becomes dominant at the distant point. By evaluating the P-wave potential $\nabla\phi$ (equation 3.61), estimate the far field term of P-wave displacement.
2. Derive equation 3.62.
3. For $X(t) = \delta(t)$, evaluate the near field term (the first term of equation 3.62).

§3.5 Reciprocity of acoustic wave

Reciprocity of acoustic wave states that an acoustic wave at point A excited by a source at B is the same as an acoustic wave at point B excited by a source at A. *"If I can hear you, you can hear me."*[4] The theorem is valid under a certain condition. For example, the "wind" effect breaks the theorem. In this section, I try to explain the physical and mathematical background of the reciprocity theorem of the acoustic wave.
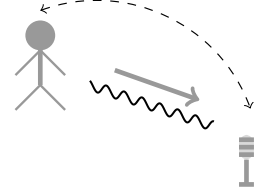
Here we consider an external force $F(\boldsymbol{x}, \omega)$ exerts the system, and it causes pressure perturbation $P(\boldsymbol{x}, \omega)$.

$$\nabla \cdot \frac{\nabla P(\boldsymbol{x}, \omega)}{\rho_0(\boldsymbol{x})} + \frac{\omega^2}{\kappa(\boldsymbol{x})} P(\boldsymbol{x}, \omega) = F(\boldsymbol{x}, \omega) \equiv \mathcal{F}\left[\nabla \cdot \left(\frac{f}{\rho_0}\right)\right]. \qquad (3.63)$$

Then we formally consider a quantity PF like work[note 8].
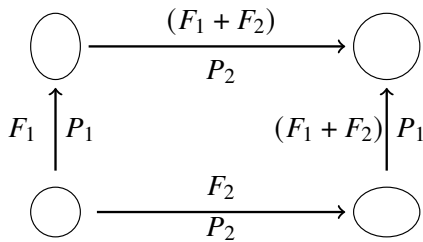
Fig. 3.4 Schematic figure of two different paths of the deformations.

Here we consider a pair of acoustic wave fields (P_1, F_1 and P_2, F_2), which satisfy $P = P_1 + P_2$, $F = F_1 + F_2$ [note 9].

$$\nabla \cdot \frac{\nabla P_1(\boldsymbol{x}, \omega)}{\rho_0(\boldsymbol{x})} + \frac{\omega^2}{\kappa(\boldsymbol{x})} P_1(\boldsymbol{x}, \omega) = F_1(\boldsymbol{x}, \omega), \qquad (3.64)$$

$$\nabla \cdot \frac{\nabla P_2(\boldsymbol{x}, \omega)}{\rho_0(\boldsymbol{x})} + \frac{\omega^2}{\kappa(\boldsymbol{x})} P_2(\boldsymbol{x}, \omega) = F_2(\boldsymbol{x}, \omega). \qquad (3.65)$$

Here we consider two types of virtual deformations: (i) forcing by $F_1 + F_2$ after F_1, (ii) forcing by $F_1 + F_2$ after F_2. Multiple equation 3.64 with P_2, multiply equation 3.65 with P_1, and subtract the resulting expressions. Integration over volume within Σ leads to [note 10]

$$\int_V (P_2 F_1 - P_1 F_2) dV = \int_\Sigma \frac{1}{\rho} (P_2 \nabla P_1 - P_1 \nabla P_2) \cdot \hat{\boldsymbol{n}} d\Sigma. \qquad (3.66)$$

Here we consider a problem under a homogeneous boundary condition (on the boundary Σ, $P = 0$ or $\nabla P = 0$). The left-hand side of equation 3.66 disappears. Green's function for $F_1 = \delta(\boldsymbol{x})$, $F_2 = \delta(\xi)$ exhibits the spatial symmetry as,

$$G(\boldsymbol{x}, \boldsymbol{x}_1, \omega) = G(\boldsymbol{x}_1, \boldsymbol{x}, \omega). \qquad (3.67)$$

[note 8] convolution between P and F in the frequency domain

[note 9] In this case, because we neglect the advection term due to the smaller amplitude, the wavefield can be characterized by pressure perturbation.

[note 10] de Hoop [1988][3] wrote "As far as acoustic wave fields are concerned, Lord Rayleigh is commonly credited as the first to derive a reciprocity theorem; it applies to harmonic sound vibrations in a homogeneous, ideal fluid. (He denotes it as Helmholtz's theorem but gives no reference to Helmholtz.)"

This equation is known as reciprocity, which is not crucial for theoretical consideration but also for numerical applications.

In the case of the Earth, the ground can be approximated by free surface ($p = 0$). I note that Coriolis force owing to Earth's rotation, breaks the reciprocity at very low frequency ($< 10^{-3}$ Hz). When we consider an advection term of the mean flow, such as infrasound propagation within a layer of a westerly jet, the reciprocity is also broken.

†Because the mathematical operations are a bit abstract, you may find it difficult to understand the physical meanings. Here we will try to explore the physical implications a little further. However, you may skip the following, as it anticipates the contents of the later further chapter (9 chapter).

First, the governing equations are abstracted as linear partial differential operators.

$$\mathcal{L} \equiv \nabla \cdot \frac{\nabla}{\rho_0(\boldsymbol{x})}. \tag{3.68}$$

Here we consider arbitrary functions u and v.

The operator $\bar{\mathcal{L}}$ that satisfies

$$\left(\int u^* \mathcal{L} v dV \right)^* = \int u^* \bar{\mathcal{L}} v dV. \tag{3.69}$$

is called the Hermitian conjugate operator with $\mathcal{L}$. If $\mathcal{L}$ satisfies

$$\mathcal{L} = \bar{\mathcal{L}}, \tag{3.70}$$

we call $\mathcal{L}$ the Hermite operator or self adjoint operator [note 11].

The Hermitian operator has two important characteristics[note 12]: (i) the eigenvalues are real, and (ii) the eigenfunctions are orthogonal and form a complete system. Therefore any function can be expanded in terms of eigenfunctions.

Here we consider eigenvalues λ_n and eigenfunctions u_n for an operator $\mathcal{L}$ as:

$$\mathcal{L} u_n = -\frac{\lambda_n}{\kappa(\boldsymbol{x})} u_n. \tag{3.71}$$

Expanding the Green's function in terms of eigenfunctions yields

$$G = \sum_n a_n u_n. \tag{3.72}$$

The insertion of the expansion into the wave equation leads to

$$\sum \left(\frac{\omega^2 - \lambda_n}{\kappa(\boldsymbol{x})} \right) a_n u_n = \delta(\boldsymbol{x} - \boldsymbol{x}_1). \tag{3.73}$$

From the orthonormality of the eigenfunctions:

$$\int \frac{u_n^*(\boldsymbol{x}) u_{n'}(\boldsymbol{x})}{\kappa(\boldsymbol{x})} dV = \delta_{nn'}, \tag{3.74}$$

[note 11] In the case of one-dimensional problems, the equations can be reduced to ordinary differential equations of the Sturm-Liouville type. In the case of horizontally stratified structures, the equation can be rewritten in the Sturm-Liouville form by separating variables. Therefore, the various properties have been studied in detail and are easy to treat.

[note 12] Remember the Hermitian matrix

the coefficients a_n are given by

$$a_n = \frac{u_n(x_1)}{\omega^2 - \lambda_n}.$$ (3.75)

Accordingly, Green's function can be written by

$$G = \sum \frac{u_n(x_1)u_n(x_2)}{\omega^2 - \lambda_n}.$$ (3.76)

From this expression, Green's function satisfies the reciprocity property. This discussion also shows that, generally, when the eigenfunctions can be described as self-adjoint operators, the eigenfunctions satisfy orthogonality and completeness, and therefore, the reciprocity is satisfied. For example, in the case of sound waves with mean wind, when the sound wave propagates upwind or downwind, the travel time changes due to the effect of the mean wind, and thus, the reciprocity is not satisfied. In this case, the governing equations do not satisfy the self-associative property.

Also, the definition of the Hermite operator shows that checking the interaction quantity is checking whether the self-adjoint property is satisfied. When rewritten in matrix form, the Hermitian operator corresponds exactly to the Hermitian matrix, and the various properties become easier to understand [note 13].

Problem 3.11

1. Derive Green's theorem:

$$\int (f\nabla^2 g - g\nabla^2 f)dV = \int (f\nabla g - g\nabla f) \cdot d\Sigma,$$ (3.77)

where f and g are arbitrary scalar functions. Hint : Use $\nabla \cdot (Fu) = F(\nabla \cdot u) + u \cdot \nabla F$, and Gauss's divergence theorem.
2. Using Green's theorem, Derive equation 3.66.

[note 13] For example, the Hermitian matrix corresponds to an orthogonal matrix that is diagonalizable and whose eigenvalues are real numbers

§3.6 Representation theorem: as a natural extension of Huygens's principle

The representation theorem is key for interpreting seismic wave propagation. In this section, I show the theorem is a natural extension of Huygens's principle, which does not predict the wavefront but also the amplitudes. For simplicity, we start a case of an acoustic (scalar) wave equation.

With an assumption that F_1 is 0 within a volume V ($P_1 = P$) and $F_2 = \delta(x - x_1)$, we obtain the equation,

$$P(x_1, \omega) = \int_\Sigma \frac{1}{\rho} (P(x, \omega)\nabla G(x, x_1, \omega) - G(x, x_1, \omega)\nabla P(x, \omega)) \cdot \hat{n}\Sigma. \qquad (3.78)$$

For a better description of the boundary condition, we rewrite pressure gradient by displacement $S(x, \omega)$ as,

$$P(x_1, \omega) = \int_\Sigma \frac{1}{\rho} \{P(x, \omega)\nabla G(x, x_1, \omega) - \rho\omega^2 G(x, x_1, \omega)S(x, \omega)\} \cdot \hat{n}d\Sigma. \qquad (3.79)$$

For a given region surrounded by a boundary Σ, the displacement and the pressure distribution on the surface Σ give us a complete description of the acoustic wavefield within the surface.

To compare Huygens's principle we replace a source at x_1 by receiver at x using the reciprocity as,

$$P(x_1, \omega) = \int_\Sigma \frac{1}{\rho} \{P(x, \omega)\nabla G(x_1, x, \omega) - \rho\omega^2 G(x_1, x, \omega)S(x, \omega)\} \cdot \hat{n}d\Sigma. \qquad (3.80)$$
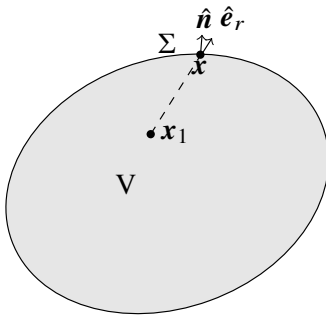
Fig. 3.5   Geometry of the fluid body.

> ### Problem 3.12
>
> To understand the nature of the representation theorem, let us consider a one-dimensional problem for simplicity. As described in the chapter on the Green function, we consider a plate-like region $0 \leq x \leq L$ as the domain of Σ, corresponding to the case where P is the function of only x.
>
> 1. Derive the following form of the representation theorem:
>
> $$P(x_1, \omega) = \left[\frac{P(x, \omega)}{\rho(x)} \left(\frac{\partial}{\partial x} G^{1D}(x_1, x, \omega) \right) - G^{1D}(x_1, x, \omega) \frac{\partial P(x, \omega)}{\partial x} \right]_{x=0}^{L}.$$
> (3.81)
>
> 2. In a case of a homogeneous medium ($\rho(x) = \rho_0$, $k = \omega/\alpha_0$), the 1-D Green's function is given by
>
> $$G^{1D}(x_1, x, \omega) = \frac{\rho_0 i}{2k} e^{-ik|x_1 - x|}.$$
> (3.82)
>
> Here we consider a propagation wave solution $P(x, \omega) = P_0(\omega) e^{-ik|x|}$. Show that the representation theorem holds in this case.
>
> The representation theorem shows that the wave field inside the boundary can be completely reproduced by information on the boundaries describing the wave inward and outward.

For a better understanding of the equation, let us consider a simple situation the Green function $G(r)$ is a function of only r using a spherical coordinate at the origin $\boldsymbol{x}_1$. Because $\nabla G = \partial_r G \hat{\boldsymbol{e}}_r$, $\nabla G = \partial_r G \hat{\boldsymbol{e}}_r$, the equation can be rewritten by,

$$P(\boldsymbol{x}_1, \omega) = \int_\Sigma \left\{ \frac{1}{\rho} P \frac{\partial G(r)}{\partial r} (\hat{\boldsymbol{e}}_r \cdot \hat{\boldsymbol{n}}) - \omega^2 G(r)(S \cdot \hat{\boldsymbol{n}}) \right\} d\Sigma, \qquad (3.83)$$

The first term of the right-hand side corresponds to a dipole source, whereas the second one corresponds to a monopole. The combination of the radiation patterns gives us a prediction of amplitudes of refracted and reflected wave fields. This formulation is known as the Fresnel-Kirchhoff diffraction formula in optics.

If you interpret the representation theorem as an extension of Huygens' principle, you have understood the physical implications. However, a closer look at the formula raises many questions. For example, if the boundary conditions do not satisfy the homogeneous boundary condition in a supposed medium (e.g., if stress and displacement are given at the boundary, as in a speaker), does the condition break the reciprocity of Green's function? This is a typical example. Actually, this problem can be avoided. That is, the wavefield combination we are considering ((F_1, P_1) and (F_2, P_2)): they are same within the region V, but not necessarily outside it.

First, as a simple case, let us consider a spherical region as the region V. Suppose that at the sphere surface, we have a free surface (satisfying the homogeneous boundary condition). In this field, you would think of a Green's function that naturally satisfies the homogeneous boundary condition on the surface of V. However, it is not necessary to choose so, and there is no problem choosing a Green's function in full space (see section 3.3.4), considering the situation where the medium continues infinitely outside the domain as well.

Next, consider the case where the homogeneous boundary condition is broken on the sphere (for example, there is a source on the boundary, such as a speaker in part). In this case, we can still choose an infinite Green's function (also called the fundamental or principal solution), and the reciprocity can be applied without any problem. In other words, the representation theorem can be applied similarly.

We can reconstruct all the seismic wavefields within the Earth's interior from the surface observations if we know Green's function of the medium. Based on the reconstructed seismic wavefield within the Earth, we can infer elastic constant at a given point from the ratio between the spatial gradient of pressure and the time derivative at the point. This is the basic principle of seismic imaging in seismic exploration. However, we must know the seismic structure in advance to calculate Green's function. At a glance, the logic seems to be a circular argument. From a practical point of view, we start "an initial model," then we update it with a modification based on the surface observation and the initial Green's function. Updating the information based on the observed wavefield is essential for exploring Earth's interior using seismic exploration techniques.

§3.7 Reciprocity of elastic medium

The reciprocity of an acoustic medium can be extended to an elastic medium. First, we extend equation 3.66 to that for an elastic medium, known as Betti's theorem. Here I show only the results [note 14)] as,

---

note 14) read Aki and Rechards[1] for details.

Betti's theorem

As in the case of the acoustic wave, we consider two types of wave fields as follows. Let us consider a pair of elastic wave fields: (i) elastic wavefield s_1 excited by forcing f_1 and (ii) elastic wavefield s_2 excited by forcing f_2. Then integrate the inner product between the equation of motions for (i) and s' for (ii), and vice versa.

$$\int_V \left\{ s_1(x,t) \cdot (f_2(x,\tau) - \rho \partial_t^2 s_2) - s_2(x,\tau) \cdot (f_1(x,t) - \rho \partial_t^2 s_1) \right\} dV \qquad (3.84)$$

$$= \int_\Sigma \left\{ [s_2(x,\tau) \cdot T_1(s_1(x,t)) \cdot \hat{n}] - [s_1(x,t) \cdot T_2(s_2(x,\tau)) \cdot \hat{n}] \right\} d\Sigma \qquad (3.85)$$

The derivation requires the following relation,

$$\sum_{ij} E_{ij} T'_{ij} = \sum_{ij} E'_{ij} T_{ij}, \qquad (3.86)$$

according to the symmetry of elastic tensor as $C_{ijkl} = C_{klij}$[note 15].

By time integration of the above equation with the change of variables $\tau = \tau - t$, we get the following relation:

$$\int_{-\infty}^{\infty} dt \int_V [s_1(x,t) \cdot f_2(x,\tau-t) - s_2(x,\tau-t) \cdot f_1(x,t)] dV \qquad (3.87)$$

$$= \int_{-\infty}^{\infty} dt \int_\Sigma \left\{ [s_2(x,\tau-t) \cdot T_1(s_1(x,t)) \cdot \hat{n}] - [s_1(x,t) \cdot T_2(s_2(x,\tau-t)) \cdot \hat{n}] \right\} d\Sigma. \qquad (3.88)$$

Here we use the relation shown in problem 3.11.

Problem 3.13

Show the following relation:

$$\int_{-\infty}^{\infty} \left\{ s_1(x,t) \cdot \partial_t^2 s_2(\tau-t) - s_2(x,\tau) \cdot \partial_t^2 s_1(\tau-t) \right\} dt = 0, \qquad (3.89)$$

for given a finite time τ by partial integration under the following condition $s_1(\infty) = s_1(-\infty)$ and $s_2(\infty) = s_2(-\infty)$.

Reciprocity of Green's function

When we consider homogeneous boundary conditions (on a boundary Σ ⊥, $s = s' = 0$ or $T_n[s)] = T_n[s')] = 0$), the right-hand side vanishes. With the transnational symmetry of Green's function, we obtain reciprocity of elastic Green's function as,

$$G_{lm}(x_2, \tau; x_1, 0) = G_{ml}(x_1, \tau; x_2, 0) \qquad (3.90)$$

$$G_{lm}(x_2, \tau_2; x_1, \tau_1) = G_{ml}(x_1, -\tau_1; x_2, -\tau_2). \qquad (3.91)$$

---

note 15) this relation is based on the independence of elastic energy on deformation paths, as explained in the previous chapter.

§3.8 Representation theorem of an elastic medium

Let us insert $G_{pm}(x,t;\eta,0)$, which represents the p component of displacement for an external force toward mth direction at η into s_2 of **Betti's theorem (equation3.7)**. Now, considering the translational symmetry with respect to time, Fourier transform with respect to τ leads to the following equation

$$s_m(\omega,x) = \int_V f_p(\omega,\eta) \cdot G_{pm}(\omega,\eta,x)dV(\eta)$$
$$+ \int_\Sigma \{G_{pm}(\omega,\eta,x)T_{pq}(u(\omega,\eta))\hat{n}_q - s_p(\omega,\eta)T_{pq}\hat{n}_q(G_p(\omega,x,\eta))\}d\Sigma. \quad (3.92)$$

In this equations To obtain displacement s at x, the above equation evaluates the convolution between Green's function for an impulsive force applied at the observed point x and the distributed sources. The evaluation makes the equation difficult to understand. Assuming that Green's function satisfies a homogeneous boundary condition, reciprocity of Green's function can simplify the formulation [note 16]. With the reciprocity, the representation theorem can be simplified as

$$s_m(\omega,x) = \int_V f_p(\omega,\eta)G_{np}(\omega,x,\eta)dV(\eta)$$
$$+ \int_\Sigma \{G_{np}(\omega,x,\eta)T_p(\eta) - s_p(\eta)C_{pqkl}\partial_l G_{nk}(\omega,x,\eta)\hat{n}_q\}d\Sigma, \quad (3.93)$$

where $\hat{n}$ is normal vector ont the boundary.

$$s_m(\omega,x) = \int_V f_p(\omega,\eta)G_{np}(\omega,x,\eta)dV(\eta)$$
$$+ \int_\Sigma \{G_{np}(\omega,x,\eta)T_p(\eta) - s_p(\eta)C_{pqkl}\partial_l G_{nk}(\omega,x,\eta)\hat{n}_q\}d\Sigma, \quad (3.94)$$

where $\hat{n}$ is a normal vector to Σ.

The Representation Theorem is very important when considering the excitation of seismic waves. The Representation Theorem assures us that cutting out a part of an elastic body has no effect on the motion of the elastic body outside it as long as the displacement and stress conditions at the boundary are known. Consider, for example, the phenomenon of earthquakes, which are caused by brittle fractures in a part of the earth. The area near the fault cannot be represented by an elastic body. However, if we consider the operation of hypothetically replacing the brittle region with an elastic body through it with a closed surface that surrounds it. Then, as long as the stresses and displacements on the boundary are identical to each other, we can completely describe the motion in the elastic body. We will see this in detail in the next chapter.

[note 16] The confusion originates that the boundary conditions for the Green function can be independent of the boundary conditions for the displacement s. This means that the choice of Green's function is arbitrary, which causes confusion. For example, when considering a homogeneous medium but complex boundaries, using the infinite medium Green's function (the fundamental solution) improves the outlook.
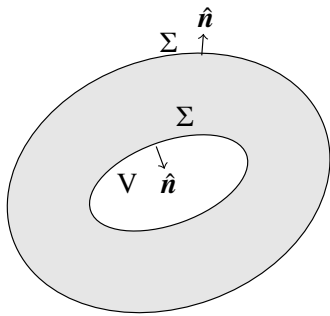
Fig. 3.6 *

§3.A Bessel function

$$\frac{1}{r}\frac{1}{dr}\left(r\frac{dR}{dr}\right)+\left(k^2-\frac{m^2}{r^2}\right)R=0,$$ (3.95)

is a differential equation of Bessel, and the solutions are known as Bessel function of the first kind $J_m(kr)$, and Neumann function $Y_m(kr)$. $J_0(0)=1$, $J_m(0)=0$, $m \neq 0$, whereas Neumann function diverges at $r=0$. Both functions converge to $1/\sqrt{r}$ for $r \to \infty$. Read Mathematical Methods for Physicists[2] for details.
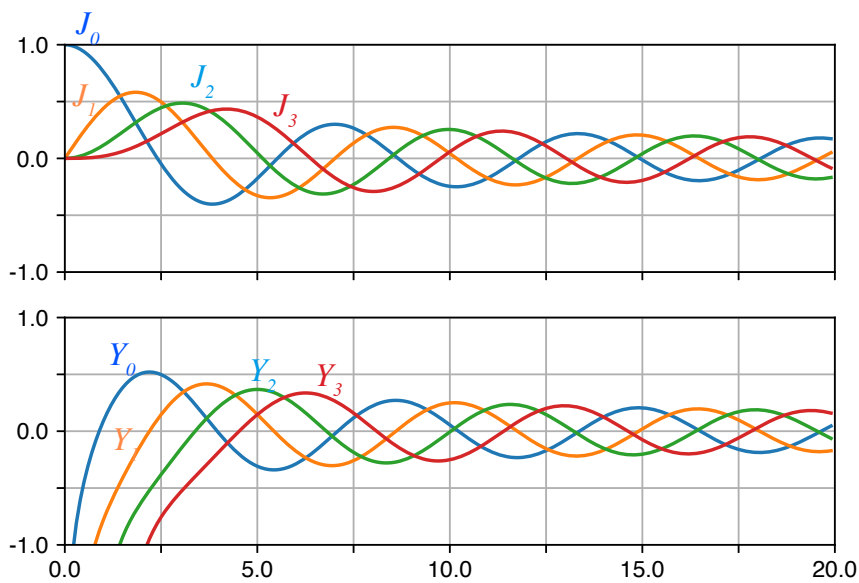
Fig. 3.7   Plots of Bessel functions and Neumann functions.

3.A.1 Properties

$$J_{-m}(x)=(-1)^n J_m(x)$$ (3.96)

$$J_{m-1}(x)+J_{m+1}(x)=\frac{2m}{x}J_m(x)$$ (3.97)

$$J_{m-1}(x)-J_{m+1}(x)=2J'_m(x)$$ (3.98)

3.A.2 Asymptotic for $x \to 0$

$$J_m(x) \sim \frac{1}{m!} \left(\frac{x}{2}\right)^m \tag{3.99}$$

$$Y_0(x) \sim \frac{2}{\pi} \ln \frac{x}{2}, \tag{3.100}$$

$$Y_m(x) \sim -\frac{(m-1)!}{\pi} \left(\frac{2}{x}\right)^m, \, m \geq 0 \tag{3.101}$$

3.A.3 Asymptotic for $kr \gg 1$

$$J_m(kr) \sim \sqrt{\frac{2}{\pi kr}} \cos\left(kr - \frac{2m+1}{4}\pi\right) \tag{3.102}$$

$$Y_m(kr) \sim \sqrt{\frac{2}{\pi kr}} \sin\left(kr - \frac{2m+1}{4}\pi\right) \tag{3.103}$$

$$H_m^{(1)}(kr) \sim \sqrt{\frac{2}{\pi kr}} e^{i\left(kr - \frac{2m+1}{4}\pi\right)} \tag{3.104}$$

Here $H_m^{(2)}(kr) = H_m^{(1)*}(kr)$.

§3.B Fourier transform

For time series $u(t)$, the Fourier transform $\mathcal{F}$ and the inverse Fourier transform $\mathcal{F}^{-1}$ are defined as

---
Definitions of Fourier transform

$$U(f) \equiv \qquad \mathcal{F}(u) = \int_{-\infty}^{\infty} u(t)e^{-i2\pi ft}\,dt, \tag{3.105}$$

$$u(t) = \qquad \mathcal{F}^{-1}(U) \equiv \int_{-\infty}^{\infty} U(f)e^{i2\pi ft}\,df, \tag{3.106}$$

$$\tag{3.107}$$
---

where U represents Fourier components of u.

Summary of Fourier transform

- If $u(t)$ is a real function, $U(f) = U^*(-f)$,
- Parseval's theorem: $\int_{-\infty}^{\infty} u(t)^2 dt = \int_{-\infty}^{\infty} U(f)^2 df$,
- Cross spectrum $C(u, v; f) = \mathcal{F}(\psi) = U^*\tilde{v}$
- Wiener- Khinchin theorem: $p(f) = \mathcal{F}(\phi) = |U|^2$.
---

§3.C Hilbert transform

Hilbert transform of $f(t)$ $\mathcal{H}f(t)$ is difined by

$$\mathcal{H}f(t) = \frac{1}{2\pi} \int_{-\infty}^{\infty} [-i\,sign(\omega)]F(\omega)e^{-i\omega t}\,d\omega. \qquad (3.108)$$

This can be interpreted as phase advance of 90° to the original signal in frequency domain. In time domain, it can be written as,

$$\mathcal{H}f(t) = \frac{1}{\pi}\mathcal{P} \int_{-\infty}^{\infty} \frac{f(\tau)}{\tau - t}\,d\tau. \qquad (3.109)$$

Here $\mathcal{P}\int$ is Cauchy's principle integral

For details. read textbooks of applied mathematics (e.g. Yomogida 2007,[6] Mathematical Methods for Physicists[2]).

§3.4 Bibliography

[1] K. Aki and P.G. Richards. *Quantitative Seismology*. Univ Science Books, 2nd edition, 2009.

[2] G.B. Arfken and H.J. Weber. *Mathematical Methods for Physicists*. Elsevier Science, 2013.

[3] Adrianus T de Hoop. Time‐domain reciprocity theorems for acoustic wave fields in fluids with relaxation. *J. Acoust. Soc. Am.*, Vol. 84, No. 5, pp. 1877–1882, November 1988.

[4] Roel Snieder and Kasper van Wijk. *A Guided Tour of Mathematical Methods for the Physical Sciences*. Cambridge University Press, 3 edition, 2015.

[5] 斎藤正徳. 地震波動論. 東京大学出版会, 2009.

[6] 蓬田清. 演習形式で学ぶ特殊関数・積分変換入門. 共立出版, 2007.

Excitation of seismic wave

Chapter 4

Various phenomena excite seismic waves. For example, fault slips and volcanic eruptions excite them. This chapter explains that these phenomena can be described by "equivalent body force" in a framework of linear elasticity. In other words, we can only guess the force system of the excitation sources from seismological methods. source characteristics inferred by seismology

Although seismological techniques are feasible for characterizing the source, we note that they can provide only information about the "force system". In order to infer physical properties (e.g. fault slip and volumetric change of an explosion source), we must interpret the "equivalent body force" based on a physical model. An inferred physical parameter depends on an assumed physical model. These two steps are essential for a seismic source study.

The following section introduces a concept of "indigenous source" for understanding equivalent body force and then moment tensor.

§4.1 Indigenous source

Without a seismic excitation source, the Earth does not oscillate. An external force at a time excites seismic waves. For example, a meteorite is an external force. In this case, according to the impulse, the momentum of the Earth changes. Mass injection by a volcanic eruption is another example. When we consider such an external force, the total momentum changes according to the impulse by the external force.

The solid Earth can be approximated by a closed system in most situations. A physical process inside the Earth, of course, can also excite seismic waves. An earthquake is a typical example of such a source. Volcanic processes inside the Earth, such as volcanic tremors, are another example. Excitation sources inside the system of the solid Earth are called indigenous sources. The physical processes are thermoelasticity, phase transition, fault slip, movement of fluid, and so on. The total momentum and angular momentum conserve

For the seismic excitation by an "indigenous source" in the source region, Hooke's law should be broken because the Earth keeps the equilibrium otherwise. For example, in a fault zone, the law is broken down. Let us consider a localized volume V. According to the exchange of momentum between V and the other body, "indigenous sources" can be

categorized into two.

The first case is that the exchange of the momentum and angular momentum between V and the other can be negligible. A fault motion is such an example. In this case, the momentum and angular momentum in the other region conserve in all instances.

The second case is that the momentum and angular momentum exchange with each other. Let us consider a landslide, which can be approximated by a sliding rigid block on a slope. In this case, the momentum at the beginning and the end is zero, but nonzero in between. Because the total momentum in the whole system (e.g. the whole Earth) conserves, the momentum of the other region ($\notin V$) is nonzero. In other words, the block imposes the impulse [note 1].

These features are crucial for characterizing "equivalent body force" in the following sections.

§4.2 Equivalent body force and Stress glut

Let us consider an earthquake as a typical example of an indigenous source. An earthquake can be described as a fault dislocation physically. Because the dislocation cannot be described by a theory of elasticity (breakdown of Hooke's law), here we consider a closed surface, which includes the fault plain. Governing equations other than Hooke's law should be satisfied exactly[note 2]. An elastic medium out of the surface Σ can be described by a framework of elasticity.
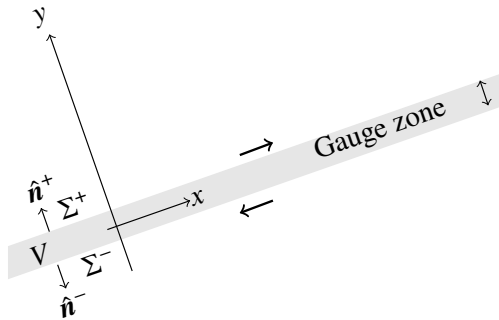
Fig. 4.1   Schematic figure of a right-lateral vertical strike-slip fault.

Representation theorem guarantees that stress and displacement on Σ without the information inside the volume V describe the elastic deformation outside the V. Here we consider an embedded transformation that a virtual elastic body is filled inside Σ. Below we show that the breakdown of Hooke's law can be represented by "equivalent body force", which exerts the virtual elastic body.

Let us consider the deformation associated with the earthquake inside the volume. An earthquake can be described as fault dislocation physically. Inside the volume V (gouge layer), brittle failure occurs, and then Hooke's law is broken down[note 3].

---

note 1) See Takei and Kumazawa [1994, 1995][11], [12] for details.
note 2) See Dahlen and Tromp 1998[2] for details.
note 3) gouge is Fault gouge is minerals formed by brittle failure with a very small grain size in a rock.

The true stress is written by T_{true}.
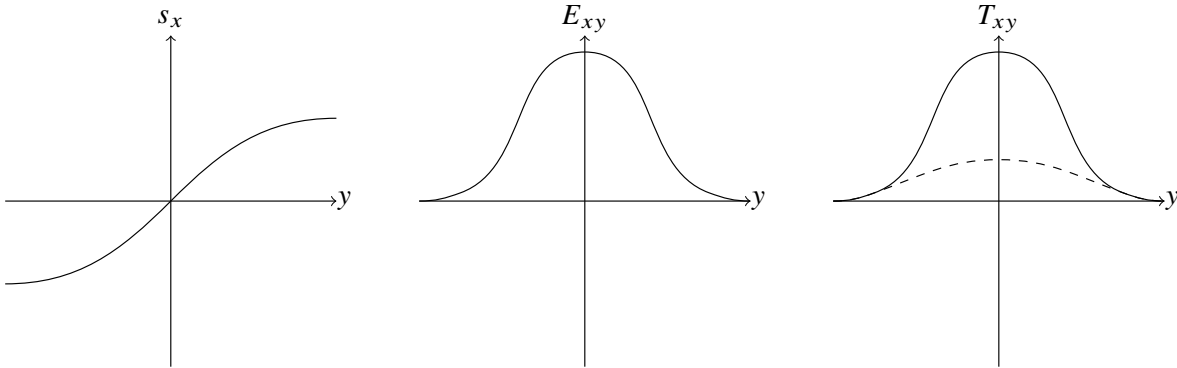
Fig. 4.2 Schematic figure of the displacement, strain and stress.

Then let us consider modeled stress T_{model} assuming Hooke's law for the deformation. As shown in Figure 4.2, the modeled stress is larger than the true stress.

Stress glut Γ is defined by $\Gamma = T_{\text{model}} - T_{\text{true}}$. Note that $\Gamma = 0$ on Σ.

Seismic waves excited by an earthquake can be described by excitation by stress glut[1] in the elastic medium. In a framework of elasticity with stress glut, we can calculate the seismic wave propagations. $-\partial_j \Gamma_{ij}$ is equivalent body force. This result guarantees that we can describe the excitation problem completely in a framework of linear elasticity.

Because this system is closed, the net force of the equivalent body force and the net torque are 0. Based on mathematical consideration, the "equivalent body force" of the fault dislocation in a small spatial dimension can be described by a point double couple source.
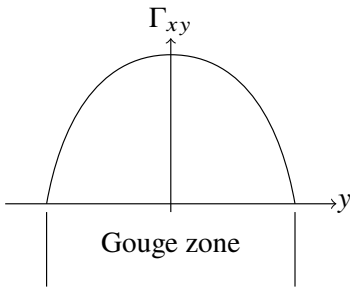
Fig. 4.3 Schematic figure of the stress glut.

When we want to know source characteristics by observations of seismic wave propagations, **we can know only "equivalent force system" of the excitation sources**. There are many possible physical mechanism for the force system. With the help of other independent knowledge, we can infer the the mechanism of the sources.

§4.3 Multipole expansion
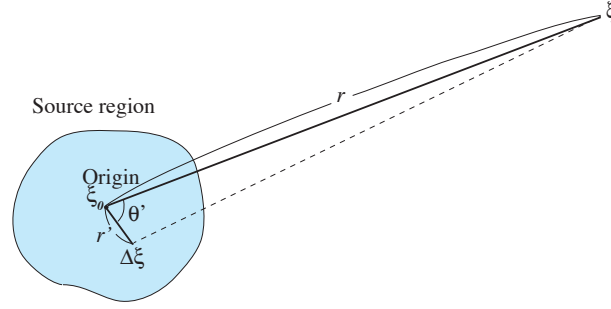
Fig. 4.4   Schematic figure of the source-receiver geometry.

Equivalent body force can be defined by stress glut $\mathbf{\Gamma}$ as,

$$\mathbf{f} = -\nabla \cdot \mathbf{\Gamma}(\mathbf{x}, t). \qquad (4.1)$$

Displacement $\mathbf{S}$ excited by equivalent body force can be given by convolution between the corresponding Green's functions and the equivalent body force as

$$\mathbf{S}(\mathbf{x}, \omega) = \int_V \mathbf{G}(\mathbf{x}, \mathbf{\xi}, \omega) \mathbf{f}(\mathbf{\xi}, \omega) dV(\xi). \qquad (4.2)$$

Let us expand Green's function at around $\mathbf{\xi}_0$ with respect to $\Delta\mathbf{\xi}$. An amplitude of the nth spatial derivative of the Green's function G can be estimated to be $k^n G$ with a typical wavenumber k of the Green's function. Therefore the nth order term of the Tayler expansion can be estimated by

$$\frac{1}{n!}k^n G \Delta\xi^n = \frac{1}{n!}G(k\Delta\xi)^n. \qquad (4.3)$$

When $k\Delta\xi$ is enough small: a typical spatial scale of volume Σ is smaller than the wavelength of the seismic wave (Figure 4.4), the expansion converges. Here we expand the Green's function up to degree 2 with respect to $\Delta\mathbf{\xi}$ as,

$$\mathbf{G}(\mathbf{x}, \mathbf{\xi}, \omega) \approx \mathbf{G}(\mathbf{x}, \mathbf{\xi}_0, \omega) + \nabla_\xi \mathbf{G}(\mathbf{x}, \mathbf{\xi}_0, \omega)\Delta\mathbf{\xi} + \frac{1}{2}\Delta\mathbf{\xi}^T \mathcal{H}_\xi \mathbf{G}(\mathbf{x}, \mathbf{\xi}_0, \omega)\Delta\mathbf{\xi} + O(\Delta\mathbf{\xi}^3). \qquad (4.4)$$

The insertion into equation 4.2 leads to

$$S_i(\mathbf{x}, \omega) \approx G_{ij}(\mathbf{x}, \mathbf{\xi}, \omega) \int_V f_j(\mathbf{\xi}, \omega) dV(\xi) \qquad (4.5)$$

$$+ \partial_k G_{ij}(\mathbf{x}, \mathbf{\xi}_0, \omega) \int_V f_j \Delta\xi_k dV(\mathbf{\xi})$$

$$+ \partial_k \partial_l G_{ij}(\mathbf{x}, \mathbf{\xi}_0, \omega) \int_V f_j \Delta\xi_k \Delta\xi_l dV(\mathbf{\xi}).$$

The first term represents the impulse, whereas the second term does the torque. When we can neglect the exchange of momentum and angular momentum between the volume Σ and the other region, these two terms vanish exactly. The terms with an order higher than 3 have

significant value. Because the field term of 3D Green's function in an infinite homogeneous medium is proportional to r^{-1}, nth order term attenuates with distance as r^{-n-1}. Therefore higher-order term tends to attenuate more rapidly. As the result, 3rd order term known as "moment tensor" becomes dominant.

For simplicity, let us consider an excitation of a 3D acoustic wave in an infinite homogeneous medium. The excitation source is assumed to be localized at around $\boldsymbol{x}_0$

$$\frac{1}{|\boldsymbol{\xi} - \boldsymbol{\xi}'|} = \frac{1}{r} \sum_{l=0}^{\infty} \left(\frac{r'}{r}\right)^l P_l(\cos \theta'). \tag{4.6}$$

Here we assume again that the source dimension is smaller than the wavelength of the acoustic wave.

When we can neglect the exchange of momentum and angular momentum between the volume Σ and the other region, these impulse and torque terms vanish exactly. The next section explains the details of the third term: moment tensor.

§4.4 Excitation by moment tensor

When the spatial scale of the source is enough smaller than the wavelength, the stress glut can be written by

$$\Gamma_{ij}(\boldsymbol{x}, t) = M_{ij}(t)\delta(\boldsymbol{x} - \boldsymbol{x}_0). \tag{4.7}$$

Here $\boldsymbol{M}$ is moment tensor. The trace of M_{ij} shows the volumetric change. When a normal earthquake, two eigenvalues are much larger than the other (double coupled force)[note 4].

At low frequencies, the moment tensor of an earthquake can be simplified as,

$$\Gamma_{ij} = \sqrt{2}M_0\hat{\boldsymbol{M}}\delta(\boldsymbol{x} - \boldsymbol{x}_0)m(t), \tag{4.8}$$

where M_0 is seismic moment, and $m(t)$ is an increasing function with the normalization of $\int m(t)dt = 1$. Here we assume that the moment function is synchronous.

At a distant station from a seismic source, displacement of body wave (U) in an infinite the homogeneous elastic medium can be written by

$$U \sim \frac{1}{r}M_0\dot{m}_0(t)(t - r/c), \tag{4.9}$$

where r is the distance between the station and the source. This means that displacement of teleseismic body wave gives us the shape of the moment rate function $M_0\dot{m}_0$.

[note 4] For example, an explosion source can be represented by a moment tensor. See Julian et al. [1998] for a generalized case of non-double coupled components[4]
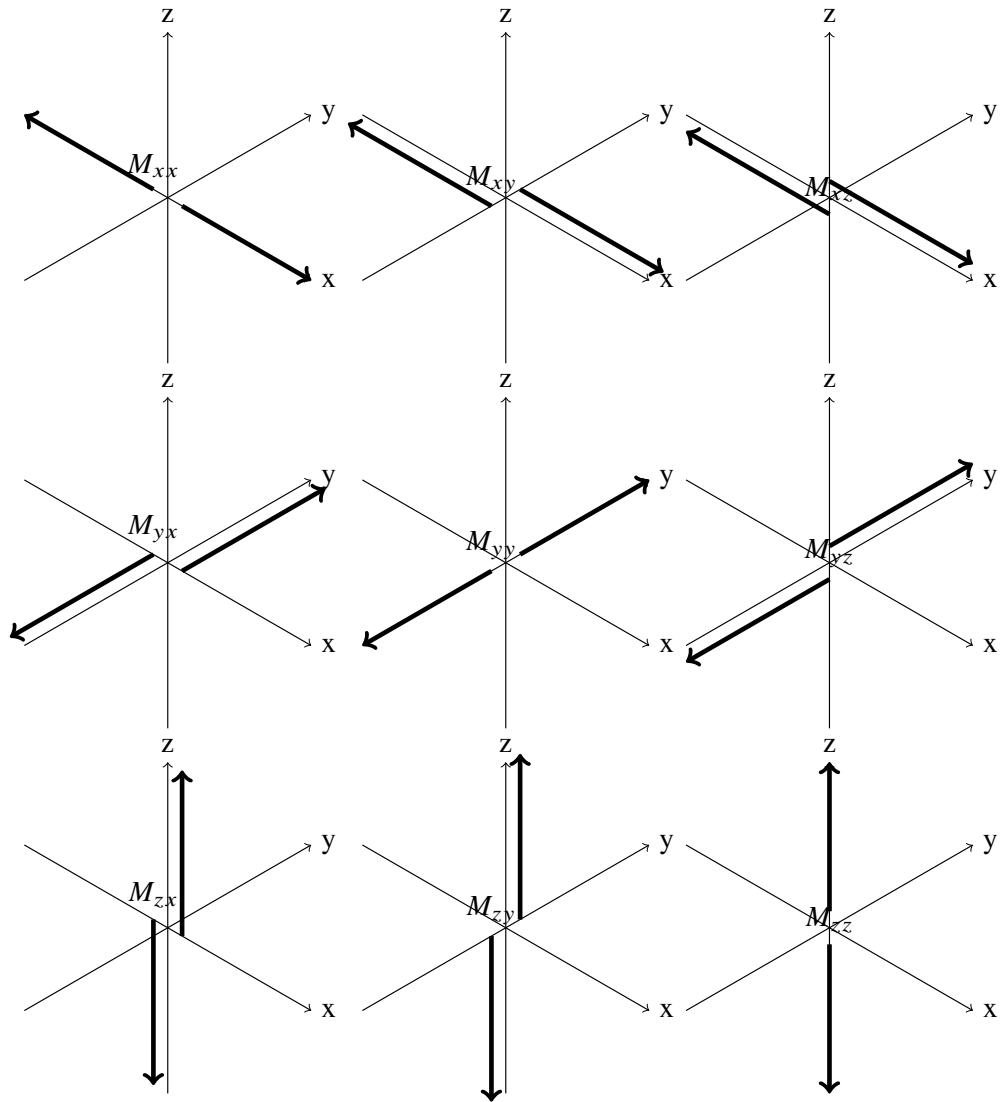
Fig. 4.5   Components of moment tensor

Problem 4.1

1. In subsection 3.4.2 we consider an explosion source. In this case, the source mechanisms can be represented by a moment tensor. When Δr is enough small, derive the corresponding moment tensor.

2. When moment tensor has only one non-zero value ($M_{xx} = 1$), show the P-wave radiation pattern .

3. For double couple source ($M_{xx} = 1, M_{yy} = -1$, and other components are zero), derive the P-wave radiation pattern (Figure 4.6).
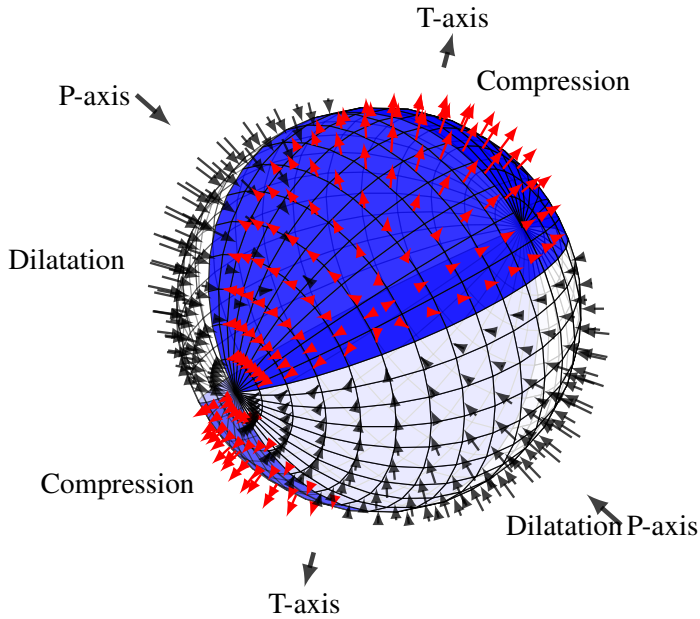
Seismic focal mechanism and Pression-Tension axis.

Fig. 4.6   P wave radiation pattern for a double couple source. Taken from Cyril Langlois (2010)/ CC BY 2.5.

§4.5 Work by Moment tensor

   In this section, we will consider the work that moment tensors act on elastic bodies. First, consider the stress glut $\mathbf{\Gamma}$ and the corresponding equivalent volume force $\mathbf{f}$.

$$f = -\nabla \cdot \mathbf{\Gamma}(\mathbf{x}, t). \tag{4.10}$$

is applied to the elastic body. If the displacement of the elastic body is $\mathbf{s}$, the work W done by the equivalent volume force on the elastic body is written by

$$W = \int_V \mathbf{f} \cdot \mathbf{s}\, dV. \tag{4.11}$$

With partial integrals (Problem 4.2), the above equation can be rewritten by

$$W = \int_V \mathbf{f} \cdot \mathbf{s}\, dV = \sum_{ij} \int_V E_{ij} \Gamma_{ij}\, dV. \tag{4.12}$$

Here we assumed that the stress glut is 0 on the surface σ of the elastic body When stress glut can be represented by a moment tensor as equation (4.7), the equation can be simplified as

$$W = \sum_{ij} E_{ij} M_{ij}(t). \tag{4.13}$$

Thus, the work is given by the production between strain E_{ij} caused by the earthquake and moment tensor M_{ij}. Based on the conservation of energy, work done by the stress glut Γ is transferred to kinematic energy and elastic energy.

> ### Problem 4. 2
>
> Derive equation (4.12) assuming the following conditions:
>
> - Consider an elastic body within a volume V, stress glut Γ exists only inside Σ.
> - On Σ, stress glut $\Gamma_{ij} = 0$.
> - Assuming that the elastic body is an isolated system, imposed torque is 0 as $\Gamma_{ij} = \Gamma_{ji}$.
> - Use partial integrals and Gaussian divergence theorem.

§4.6 Effects of free surface on the seismic excitations

In this section, let's consider how free surfaces affect the excitations of seismic waves.[13] In conclusion, we obtain the strange result that M_{xz}, M_{yz} does not excite seismic waves by shallow earthquakes.

For simplicity, we consider a semi-infinite medium. If $z = 0$ is the ground surface now, the free boundary surface condition is $T_{xz} = T_{yz} = T_{zz} = 0$ at $z = 0$. and $T_{xz} = T_{yz} = T_{zz} = 0$. Rewriting these first two conditions in terms of distortion, we get

$$E_{xz}|_{z=0} = \left.\frac{T_{xz}}{\mu}\right|_{z=0} = 0 \quad E_{yz}|_{z=0} = \left.\frac{T_{yz}}{\mu}\right|_{z=0} = 0 \tag{4.14}$$

We have shown that the work W done by the moment tensor can be written as $\sum_{ij} E_{ij}T_{ij}$. Since $E_{xz} = E_{yz} = 0$ at $z = 0$, the components M_{xz} and M_{yz} of the corresponding moment tensor M_{xz} and M_{yz} do not contribute to the excitation. This means that M_{xz} and M_{yz} cannot excite seismic waves near the free surface (sufficiently shallow in depth compared to the wavelength). What happens in relation to actual phenomena?

For example, in shallow earthquakes near the trench, if the subduction angle is gentle, a low-angle reverse fault earthquake occurs. In such cases, M_{xz} and M_{yz} components do not excite seismic waves very much, and it is known that it is difficult to determine these components from seismic wave data. This is a serious problem, especially when estimating moment tensors for long-period seismic waves. When determining the moment of an earthquake on a shallow low-angle reverse fault, there is a trade-off with the tilt angle of the fault, which leads to large uncertainties in the moment estimate.

§4.7 Single force source

When the source region (non-elastic part) is enough large, we cannot neglect the exchange of momentum between them. The single force term represents the impulse owing to the exchange. This term becomes important when a landslide excites seismic waves (Figure 4.7). Of course, the total momentum of the system is conservative.

Examples of source processes represented by a single force are (i) glacial earthquake and (ii) microseisms excited by ocean swell. In both cases, we cannot neglect the source volume.

$$\int M|v(t)|dt \qquad \text{Momentum } Mv(t) = -\int f^e(t)dt$$

Landslide
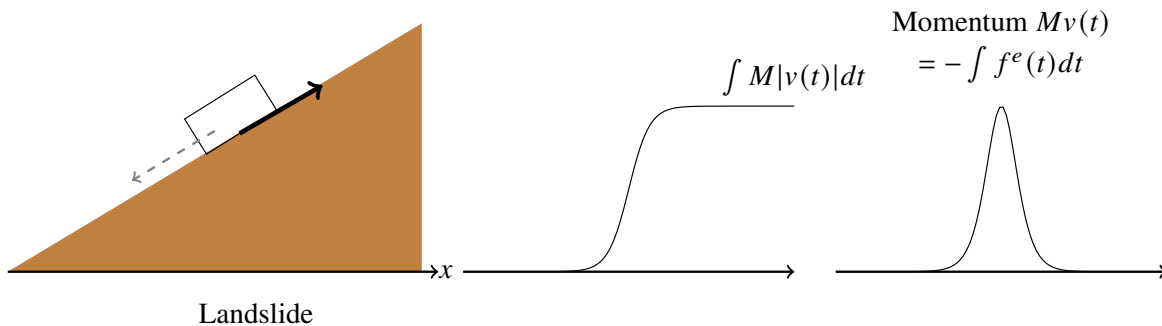
Fig. 4.7   Schematic figure of the single force.[5]

4.7.1 Origin of ambient noise: ocean swell shakes the Earth

Even on seismically quiet days, the Earth oscillates persistently. At frequencies higher than 1 Hz, human activities cause a background seismic wavefield. At a frequency lower than 1 Hz, the contribution becomes smaller. The human activity is not enough energetic to excite it because the wavelength of the seismic wave becomes an order of km. At this frequency, ocean swell activities are more energetic, and they excite seismic surface waves (Rayleigh wave and Love wave) persistently. This phenomenon is known as ambient noise or microseisms.

Figure 4.8 shows two peaks at around 0.1 Hz and 0.2 Hz. Ambient

Fig. 4.8   Probability density of power spectrum of horizontal acceleration at a Hi-net station in Japan.[9] A reddish color means more probable. The thick red line represents the power spectral densities of ambient noise.

noise at the lower peak is called primary microseisms, whereas the other one is called secondary microseisms. The frequency of primary microseisms corresponds to that of ocean swells, whereas that of secondary microseisms corresponds to double the frequency. Against our instinct, amplitudes of secondary microseisms are larger than primary microseisms be-

cause the nonlinear effect of the ocean, known as the Longuet-Higgins mechanism (Longuet-Higgins), is dominant. The amplitudes of secondary microseisms are several orders of magnitudes larger than those of primary microseisms. Even at a continental station distant from a coastal area, these microseisms are observed because of the large amplitudes.

A ripple pattern by raindrops is analogous to those of microseisms. Please run an application at the website. An impulsive force at a point generates an outgoing concentric wave. On the other hand, we can trace wavefront generated by many random sources at first. Gradually inside the circle, the wave field becomes quite random. We cannot identify any specific direction.

Here we pick up a typical example of microseisms when a typhoon because the high ocean swell activities excite the larger amplitudes of microseisms in the area of the center of the typhoon. Figure 4.9 shows running spectrum[note 5)] at a station (Minami Daito) when typhoon Songda in 2004 hit the Japan island. The typhoon became weaker

Fig. 4.9 Left: Running spectrum from Sept. 7th to Sept. 8th in 2004. The vertical axis shows frequency, and the horizontal one shows time. Right: Track information about the typhoon. The red line shows the track. The thick red line corresponds to the time period of the running spectrum.

with time in this time. With time increasing, the peak frequency becomes higher. We can also identify a vertical line at around 3:00 on 9/7, which corresponds to a teleseismic earthquake. In this case, the teleseismic earthquake was masked by the microseisms in this frequency. Thus, microseisms are major noise for earthquake observations, as noted before.

4.7.2 The excitation mechanism of secondary microseisms: Longuet-Higgins mechanism

In this section, I explain the excitation mechanism of secondary microseisms, also known as Longuet-Higgins mechnism[7)][note 6)]. Because the math of the theory is complicated, I introduce a simplified model by Longuet-Higgins[note 7)].

Let us consider an analogy by a pendulum proposed by Longuet-Higgins [1953][8)] (Figure 4.10 right). The left panels show a standing wave with vertical motions, which does not propagate toward a specific direction. Therefore, the center of mass of (a) and (c) is higher than that of (b) and (d). To cause the periodic vertical oscillations of the center, a periodic external force with frequency 2ω is required. A pendulum depicted by the right panels could be a good analogy. The location of the weight of the pendulum represents the center of the mass, force at the pivot point represents pressure on the bottom, and displacement of the pendulum represents the displacement of the center. Displacement of the pendulum corresponds to the movement of water (see streamline of Figure 4.10 (e)). The period of forcing at the pivot point is estimated to be 2ω, which leads to pressure on the bottom with frequency 2ω. The amplitude of the forcing can be estimated by $m(d\omega)^2/R$, where m is the mass, d is the displacement, R is length of the leg, and ω is angler frequency of the pendulum. Thus, pressure fluctuations, which correspond to the forcing at the pivot point, should be proportional to the power of the amplitudes of ocean swell (nonlinear).

Next, let us consider a propagating wave without dispersion. Because the wave keeps its shape with the propagation, no vertical movement of the center of the mass occurs. This means that the ocean wave cannot excite pressure fluctuations on the bottom. Because the

---

note 5) A running spectrum shows the time evolution of frequency spectra. We calculate the power spectra of sliding windows and align the spectra with respect to time

note 6) Longuet-Higgins is an applied mathematician and physical oceanographer. In particular, he is a pioneer in the statistics of ocean waves. Unfortunately, he passed away in 2016.

note 7) Read Longuet-Higgins (1950),[7)] Hasselemann (1963),[3)] Kedar et al. (2008)[6)] for details.

(a) $t=0$
$\zeta=\zeta_0 \cos kx \cos \omega t$
Center of mass
The pivot point

(b) $t=T/4$
Bottom pressure
Force

(c) $t=T/2$

(d) $t=3T/4$

(e)
Displacement
Pressure
$\frac{\rho(\zeta_0 \omega)^2}{2}$
Displacement
Pressure change
$-\frac{\rho(\zeta_0 \omega)^2}{2}$
Time
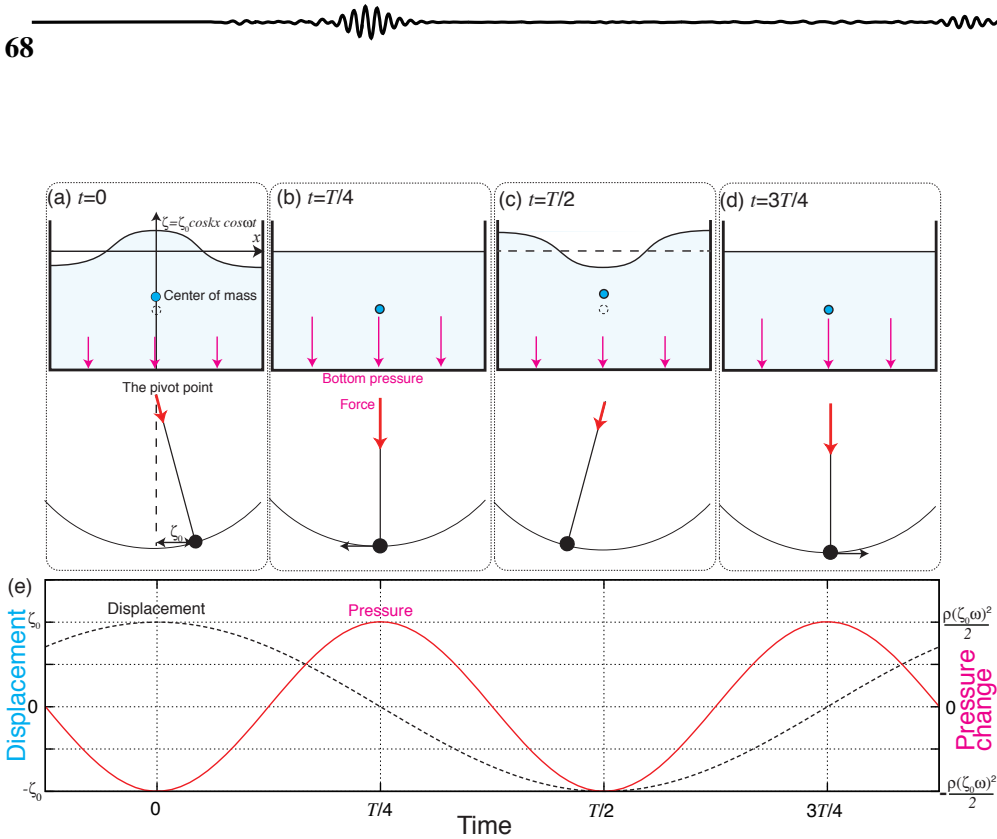
Fig. 4.10　Upper: a schematic model and the analogy of a pendulum (a-d). Here we consider a standing wave. Taken from Nishida (2017).[10]

Longeut-Higgins mechanism is not efficient for a propagating wave, this mechanism requires two waves with an opposite direction pair at least. The extent of ocean swell activities and the coastal reflection is crucial for realizing random propagations of the ocean swell. Now we have a good stochastic wave action model, a theory that can predict observed secondary microseisms well (e.g. Kedar *et al.* (2008),[6]

§4.8 Bibliography

[1] George Backus and Marjorie Mulcahy. Moment tensors and other phenomenological Discontinuous descriptions of seismic sources - I. displacements. *Geophys. J. R. Astron. Soc.*, Vol. 46, No. 2, pp. 341–361, 1976.

[2] F.A. Dahlen and J. Tromp. *Theoretical Global Seismology*. Princeton University Press, Princeton, 1998.

[3] K. Hasselmann. A statistical analysis of the generation of miceoseisms. *Rev. Geophys.*, Vol. 1, pp. 177–210, 1963.

[4] Bruce R. Julian, Angus D. Miller, and G. R. Foulger. Non-double-couple earthquakes 1. Theory. *Rev. Geophys.*, Vol. 36, No. 4, p. 525, 1998.

[5] Hitoshi Kawakatsu. Centroid single force inversion of seismic waves generated by landslides. *J. Geophys. Res.*, Vol. 94, No. B9, p. 12363, 1989.

[6] S. Kedar, M. Longuet-Higgins, F. Webb, N. Graham, R. Clayton, and C. Jones. The origin of deep ocean microseisms in the northern atlantic ocean. *Proc. R. Soc. A*, Vol. 464, pp. 777–793, 2008.

[7] M. Longuet-Higgens. A theory of the origin of microseisms. *Phil. Trans. of the Roy. Soc. of London*, Vol. 243, pp. 1–35, 1950.

[8] M. S. Longuet-Higgins. Can sea waves cause microseisms? *Proc. Symposium on Microseisms, Harriman 1952*, No. 306, pp. 74–93, 1953.

[9] K Nishida, H Kawakatsu, and K Obara. Three-dimensional crustal S wave velocity structure in japan using microseismic data recorded by hi-net tiltmeters. *J. Geophys. Res.*, Vol. 113, No. B10, p. B10302, October 2008.

[10] Kiwamu Nishida. Ambient seismic wave field. *Proc. Jpn. Acad. Ser. B Phys. Biol. Sci.*, Vol. 93, No. 7, pp. 423–448, 2017.

[11] Yasuko Takei and Mineo Kumazawa. Why have the single force and torque been excluded from seismic source models? *Geophys. J. Int.*, Vol. 118, No. 1, pp. 20–30, jul 1994.

[12] Yasuko Takei and Mineo Kumazawa. Phenomenological representation and kinematics of general seismic sources including the seismic vector modes. *Geophys. J. Int.*, Vol. 121, No. 3, pp. 641–662, jun 1995.

[13] 川勝均. 地震の大きさと多様性. 地震 第 2 輯, Vol. 44, No. Supplement, pp. 265–277, 1991.

Elastic wave propagation in a half space

Chapter 5

The previous chapter explained Green's function in an infinite medium. However, the structure of the real Earth is not so simple. The lateral heterogeneity causes the complexity of seismic wave propagations. This figure shows SH wave propagations from an earthquake. At frequencies lower than several Hz, a stratified Earth's structure (a seismic wave velocity structure depending only on depth) is a good approximation. Even the simple Earth's structure still shows complexities, but we can trace the wavefront. The figure shows the waves can be approximated by plane waves.

In this figure, we can see reflections and conversions on the discontinuities (at the surface, 410 km, 660 km, and core-mantle boundary (CMB)). Because the free surface is the biggest boundary, we introduce the free surface first in this chapter.

First, I introduce the concept of a plane wave, then I will show we can separate the wavefield into P-SV and SH waves according to the wave type and the polarization direction. This chapter describes the effects of a free surface: the reflection and the P-S conversion at a free surface.

§5.1 Review of seismic wave propagation: body waves and surface and boundary waves

Nature is full of waves. For example, if we look at the water's surface, we can see ripples spreading as the wind blows. When some restoring force acts on the medium, they propagate at a certain speed while maintaining their shape ($f(x - ct)$ (x is position, c is propagation speed, t is time)). Let us consider sound waves specifically.

1. Gas moves and density changes
2. Density change produces pressure change
3. pressure gradient moves gas

Sound waves propagate by repeating this cycle. Seismic waves propagate in solids in a similar cycle (see the next chapter for details). If the wave's amplitude is sufficiently small, it is linear, and the principle of superposition holds. In other words, if the wave of interest can be taken out and understood, the whole can simply be understood as a superposition of the waves.

§5.2 Plane wave

To be revised Elastic wave propagation becomes more complex than a homogeneous infinite medium when considering free surfaces. For example, when trying to evaluate the Green function for half-space with a free surface, it can only be expressed analytically in limited cases, such as when the source is located on the ground surface (e.g., chapter 5.7). Even in the case of the Green function for a homogeneous infinite elastic medium, the analytical form of the near-field term becomes complex. When considering Green's function for the infinite medium, the near-field term changes shape depending on the distance from the epicenter, while the far-field term remains the shape. On the other hand, the far-field term propagates with keeping its shape[note 1]. Therefore, this chapter will focus only on the far-field term.

Let us first consider the 3-dimensional scalar case for simplicity. Consider the case of an external force $\delta(x)$ acting at the epicenter. As we learned previously, the Green function, in this case, is given [note 2] by

$$G^\phi(r, \omega) = -\frac{1}{4\pi\kappa}\frac{e^{-ikr}}{r}. \tag{5.1}$$

We can define an isosurface where the phase of e^{-ikr} is constant and is generally referred to as a "wavefront." The trajectory orthogonal to the wavefront is called the ray (see Chapter **??** for details). In regions where r is sufficiently distant, the wavefront curvature can be neglected.[note 3]. The wave can be treated as a plane wave in the region e^{-ikr}, where e^{-ikr} is the radius of curvature.

Let us go back to the wave equation for once: the Green function G^ϕ in the frequency domain satisfies

$$-rho_0\omega^2 G^\phi - \kappa\nabla^2 G^\phi = -\delta(x). \tag{5.2}$$

The Fourier transform in the space, and Fourier inverse transform again gives

$$G^\phi = -\frac{1}{\kappa}\iiint \frac{\alpha^2 e^{i(k_x x + k_y y + k_z z)}}{\alpha^2(k_x^2 + k_y^2 + k_z^2) - \omega^2}dk_x dk_y dk_z \tag{5.3}$$

We can write that this equation shows that the Green function can be represented by a superposition of plane waves.

[note 1] As explained in the section of Ray Theory, the far-field term keeps its shape when the typical spatial scale of the velocity structure is longer than the wavelength of interest.

[note 2] In the 2-dimensional case as well as in the 3-dimensional case, the far-field of the Green function can be approximated as e^{-ikr} **??**.

[note 3] More exact conditions are required for the approximation of plane waves: (i) the curvature of the wavefront can be neglected when focusing on wave propagation on spatial scales sufficiently short compared to the radius of curvature of the wavefront. (ii) Near the epicenter, the radius of curvature becomes so small that a plane wave cannot approximate it. From a simple estimation, it can be seen that the wave can be treated as a plane wave in the region of approximately $r > 1/k$

When considering the Green's function of a semi-infinite medium, if we understand the behavior of the "element" $e^{-i\boldsymbol{k}\cdot\boldsymbol{x}}$ at the free boundary surface, we can understand the overall behavior by superposition (inverse Fourier transform in the frequency domain). In other words, understanding the behavior of the plane wave, $e^{-i\boldsymbol{k}\cdot\boldsymbol{x}}$ on the free surface is the key to understanding elastic wave propagation in a semi-infinite medium.
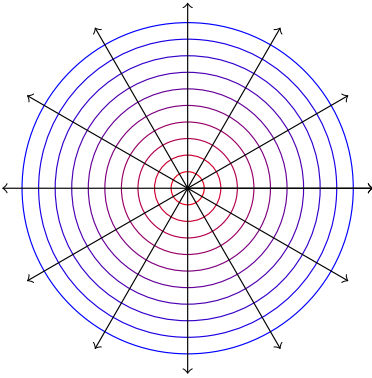
Fig. 5.1   Wavefront and ray for Green's function for a 3-D in an infinite medium.

--- Summary of plane wave ---

When the source is enough far away from the source, the curvature of the wavefront becomes small. In this case, the waveform can be approximated by a plane wave:

1. Plane wave is preserving its shape,
2. Plane wave has a plane wavefront,
3. Plane wave propagates perpendicular to the wavefront[a].

In this case, the scalar variable $\phi(t - \boldsymbol{p} \cdot \boldsymbol{x})$ can be represented as a function of $t - \boldsymbol{k} \cdot \boldsymbol{x}$. $\boldsymbol{p}$ is quantity called as slowness defined as $\boldsymbol{p} = \boldsymbol{k}/\alpha$ (acoustic wave).

---

[a] Exactly speaking, here we neglect the dispersion for simplicity.

Here we consider a propagating wave into the x axis ($p_y = 0$). When $p_x > 1/\alpha$, p_z has real value. Then it propagates into the z direction (plane wave). with P-wave speed α along the slowness vector. On the ground ($z = 0$), at $t = 0$ the wavefront is at the point of $x = z = 0$. At $t = \tau$ it is at the point of $(\tau/p_x, 0, \tau/p_z)$. When we observed the waveform on the ground using seismometers, it propagates in the x direction with "apparent velocity" with $1/p_x$. Thus we can estimate the horizontal apparent velocity from the surface seismic observations.

5.2.1 Plane wave in an elastic medium

Next, Let us consider an elastic wave with a sinusoidal shape at angular frequency ω[note 4)], and slowness vector p. Elastic potential ϕ and ψ can be written by [note 5)]

$$\phi = A_\alpha e^{i(k_\alpha \cdot x - \omega t)} = A_\alpha e^{i\omega(p_\alpha \cdot x - t)} \qquad (5.4)$$

$$\psi = A_\beta e^{i(k_\beta \cdot x - \omega t)} = A_\beta e^{i\omega(p_\beta \cdot x - t)}. \qquad (5.5)$$

The corresponding displacement is given by,

$$s_\alpha(x, t) = A_\alpha k_\alpha e^{i(k_\alpha \cdot x - \omega t)} = \omega A_\alpha p_\alpha e^{i\omega(p_\alpha \cdot x - t)} \qquad (5.6)$$

$$s_\beta(x, t) = k_\beta \times A_\beta e^{i(k_\beta \cdot x - \omega t)} = p_\beta \times A_\beta \omega e^{i\omega(p_\beta \cdot x - t)}. \qquad (5.7)$$

The polarization vector of the P wave is parallel to the propagation direction p_α, whereas that of the S wave is perpendicular with an ambiguity of the direction.

p is called as **Slowness** defined by $p = k/\omega$. The dimension is inverse of speed and is parallel to the propagation direction. For example, the squared norm can be written by

$$p_x^2 + p_y^2 + p_z^2 = \frac{1}{\alpha^2}. \qquad (5.8)$$

Inverse Fourier transform of $e^{i\omega(p \cdot x - t)}$ gives us formula of general waveform. A waveform of P wave propagates with keeping the shape as $s_\alpha(x, t) = p_\alpha f(t - p_\alpha \cdot x)$, whereas that of S wave propagate as $s_\beta(x, t) = p_\beta \times A_\beta f(t - p_\beta \cdot x)$.

5.2.2 Body wave and inhomogeneous wave

When $p^2 > 1/\alpha^2$, p_z becomes imaginary. Using an definition of $p_z = \xi i$, the corresponding potential is given by

$$\phi = A_\alpha e^{i\omega(p_x x - \omega t)} e^{-\xi z}. \qquad (5.9)$$

This equation shows that it decreases exponentially in the z direction. The wave is called an inhomogeneous wave[note 6)] In an infinite medium, it diverges at infinity, it is a trivial solution physically. However, when boundaries exist, it is possible to learn the boundary. Section 5.6

[note 4)] When we consider seismic wave propagation, the sign of the Fourier convention is different from other physical cases, including the appendix of the previous chapter. To keep consistency a propagation in positive x direction as $e^{i(k \cdot x - \omega t)}$. Read the box of Aki and Richards for details. Please take care of the Fourier convention when you read a paper of a textbook.

[note 5)] In seismology, when considering wave propagation, the sign on ω is often taken to be negative. The definition of the Fourier transform is also often changed. This is to treat traveling waves as positive, and this is the sign taken by Aki and Richards (2002) and Saito (2009). In seismology, too, Dahlen and Tromp (1998) use the opposite sign, so it is important to be careful about which definition you are following.

[note 6)] This wave is also known as an evanescent wave or external wave in physics or meteorology.
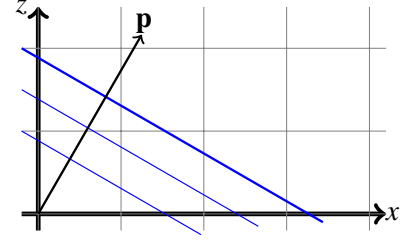
explains Rayleigh wave as a kind of inhomogeneous wave in a semi-infinite medium with a free boundary.

Let us review the global propagation of seismic waves. We can categorize it into body wave, which propagates in the Earth's interior, and boundary/surface wave, which propagates along a boundary including the Earth's surface (Figure 5.2left). Figure 5.2 shows such an example of Green's functions using seismic interferometry. The Horizontal axis shows the epicentral distance, whereas the vertical one shows the travel time[note 7]. The figures show global propagations of seismic surface waves and body waves. This section describes a brief summary of seismic wave types.

In general, we can categorize seismic waves into body waves and boundary waves. Body waves propagate in an internal body, whereas boundary waves travel along a boundary. A surface wave is a kind of boundary wave trapped close to the free surface.

[note 7] travel time is defined as the time from the origin time to the arrival time
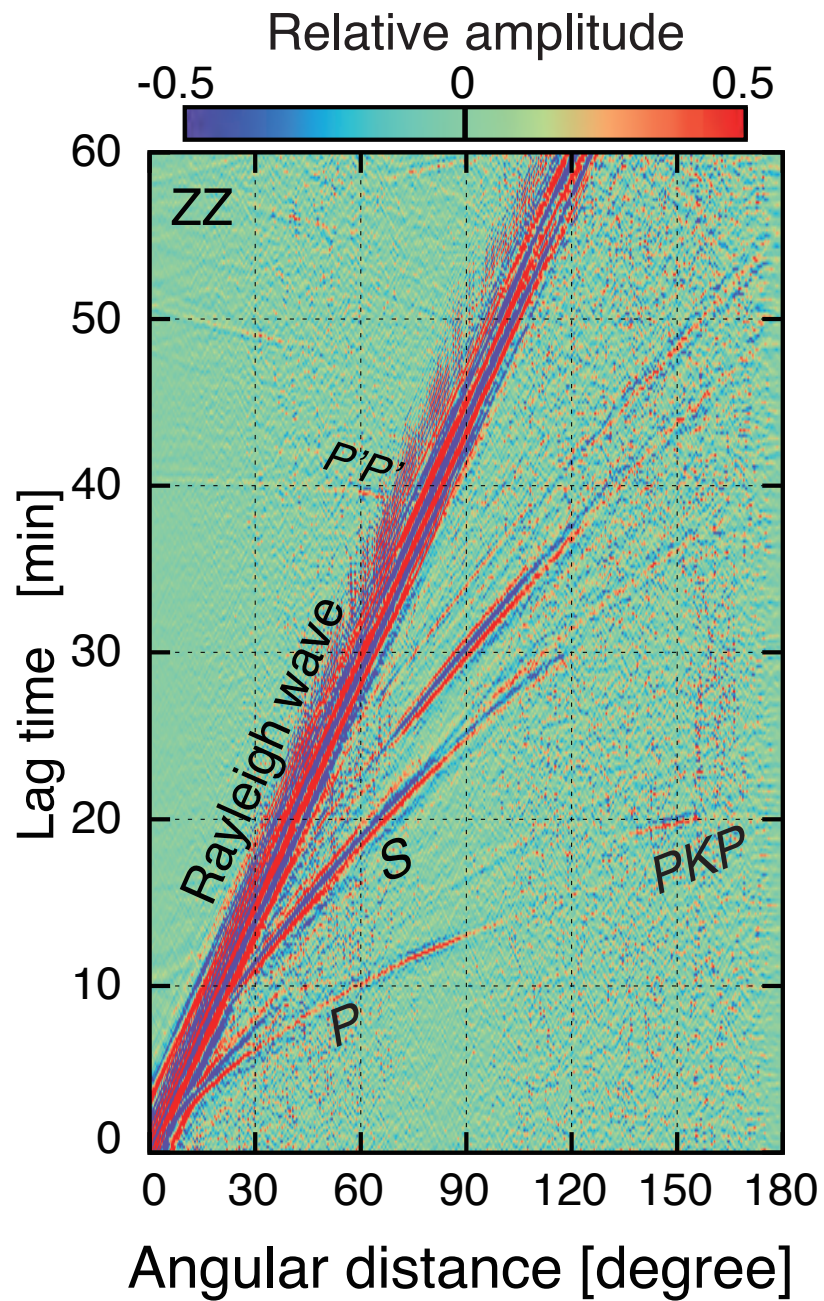
Fig. 5.2 Global propagation of body and surface waves. The waveforms are virtual Green's functions retrieved by cross-correlating ambient seismic wave field, also known as microseisms[3] (see chapter 10 for details of seismic interferometry.)

Body wave
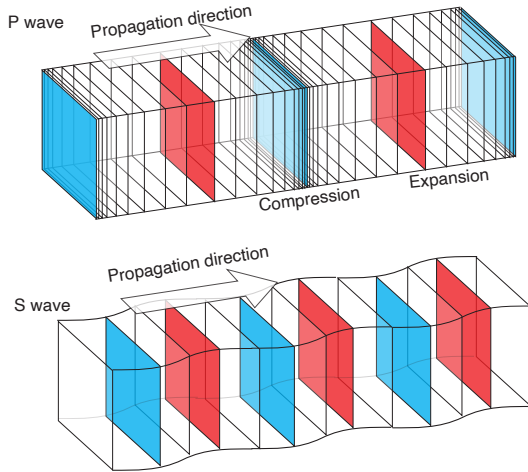
Fig. 5.3 A schematic figure of P and S wave propagation.

We can categorize body waves into P and S waves; the polarization of the P wave is parallel to the propagation direction, whereas that of the S wave is perpendicular to the propagation direction (Figure 5.3). "P" originated from the Primary wave, and "S" originated from the Secondary wave. The deformation of the P wave is volumetric, whereas that of the S wave is shear. [note 8]。 In general, with the decreasing temperature of the material, the stiffness increases, which causes an increase in the P wave and S wave velocities.

We all know well that P-waves propagate faster than S-waves, and the Omori formula for determining the distance to the epicenter from the difference in the arrival times of P-waves and S-waves [note 9]. You may have also heard of the Earthquake Early Warning, which estimates the hypocenter from the fast-moving P-waves and predicts the arrival of large tremors (S-waves).

Inhomogeneous waves: surface waves and boundary wave

Surface waves in an elastic medium can be categorized into Rayleigh waves, associated with volumetric changes, and Lave waves associated with multiple reflections of SH waves in a surface low-velocity layer.

5.2.3 Energy flux

The total energy of elastic medium per unit volume $\mathcal{U}$ can be written by the sum of the kinetic energy $\mathcal{U}^k$ and the strain energy $\mathcal{U}^p$ as

$$\mathcal{U} = \mathcal{U}^k + \mathcal{U}^p. \tag{5.10}$$

Energy flux $\boldsymbol{K}$ perpendicular to a unit area is given by[1]

$$\boldsymbol{K} = -\boldsymbol{T} \cdot \partial_t \boldsymbol{s}. \tag{5.11}$$

---

note 8) A Web site of demonstration of body wave propagation.http://www.eri.u-tokyo.ac.jp/knishida/
Seismology/body_wave.html
note 9) [4] is available at http://hdl.handle.net/2261/32677
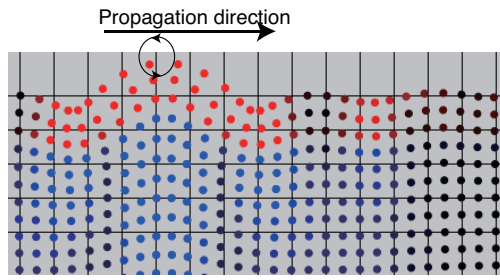
Fig. 5.4 Rayleigh wave propagation. The red color shows particle motions in retrograde, and the blue color shows those in prograde.
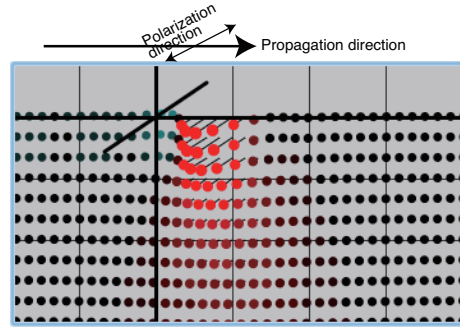
Fig. 5.5 Love wave propagation.

By equipartition between the kinetic energy and the strain energy, the total energy $\mathcal{U}$ can be written by,

$$\mathcal{U} = \rho \left| \frac{\partial s}{\partial t} \right| \tag{5.12}$$

where A is the displacement.

In particular, the energy flux of the P wave and that of the S wave are given by

$$\boldsymbol{K} = \begin{cases} \alpha \hat{\boldsymbol{n}} \mathcal{U} & \text{P wave} \\ \beta \hat{\boldsymbol{n}} \mathcal{U} & \text{S wave,} \end{cases} \tag{5.13}$$

where $\hat{\boldsymbol{n}}$ is a unit vector of the propagation direction. Conservation of energy is represented by

$$\frac{\partial \mathcal{U}}{\partial t} + \nabla \cdot \boldsymbol{K} = 0. \tag{5.14}$$

Problem 5.1

1. For a plane P wave, show that the kinetic energy is equal to the strain energy as,

$$\frac{1}{2} T_{ij} E_{ij} = \frac{1}{2} \rho \left| \frac{\partial s}{\partial t} \right|^2. \tag{5.15}$$

2. Here we consider a wave form of P wave $\boldsymbol{s} = \boldsymbol{p} f(t - \boldsymbol{p} \cdot \boldsymbol{x})$. Calculate the energy flux from equation 5.11.

3. For the inhomogeneous P wave with propagation in $z < 0$ given by P wave potential $\phi = \sin(\omega t - kx) \exp(\xi z)$. Then the displacement is written by

$$s_x = -k \cos(\omega t - kx) \exp(\xi z) \tag{5.16}$$
$$s_z = \lambda \sin(\omega t - kx) \exp(\xi z). \tag{5.17}$$

Calculate the energy flux.

§5.3 SH wave and P-SV wave

Free surface condition on the ground is crucial for seismic wave propagations. For simplicity, let us consider semi-infinite homogeneous medium in $z < 0$ with free surface condition on $z = 0$ (T_{iz}=0) (Figure 5.7). By introducing the free surface, we can categorize S wave into two. Figure 5.6 shows (1) vertically polarized S wave in xz plane (SV wave) and (2) horizontally polarized S wave (SH wave). This category is also crucial for stratified Earth, which is a good approximation at frequencies lower than several Hz.

In this chapter, the first section explains reflections and refraction of SH wave, and then we will explain reflection, refraction, and conversion of SV waves.

5.3.1 Equations of motion and Hooke's law

As shown in Figure 5.6, we take the y axis along the wave front,

$$\frac{\partial}{\partial y} = 0. \qquad (5.18)$$

Then, the equations of motion are given by

$$\rho \frac{\partial^2 s_x}{\partial t^2} = \frac{\partial T_{xx}}{\partial x} + \frac{\partial T_{xz}}{\partial z} \qquad (5.19)$$

$$\rho \frac{\partial^2 s_y}{\partial t^2} = \frac{\partial T_{yx}}{\partial x} + \frac{\partial T_{yz}}{\partial z} \qquad (5.20)$$

$$\rho \frac{\partial^2 s_z}{\partial t^2} = \frac{\partial T_{zx}}{\partial x} + \frac{\partial T_{zz}}{\partial z}, \qquad (5.21)$$

Fig. 5.6 Propagations of SH wave and SV waves and the polarization.

and Hooke's law is given by

$$T_{xx} = (\lambda + 2\mu)\frac{\partial s_x}{\partial x} + \lambda \frac{\partial s_y}{\partial y} + \lambda \frac{\partial s_z}{\partial z} \qquad (5.22)$$

$$T_{xz} = \mu \left(\frac{\partial s_x}{\partial z} + \frac{\partial s_z}{\partial x} \right) \qquad (5.23)$$

$$T_{yx} = \mu \left(\frac{\partial s_y}{\partial x} + \frac{\partial s_x}{\partial y} \right) \qquad (5.24)$$

$$T_{yz} = \mu \left(\frac{\partial s_y}{\partial z} + \frac{\partial s_z}{\partial y} \right) \qquad (5.25)$$

$$T_{zz} = \lambda \frac{\partial s_x}{\partial x} + \lambda \frac{\partial s_y}{\partial y} + (\lambda + 2\mu)\frac{\partial s_z}{\partial z}. \qquad (5.26)$$

Let us drop the stress term and rearrange the equations as,

$$\rho \partial_t^2 s_x = (\lambda + \mu)\partial_x(\partial_x s_x + \partial_z s_z) \qquad\qquad +\mu(\partial_x^2 s_x + \partial_z^2 s_x) \qquad (5.27)$$

$$\rho \partial_t^2 s_y = \qquad\qquad\qquad\qquad\qquad +\mu(\partial_x^2 s_y + \partial_{z^2} s_y) \qquad (5.28)$$

$$\rho \partial_t^2 s_z = (\lambda + \mu)\partial_z(\partial_x s_x + \partial_z s_z) \qquad\qquad +\mu(\partial_x^2 s_z + \partial_z^2 s_z) \qquad (5.29)$$

s_x and s_y are coupled with each other, whereas, s_y is decoupled with the others. Because s_y is polarized in a horizontal plane, the wave is called an SH wave. On the other hand, because s_x and s_z are composed of the P wave and vertical polarized S wave. the wave is called as P-SV wave. As described in later sections, the separation of the SH wave field and P-SV wave field is possible for a stratified Earth mode. Therefore, when we analyze seismic waveforms, rotations of horizontal components from north-south component and east-west component to transverse component (perpendicular to the great circle path between the source and the receiver) and radial component (parallel to the path). The transverse component represents the SH wave, and the radial component represents P-SV wave[note 10].

5.3.2 Plane waves in the case of P-SV and SH waves: how to take the vector potential

When considering seismic wavefields, in particular, plane waves in the P-SV case (see next section for details), it is useful to introduce a potential as explained in the 3.4.1 section. As already mentioned, there is one degree of freedom in the vector potential. When considering wave propagation in a horizontal multilayer structure in Cartesian coordinates

$$\mathbf{A} = \underbrace{\begin{pmatrix} 0 \\ 0 \\ \chi \end{pmatrix}}_{SH} \qquad \underbrace{+\nabla \times \begin{pmatrix} 0 \\ 0 \\ \psi \end{pmatrix}}_{SV} \tag{5.30}$$

SV and SH can be separated,[6] and the outlook improves if we use the following formula. Because of the arbitrary property of the vector potential, we can choose a convenient way to take the vector potential for our problem. For future calculations, we will write down the case of propagation along a two-dimensional xz plane. Assuming that the potential does not depend on y, the partial derivative with respect to y disappears, and we have a simple form. Below unexplained components are set to zero.

P wave

$$s_x = \frac{\partial \phi}{\partial x}, \qquad s_y = 0, \qquad s_z = \frac{\partial \phi}{\partial z} \tag{5.31}$$

$$E_{xx} = \frac{\partial^2 \phi}{\partial x^2}, \qquad E_{xz} = \frac{\partial^2 \phi}{\partial x \partial z}, \qquad E_{zz} = \frac{\partial^2 \phi}{\partial z^2} \tag{5.32}$$

$$T_{xx} = E \frac{(1-\nu)\frac{\partial^2 \phi}{\partial x^2} + \nu \frac{\partial^2 \phi}{\partial z^2}}{(1+\nu)(1-2\nu)}, \quad T_{xz} = \frac{E}{1+\nu} \frac{\partial^2 \phi}{\partial x \partial z}, \quad T_{zz} = E \frac{(1-\nu)\frac{\partial^2 \phi}{\partial z^2} + \nu \frac{\partial^2 \phi}{\partial x^2}}{(1+\nu)(1-2\nu)} \tag{5.33}$$

---

note 10) Exactly speaking, this separation valid for the far field.

SV wave

$$s_x = \frac{\partial^2 \psi}{\partial x \partial z}, \qquad\qquad s_y = 0, \qquad\qquad s_z = \frac{\partial^2 \psi}{\partial x^2} \qquad (5.34)$$

$$E_{xx} = \frac{\partial^3 \psi}{\partial x^2 \partial z}, \qquad\qquad E_{xz} = \frac{1}{2}\left(\frac{\partial^3 \psi}{\partial x \partial z^2} - \frac{\partial^3 \psi}{\partial x^3}\right), \qquad\qquad E_{zz} = -E_{xx} \qquad (5.35)$$

$$T_{xx} = -E\frac{(2\nu - 1)\frac{\partial^3 \psi}{\partial x^2 \partial z}}{(1 + \nu)(1 - 2\nu)}, \qquad T_{xz} = \frac{E}{1 + \nu}\frac{1}{2}\left(\frac{\partial^3 \psi}{\partial x \partial z^2} - \frac{\partial^3 \psi}{\partial x^3}\right), \qquad T_{zz} = -T_{xx} \qquad (5.36)$$

SH wave

$$s_x = 0, \qquad\qquad s_y = -\frac{\partial \chi}{\partial x}, \qquad\qquad s_z = 0 \qquad (5.37)$$

$$E_{xx} = 0, \qquad\qquad E_{xy} = -\frac{1}{2}\frac{\partial^2 \chi}{\partial x^2}, \qquad\qquad E_{yz} = -\frac{1}{2}\frac{\partial^2 \chi}{\partial x \partial z}, \qquad (5.38)$$

$$T_{xx} = 0, \qquad\qquad T_{xz} = -\frac{E}{1 + \nu}\frac{1}{2}\frac{\partial^2 \chi}{\partial x^2}, \qquad\qquad T_{yz} = -\frac{E}{1 + \nu}\frac{1}{2}\frac{\partial^2 \chi}{\partial x \partial z} \qquad (5.39)$$

In the following, the plane wave amplitudes are variables (e.g. A, B, C). In the next section, we will use

$$\phi = \frac{A}{\omega i}e^{i(k \cdot x - \omega t)} \psi \qquad\qquad = -\frac{B}{p_x \omega^2}e^{i(k \cdot x - \omega t}\frac{C}{\cdot x - \omega t)} \qquad (5.40)$$

and we will discuss the corresponding amplitudes by considering the potential that

§5.4 Reflection of SH-wave at a free surface

Let us consider the reflection and refraction of SH wave in a semi-infinite elastic medium $z <= 0$ with a free surface on $z = 0$. An incident SH wave enters with incident angle φ can be represented by a general solution of equation 5.28 as

$$s_y = Ae^{-i\omega(t-p_x x - p_z z)} + Be^{-i\omega(t-p_x x + p_z z)},$$
(5.41)

z axis

x axis

Fig. 5.7

where A and B are integral constants. The first term shows incident waves, and the second term shows the reflected wave. The free surface condition is written by

$$T_{zy} = -\mu\frac{\partial s_y}{\partial z} = 0.$$
(5.42)

Then the result of $A = B$ exhibits the phase of the reflected wave is the same as that of the incident wave. Displacement on the free surface is given by,

$$s_y = 2Ae^{-i\omega(t-px)},$$
(5.43)

which is double as large as the incident wave.
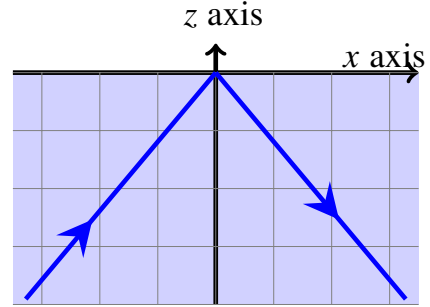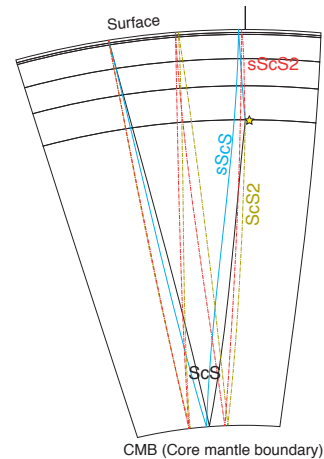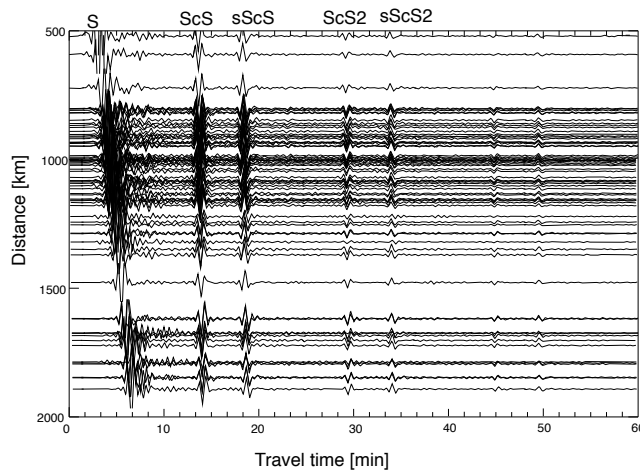
Fig. 5.8   Left: An example of seismograms of ScS reverberations when a deep earthquake of Ogasawara on 2015/5/30. They are vertical components of broadband seismometers of F-net band-pass-filtered from 30 s to 200 s. 。 Right: Ray paths of ScS, sScS, ScS2, sScS2.

This reflected wave can be interpreted as the "mirror" of the incident wave to meet the boundary condition. When we consider an incident wave $Ae^{-i\omega(t-p_x x - p_z z)}$, superposition between a mirror described by $Ae^{-i\omega(t-p_x x + p_z z)}$ and the incident wave satisfy the boundary condition.

Governing equation of SH wave is the same as the acoustic wave equation. However, the boundary conditions are different. For the SH wave, stress T_{zx} and T_{zy} are vectors, whereas the pressure for the acoustic wave is scalar. To meet the free surface condition of acoustic wave at $z = 0$, a mirror of $-Ae^{-i\omega(t-p_x x+p_z z)}$ is needed. The sign is different from the SH wave.

Figure 5.8 shows an example of reverberations of SH waves between the surface and the core-mantle boundary (CMB). Because the outer core is liquid, CMB is also a free surface. The figure shows many wave packets with fast apparent velocities, which correspond to multiple reflections of vertically propagating SH waves between the surface and CMB[note 11] The figure also shows the phase of ScS (reflected at CMB once) is the same as that of ScS2 (reflected at CMB twice).

[note 11] The amplitudes attenuate with distance due to intrinsic attenuation of the material.

§5.5 Reflection and conversion of P-SV wave at a free surface

For a given angular frequency ω, let us consider an incident P wave ($\boldsymbol{p}_\alpha^{in}$), and an incident SV wave ($\boldsymbol{p}_\beta^{in}$). The reflected P wave ($\boldsymbol{p}_\alpha^{refl}$), and the reflected SV wave ($\boldsymbol{p}_\beta^{refl}$) can be related by,

$$\boldsymbol{s} = A_\alpha^{in} e^{i\omega(\boldsymbol{p}_\alpha^{in}\cdot\boldsymbol{x}-t)} + A_\alpha^{refl} e^{i\omega(\boldsymbol{p}_\alpha^{refl}\cdot\boldsymbol{x}-t)} + A_\beta^{in} e^{i\omega(\boldsymbol{p}_\beta^{in}\cdot\boldsymbol{x}-t)} + A_\beta^{refl} e^{i\omega(\boldsymbol{p}_\beta^{refl}\cdot\boldsymbol{x}-t)}, \quad (5.44)$$

where $\boldsymbol{s}$ is displacement, and $\boldsymbol{A}$ represents polarization vector with the amplitudes. For simplicity, we solve a problem in the xz plane for propagating wave into y direction. The slowness vectors and the polarization vectors are given by,

$$\boldsymbol{p}_\alpha^{in} = \begin{pmatrix} p \\ \xi \end{pmatrix}, \qquad \boldsymbol{p}_\alpha^{refl} = \begin{pmatrix} p \\ -\xi \end{pmatrix}, \qquad \boldsymbol{p}_\beta^{in} = \begin{pmatrix} p \\ \eta \end{pmatrix}, \qquad \boldsymbol{p}_\beta^{refl} = \begin{pmatrix} p \\ -\eta \end{pmatrix}, \qquad (5.45)$$

$$\boldsymbol{A}_\alpha^{in} = A \begin{pmatrix} p \\ \xi \end{pmatrix}, \qquad \boldsymbol{A}_\alpha^{refl} = B \begin{pmatrix} p \\ -\xi \end{pmatrix}, \qquad \boldsymbol{A}_\beta^{in} = C \begin{pmatrix} \eta \\ -p \end{pmatrix}, \qquad \boldsymbol{A}_\beta^{refl} = D \begin{pmatrix} \eta \\ p \end{pmatrix}, \qquad (5.46)$$

Then we can simplify the equations as,

$$s_x(x,z)e^{i\omega(t-px)} = p(Ae^{i\omega\xi z} + Be^{-i\omega\xi z}) + \eta(Ce^{i\omega\eta z} + De^{-i\omega\eta z}) \qquad (5.47)$$

$$s_z(x.z)e^{i\omega(t-px)} = \xi(Ae^{i\omega\xi z} - Be^{-i\omega\xi z}) + p(-Ce^{i\omega\eta z} + De^{-i\omega\eta z}). \qquad (5.48)$$

Later, this chapter explains the reflection and transmission coefficients of two cases: (1) incident SV wave ($A = 0$), (2) incident P wave ($C = 0$) with boundary conditions of $T_{zx}(0) = 0$, and $T_{zz}(0) = 0$ as

$$2p\xi(A - B) + (\eta^2 + p^2)(C + D) = 0, \qquad (5.49)$$

$$(\eta^2 - p^2)(A + B) - 2p\eta(C + D) = 0. \qquad (5.50)$$

Here we define polarization vectors as

$$\hat{\boldsymbol{n}}_\alpha^{in} = \begin{pmatrix} p \\ \xi \end{pmatrix}\alpha, \qquad\qquad \hat{\boldsymbol{n}}_\alpha^{refl} = \begin{pmatrix} p \\ -\xi \end{pmatrix}\alpha, \qquad (5.51)$$

$$\hat{\boldsymbol{n}}_\beta^{in} = \begin{pmatrix} \eta \\ -p \end{pmatrix}\beta, \qquad\qquad \hat{\boldsymbol{n}}_\beta^{refl} = \begin{pmatrix} \eta \\ p \end{pmatrix}\beta \qquad (5.52)$$

In order to estimate the coefficients, we calculate the inner product between the polarization vectors and displacement $\boldsymbol{s}$.

5.5.1 P-wave incidence

The reflection coefficient from P wave to P wave $R_{PP} = (B/\alpha)/(A/\alpha)$ is given by,

$$R_{PP} = -\frac{(\eta^2 - p^2)^2 - 4p^2\xi\eta}{(\eta^2 - p^2)^2 + 4p^2\xi\eta}. \qquad (5.53)$$
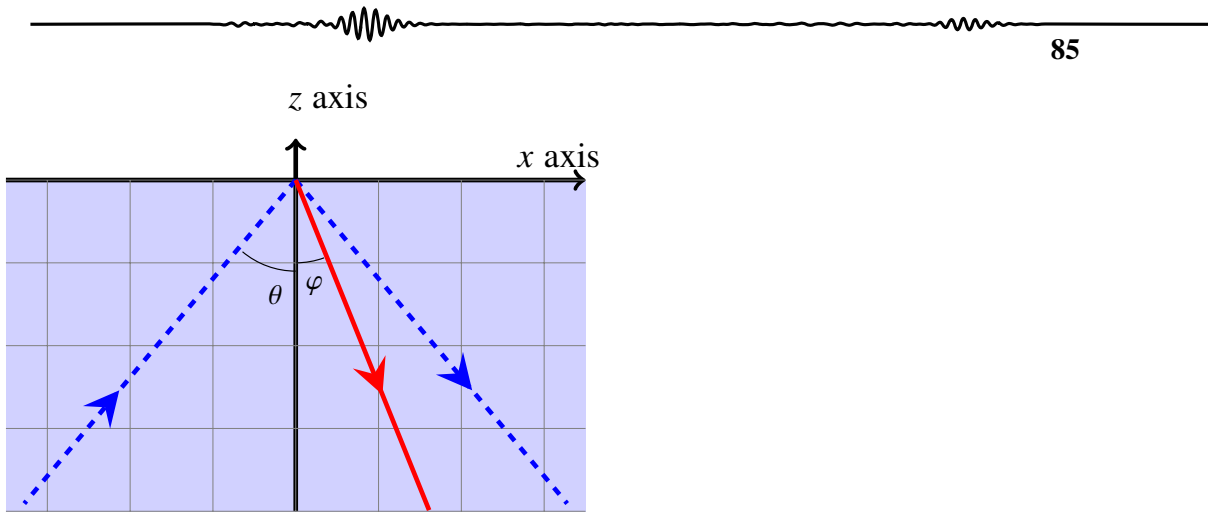
Fig. 5.9   P-wave incidence

The reflection coefficient from P wave to S wave $R_{PS} = (D/\beta)/(A/\alpha)$ is given by

$$R_{PS} = \frac{4p\xi(\eta^2 - p^2)}{(\eta^2 - p^2)^2 + 4p^2\xi\eta}\frac{\alpha}{\beta}. \tag{5.54}$$

Snell's Law

As already explained, both incident and reflected waves must have a dependence of e^{-px} in order to satisfy the boundary conditions p. [note 12]. In order for p to be a conserved quantity, the incident and reflected angles must satisfy the following relation: i.e., Snell's law,

$$\frac{\sin\varphi}{\beta} = \frac{\sin\theta}{\alpha}. \tag{5.55}$$

Conservation of energy

Consider the energy balance in a region on a thin region that includes the ground surface. The vertical energy flux must be balanced between the incident and reflected waves. The energy conservation law is given by

$$\alpha\cos\theta = \beta\cos\varphi|R_{PS}|^2 + \alpha\cos\theta|R_{PP}|^2. \tag{5.56}$$

Problem 5.2

1. Derive equation 5.53.
2. Derive equation 5.54.

[note 12] as explained in the ray theory in chapter **??**, where p is a quantity that can be related to momentum. Therefore we use p associated with momentum

5.5.2 SV-wave incidence
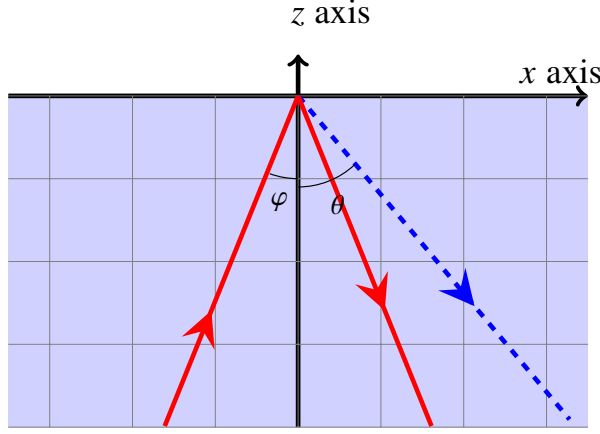
Fig. 5.10   SV-wave incidence

Consider the case of an SV wave with unit amplitude ($C = 1$) incident at an angle of 25° (φ in figure5.10). Figure5.10 shows that each of them takes a non-zero value. In order to satisfy the boundary condition, the stress must be zero when the superposition. In fact, the resultant wavefield in the figure shows that the stress T_{zz} is zero at the surface. We search the values of B and D to meet the boundary condition: $T_{zz} = T_{xz} = 0$. Since the sum of the unknowns and the number of boundary conditions are equal, we can find B and D.

Reflection coefficient from S wave to S wave $R_{ss} = (D/\beta)/(C/\beta)$ is written by

$$R_{SS} = \frac{(\eta^2 - p^2)^2 - 4p^2\xi\eta}{(\eta^2 - p^2)^2 + 4p^2\xi\eta}. \tag{5.57}$$

Here slowness and the incidental angles are related as, $p = \frac{\sin\theta}{\alpha} = \frac{\sin\varphi}{\beta}, \xi = \frac{\cos\theta}{\alpha}, \eta = \frac{\cos\varphi}{\beta}$.

Reflection coefficient from S wave to P wave $R_{SP} = (B/\alpha)/(C/\beta)$ is given by,

$$R_{SP} = \frac{4p\eta(\eta^2 - p^2)}{(\eta^2 - p^2)^2 + 4p^2\xi\eta}\frac{\beta}{\alpha}. \tag{5.58}$$

Corresponding conservation of energy is represented by

$$\beta\cos\varphi = \beta\cos\varphi|R_{SS}|^2 + \alpha\cos\theta|R_{sp}|^2. \tag{5.59}$$

Figure 5.12 shows the reflection coefficients.
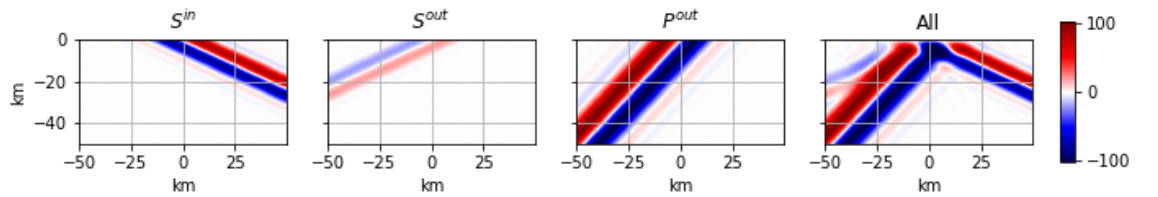
Fig. 5.11   The stresses T_{zz} for reflected SV and reflected P waves when the SV wave is incident at an angle of incidence (φ) of 25°. This figure shows that the stress for the superposed wave field is zero at the ground surface.
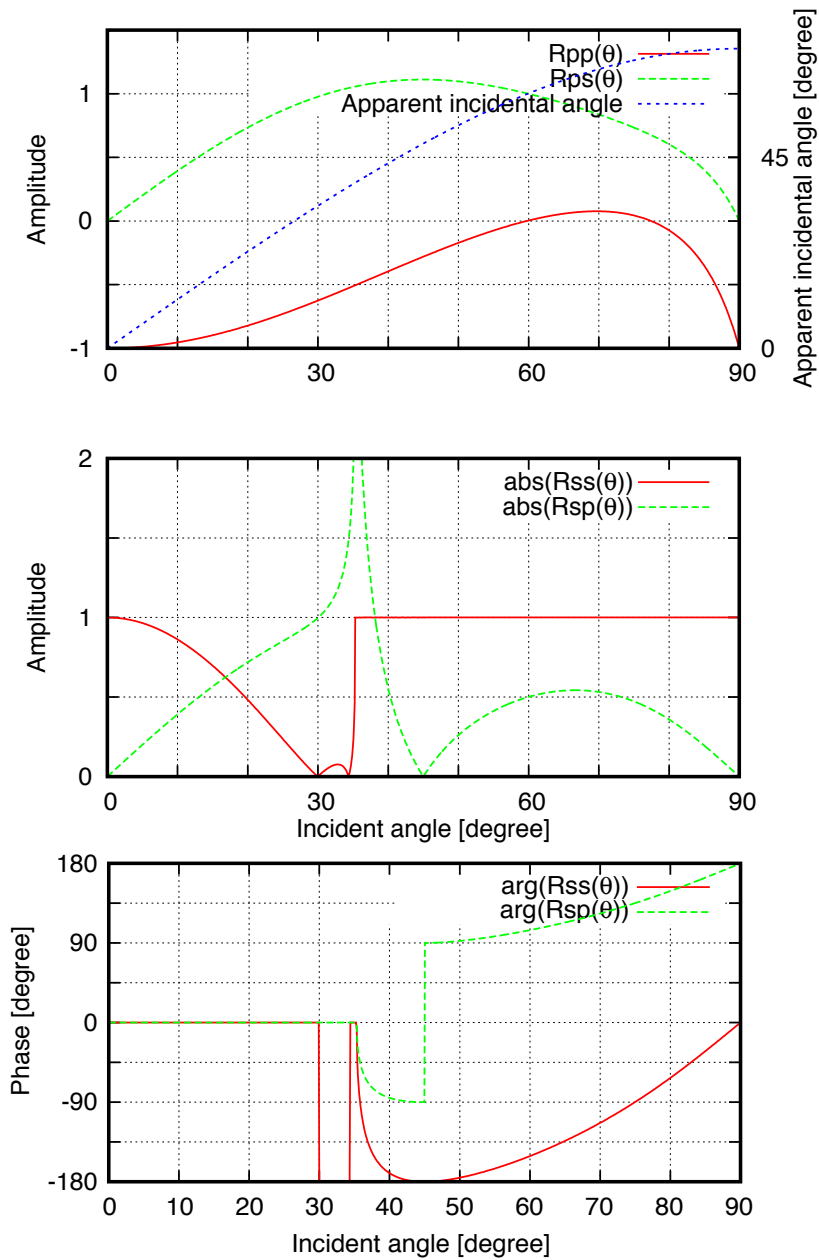
Fig. 5.12 R_{sp} has the finite value at its critical angle.

Snell's law

Similarly, the continuity of displacement and stress at the boundary leads to Snell's law. The conservation of p and Snell's law hold as well as P-wave:

$$\frac{\sin \varphi}{\beta} = \frac{\sin \theta}{\alpha}. \tag{5.60}$$

Critical angle

After the critical angle φ_c

$$\varphi_c = \sin^{-1} \frac{\beta}{\alpha}, \tag{5.61}$$

total reflection occurs. In this case, the z component of the slowness of the converted P wave becomes imaginary and cannot carry net energy in the vertical direction (known as an inhomogeneous wave). The S-wave will be out of phase due to the inhomogeneous P-wave sticking near the ground surface. [note 13].

Inhomogeneous P wave

Let us consider the stress T_{zz} for the case where the SV wave is incident at an angle of $75°$ (φ) beyond the critical angle. Figure 5.13 shows the incident SV wave and the reflected SV wave. The figure also shows that the phase of the reflected SV wave is out of phase by about 90 degrees (the incident SV wave is shaped like a half period of the sin function, while the reflected SV wave is shaped like one period of the cos function). The figure also shows that there are inhomogeneous P waves to meet the boundary conditions because of the phase shift of the reflected SV. The inhomogeneous P-wave is localized at the reflection point, and we can see that it is consistent with $Tzz = 0$.
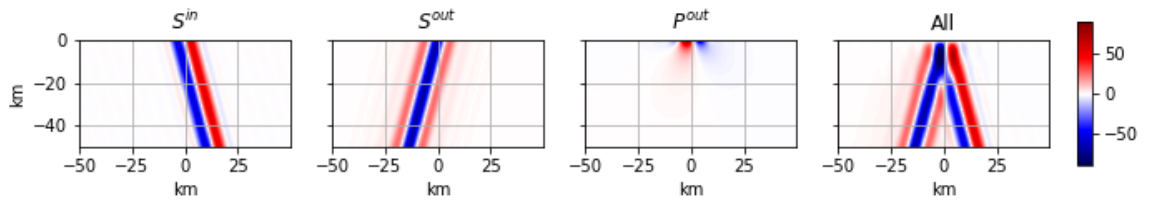
Fig. 5.13 Stress T_{zz} for SV wave incident with angle φ of $75°$, the reflected SV wave and the reflected P wave. wave. The superimposed stress field satisfies the boundary condition of the free surface.

Conservation of energy

Let us consider the energy balance in a thin region along the Earth's surface. surface. The vertical energy flux must be balanced between the incident and reflected energy flux. Before the critical angle, the energy conservation law is given by

$$\beta \cos \varphi = \beta \cos \varphi |R_{SS}|^2 + \alpha \cos \theta |R_{SP}|^2. \tag{5.62}$$

Since the reflected wave becomes evanescent after the critical angle, the net energy flux becomes 0, which leads to the following relation,

$$1 = |R_{SS}|^2. \tag{5.63}$$

[note 13] As calculated in Problem 5.1, the inhomogeneous waves carry energy up and down at a local scale but zero on a larger scale. When the wave incidents after the critical angle, the inhomogeneous P-wave accompanies the S-wave at the surface. The inhomogeneous P wave receives energy vertically from the S-wave and returns the energy with a slight time delay. The S wave is out of phase because of the temporary energy transfer by the inhomogeneous P wave

> **Problem 5.5**
>
> 1. Derive equation 5.57.
> 2. Derive equation 5.58.

Similarities and differences between SH and P waves

Both SH and P waves can be described by a single variable and behave very similarly because they satisfy the scalar wave equation. However, the reflection coefficient changes because the boundary conditions appear differently. Let us focus on this point here.

Here we consider an acoustic and an SH wave propagated in a xz plane. The governing equations are given by

$$\rho \frac{\partial^2 p}{\partial t^2} = \kappa \left(\frac{\partial^2 p}{\partial x^2} + \frac{\partial^2 p}{\partial y^2} \right) \tag{5.64}$$

$$\rho \frac{\partial^2 s_y}{\partial t^2} = \mu \left(\frac{\partial^2 s_y}{\partial x^2} + \frac{\partial^2 s_y}{\partial y^2} \right). \tag{5.65}$$

The equations show that both can be described by a two-dimensional scalar wave equation. For example, if the speed of sound and SH wave velocity is the same, p and s_y have the same solution.

One point should be noted, however. The acoustic wave takes pressure as a variable, while the SH wave takes displacement as a variable. There is a big difference when considering free surface. When considering acoustic waves, $p = 0$ is the boundary condition at the free surface. On the other hand, when we consider a free surface at $z = 0$, the boundary condition at the free surface for SH waves is given by

$$-\rho \frac{\partial s_y}{\partial z} = 0. \tag{5.66}$$

This corresponds to the boundary condition of a rigid wall for acoustic waves. The reflection coefficient at the surface with respect to pressure for P waves is -1, while for SH waves, the reflection coefficient at the surface is 1. The difference is whether stress or displacement is taken as the variable; in both cases, the stress at the surface is zero. The analogy with acoustic waves is valid, but be careful how you choose the variables.

Problem 5.4

Let us consider P wave propagation in a 3-D half space of fluid.

1. As in the case of SH wave, estimate reflection coefficients for an incident plane wave (P-wave) as a function of incident angle.
2. Compare the above result with P-wave reflection coefficients for the P-SV problem. In particular, discuss it for the incidental angles of about 0° and 90°.
3. As in the case of full space (see subsection 3.4.2), estimate the Green's function for an explosion source in a half-space of fluid. Discuss the behavior as the source depth approach the free surface.

5.5.3 Apparent incidental angle of P-SVwave

When we analyze seismic waveform, the particle motion is informative. For example, Figure 5.5.3 shows the particle motion of P wave against radial and vertical components when the deep earthquake at Ogasawara was recorded by the F-net station at Fukue. The figure shows an inclined linear polarization. The inclination shows the approximate incidental angle. This subsection describes this relation.

First, let us consider that the P wave enters the free surface. The ratio between the vertical displacement s_x and the horizontal one s_y is given by

$$\frac{s_x}{s_z} = \frac{p(A + B) + \eta D}{\xi(A - B) + pD} = \frac{2p\eta}{\eta^2 - p^2} = \tan 2\varphi. \tag{5.67}$$

The inclination of P wave polarization (or apparent incidental) θ' is twice as large as the S-wave reflected angle as (Figure 5.12,

$$\theta' = 2\varphi. \tag{5.68}$$

When the incident angle is enough small for a Poisson medium ($\alpha = \sqrt{3}\beta$) relation between the apparent incidental angle and the P-wave incidental angle can be simplified as

$$\theta' = 2\varphi \sim \frac{2\beta}{\alpha}\theta \sim 1.15\theta. \tag{5.69}$$

Fig. 5.14 An example of particle motion of P-wave against radial and vertical components of F-net station at Fukue.

This result shows that the P-wave incidental angle can be approximated by the apparent incidental angle.

In the same manner, the incidental angle of the S wave can be related to apparent incidental angle as.

$$\frac{s_x}{s_z} = \frac{pB + \eta(C + D)}{-\xi B + p(-C + D)} = -\frac{\eta^2 - p^2}{2p\xi} \tag{5.70}$$

When the incidental angle is small (this assumption is valid for teleseismic events), the apparent incident angle can be related to the incident angle by

$$\varphi' = 2\frac{\beta^2}{\alpha^2}\varphi = 2\frac{\beta}{\alpha}\varphi. \tag{5.71}$$

Here we assumed that the incidental angle is smaller than the critical angle.

It may seem somewhat intuitive that the direction of oscillation of the P wave coincides with the direction of incidence, but it is by no means obvious. For example, consider the limit $\beta \rightarrow 0$, assuming a medium similar to a fluid. In this case, the direction of oscillation is 0 degrees. Let us consider the case of a fluid. In Fig 5.15, we consider a pressure source in the ground. To satisfy the boundary conditions at the water surface, we consider a pressure source with the opposite sign at the mirror-symmetric location. In this case, considering the particle trajectory at the ground surface, it will move up and down. Since this relationship holds at any time, the particle trajectory at the water surface is always vertical, regardless of the angle of incidence.

Fig. 5.15   Particle motion near the surface in fluid.

Problem 5.5

1. Derive equation 5.67.
2. Derive equation 5.70.

§5.6 Rayleigh wave

Before this section, this chapter explains body waves that can propagate freely in the vertical direction. Inhomogeneous waves accompany incoming SV after the critical angle. Can inhomogeneous waves exist on their own? Rayleigh waves have energy near the surface and are known to propagate horizontally. Figure 5.16 shows the observation record during the 2014 Chilean earthquake. The waves labeled R1 and R2 are Rayleigh waves, which propagate at an approximately constant speed. The Chilean earthquake excited Rayleigh waves efficiently because the depth of the epicenter is 35 km, which is much shorter than the wavelength of the waves. First, let us consider qualitatively the nature of Rayleigh waves.
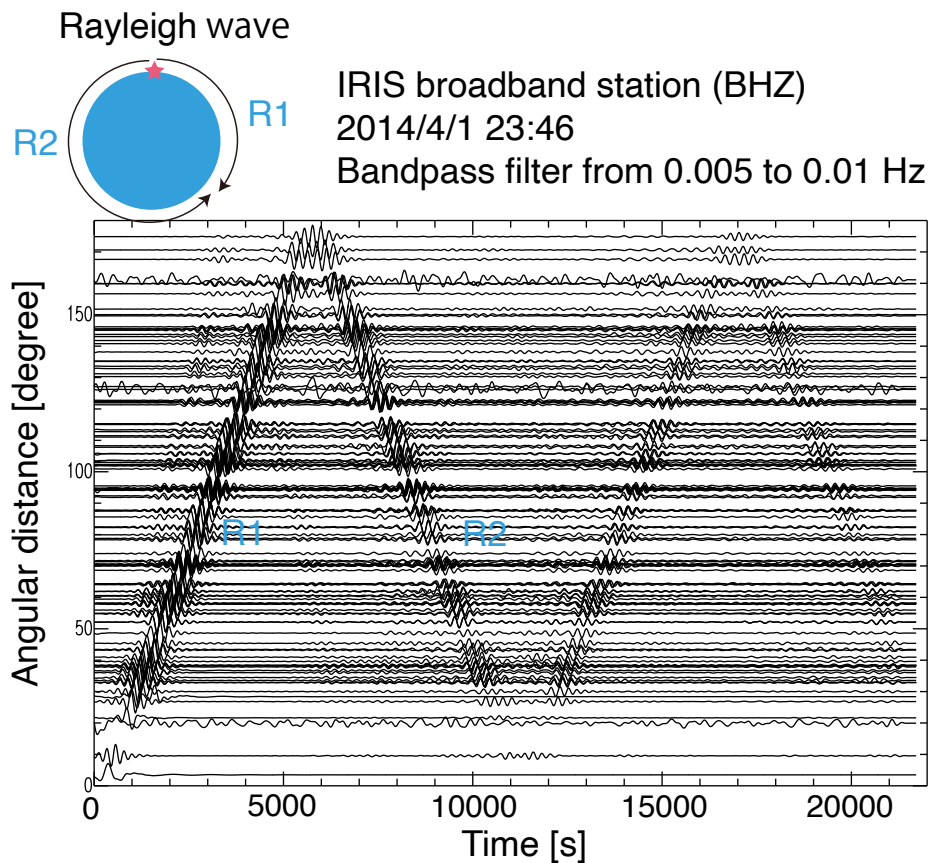
Fig. 5.16 Waveforms in vertical components recorded by broadband seismometers when the 2014 Chilean earthquake.

When considering acoustic or SH wave propagation in a half-space, inhomogeneous waves cannot exist alone because they cannot satisfy the boundary conditions at the free surface. On the other hand, they can exist for P-SV propagations: known as Rayleigh waves.[5] Rayleigh waves satisfy the free surface condition because P-wave-like and S-wave-like deformations can exist simultaneously, which lean against each other at the surface. Rayleigh waves have energy concentrated near the surface so that we can observe global propagation (Fig. 5.17). We will first consider its properties qualitatively. First, let us consider the Rayleigh wave [note 14].

Let us consider a situation where an S-wave enters the right direction while oscillating vertically through an infinite medium. We then cut out an infinite medium in the middle. Then, to satisfy the boundary condition of zero stress at the free surface, the large stress part will bulge out (the part with large volumetric strain). The free surface causes a large deformation, and the effective elastic constant decreases. As a result, the Rayleigh wave propagates slower than the S-wave (about 90% of the S-wave velocity). The particle motion becomes elliptical because the phase of the

Fig. 5.17 Schematic figure of Rayleigh propagation. Red circles show particle motions in retrograde, whereas blue ones show those of prograde.

volume deformation is shifted by 90 degrees compared to that of the S-wave. Because the horizontal propagation velocity is slower than the S-wave and P-wave velocities, they can only exist as inhomogeneous wave. The amplitude decreases exponentially in the depth direction. At the surface, the particle motion is in the opposite direction of the rotation of a bicycle wheel (retrograde). On the other hand, in deeper regions (blue in the figure), the direction is the same as the rotation of a bicycle wheel (prograde).

5.6.1 Can elastic waves along a free surface exist?

To consider this a little more quantitatively, let us now clarify the problem. Let us consider the propagation in the xz plane and assume that it does not change in the y direction, just as we would consider the reflection and transformation of a P-SV wave at the free plane. The boundary condition is given by $T_{zz} = T_{zx} = 0$ at the surface. To begin with, let us simply consider if acoustic waves and SH waves can propagate horizontally in half space.

As you may recall from Figure 5.15, the reflection coefficient of an acoustic wave at a free surface is -1. Because the incident and reflected waves cancel each other out, the acoustic wave is not excited when an excitation source is near the free surface. Since the sign of the mirror image is reversed in Figure 5.15, it can be interpreted that in the case of a very shallow pressure source, the waves are not excited because they cancel each other out with the pressure of the mirror image, which has the opposite sign. The fact that acoustic waves cannot be excited by an explosive source near the water surface may, at first glance, seem inconsistent with physical intuition. However, it makes physical sense when one considers that the elastic energy is zero due to the free boundary surface (see also the section 4.6).

On the other hand, in the case of SH waves, the amplitude doubles at the surface and is amplified since the reflection coefficient is 1 in the case of SH waves. In other words, horizontally propagating waves do exist in the case of SH waves. This difference is due to the

note 14) see demo http://www.eri.u-tokyo.ac.jp/knishida/Seismology/Rayleigh_wave.html

difference in boundary conditions. As mentioned before, the difference between displacement and stress comes into play because the pressure satisfies the scalar wave equation for acoustic waves, while s_y satisfies it in the SH case. If so, is this possible for SV waves? It is impossible because SV waves do not satisfy the boundary conditions when horizontally propagating.

5.6.2 A case of the reflection coefficient of zero

Let us now reconsider the number of boundary conditions. For the $P - SV$ problem, we need two boundary conditions, $T_{zz} = 0, T_{zx} = 0$. If we now consider arbitrary incident waves, we will need to add together two independent solutions to eliminate these two. This situation corresponds exactly to the reflection/transformation wave for the incident wave at the free surface in the previous section. The similarity means that a combination of the three waves is required. So let us look at the SV incidence in Figure 5.12. R_{SS} in the figure shows two points where the amplitude of the S reflection is zero. R_{SP} in the figure shows one point where the P reflection is zero. The zeros show the possibility of combining the two waves to satisfy the boundary condition if one looks for the appropriate frequency. Let us consider the possibility of this kind of solution.

In the following, let us consider T_{zx}^P, T_{zz}^P caused by an inhomogeneous P wave and T_{zx}^S, T_{zz}^S caused by an inhomogeneous SV wave. If we can find a phase velocity p as the same stress ratio T_{zx}/T_{zz} for two waves, the difference between the two normalizing solutions satisfies the boundary condition. Now, let us look at the stress ratio for each wave.

Inhomogeneous P wave

Here, the scalar potential for an inhomogeneous P wave is defined by

$$\phi = e^{i\omega px}e^{-\omega\xi z}e^{-i\omega t}. \tag{5.72}$$

P-wave velocity α satisfies the relation $\alpha^{-2} = p^2 - \xi^2$. The result in section **??** leads to the ration betwenn T_{zz} and T_{zx}:

$$\frac{T_{zx}}{T_{zz}} = -i\frac{(1-2\nu)\xi p}{(1-\nu)\xi^2 - \nu p^2}. \tag{5.73}$$

In a case of Poisson material ($\nu = 1/4$), we can simplifies the relations by elimination of ξ:

$$\frac{T_{zx}}{T_{zz}} = -i\frac{2\sqrt{p^2 - \alpha^{-2}}p}{2p^2 - 3\alpha^{-2}}. \tag{5.74}$$

Inhomogeneous SV wave

Here, the component of vector potential for an inhomogeneous SV wave is defined by

$$\frac{\partial\psi}{\partial x} = e^{i\omega px}e^{-\omega\eta z}e^{-i\omega t}. \tag{5.75}$$

The S-wave velocity β satisfies the relation $\beta^{-2} = p^2 - \eta^2$. The result in section **??** leads to the stress ration between T_{zz} and T_{zx} as:

$$\frac{T_{zx}}{T_{zz}} = -i\frac{(\eta^2 - p^2)}{2p\eta}, \tag{5.76}$$
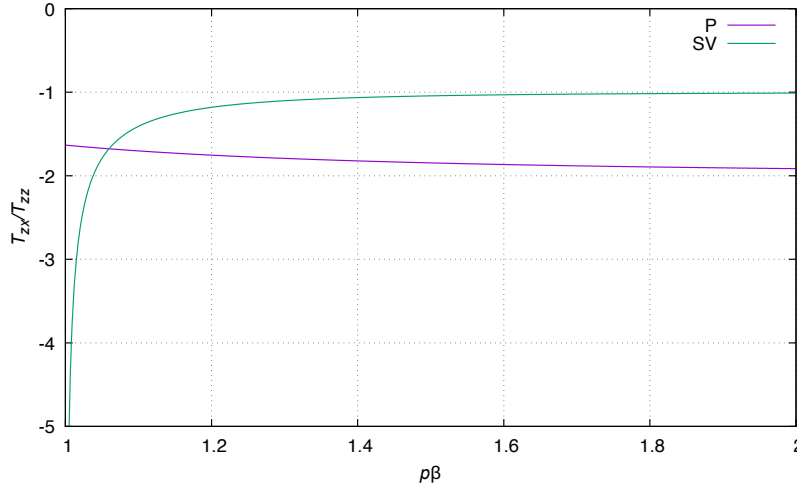
Fig. 5.18   Stress ratio T_{zx}/T_{zz} at the surface for slowness p. Here we consider a Poisson material, and the slowness is normalized by the S-wave velocity. We plot them for $p\beta > 1$ because the vertical wavenumber becomes pure imaginary (which can propagate in the vertical direction as body waves) for $p\beta < 1$

In a case of Poisson material $\alpha = \sqrt{3}\beta$ Elimination of η leads to

$$\frac{T_{zx}}{T_{zz}} = -i\frac{2p^2 - \beta^{-2}}{2p\sqrt{p^2 - \beta^{-2}}}. \tag{5.77}$$

Let us compare the two stress ratios. Figure 5.18 shows that the two curves intersect when p is slightly greater than β^{-1}, which would represent the condition under which inhomogeneous waves can exist alone. This corresponds to Rayleigh waves. Let us consider in more detail the conditions under which the stress ratio at the surface is constant. The condition of equal stress ratio leads to the following relation;

$$(\eta^2 - p^2)^2 + 4p^2\xi\eta = 0. \tag{5.78}$$

For the better understandings of the equation, we define $X \equiv p^2\beta^2$ and $\gamma^2 \equiv \alpha^{-2}/\beta^{-2}$. With the squared stress ratios of the inhomogeneous P wave and the inhomogeneous SV wave, we can rearrange the equation is as follows:

$$16(1 - \gamma^2)X^3 - (24 - 16\gamma^2)X^2 + 8X - 1 = 0. \tag{5.79}$$

In the case of Poisson material, the equation can be simplified as,

$$32X^3 - 56X^2 - 24X - 3 = 0, \tag{5.80}$$

and the analytic solutions are given by

$$X = \frac{1}{4}, \frac{3}{4} \pm \frac{\sqrt{3}}{4}. \tag{5.81}$$

Only the last one satisfies the condition $p > \beta^{-1}$, and the solution corresponds to the solution shown by Figure 5.18. What are the physical meanings of the other two solutions? The incident angles estimated from p are 30° and 34.3° for Poisson material. These two angles correspond exactly to the zero crossing of the R_{SS} in Figure 5.12: i.e., the case where all

incident S waves are converted to reflected P waves. Thus, the three solutions make physical sense. In other words, the problem of finding a condition where the incident S-wave reflected at the free surface is extended to the problem of finding a condition where the inhomogeneous P-wave converted only the inhomogeneous SV-wave wave. We summarize the displacement of the Rayleigh wave

$$s_x(x, z, t) = ipB \left[e^{\omega \xi z} + \frac{1 - 2p\beta}{2p\beta} e^{\omega \eta z} \right] e^{i\omega(t-px)} \tag{5.82}$$

$$s_z(x, z, t) = \xi B \left[e^{\omega \xi z} + \frac{2p\beta}{1 - 2p\beta} e^{\omega \eta z} \right] e^{i\omega(t-px)}, \tag{5.83}$$

where $\xi = \sqrt{p^2 - \alpha^{-2}}, \xi = \sqrt{p^2 - \beta^{-2}}$ and B is an integral constant. Also, in order to choose a physically meaningful solution (no divergence at $z = -\infty$), the sign is chosen so that Im $\eta < 0$, Im $\xi < 0$ The sign is chosen so that Im $\eta < 0$, Im $\xi < 0$.

Figure 5.19(a) shows the depth profile of Rayleigh wave amplitudes (s_x and s_z). It can be seen that the amplitude decreases exponentially with depth. The major difference from the entity wave is the phase shift between horizontal and vertical motion. The motion of particles at the surface is plotted in Fig 5.19(b). Taking the real parts of s_X and s_z, we see that they rotate in the direction of the arrows in the figure since $s_x - \sin \omega t, s_z = \cos \omega t$. Since the Rayleigh wave is now traveling from left to right in the figure, we call it retrograde. [note 15)] Also, the sign of s_x reverses around $z = -0.25$, so the direction of rotation is reversed at deeper points. This direction is called the forward direction (prograde).

It's hard to explain, so I created a demo page for Rayleigh waves on the web.[note 16)] Please refer to them as needed.

Rayleigh waves are two-dimensional because they have energy only near the surface. The behavior is, therefore, similar to that of a two-dimensional Green's function. Especially since the amplitude is proportional to $r^{1/2}$. [note 17)] When the epicentral distance is far, the surface waves are larger than the body waves. [note 18)] Also, surface waves are not efficiently excited when the hypocenter is deeper than the wavelength (because they decay exponentially in the depth direction).

5.6.3 As a problem of inhomogeneous S-wave incidence

Let us now interpret the Rayleigh wave as a reflection/transmission problem for P-SV inhomogeneous waves. Let us take the horizontal slowness on the horizontal axis and calculate the reflection and conversion coefficients even for values larger than the S-wave slowness (Figure 5.20). Here we consider the same formulation as in the section 5.5.2. In this case, let us assume that the incident SV waves are inhomogeneous waves and choose a solution that decays exponentially in a vertically downward direction. Then we would have to choose a solution where the reflected inhomogeneous SV waves diverge in amplitude with depth. At

---

note 15) It is easy to understand if you think of the direction of rotation of a bicycle wheel.

note 16) https://www.eri.u-tokyo.ac.jp/people/knishida/Seismology/Rayleigh_wave.html

note 17) Roughly speaking, if the epicentral distance r, amplitude A, and propagation velocity c_R, the energy flux can be written as $c_r \rho \omega A^2$ and

$$\nabla \cdot \boldsymbol{K} = \frac{1}{r} \frac{\partial}{\partial r} (Kr) = 0, \tag{5.84}$$

which leads to $A \sim r^{1/2}$.

note 18) Recalling the far-field term of Green's function, we can see that the body waves are proportional to r^{-1}. This can be derived from considering the conservation of energy as well as surface waves.

(a) $\omega = 1$, $\alpha = \sqrt{3}$, $\beta = 1$

(b) Particle motion

Rayleigh wave propagation

s_x

s_z

z axis

Vertical displacement

Horizontal displacement
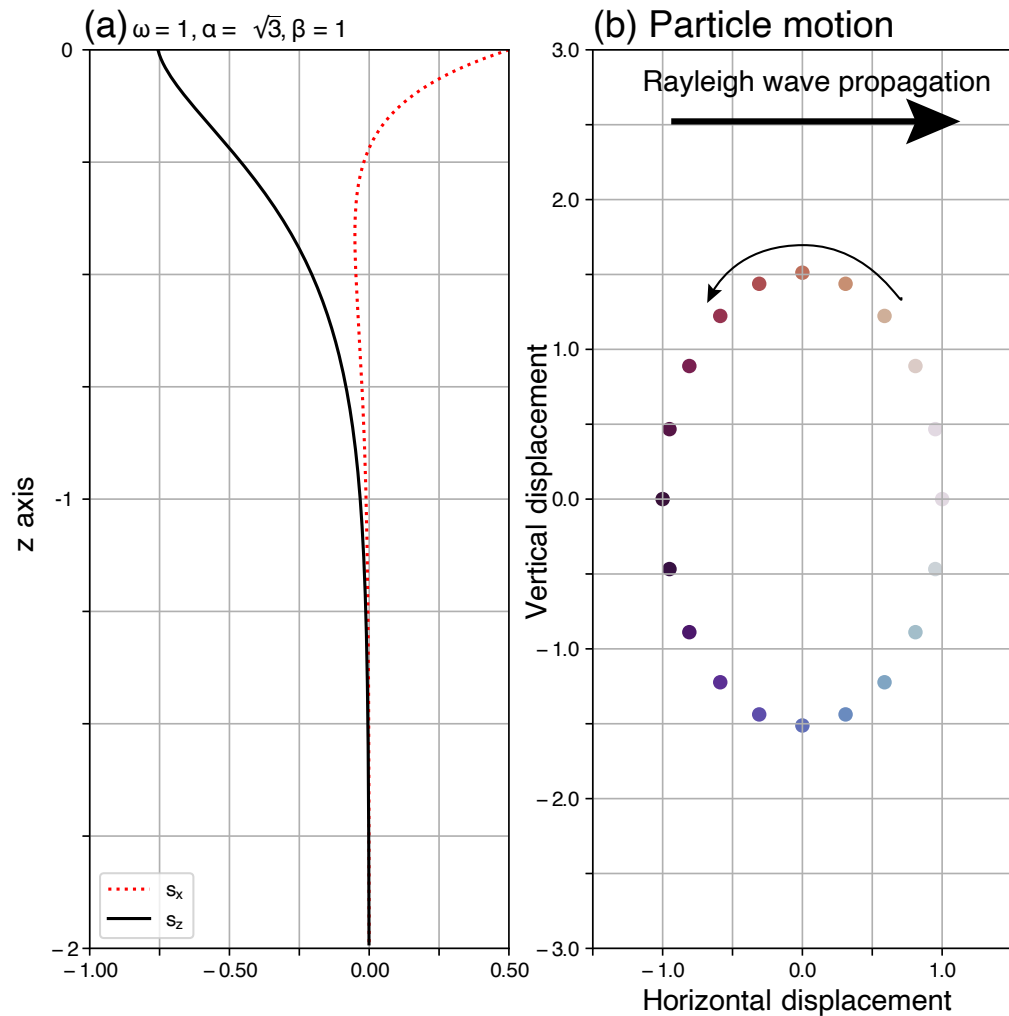
Fig. 5.19   (a) Depth profile of Rayleigh wave amplitudes. (b) Particle motion at the surface.

first glance, this seems physically impossible, but let us recall the representation theorem. By placing a boundary surface at a depth where the amplitude of the incident SV wave is sufficiently small and by imposing stress and displacement boundary conditions at the boundary surface, we can treat inhomogeneous SV waves with increasing amplitude in the depth direction. In other words, it can be realized by considering a bottom to the medium instead of a semi-infinite medium [note 19)].

Figure 5.20 is identical to Figure 5.12 when the incident angle of 90°, which corresponds to $p\beta = 1$. When $p\beta$ is larger than 1, the incident SV wave also becomes an inhomogeneous wave. There is a point where R_{ss} is zero at which $p\beta = 1$ is slightly larger than 1. This is precisely the point where there are no reflected S waves. The corresponding inhomogeneous P wave and inhomogeneous SV wave can take a downward decaying solution. Thus, the problem can also be viewed as a generalization of the SV wave reflection and transformation problem.

[note 19)] representation theorem is powerful because it makes it easy to consider virtual operations like this
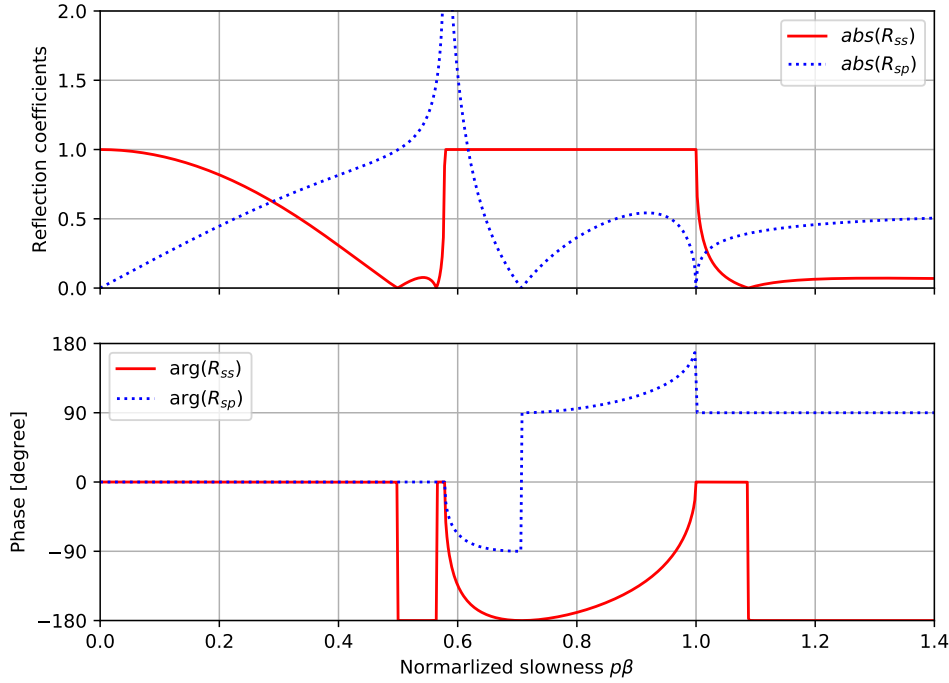
Fig. 5.20 We can see that R_{ss} is zero at the point where Slowness is slightly larger than $1/\beta$. Also, the conversion coefficient R_{sp} corresponding to Rayleigh waves is defined as $(D/\alpha)/(C/\beta)$ (see section 5.5.2), which can be related to the particle motions on the ground surface.

5.6.4 Eigen value problem

We have considered the conditions for the existence of Rayleigh waves, but the governing equation is somewhat complicated, and it is difficult to understand the mathematical setup. Therefore, for the plane wave case of the P-SV problem, we rearrange the equation of motion (equation 5.19) and Hooke's law (式 5.22). We choose s_x, s_z, T_{xz}, T_{zz} as variables to consider the boundary conditions. Since the governing equations are partial derivatives of z only, the equation can be represented by the first-order ordinary differential equations for z,

$$\frac{d}{dz}\begin{pmatrix} s_x \\ s_z \\ T_{xz} \\ T_{zz} \end{pmatrix} = \begin{pmatrix} 0 & -i\omega p & \frac{1}{\mu} & 0 \\ -i\omega p \frac{\lambda}{\lambda+2\mu} & 0 & 0 & \frac{1}{\lambda+2\mu} \\ -\rho\omega^2 + \omega^2 p^2 \frac{4\mu(\lambda+\mu)}{\lambda+2\mu} & 0 & 0 & -i\omega p \frac{\lambda}{\lambda+2\mu} \\ 0 & -\rho\omega^2 & -i\omega p & 0 \end{pmatrix}\begin{pmatrix} s_x \\ s_z \\ T_{xz} \\ T_{zz} \end{pmatrix}, \tag{5.85}$$

where 、 T_{xx}, s_x and T_{zx} are given by

$$T_{xx} = i\omega p(\lambda + 2\mu)s_x + \lambda \frac{ds_z}{dz}. \tag{5.86}$$

In other words, it is a problem of integrating an ordinary differential equation from one boundary to find p such that the boundary condition is satisfied on the other. This is nothing

but an eigenvalue problem. The setup of the problem in section 5.6.2 corresponds to starting the integration from the bottom to meet the boundary conditions at the other side. The result in section 5.6.3 corresponds to matching the boundary condition at infinity depth-integrated from the ground surface. This treatment as an eigenvalue problem will be discussed in detail in the chapter on normal mode theory.

ToDO: Excitation of Rayleigh wave

Polar phase shift

Problem 5.6

1. Show that the equation 5.79 has a solution with slowness greater than $p = 1/\beta$ for any elastic constant.
2. Illustrate the Rayleigh wave velocity versus Poisson's ratio when $\beta = 1$. Also, discuss the physical meanings.
3. Calculate the ellipticity of the particle motion at the earth's surface in the same way and discuss it physically.

§5.7 Lamb's solution

We show a solution for Lamb's solution for a half-space of 3-D elastic medium given by Kausel 2014.[2] r is distance, θ is azimuth, μ is shear modulus, ρ is density, ν is Poisson's ratio, C_R is Rayleigh wave velocity, C_s is S-wave velocity, C_P is P-wave velocity, t is time, a is C_S/C_P, κ_j is three dimensionless solution to the Rayleigh characteristic equation ($= C_S/C_j$), $\gamma \equiv \kappa_1 = C_S/C_R$ is true Rayleigh root, and τ is dimensionless time tC_S/r.

The Rayleigh characteristic equation is given by

$$16(1 - a^2)\kappa^6 - 8(3 - 2a^2)\kappa^4 + 8\kappa^2 - 1 = 0. \tag{5.87}$$

$$A_j = \frac{\left(\kappa_j^2 - \frac{1}{2}\right)^2 \sqrt{a^2 - \kappa_j^2}}{D_j}, \quad B_j = \frac{\left(1 - 2\kappa_j^2\right)\left(1 - \kappa_j^2\right)}{D_j}, \quad C_j = \frac{\left(1 - \kappa_j^2\right)\sqrt{a^2 - \kappa_j^2}}{D_j}$$

$$D_j = \left(\kappa_j^2 - \kappa_i^2\right)\left(\kappa_j^2 - \kappa_k^2\right), \quad i \neq j \neq k \tag{5.88}$$

$$u_{zz}(r, \tau) = \frac{(1 - \nu)}{2\pi\mu r} \begin{cases} \frac{1}{2}\left(1 - \sum_{j=1}^{3} \frac{A_j}{\sqrt{\tau^2 - \kappa_j^2}}\right), & a < \tau < 1 \\[2ex] 1 - \frac{A_1}{\sqrt{\tau^2 - \gamma^2}}, & 1 \leq \tau < \gamma \\[2ex] 1, & \tau \geq \gamma \end{cases} \tag{5.89}$$

$$u_{rx} = \frac{(\cos\theta)}{2\pi\mu r} \begin{cases} \frac{1}{2}(1 - \nu)\tau^2 \sum_{j=1}^{3} \frac{C_j}{\sqrt{\tau^2 - \kappa_j^2}}, & a < \tau < 1 \\[2ex] 1 + (1 - \nu)\tau^2 \frac{C_1}{\sqrt{\tau^2 - r^2}}, & 1 \leq \tau < \gamma \\[2ex] 1, & \tau \geq \gamma \end{cases} \tag{5.90}$$

$$u_{\theta x} = \frac{(1 - \nu)(-\sin\theta)}{2\pi\mu r} \begin{cases} \frac{1}{2}\left[1 - \sum_{j=1}^{3} C_j \sqrt{\tau^2 - \kappa_j^2}\right], & a < \tau < 1 \\[2ex] 1 - C_1 \sqrt{\tau^2 - \gamma^2}, & 1 \leq \tau < \gamma \\[2ex] 1, & \tau \geq \gamma \end{cases} \tag{5.91}$$

§5.8 Bibliography

[1] F.A. Dahlen and J. Tromp. *Theoretical Global Seismology*. Princeton University Press, Princeton, 1998.

[2] Eduardo Kausel. Lamb's problem at its simplest. *Proc. R. Soc. A Math. Phys. Eng. Sci.*, Vol. 469, No. 2149, pp. 20120462–20120462, nov 2012.

[3] K Nishida. Global propagation of body waves revealed by cross-correlation analysis of seismic hum. *Geophys. Res. Lett.*, Vol. 40, No. 9, pp. 1691–1696, May 2013.

[4] F. Omori. Note on the preliminary tremor of earthquake motion. The journal of the College of Science, Imperial University of Tokyo, Japan = 東京帝國大學紀要. 理科, Vol. 11, No. 3, pp. 147–159, 1899.

[5] John William Strutt Rayleigh. On waves propagated along the plane surface of an elastic solid. *Proc. Lond. Math. Soc.*, Vol. s1-17, No. 1, pp. 4–11, November 1885.

[6] 斎藤正徳. 地震波動論. 東京大学出版会, 2009.

SH-wave propagation from a point source in a medium with two layers

Chapter 6

On 8 October 1909, at Kulpa Valley, a huge earthquake occurred, then it caused severe damage. A Croatian meteorologist/seismologist Andrija Mohorovičić collected seismograms in Europe, and plot the travel time curve as shown in Figure 6.1. He discovered a discontinuity at depth of 54 km. The P-wave velocity of the crust is 5.68 km/s, whereas that of the mantle is 7.75 km/s. Now it is known as Mohorovičić discontinuity (Moho discontinuity).[2] In this chapter, we learn how to infer discontinuity based on behaviors of reflected and refracted waves from a point source. For simplicity, we focus on SH wave propagations.

In the previous chapter, we learned the reflection and refraction of plane waves. They are fundamental to interpreting seismic wave propagation because a seismic wave field can be represented by a superposition of plane waves as,

$$\phi(\boldsymbol{x}, t) = \int_{-\infty}^{\infty} d\omega \int_{-\infty}^{\infty} dk_x dk_y A(k_x, k_y, \omega) e^{i\left[k_x x + k_y y + \left(\frac{\omega^2}{\alpha^2} - k_x^2 - k_y^2\right)^{1/2} z - \omega t\right]}. \tag{6.1}$$

Based on the results, we consider seismic wave propagations in a two-layer medium together with features of Green's function in an infinite medium. For simplicity, we will consider SH wave (or acoustic wave equivalently) in this chapter.
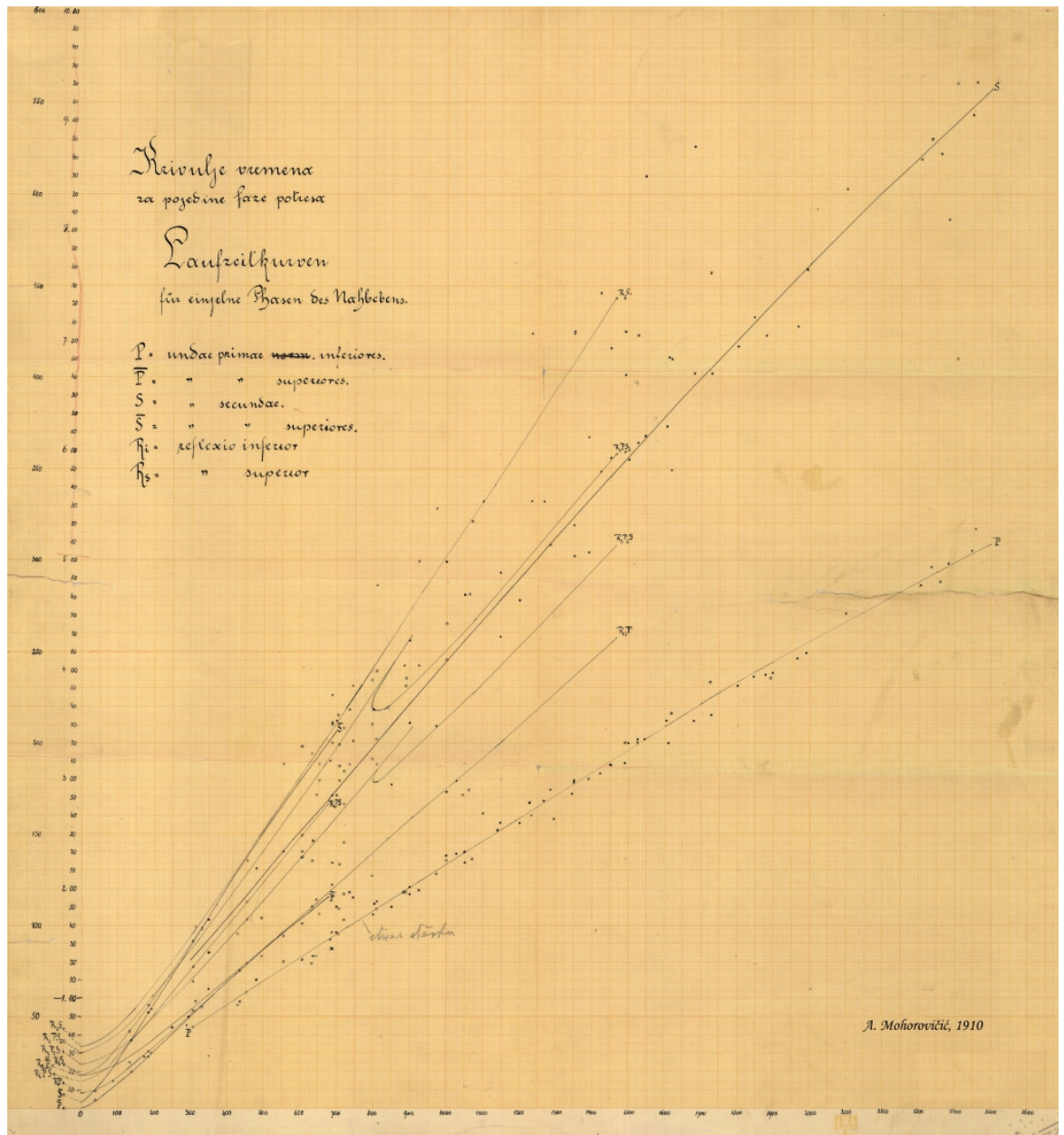
Fig. 6.1   Observed travel-time curves for the 1909 earthquake, taken from a paper trans-
lated into English (4) from Croatian[4] by Mohorovičić (1910).

§6.1 Reflection and refraction on an internal boundary

6.1.1 SH wave

Next, we consider reflection and refraction on a boundary inside an infinite elastic medium (Figure 6.2). A semi-infinite medium 2 $z < 0$ is welded to the medium 1 $z > 0$. The incident SH wave enters downward in medium 1, then it is reflected in medium 1 and refracted to medium 2. Corresponding plane wave solutions are given by

Fig. 6.2

$$z > 0 : s_y = A_1 e^{-i\omega(t - p_{1x}x - p_{1z}z)} + B_1 e^{-i\omega(t - p_{1x}x + p_{1z}z)}$$
$$\tag{6.2}$$

$$z < 0 : s_y = A_2 e^{-i\omega(t - p_{2x}x - p_{2z}z)}. \tag{6.3}$$

The first term of s_1 shows incident wave, the second term shows reflected wave, and s_2 shows refracted wave in medium 2. To meet the boundary condition of the continuity of displacement, the horizontal slowness should be the same as $p_{1x} = p_{2x}$. The condition is identical to Snell's law as

$$\frac{\sin \theta_1}{\beta_1} = \frac{\sin \theta_2}{\beta_2}. \tag{6.4}$$

To meet the condition of continuity of displacement on $z = 0$, $A_1 + B_1 = A_2$ is required. Moreover, to meet the boundary condition of continuity of stress, $\mu_1 p_{1z}(A_1 - B_1) = \mu_2 p_{2z}A_2$ is also required. Then corresponding the reflection coefficient R_{12} and the transition coefficient T_{12} are given by

$$R_{12} = \frac{B_1}{A_1} = \frac{\mu_1 p_{1z} - \mu_2 p_{2z}}{\mu_1 p_{1z} + \mu_2 p_{2z}} = \frac{\rho_1 \beta_1 \cos \theta_1 - \rho_2 \beta_2 \cos \theta_2}{\rho_1 \beta_1 \cos \theta_1 + \rho_2 \beta_2 \cos \theta_2} \tag{6.5}$$

$$T_{12} = \frac{A_2}{A_1} = \frac{2\mu_1 p_{1z}}{\mu_1 p_{1z} + \mu_2 p_{2z}} = \frac{2\rho_1 \beta_1 \cos \theta_1}{\rho_1 \beta_1 \cos \theta_1 + \rho_2 \beta_2 \cos \theta_2}. \tag{6.6}$$

Conservation of energy

Sum Energy flux which enters a unit area on $z = 0$ is $K_{in} \cos \theta_1$ should be same as the sum of the reflected wave ($K_{refl} \cos \theta_1$), and refracted wave ($K_{trans} \cos \theta_2$). In the case of SH wave, the conservation of energy is given by

$$\rho_1 \beta_1 \cos \theta_1 = \rho_1 \beta_1 \cos \theta_1 |R_{12}|^2 + \rho_2 \beta_2 \cos \theta_2 |T_{12}|^2. \tag{6.7}$$

Total reflection

When $\theta_2 > \theta_1$, total reflection occurs for incident angle θ_1 is larger than the critical angle θ_c defined by

$$\theta_c = \sin^{-1} \frac{\beta_1}{\beta_2}. \tag{6.8}$$

In this case, since p_{2z} becomes imaginary, the refracted wave in medium 2 decreases exponentially with z. The refracted wave cannot transfer energy downward in medium 2.
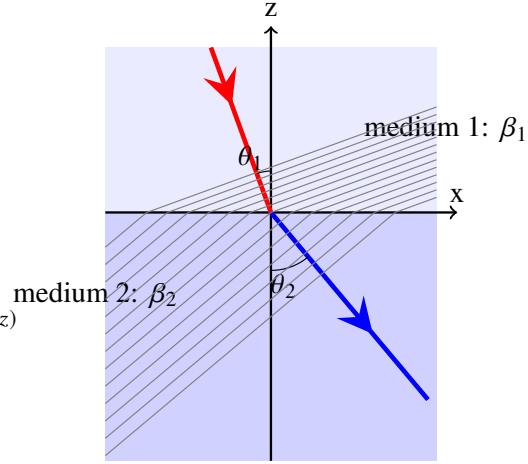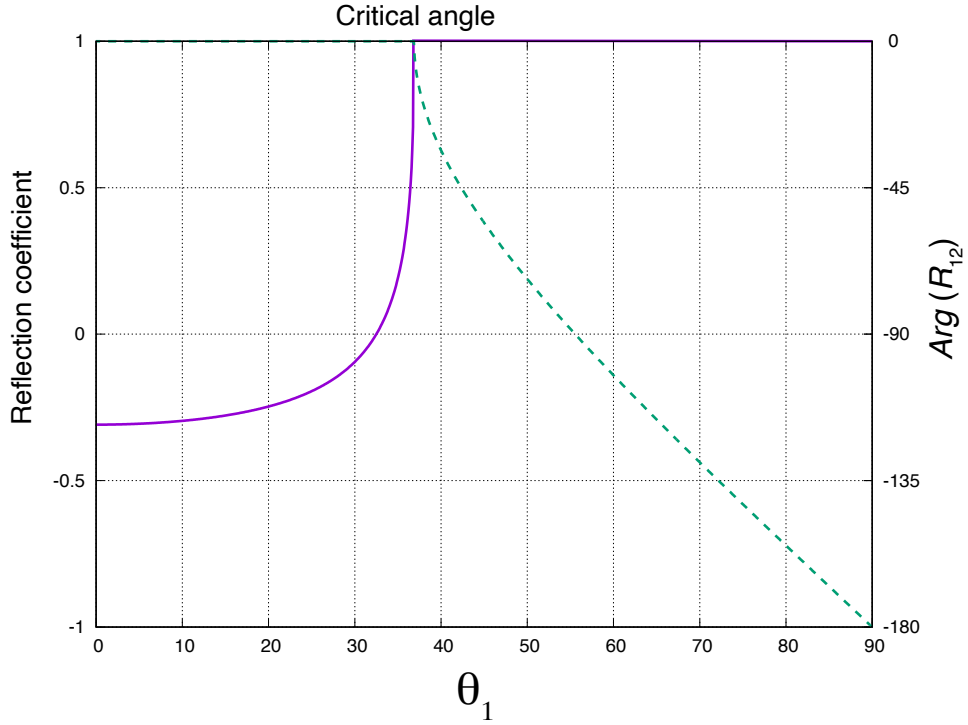
Fig. 6.3 Reflection coefficient R_{12} of SH wave on the internal boundary. The coefficient is real before the critical angle, and it becomes complex after the angle. The solid line shows the reflection coefficient, and the broken line shows the phase. $\rho_1 = 2.2 \times 10^3$ [kg/m^3], $\rho_2 = 2.5 \times 10^3$ [kg/m^3], $\beta_1 = 3$ [km/s], $\beta_2 = 5$ [km/s].

On the other hand, although the reflection coefficient R_{12} is imaginary, the absolute value is 1 (the numerator is complex conjugate to the denominator). When we consider conservation of energy of equation 6.7, $|R_{12}|^2$ is 1 and $|T_{12}|^2 = 0$. This also means the phase of the reflected wave is advanced when the total reflection is. The phase of R_{12} is given by

$$arg R_{12} = -2 \tan^{-1} \frac{\mu_2 i p_{2z}}{\mu_1 p_{1z}} = -2 \tan^{-1} \frac{\mu_2 \sqrt{p^2 - \beta_2^{-2}}}{\mu_1 \sqrt{\beta_1^{-2} - p^2}} \tag{6.9}$$

When μ_2 goes infinity, the reflection coefficient $R_{12} = -1$ represents reflection at a rigid wall.

Acoustic impedance

For simplicity, here we consider equation 6.10 for vertically propagating wave ($\theta = 0$). The reflection and transmission coefficients are give by

$$R_{12} = \frac{\rho_1 \beta_1 - \rho_2 \beta_2}{\rho_1 \beta_1 + \rho_2 \beta_2} \tag{6.10}$$

$$T_{12} = \frac{2 \rho_1 \beta_1}{\rho_1 \beta_1 + \rho_2 \beta_2}. \tag{6.11}$$

$\rho\beta$ is called acoustic impedance, which shows resistance of entering wave. The equation shows the impedance contrast determines the reflection and transmission coefficients. The

acoustic impedance is defined as the ratio between stress and particle velocity as an analogy of resistance of the electric circuit.

With increasing $\rho_2\beta_2$, the transmitted wave is harder to enter. When the two acoustic impedances match with each other as $\rho_1\beta_1 = \rho_2\beta_2$, no reflection occurs. Even if seismic velocities of two media are the same, a reflected wave occurs owing to the density contrast. In summary, the reflection and transmission coefficients do not contain information on seismic velocity contrast but also on density contrast. The coefficients are crucial for exploring density contrast at discontinuities of the Earth.

6.1.2 Reflection, refraction, and conversion of P-SV at an internal boundary

Because the calculation is complex, here I show only the results [note 1)]

$$a = \rho_2 - 2(\mu_2 - \mu_1)p^2 \qquad K = a\xi_1 + b\xi_2 \qquad N = a\eta_1 + b\eta_2 \qquad (6.12)$$

$$b = \rho_1 + 2(\mu_2 - \mu_1)p^2 \qquad L = d - 2(\mu_2 - \mu_1)\xi_1\eta_2 \quad M = d - 2(\mu_2 - \mu_1)\xi_2\eta_1 \quad (6.13)$$

$$d = \rho_2 - \rho_1 - 2(\mu_2 - \mu_1)p^2 \quad D = KN + p^2LM \qquad\qquad (6.14)$$

SV wave incidence

$$R_{SS} = \frac{1}{\Delta}\{-(a\eta_1 - b\eta_2)K + p^2[d + 2(\mu_2 - \mu_1)\xi_2\eta_1]L\}$$
$$(6.15)$$

$$R_{SP} = -\frac{\beta_1}{\alpha_1}\frac{2p\eta_1}{\Delta}[ad + 2(\mu_2 - \mu_1)b\xi_2\eta_2]$$
$$(6.16)$$

$$T_{SS} = \frac{\beta_1}{\beta_2}\frac{2\rho_1\eta_1 K}{\Delta} \qquad (6.17)$$

$$T_{SP} = \frac{\beta_1}{\beta_2}\frac{2\rho_1 p\eta_1 L}{\Delta} \qquad (6.18)$$
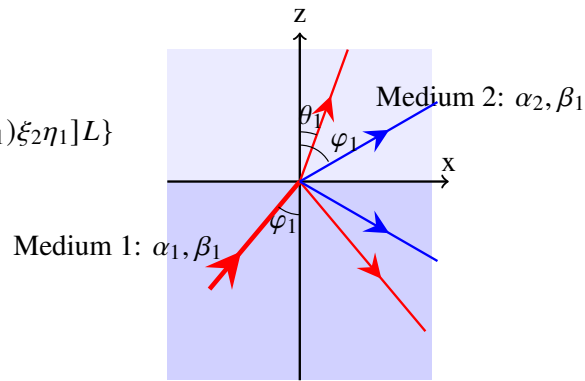
Fig. 6.4

ここで

$$p = \frac{\sin\theta_1}{\alpha_1} = \frac{\sin\theta_2}{\alpha_2} = \frac{\sin\varphi_1}{\beta_1} = \frac{\sin\varphi_2}{\beta_2} \qquad (6.19)$$

$$\xi_i^2 = \frac{1}{\alpha_i^2} - p^2, \eta_i^2 = \frac{1}{\beta_i^2} - p^2, \gamma_i^2 = 2\beta_i^2 p^2. \qquad (6.20)$$

P wave incidence

[note 1)] Read ki and Richards (2002) or 斎藤 (2009) in detail.

Fig. 6.5

$$R_{PP} = \frac{1}{\Delta}\{(a\xi_1 - b\xi_2)N - p^2[d + 2(\mu_2 - \mu_1)\xi_1\eta_2]M\}$$

(6.21)

$$R_{PS} = -\frac{\alpha_1}{\beta_1}\frac{2p\xi_1}{\Delta}[ad + 2(\mu_2 - \mu_1)b\xi_2\eta_2]$$

(6.22)

$$T_{PP} = \frac{\alpha_1}{\alpha_2}\frac{2\rho_1\xi_1 N}{\Delta}$$

(6.23)

$$T_{PS} = \frac{\alpha_1}{\alpha_2}\frac{2\rho_1 p\xi_1 M}{\Delta}$$

(6.24)

$$R_{PP} = \frac{1}{\Delta}\{(a\xi_1 - b\xi_2)N - p^2[d + 2(\mu_2 - \mu_1)\xi_1\eta_2]M\}$$

(6.25)

$$R_{PS} = -\frac{\alpha_1}{\beta_1}\frac{2p\xi_1}{\Delta}[ad + 2(\mu_2 - \mu_1)b\xi_2\eta_2]$$

(6.26)

$$T_{PP} = \frac{\alpha_1}{\alpha_2}\frac{2\rho_1\xi_1 N}{\Delta}$$

(6.27)

$$T_{PS} = \frac{\alpha_1}{\alpha_2}\frac{2\rho_1 p\xi_1 M}{\Delta}$$

(6.28)

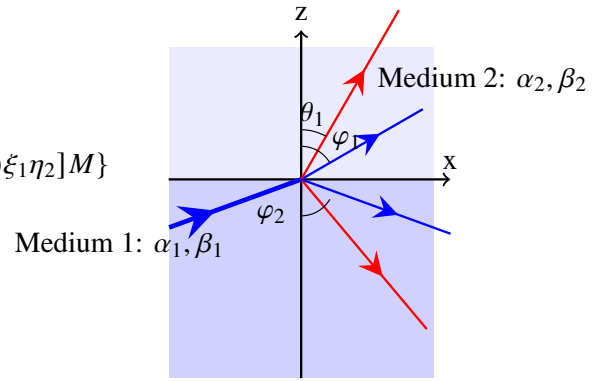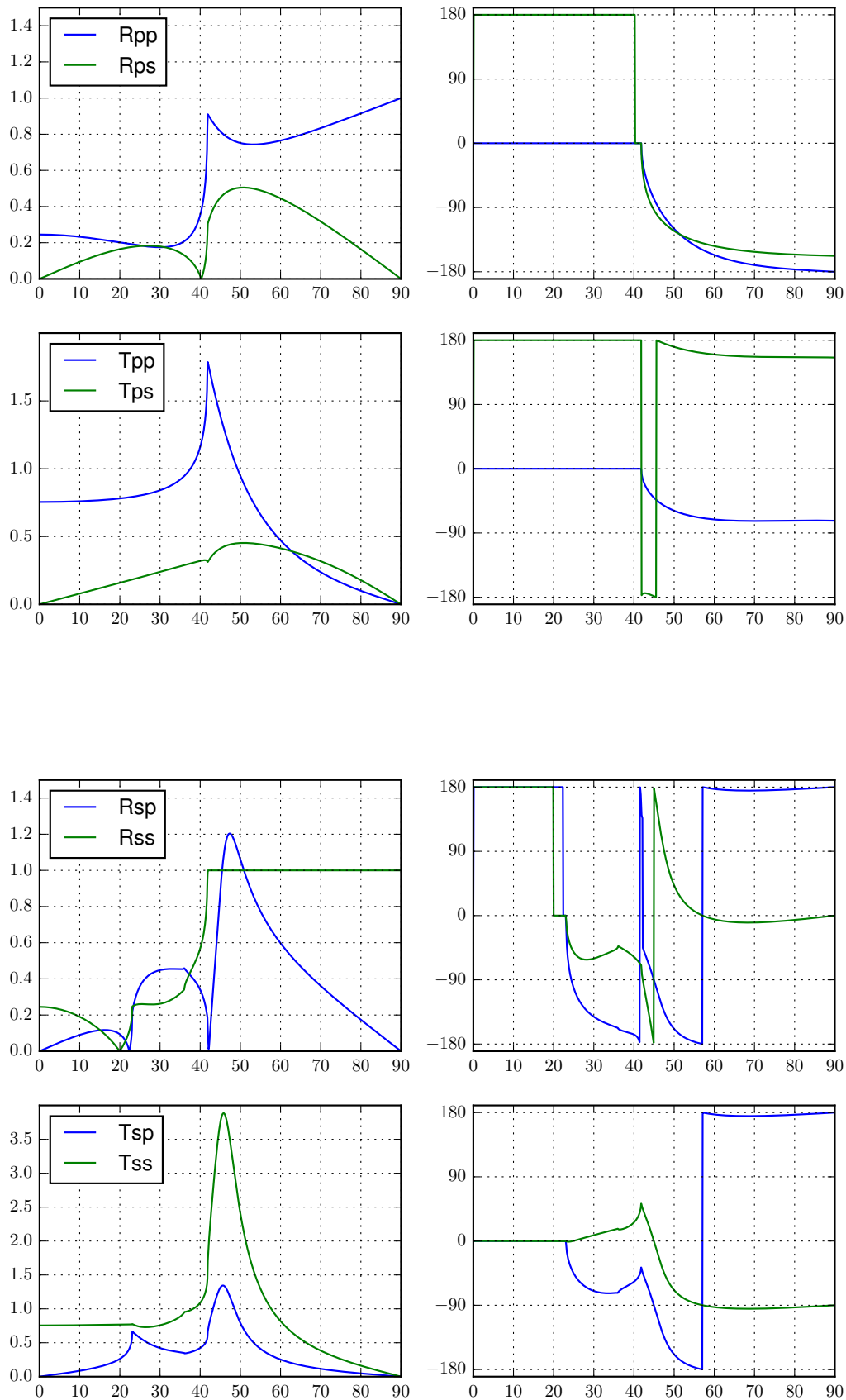Fig. 6.6   Reflection, transmission and conversion coefficients at a boundary taken from 斎
藤 (2009).[9]

6.1.3 Asymptotics for near vertical incident

This section describes the asymptotics of the coefficients for the near-vertical incident (p is enough small). Here we neglect higher-order terms of p than 2.

P wave incident

$$R_{PP} = \frac{\rho_2\alpha_2 - \rho_1\alpha_1}{\rho_2\alpha_2 + \rho_1\alpha_1} \tag{6.29}$$

$$R_{PS} = -\frac{2\alpha_1 p[\rho_2(\rho_2 - \rho_1)\alpha_2\beta_2 + 2\rho_1(\mu_2 - \mu_1)]}{(\rho_2\alpha_2 + \rho_1\alpha_1)(\rho_2\beta_2 + \rho_1\beta_1)} \tag{6.30}$$

$$T_{PP} = \frac{2\rho_1\alpha_1}{\rho_2\alpha_2 + \rho_1\alpha_1} \tag{6.31}$$

$$T_{PS} = \frac{2\rho_1\alpha_1 p[(\rho_2 - \rho_1)\alpha_2\beta_1 - 2(\mu_2 - \mu_1)]}{(\rho_2\alpha_2 + \rho_1\alpha_1)(\rho_2\beta_2 + \rho_1\beta_1)}. \tag{6.32}$$

S wave incident

$$R_{SS} = \frac{\rho_2\beta_2 - \rho_1\beta_1}{\rho_2\beta_2 + \rho_1\beta_1} \tag{6.33}$$

$$R_{SP} = -\frac{2\beta_1 p[\rho_2(\rho_2 - \rho_1)\alpha_2\beta_2 + 2\rho_1(\mu_2 - \mu_1)]}{(\rho_2\alpha_2 + \rho_1\alpha_1)(\rho_2\beta_2 + \rho_1\beta_1)} \tag{6.34}$$

$$T_{SS} = \frac{2\rho_1\beta_1}{\rho_2\beta_2 + \rho_1\beta_1} \tag{6.35}$$

$$T_{SP} = \frac{2\rho_1\beta_1 p[(\rho_2 - \rho_1)\alpha_2\beta_1 - 2(\mu_2 - \mu_1)]}{(\rho_2\alpha_2 + \rho_1\alpha_1)(\rho_2\beta_2 + \rho_1\beta_1)}. \tag{6.36}$$

R_{PP} and R_{SS} can be represented by impedance as in SH wave. Surprisingly, the conversion coefficients (e.g. T_{PS}, R_{PS}) is sensitive to density contrast and S-wave contrast explicitly. Figure 6.6 shows that this first-order approximation is valid for a large extent of slowness p.

§6.2 Radiation of seismic wave from a point source: wavefront and ray path

Here we consider propagations of a wave packet $f(t)$. Amplitude in y component s_y is given by

$$s_y(\boldsymbol{x}, t) = A(\boldsymbol{x})f(t - T(\boldsymbol{x})), \tag{6.37}$$

where $T(\boldsymbol{x})$ is the arrival time at a location $\boldsymbol{x}$, and $A(\boldsymbol{x})$ is the amplitude. The isocontour for the same arrival time of $T(\boldsymbol{x})$ is known as the "wavefront". The ray is perpendicular to the
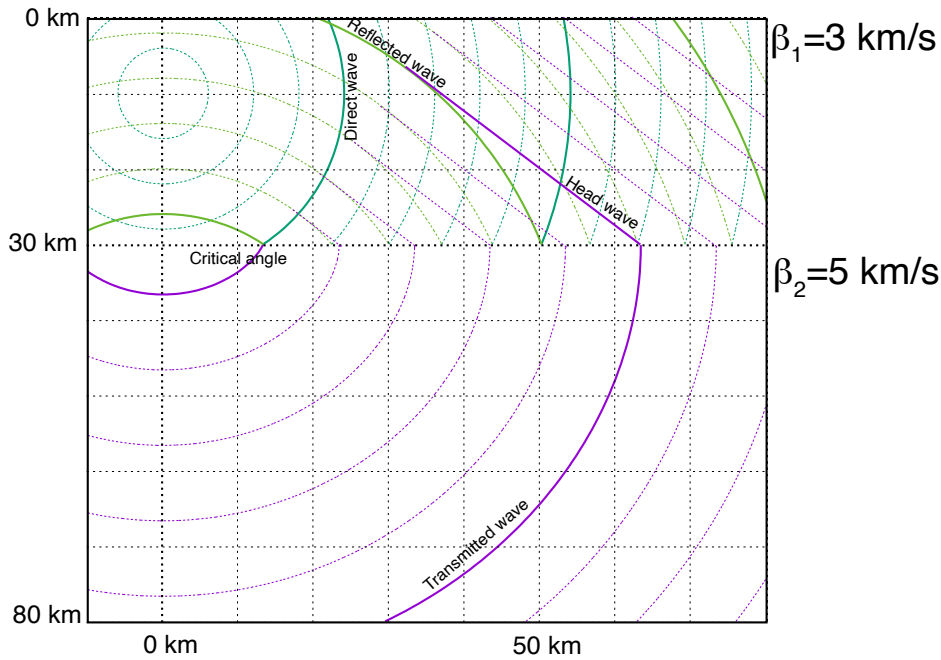
Fig. 6.7

wavefront. The direction of the ray is represented by $\hat{n} \equiv \beta \nabla T$, where β is the S-wave velocity. The comparison with a plane wave shows that ∇T corresponds to the slowness vector.

Figure 6.7 shows a typical example of wavefronts for two-layer medium. The wavefronts are associated with ripples spread out when a single pebble is dropped into water.

For understanding ray paths, the physical interpretation is feasible. Here we consider that the spatial variation of A is enough loner than the wavelength. Because the spatial derivative of A is negligible, the displacement is written as,

$$\nabla s_y = -A \nabla f = -A \frac{df}{dt} \nabla T \tag{6.38}$$

The energy flux $\boldsymbol{K}$ is given by

$$\boldsymbol{K} = \beta \hat{\boldsymbol{n}} \rho \dot{f}^2 A^2. \tag{6.39}$$

Conservation of energy along the ray path gives us the information of the amplitude. Figure 6.8 shows a typical example of ray paths.

A comparison of ray paths for reflection before the critical angle with the corresponding wavefronts in Figure 6.7 is easy to interpret. On the other hand, the behavior after the critical angle is complex. Total reflection after the critical angle causes the split between the transited and reflected wave packets. The following section explains the behavior.

§6.3 Behaviors at a discontinuity of seismic wave

In the previous chapter, we learned about reflection and transmission at a discontinuity for a plane wave. Based on the results, let us consider behaviors of seismic waves excited by a point source (Green's function) on the discontinuity. They are categorized into 4 types: direct wave, reflection wave, head wave, and transmitted wave.
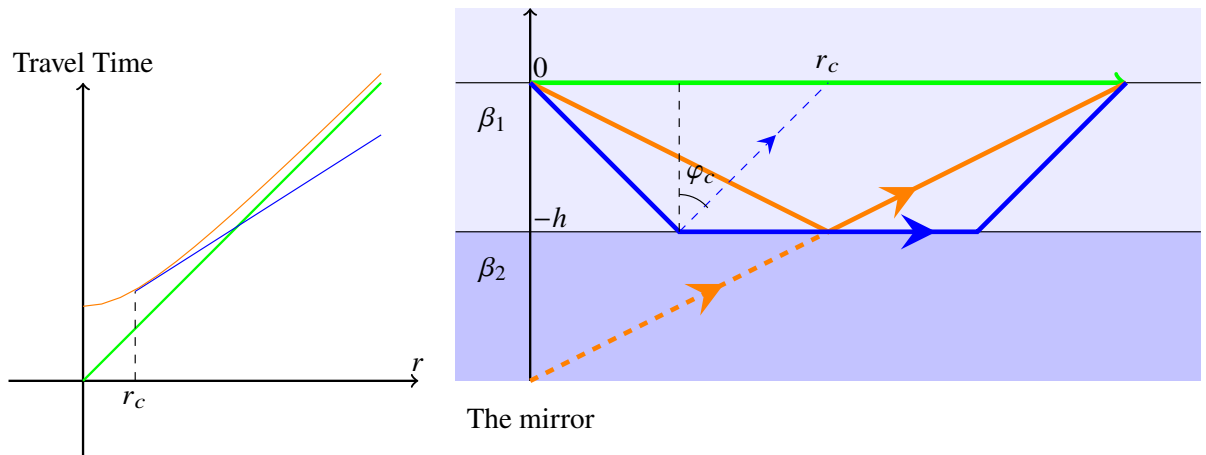
Fig. 6.8

6.3.1 Direct wave

First, let us consider the direct wave. For simplicity, we neglect free surfaces on the ground. The green line in Figure 6.8 shows the direct wave. The SH-wave propagation can be represented by a Green's function in an infinite homogeneous medium. Of course, the travel time T is proportional to the epicentral distance between the source and the station as

$$T(r) = r/\beta_1, \tag{6.40}$$

where r is the epicentral distance for the station and source in the xy plane. For a point source in the 3-D medium, the amplitude decreases with $1/r$, which is given by the conservation of energy along the path as,

$$A_d \sim \frac{1}{4\pi r} e^{ik_{\beta_1} r \mu_1 \beta_1} \tag{6.41}$$

6.3.2 Reflected wave

Next, let us consider the reflection wave. The orange line shows the reflection wave. The mirror symmetric source for the discontinuity ($z = -h$) help us to understand the ray path. The travel time is given by

$$T = 2\sqrt{h^2 + (r/2)^2}/\beta_1, \tag{6.42}$$

and the amplitude is given by

$$A_r \sim \frac{1}{4\pi R_0 \mu_1 \beta_1} R_{12}(\boldsymbol{p}) e^{i k_{\alpha_1} R_0},$$ (6.43)

where R_{12} is the reflection coefficient again. Because R_{12} is real before the critical angle, the reflection does not cause the phase shift. However, total reflection after the critical angle causes the phase shift, and the amplitude equals to 1. They are also known as post-critical reflections or wide-angle reflections.

After a critical angle, the behaviors become complex such as the splits of wavefronts and the phase shift. Behaviors of a head wave are key to understanding the complexity, as explained in the next subsection.

Fig. 6.9 Example of wide-angle reflection. After the critical angle, we can see the reflected wave arrives before the ray theoretical value because of the phase shift due to the inhomogeneous wave.

6.3.3 Head wave

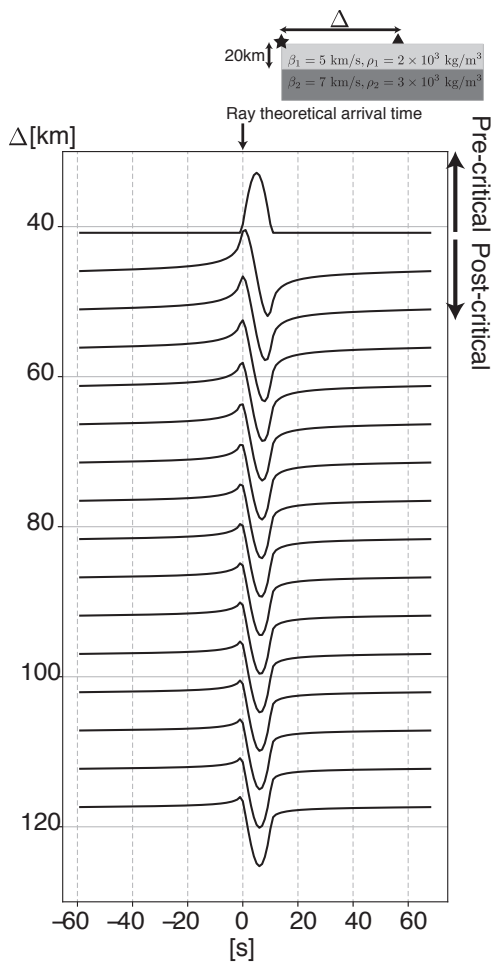The third type is a head wave (also known as a refracted wave). The wave enters the second layer with a critical angle, and it propagates in the horizontal direction along the uppermost part of the second layer (Figure 6.8). The travel time T_H is given by

$$T_H(r) = \frac{r - r_c}{\beta_2} + \frac{r_c}{\cos \varphi_c \beta_1}. \quad (6.44)$$

The amplitude A is written by

Fig. 6.10   A schematic figure of head wave based on Huygens' principle.

$$A_{head} \sim \frac{i}{2\pi\omega\mu_1\beta_1} \frac{\rho_2\beta_2}{\rho_1(1 - \beta_1^2/\beta_2^2)} \frac{1}{\sqrt{r}D^{3/2}} e^{i\omega t_h}$$
$$(6.45)$$

Although the frequency- and distance- dependencies are difficult to understand, I try to explain in an intuitive manner.

Figure 6.7 shows wavefronts of the direct and the reflected and refracted wave share a point on the boundary. After the critical reflection, they are split into two groups: one is a direct and reflected wave, and the other is a head wave and transmitted wave. Exactly speaking, inhomogeneous waves along the boundary also exists.

Let us consider the details of the split. A major difference between the two groups originated from the fact that the direct wave cannot enter the second layer into the second medium. When the transition from the transmitted wave to the inhomogeneous wave in the second layer, let us consider a secondary point source with a spatial scale of about the wavelength at r_c (finite frequency effect) based on the representation theorem, which is a natural extension of Huygens principle. As in the case of diffraction at a narrow slit, an SH wave is radiated in the right direction. Although the ray path of the head wave seems to be parallel to the boundary in layer 2, the path is slightly inclined to owe the source depth of an about wavelength. Thus SH wave is transmitted toward layer 1, as predicted by the Huygens principle. The incident angle can be estimated to be $90°\varphi_1 \sim D/\lambda$ The corresponding transmission coefficient T_{12} can be approximated by

$$T_{21} = \frac{2\rho_2\beta_2 \cos \varphi_2}{\rho_1\beta_1 \cos \varphi_1 + \rho_2\beta_2 \cos \varphi_2} \sim \frac{2\rho_2\beta_2\lambda/D}{\rho_1\beta_1 \cos \varphi_c} \sim \frac{1}{D\omega} \quad (6.46)$$

The amplitude decreases as $r^{-1/2}D^{-1}D^{-1/2}$, where (1) $r^{-1/2}$ represents geometrical spreading of the wavefront in xy plane, (2) $D^{-1/2}$ represents geometrical spreading of the wavefront in xz plane, and (3) D^{-1} represents contribution by the transmission coefficient. The frequency dependence of ω can be explained by the frequency dependence of the incident angle φ_1, which is proportional to the inverse of the wavelength. This is why the low-frequency component of the head wave is emphasized. This equation exhibits that the head wave can be represented by the integration of the direct wave in time domain[note 2]. An example of observation in Figure 6.17 shows the dominance of low-frequency components in the head wave.

Because a realistic Earth structure is more complex, the ray path is not so simple. For example, the Pn wave (head wave for Moho discontinuity) is refracted in the uppermost mantle: the behavior may be easy to understand. The next section explains such a case. [note 3]。
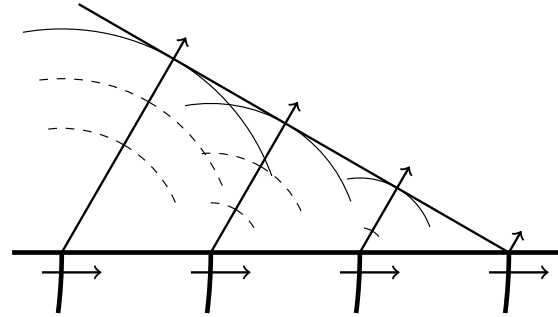
[note 2] The phase delay of i is explained by caustic introduced in the next section. A more exact discussion mathematically is given by Aki and Richards[1] for example. In the textbook, the complex integral is used for the evaluation. On the other hand, I try to explain these features in a physically intuitive manner in this lecture.

[note 3] See Stein and Wysession[8] §3.2.3 for details.

6.3.4 Transmitted wave

Last, let us consider the transmitted wave. Because this wave does not return to the surface, of course, we cannot measure the travel time at a surface station.

$$A_t \sim \frac{1}{4\pi\sqrt{r}} T_{12}(\boldsymbol{p}) \left(r_1 + r_2 \frac{\beta_2 \cos^2 \varphi_1}{\beta_1 \cos^2 \varphi_2} \right)^{-1/2} , e^{i(k_{\alpha_1} r_1 + k_{\alpha_2} r_2)}$$

(6.47)

where r_1 is the length of line OA, r_2 is length of line AB, and r is length of line OB. A wavefront enters the discontinuity with incident angle φ_1, and it is transmitted with the emergency angle φ_2. Let us estimate the amplitude at point B based on energy conservation. Figure 6.11 shows a cross-section of the 3-D medium along line OB. δl shows interception length at point B perpendicular to the ray path. A simple geometrical estimation leads to
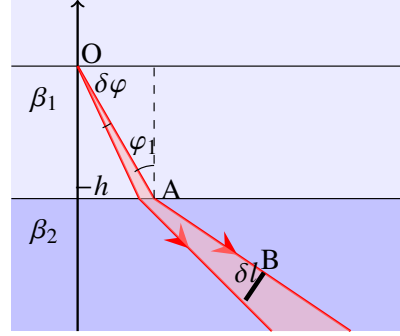
Fig. 6.11

$$\delta l = \frac{\cos \varphi_2}{\cos \varphi_1} \left(r_1 + r_2 \frac{\beta_2 \cos^2 \varphi_1}{\beta_1 \cos^2 \varphi_2} \right) \delta\varphi.$$

(6.48)
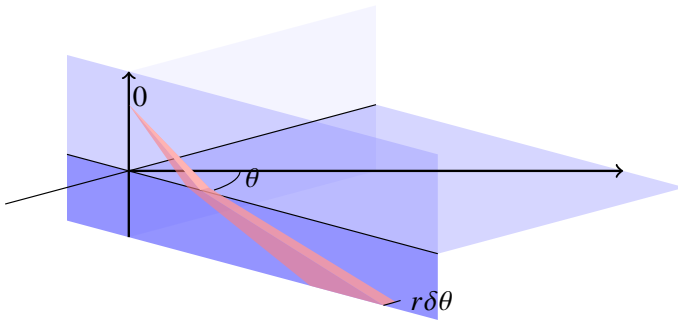
Fig. 6.12 Enter of a ray path toward the discontinuity. The ray path is refracted to the radial direction, whereas it is not toward the tangential direction.

Figure 6.12 shows a bird's view of the ray path. The ray path is refracted to the radial direction (on rz plane), whereas it is not toward the tangential direction (θ). Therefore a cross-section area at point δr away from the origin is given by $\delta r^2 \delta\theta\delta\varphi$, and a cross-section area at point B is given by $r\delta\theta\delta l$. Here we define amplitude A_i on a unit sphere in medium 1. The conservation of energy along the ray leads to

$$\left(\frac{\rho_2 \beta_2 \cos \varphi_2}{\rho_1 \beta_1 \cos \varphi_1} |T_{12}|^2 \right) \rho_1 A_1^2 \omega^2 \beta_1 \delta\varphi\delta\theta = \rho_2 A_t^2 \omega^2 \beta_2 \delta l r \delta\theta.$$

(6.49)

Note that the transmission coefficient is multiplied by $\frac{\rho_2 \beta_2 \cos \varphi_2}{\rho_1 \beta_1 \cos \varphi_1}$.

Energy normalization of reflection and transmission coefficients

In the previous chapter, I explained the reflection and transmission coefficients. They are defined by the amplitude ratio between the incident wave and the transmitted or reflected

wave. When we consider energy conservation, energy normalization of the coefficients gives us the physical meaning explicitly.

Conservation of energy (eq. 6.50) for the reflection and transmission is given by

$$\rho_1 \beta_1 \cos \varphi_1 = \rho_1 \beta_1 \cos \varphi_1 |R_{12}|^2 + \rho_2 \beta_2 \cos \varphi_2 |T_{12}|^2. \tag{6.50}$$

Both sides divided by $\rho_1 \beta_1 \cos \varphi_1$ leads to

$$1 = |R_{12}|^2 + \left| \frac{\rho_2 \beta_2 \cos \varphi_2}{\rho_1 \beta_1 \cos \varphi_1} T_{12} \right|^2. \tag{6.51}$$

Here we define a energy normalized transmission coefficient T_{12}^{norm} as,

$$T_{12}^{norm} = \sqrt{\frac{\rho_2 \beta_2 \cos \varphi_2}{\rho_1 \beta_1 \cos \varphi_1}} T_{12}^{\text{note 4)}}. \tag{6.52}$$

Thus, this section explains the behaviors of Green's function for a two-layer medium. In the next section, I will introduce ray theory for discussions of seismic wave propagations in a multi-layer structure.

──── Problem 6.1 ────

Derive eq. 6.48. This is a simple geometrical problem.

[note 4)] See a textbook by Shearer[7] for details. Sections of ray theory are easy-to-grasp.
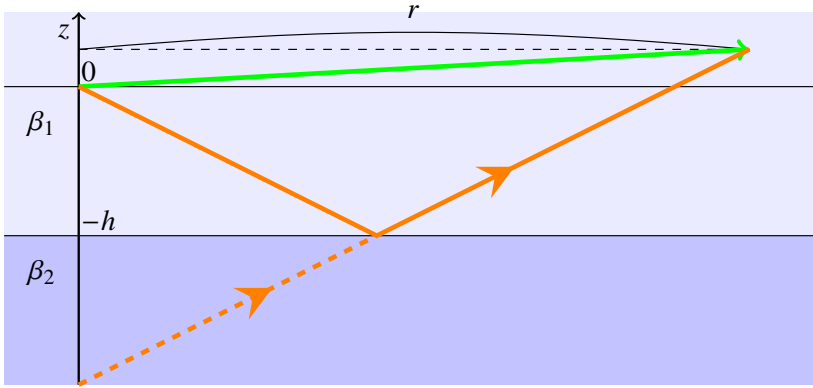
The mirror

Fig. 6.13

▌ 6.3.5 Evaluation of integral: stationary phase approximation

The previous sub-section physically interpreted direct, reflected, transmitted, and head waves. Now let us consider them more quantitatively.

As mentioned at the beginning of this chapter, wave propagation in a two-layer medium can be exactly evaluated by decomposing it into plane waves and multiplying each plane wave by the reflection-transmission coefficient and integrating it in the wavenumber domain. This expression can be naturally extended to cylindrical waves (Hankel function) and is expressed as The potential χ_d representing a direct wave is given by the integration of slowness as

$$\chi_d = \frac{\omega}{4\pi\mu_1} \int_{-\infty}^{\infty} H_0^{(1)}(\omega p r) \frac{e^{i\omega\xi_1|z|}}{-2i\xi_1} p\, dp. \tag{6.53}$$

Here, let us consider a case of ξ_1 becomes imaginary. As χ_d is physically meaningful (not diverging) for $p \longrightarrow \infty$, we define the sign as

$$\xi_1 = \begin{cases} \sqrt{\beta_1^{-2} - p^2} & |p| \leq 1/\beta_1, \\ \sqrt{p^2 - \beta_1^{-2}}\, i & |p| > 1/\beta_1. \end{cases} \tag{6.54}$$

Potentials χ_r and χ_t for reflected and transmitted waves are also given by

$$\chi_r = \frac{\omega}{4\pi\mu_1} \int_{-\infty}^{\infty} R_{12}(p) H_0^{(1)}(\omega p r) \frac{e^{i\omega\xi_1|z+2h|}}{-2i\xi_1} p\, dp, \tag{6.55}$$

$$\chi_t = \frac{\omega}{4\pi\mu_1} \int_{-\infty}^{\infty} T_{12}(p) H_0^{(1)}(\omega p r) \frac{e^{i\omega(\xi_1 h - \xi_2(z+h))}}{-2i\xi_1} p\, dp. \tag{6.56}$$

It is important to note that the reflection potential χ_r represents both reflected and head waves.

This integral is numerically evaluated in Figure 6.14. [note 5)]. The direct wave is impulsive, showing that it propagates without changing its shape. The head wave is clearly visible from

---

[note 5)] ξ_1 has a singularity. In order to avoid the singularity in the numerical integration, we gave a very small imaginary part to the elastic constants. This physically corresponds to giving a weak damping

around 60 km, and it is also evident that it is predominantly long-period. The reflected waves are pulse-like at stations close to the epicenter (up to about 20 km), but when it exceeds the critical angle (wide-angle reflection), the reflected waves gradually shift in phase.

The numerical integration results show that, indeed, this integral (Weyl's table expression) seems to be correct. To grasp this integral roughly, let us consider its approximate behavior. Here we will consider direct-directed wave as the simplest case.

First, assuming that the propagation distance is sufficiently large compared to the wavelength, the Hankel function is approximated by

$$H_0^{(1)}(z) \sim \sqrt{\frac{2}{\pi z}} e^{i(z-\pi/4)}. \tag{6.57}$$

Then, χ_d can be approximated by

$$\chi_d \sim \frac{1}{4\pi\mu_1} \sqrt{\frac{2\omega}{\pi r}} e^{-i\pi/4} \int_{-\infty}^{\infty} \frac{e^{i\omega(pr+\xi_1|z|)}}{-2i\xi_1} \sqrt{p}\,dp. \tag{6.58}$$

Here we consider a case for z=20 km, $r = 30$ km, $f = 2\pi 5$ [Hz], and $\beta = 3$ km/s, Figure 6.15 plot the integrand

$$\frac{e^{i\omega(pr+\xi_1|z|)}}{-2i\xi_1} \sqrt{p}. \tag{6.59}$$

The figure shows the oscillatory shape in most locations, but the oscillation stops near $p\beta_1 = 0.8$. When integrated, the contribution near this point becomes large.

Let us now evaluate the integral using stationary phase method. Because the part of the gentle oscillation shows a location where the phase change is small,

$$\frac{d\omega(pr - \xi_1|z|)}{dp} = 0. \tag{6.60}$$

Then,

$$\frac{d(pr - \xi_1|z|)}{dp} = r - |z|\frac{\xi_1}{dp} = r - \frac{|z|p}{\xi_1} = 0. \tag{6.61}$$

Therefore, the contribution of the integral near p (called the stationary point) which satisfy

$$p_0 = \sqrt{\frac{r^2}{\beta_1^2 d^2}} \tag{6.62}$$

becomes large, where d is the distance $\sqrt{r^2 + z^2}$.

Although the calculations are a little complicated [note 6)], the integrand can be evaluated by Tayler expansion up to the second order. Because the first-order term disappears from the condition to be the stationary point, we can evaluate the correpsonding phase up to the second order as

$$\omega(pr - \xi_1|z|) = \omega\left(\frac{d}{\beta_1} - \frac{d^3\beta_1}{|z|^2}\frac{(p - p_0)^2}{2}\right). \tag{6.63}$$

[note 6)] This subsection plant to explain stationary phase method. The following is a simple calculation policy, but since the calculations are complicated. You can skip over the evaluations below.

With an assumption that ξ_1 and p are small enough near the stationary point, the inegrand χ_d can be evaluated up to the second order terms of the Tayler expansion as

$$\chi_d \sim \frac{1}{4\pi\mu_1}\sqrt{\frac{2\omega}{\pi r}}e^{-i\pi/4}\int_{-\infty}^{\infty}\frac{e^{i\omega\left(\frac{d}{\beta_1}-\frac{d^3\beta_1}{|z|^2}\frac{(p-p_0)^2}{2}\right)}}{-2i\frac{|z|}{d\beta_1}}\sqrt{p_0}dp, \tag{6.64}$$

where

$$\xi_1\big|_{p=p_0} = \frac{|z|}{d\beta_1}. \tag{6.65}$$

This integral can be calculated by using the Fresnel integral

$$\int_{-\infty}^{\infty}e^{-ia^2x^2}dx = \frac{1}{|a|}\sqrt{\pi}e^{-i\pi/4}. \tag{6.66}$$

Although the calculation is complicated, the potential χ_d can be calculated as

$$\chi_d \sim \frac{1}{4\pi\mu_1}\sqrt{\frac{2\omega}{\pi r}}e^{i\left(\omega\frac{d}{\beta_1}+\frac{\pi}{4}\right)}\frac{d\beta_1\sqrt{p_0}}{2|z|}\int_{-\infty}^{\infty}e^{-i\omega\left(\frac{d^3\beta_1}{2|z|^2}p^2\right)}dp \tag{6.67}$$

$$= \frac{1}{4\pi\mu_1}\sqrt{\frac{2\omega}{\pi r}}e^{i\left(\omega\frac{d}{\beta_1}+\frac{\pi}{4}\right)}\frac{d\beta_1\sqrt{p_0}}{2|z|}\int_{-\infty}^{\infty}e^{-i\omega\left(\frac{d^3\beta_1}{2|z|^2}p^2\right)}dp \tag{6.68}$$

$$= \frac{1}{4\pi\mu_1}\sqrt{\frac{2\omega}{\pi r}}e^{i\left(\omega\frac{d}{\beta_1}\right)}\frac{\sqrt{r\pi}}{2d\sqrt{\omega}} \tag{6.69}$$

$$= \frac{1}{4\pi\mu_1 d}e^{i\omega\frac{d}{\beta_1}}. \tag{6.70}$$

For an external force

$$H(t)\nabla\times(0,0,\delta(\boldsymbol{x})), \tag{6.71}$$

we can evaluate displacement A_d from the potential χ_d as

$$A_d = \frac{1}{4\pi\mu_1\beta_1 d}e^{i\omega\frac{d}{\beta_1}}, \tag{6.72}$$

which is identical to the exact solution by chance.

Next, let's consider reflected and head waves (χ_r and χ_t). The reflected wave is similar to the direct wave, with a larger contribution from the stationary phase. Next, let's consider the envelope. You can see that the shape of the envelope changes dramatically at around $p\beta_2 = 1$. This is because the reflection coefficient changes significantly at around the critical angle. At the point, the condition of stationary phase approximation, which is required to apply the stationary phase method, does not hold. Therefore, even when oscillating rapidly outside the stationary point, the integral contribution near $p\beta_1$ does not cancel each other out. This contribution corresponds to the head wave.
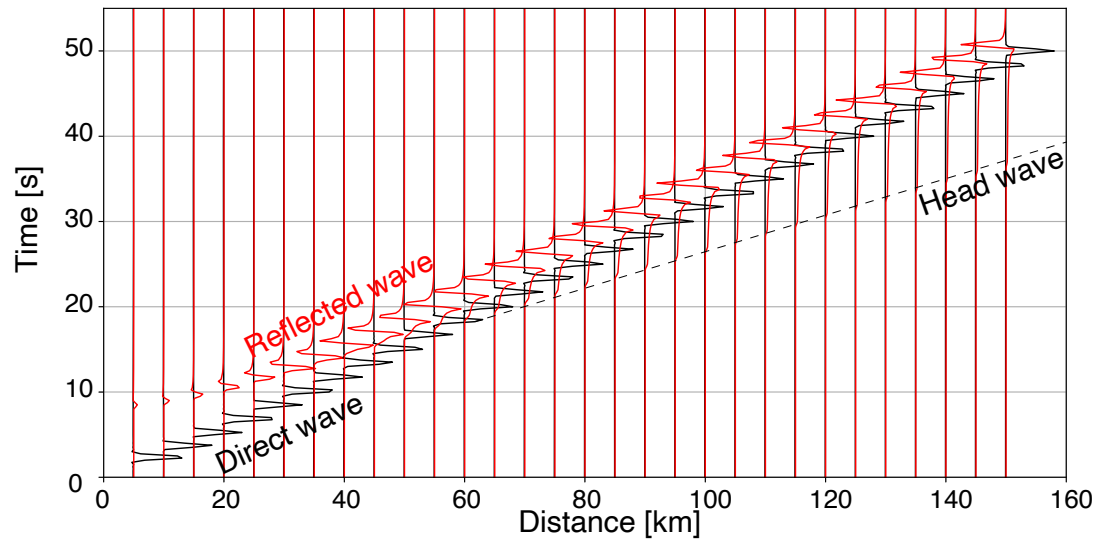
Fig. 6.14 An example of numerical evaluation of the integrated for $\beta_1 = 3$ [km/s], $\beta_2 = 5$ km/s and $rho_1 = rho_2$. The hypocenter is located at $z = 10$ km and the observed station is located at $z = 15$ km.
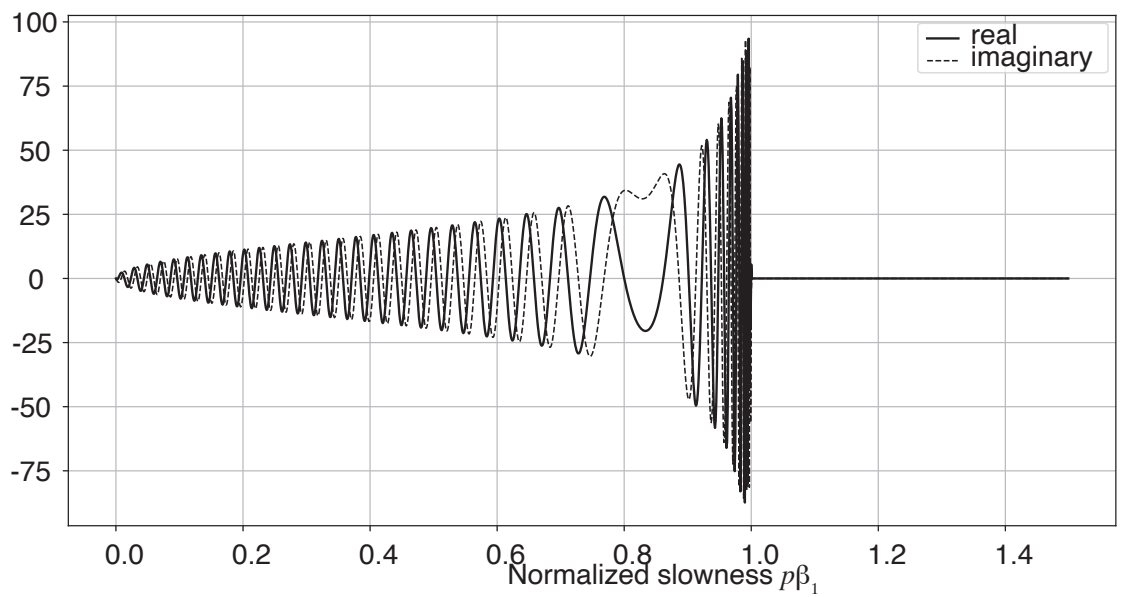
Fig. 6.15 The integrated of the direct wave for $z=20$ km, $r = 30$ km, $f = 2\pi5$ [Hz], $\beta = 3$ km/s. This figure shows rapid   oscillations.
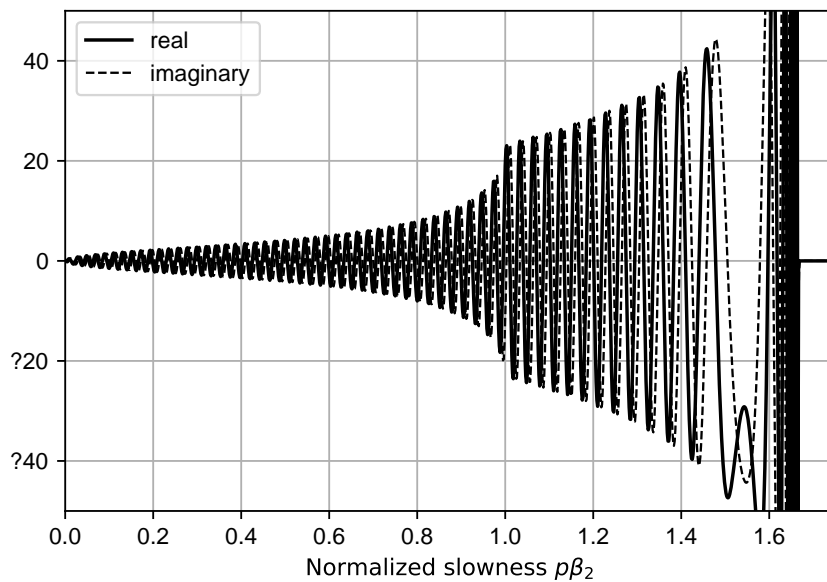
Fig. 6.16 The integrated of the reflection wave and the head wave for z=20 km, $r = 30$ km, $f = 2\pi 5$ [Hz] and $\beta = 3$ km/s. This figure shows rapid oscillations.

6.3.6 An example of actual records

Figure 6.17 shows a record section when an earthquake with Mj 5.2 at Shimane prefecture on June 4th 2011. The figure shows the first arrivals of Pg (direct wave, which propagates in the crust) up to an epicentral distance of about 170 km. Farther than the distance, the first arrivals are Pn wave arrivals (head wave for Moho discontinuity). The dominant frequency of the Pn wave is longer than the direct wave (Pg wave). In contrast, reflection phases (PmP) exhibit complex wave propagations. The complexity originated from scattering owing to lateral heterogeneities in the crust. At higher frequencies, the travel times of the first arrivals give us robust information because they are not disturbed by the scattering.

The slopes of Pg and Pn show that $\beta_1 \sim 6$ km/s, and $\beta_2 \sim 8$ km/s. A cross-over point between Pg- and Pn-arrivals at distance x_d is given by $x_d = 2h\sqrt{(\beta_1 + \beta_2)/(\beta_2 - \beta_2)}$. Based on the observed x_d of about 170 km, the crust thickness is estimated to be 30 km. Although, of course, this estimation is oversimplified, a similar simple estimation is feasible for grasping the propagation properties. For a more realistic situation, the ray theory introduced in the next chapter is feasible.
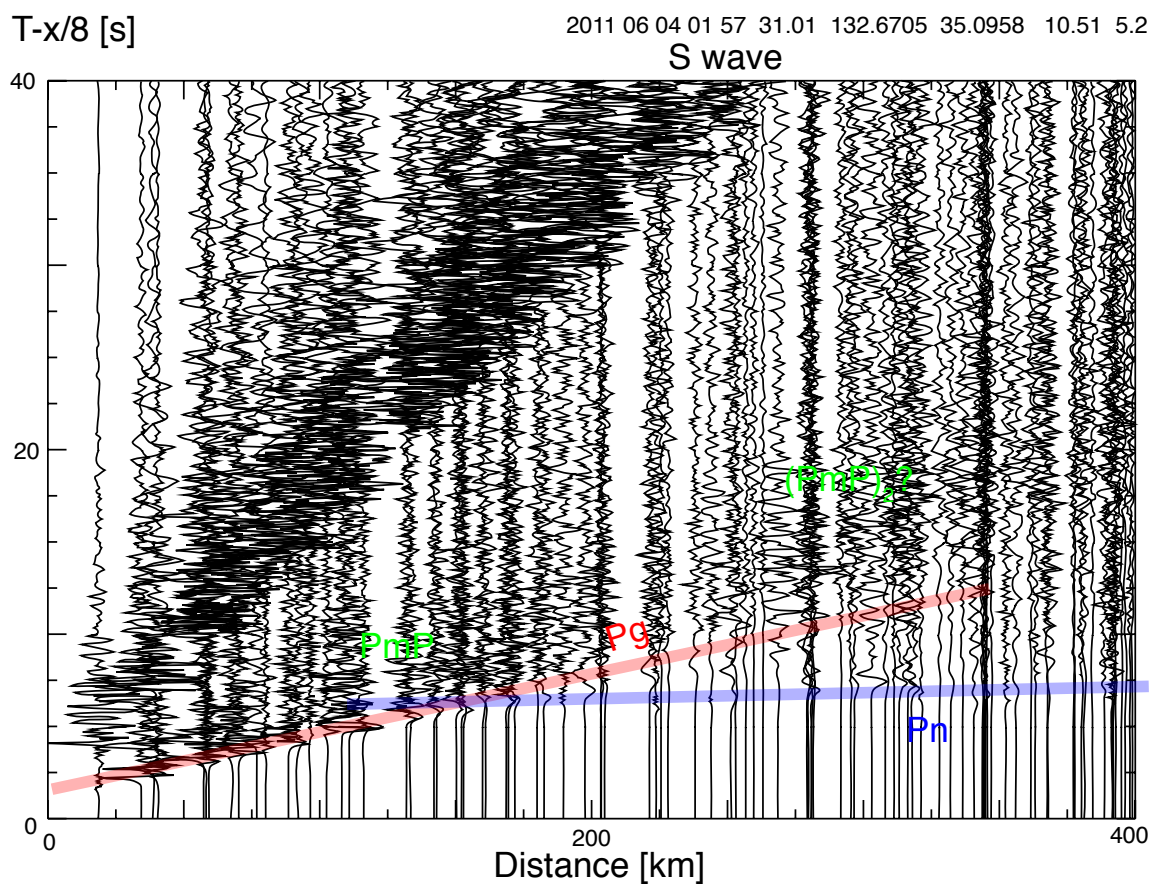
Fig. 6.17   Seismograms recorded by Hi-net station against the epicentral distances when an earthquake with Mj 5.2 at Shimane prefecture on June 4th in 2011. Although the first arrivals are easy to pick, the later phases show complex propagation properties. The complex features originated from lateral heterogeneities in the crust, although the lateral heterogeneities in the Chugoku region are weakest in Japan islands

---

Problem 6.2

The website demonstrates SH-wave propagation in a two-layer medium (2-D). Based on the seismograms, we can estimate (1) the S-wave ratio between the 1st layer and the 2nd layers and (2) the density ratio between the 1st layer and the 2nd layers.

1. Using the whole wave field (depth section in the upper panel), estimate the S-wave ratio between the layer and the density ratio.
2. Using only surface records (seismograms shown in the lower panel) estimate the S-wave ratio between the layer and the density ratio.

Here we assume that the source depth is known. You do not need to consider measurement errors.
http://www.eri.u-tokyo.ac.jp/people/knishida/Seismology/wave2D2.
html
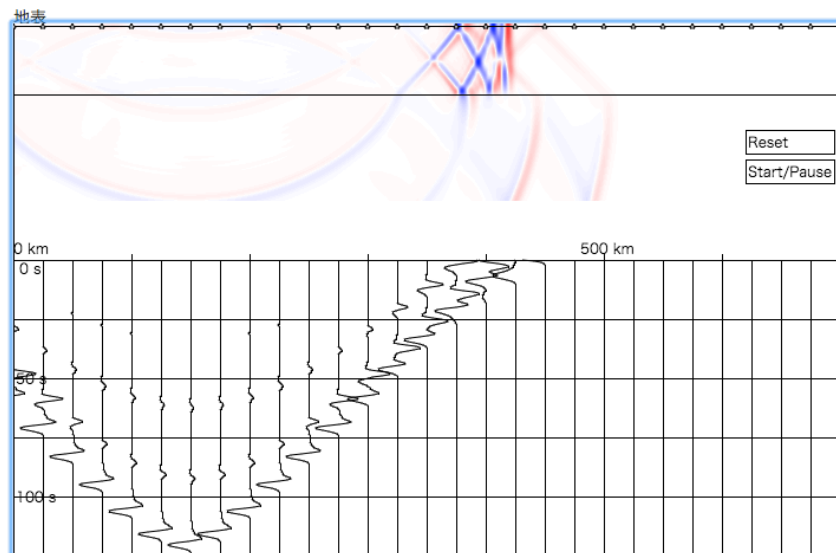
Fig. 6.18   Example of the demonstration

§6.4 Inhomogeneous wave: Love wave and Scholte wave

In the case of a semi-infinite medium, only a Rayleigh wave can exist as an inhomogeneous wave; what about the two-layer case? Let us consider the case where there is a layer of thickness h below the surface welded with a semi-infinite medium below it (Figure6.19). An inhomogeneous wave can exist because the wave is trapped in the above low-velocity layer. First, for the SH wave case, we will consider a wave known as Love wave.[3] Next, for the case where the first layer is fluid and the second layer is solid, it is known as Scholte wave.[6] We will consider each wave in this section.
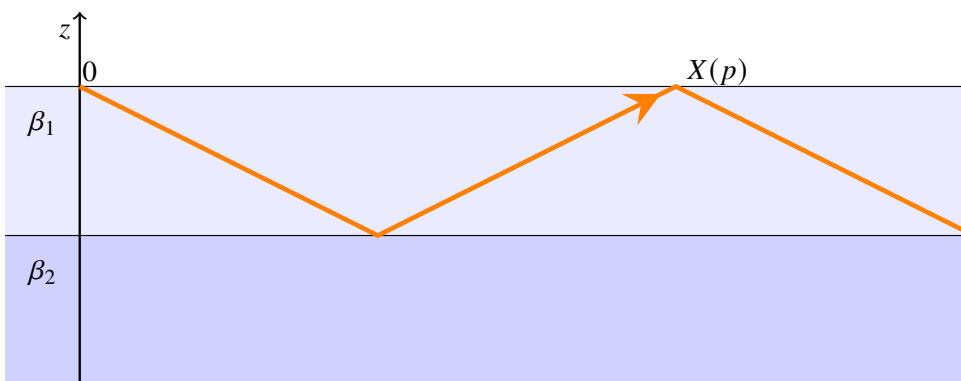
Fig. 6.19

6.4.1 Love wave

First, let us consider how the Love wave propagates (Figure6.20). ∘ in the figure shows a marker for the ground displacement. You can see in the figure how the ground is deformed horizontally. Move the cursor over the figure and press the s key on the keyboard; the Love wave starts to propagate to the right. The circle moving in the font of the page is shown in red and the circle moving in the back of the page is shown in light blue.

Love waves occur when a soft layer overlies a hard layer. For example, a soft crust overlying a stiff mantle. In this figure, circles are placed every 10 km along the vertical axis (depth) and every 6.25 km along the horizontal axis (horizontal). The fourth ∘ in the depth direction is at the boundary between the crust and the mantle (the Moho discontinuity). You can see how the waves are efficiently
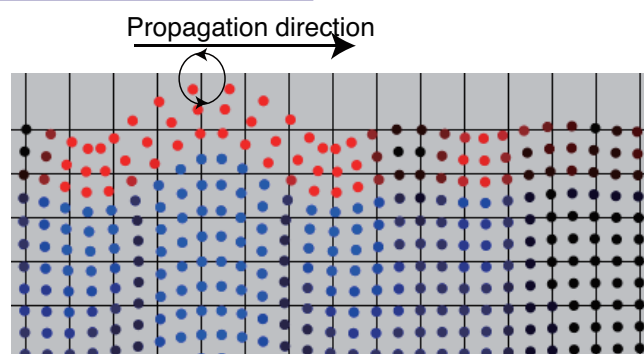
Fig. 6.20 A snapshot of a demonstration of Love wave propagation. Sea the following web application: https://www.eri.u-tokyo.ac.jp/people/knishida/Seismology/Love_wave.html. Play the application for the understandings.

propagating horizontally through the crust.

You can see how the shape of the wave has changed compared to the beginning of the wave and its propagation. The red areas extend both horizontally and vertically. On the other hand, the green part is concentrated near the surface. You can see the delayed propagation of the green part. The speed of wave propagation changes depending on the wavelength and the shape of the wave changes. This phenomenon is called dispersion. In this case, waves with longer wavelengths travel faster, and waves with shorter wavelengths travel slower. This is because long waves are strongly affected by the stiff layer (deep layer: mantle).

Standing wave

This sub-section has described the properties of the Love wave qualitatively, but physically it can be thought of as a standing wave with the energy trapped in the first layer. Let us consider the case where β_2 is infinite (bottom is a rigid wall) as an extreme limit. This is the problem of the so-called oscillation of an air column. Assuming that the wave propagates in the vertical direction, the stress is zero at the surface, so $s_y \propto \cos(kz - \omega t)$. At depth h, the phase is π shifted due to the fixed edge. At the ground surface, the phase is not shifted by reflections because of the open edge. Therefore, considering that the phase difference with the wave reflected there is 2π,

$$k \cdot 0 - \omega t = k(2h) - \omega t + \pi + 2n\pi. \tag{6.73}$$

Because $\lambda = 2\pi/k$, we obtain the following relation:

$$\lambda = -\frac{2h}{n + \frac{1}{2}}. \tag{6.74}$$

Let us make a similar estimate for the Love wave below.

Since we are now considering a situation where energy is trapped in the first layer, we assume that the incident wave is totally reflected beyond the critical angle (see section 6.1.1). The phase of the reflection at the boundary between the first and second layers is shifted by

$$arg R_{12} = -2\tan^{-1} \frac{\mu_2 i p_{2z}}{\mu_1 p_{1z}} = -2\tan^{-1} \frac{\mu_2 \sqrt{p^2 - \beta_2^{-2}}}{\mu_1 \sqrt{\beta_1^{-2} - p^2}}. \tag{6.75}$$

The difference from the air column case is that once the wave is reflected, it returns to the surface point X (Figure 6.19). This means that the phase of the incident SH wave at $(X, 0)$ must be the same as that of the reflected wave. The two-way travel time T can be written by

$$T = 2\sqrt{X^2 + h^2}. \tag{6.76}$$

During the propagation, the incident wave advances in phase by Xp. The condition requires the following relation:

$$T + arg R_{12} = pX + 2n\pi. \tag{6.77}$$

Because

$$X = \frac{ph}{\sqrt{\beta_1^{-2} - p^2}} \tag{6.78}$$

in summary, we obtain the following relation:

$$\tan\left[h\omega\sqrt{\beta_1^{-2} - p^2}\right] = \frac{\mu_2\sqrt{p^2 - \beta_2^{-2}}}{\mu_1\sqrt{\beta_1^{-2} - p^2}}. \tag{6.79}$$

This equation is known as the characteristic equation for Love waves. To improve the perspective of the equation, we can rewrite the relation as

$$\tan\left(\frac{h\omega}{\beta_1}\beta_1\eta_1\right) = \frac{\mu_2}{\mu_1}\frac{\sqrt{1 - (\beta_1/\beta_2)^2 - (\beta_1\eta_1)^2}}{\beta_1\eta_1}, \tag{6.80}$$

where we define $\eta_1 \equiv \sqrt{\beta_1^{-2} - p^2}$, and we choose $\beta_1\eta_1$ as a variable. Figure 6.21 shows t he left and right sides of the equation are plotted as functions of $\beta_1\eta_1$, respectively. When the two lines cross each other, the condition is satisfied and a Love wave can exist.
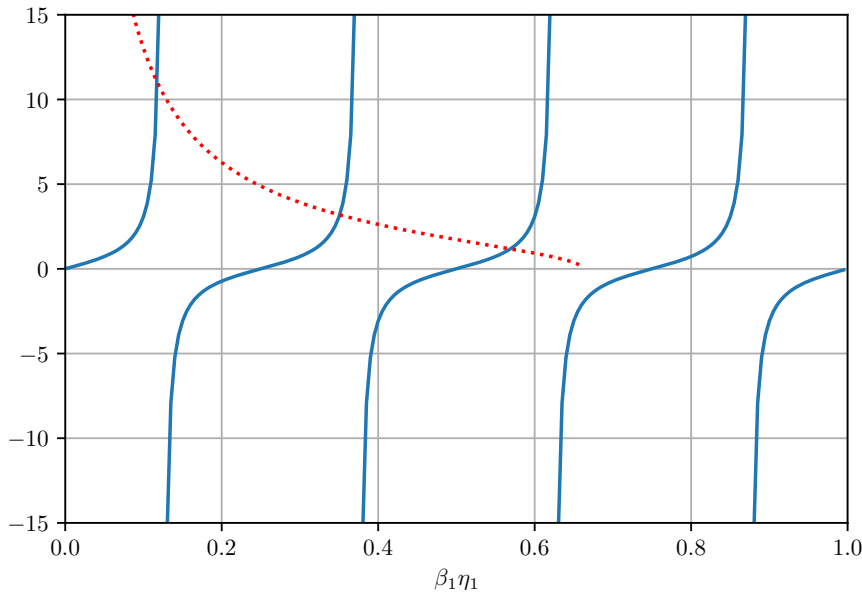
Fig. 6.21 Root of the characteristic equation of a Love wave for $h = 30$ km, 0.2 Hz, $\beta_1 = 3$ km/s, $\beta_2 = 4$ km/s, $\rho_1 = 2.5$ g/cm^3 and $\rho_2 = 2.8$ g/cm^3.

The right side can exist if $\beta_1\eta_1$ is smaller than $\sqrt{1-(\beta_1/\beta_2)^2}$. Since the left side is tan, we know that at least one solution can exist. This solution is called the fundamental mode. In the current situation (0.2~ Hz), we can see that three solutions exist. They are called the fundamental mode (zeroth-order mode), first higher mode, and second higher mode, respectively, starting from the one with smaller $\beta_1\eta_1$ (i.e., longer wavelength).

Consider the conditions for the existence of a first higher mode. As the frequency decreases, the dashed line moves to the left. It cannot exist when the phase of tan is left of $3\pi/2$. This requires

$$\pi\frac{\beta_1}{h\omega} \le \sqrt{1-(\beta_1/\beta_2)^2}. \qquad (6.81)$$

The cut-off frequency of an nth higher mode f_n^{cut} is given by

$$f_n^{cut} = \frac{n\beta_1}{2h}\frac{1}{\sqrt{1-(\beta_1/\beta_2)^2}}. \qquad (6.82)$$

Let us consider the displacement distribution as a function of depth for each mode. Figure 6.22 shows the depth distribution of displacement for each mode. You can see that the energy is confined in the low-velocity layer (layer 1), and in layer 2, it decays ex-

Fig. 6.22 Depth distribution of Love wave amplitudes. Amplitudes of each mode are normalized at the surface.

ponentially with increasing depth. The oscillation of the air column corresponds to the fundamental mode, first-order mode, and second-order mode, starting from the one with the smaller number of nodes.

Jeans relation

Phase velocity and group velocity

The phase velocity (p^{-1}) of the Love wave for each frequency is plotted in Figure 6.23. For each mode, the phase speed (solid line) is β_2 on the long-period side and monotonically decreases as the frequency increases, approaching β_1. The fundamental mode exists from frequency 0, while a higher-order mode has a cutoff frequency on the low-frequency side.

Fig. 6.23   Dispersion curves for the Love wave. Phase velocity is shown as a solid line and group velocity as a dashed line. Here we assumed that $h = 30$ km, 0.2 Hz, $\beta_1 = 3$ km/s, $\beta_2 = 4$ km/s, $\rho_1 = 2.5$ g/cm^3 and $\rho_2 = 2.8$ g/cm^3.
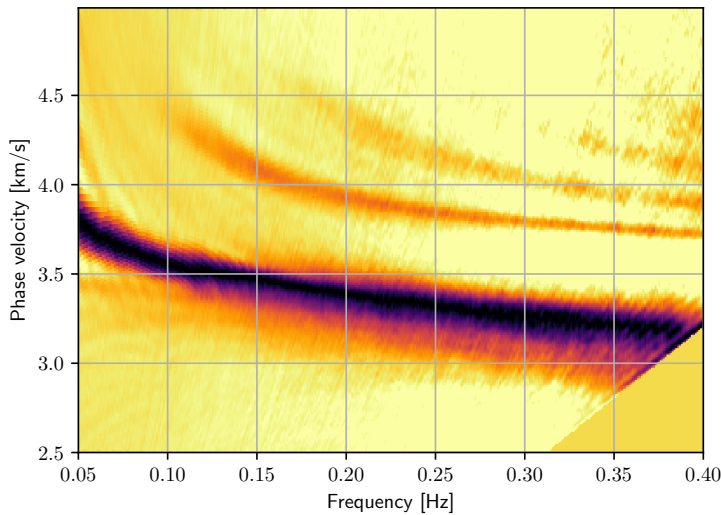
Fig. 6.24   Dispersion curves of Love waves propagating through the Japanese Islands observed by Hi-net tiltmeters. See[5] for details of the analysis.

Here is an example of an observed dispersion of Love waves. Figure 6.24 is the dispersion curve of the Love wave recorded by the Hi-net tiltmeters, which shows the fundamental mode, the first, second, and third higher modes. It represents the average features of the Japanese Islands. There is a cutoff at 4.5 km/s, indicating that the mantle S-wave velocity is approximately 4.5 km/s. In addition, the phase velocity of the fundamental mode is slower for shorter periods. This is because the crust cannot be represented as a single layer, and the shallow and slower layer reduces the phase velocity.

Surface waves have different propagation speeds at different frequencies. This phenomenon

is called dispersion. Here, for simplicity, we consider the following wave propagation:

$$\int_{\omega_0-\Delta\omega}^{\omega_0+\Delta\omega} e^{i(k(\omega)x-\omega t)}d\omega, \tag{6.83}$$

where ω is angular frequency, $k(\omega)$ is wavenumber and x represents the location.

The Taylor expansion of $k(\omega)$ around the center frequency ω_0 leads to

$$k(\omega) \approx k_0 + \frac{dk}{d\omega}(\omega - \omega_0) + O(2). \tag{6.84}$$

If $\Delta\omega$ is enough small, we can simplify the equation as

$$\int_{\omega_0-\Delta\omega}^{\omega_0+\Delta\omega} e^{i(k(\omega)x-\omega t)}d\omega \approx e^{i(k_0x-\omega_0t)}\int_{-\Delta\omega}^{\Delta\omega} e^{i\omega'\left(\frac{dk}{d\omega}x-t\right)}d\omega' = e^{i(k_0x-\omega_0t)}\frac{2\sin\left(\frac{x}{c_g}-t\right)}{\frac{x}{c_g}-t}, \tag{6.85}$$

where group velocity c_g is defined by $d\omega/dk$. The phase propagates with ω_0/k_0, and the envelope (sinc function $\sin x/x$) propagates with the group velocity c_g.

The results of the actual numerical integration are shown in Figure 6.25. Unlike the simple case with no dispersion, you can see that the waveform is propagating while changing its shape. Lines with the same amplitude (in-phase) propagate with a phase speed of ω/k. On the other hand, the entire wave group propagates with a group velocity of $d\omega/dk$. Approximating the above integral by the sum of the two frequencies, we can derive the group velocity equation from the sum-product formula for trigonometric functions.

Let up take another look at the figure 6.23. The group velocity is represented by the dotted line. The phase velocities decrease with frequency, but group velocities have minima. What happens when there is a minimum? Near the minima, the group velocity does not change much. Suppose we divide such an in-terval into a narrow frequency range (e.g., frequency width $2\Delta\omega$). Since each arrives at the same group velocity, each wave packet arrives at the same time and has a larger amplitude. Thus, the amplitude of the wave packet near the group velocity minimum becomes large, which is known as the airy phase. In figure 6.26, we have shown an example of a first-order higher-order mode of the Love wave. Indeed, it can be seen that wave packets with group velocities of 2.7 km/s, which is the minimum value of group velocity, are dominant.
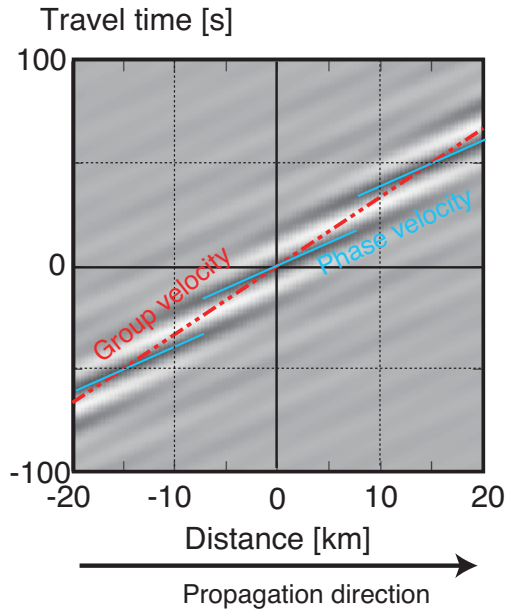
Fig. 6.25 波の分散。

Superposition of Love modes

Finally, let us superimpose all the Love modes. As we first discussed in this section, we can see the wave with wide-angle multiple reflections (at a time shortly before the blue dotted line). The blue dotted line corresponds to the travel time $T(x) = x\beta_2/(\beta_1^2)$ and represents
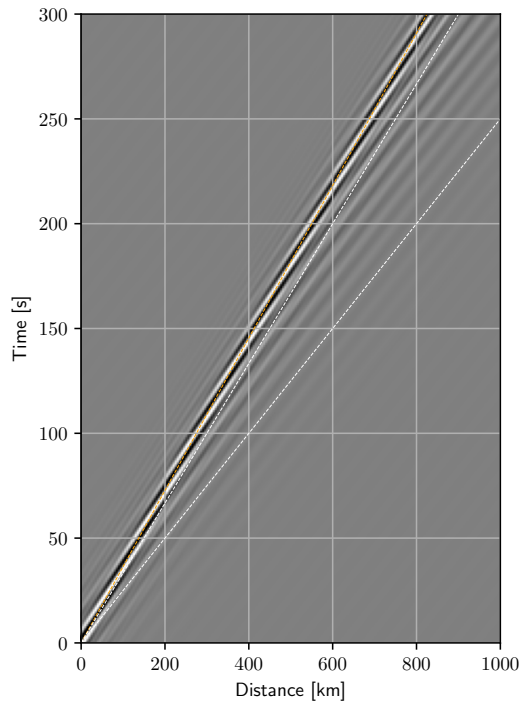
Fig. 6.26 First-order higher mode of the Love wave plotted against distance and time. The white dashed lines correspond to phase speeds of 3 km/s and 4 km/s, and the orange dashed line corresponds to 2.7 km/s (the minimum value of group velocity). You can see the dominant wave packet where the group velocity takes a minimum value.

the travel time of the wide-angle multiple reflections. The fact that the wave is not visible at times later than this line indicates that it cannot represent a wave incident at a steep angle that would transmit to the layer below. It should be noted that the superposition of modes also reproduces head wave (red dashed line in the figure). While the reflected wave is impulsive, the head wave is bordered. This is because the head wave can be estimated by an integral of the direct waveform (see chapter 6.3.3). This is due to the contribution of higher-order modes near the cutoff frequency. The wave that is parallel to the head wave and visible 20 seconds later is the wave propagating as a head wave after once being reflected wide angle.

One point to note is that we can see wave groups that are clearly physically incorrect (not satisfying the causality) before the head wave. These waves have a phase velocity of approximately 4 km/s (S-wave velocity in the second layer). This is because Love waves cannot represent waves propagating in the second layer. [note 7]. What waves cannot be represented as a sum of modes can be interpreted physically. More strict treatment will be given in the chapter on normal mode theory.

---

note 7) Strictly speaking, it is the term expressed by the branch integral contribution. See Saito (2009) chapter 9.4
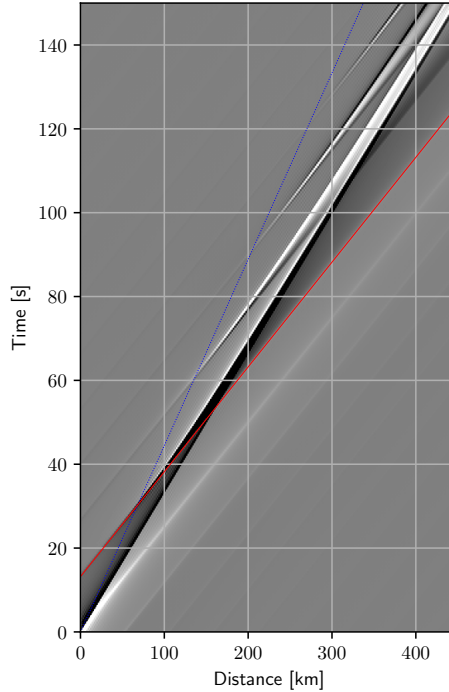
Fig. 6.27 The figure shows the superposition of Love modes up to the 14th higher-order modes. The highest frequency is 1 Hz and the structure is the same as in the previous example. The blue dotted line corresponds to the travel time $T(x) = x\beta_2/(\beta_1^2)$ and represents the wide-angle multiple reflection travel time. The red line represents the travel time of the head wave.

Problem 6.4

Let us evaluate the dispersive wave using the stationary phase approximation.

$$\frac{1}{\pi} Re \int_0^\infty e^{i(k(\omega)x - \omega t)} d\omega \tag{6.86}$$

Here we define the phase $\Psi = k(\omega)x/t - \omega$, we can rewrite the equation

$$\frac{1}{\pi} Re \int_0^\infty e^{it\Psi(\omega)} d\omega. \tag{6.87}$$

Because $e^{it\Psi}$ oscillates rapidly, the contribution near

$$\frac{d\Psi(\omega)}{d\omega}\bigg|_{\omega=\omega_0} = 0 \tag{6.88}$$

became dominant. In this case,

1. Evaluate the integral by expanding ω to the second order term of ω_0.
2. Consider the group velocity.
3. Also, consider the case where the group velocity takes the minimum.

§6.5 Bibliography

[1] K. Aki and P.G. Richards. *Quantitative Seismology*. Univ Science Books, 2nd edition, 2009.

[2] Craig M Jarchow and George A Thompson. The nature of the mohorovicic discontinuity. *Annual Reviews of Earth and Planetary Sciences*, Vol. 17, pp. 475–506, 1989.

[3] A E H Love. *Some Problems of Geodynamics*. Cambridge University Press. Reprinted in 2015 by Dover Publications, Cambridge, England, December 1911.

[4] Andrija Mohorovičić. Earthquake of 8 october 1909. *Geofizika*, Vol. 9, No. 1, pp. 3–55, 1992.

[5] K Nishida, H Kawakatsu, and K Obara. Three-dimensional crustal S wave velocity structure in japan using microseismic data recorded by hi-net tiltmeters. *J. Geophys. Res.*, Vol. 113, No. B10, p. B10302, October 2008.

[6] J G J Scholte. RAYLEIGH WAVES. IN ISOTROPIC AND ANISOTROPIC. ELASTIC MEDIA. *Meded. en Verhand. KNMI*, Vol. 72, pp. 9–43, 1958.

[7] P.M. Shearer. *Introduction to Seismology*. Cambridge University Press, 2009.

[8] S. Stein and M. Wysession. *An Introduction to Seismology, Earthquakes, and Earth Structure*. Wiley, 1991.

[9] 斎藤正徳. 地震波動論. 東京大学出版会, 2009.

Waves in a density stratified fluid

Chapter 7

§7.1 Atmospheric wave

When propagations of an atmospheric wave, buoyancy force plays a more important role than seismic wave propagations. There are two major effects of gravity [note 1)].

First, gravity force causes stratification of the atmospheric structure. Under hydrostatic equilibrium, pressure gradient equals gravity force. As a result, the density and the pressure decay exponentially with the height. With an increasing height of atmospheric scale height H_s km, the density decrease to $1/e$. The scale height is a characteristic parameter of the atmospheric structure.

Next, gravity is important as a restoring force. As already explained, gravity case stratification of the atmosphere. The change in height causes significant buoyancy force. The buoyancy force is not only the dominant restoring force for internal gravity waves but also significant for low frequency infrasound. When characterizing the buoyancy force, buoyancy frequency (or Brunt-Väisälä frequency) N and acoustic cut-off frequency N_a are defined as,

$$N^2 = -\frac{g}{\rho_0}\frac{d\rho_0}{dz} - \frac{g^2}{c_s^2},$$
$$N_a = \frac{c_s}{2H_s}, \tag{7.1}$$

where g is gravity acceleration, ρ_0 is density, z is height, and c_s is sound speed.

First, to understand buoyancy frequency N, let us consider a volume element. The stratification causes buoyancy force. The stratification is enough strong when the temperature profile is steeper than the adiabatic temperature gradient. In this case, the buoyancy force causes oscillation of the element with frequency N.

Acoustic cut-off frequency N_a represents the lowest frequency of an acoustic wave. Lower than this frequency, acoustic waves cannot exist. The definition shows that the wavelength of acoustic wave at the frequency N_a is $4\pi H_s$. This means that the acoustic restoring force

---

note 1) See details in §6.14 (Adjustment to Equilibrium in a Stratified Compressible Fluid) of Gill's textbook.[1] You can find more details about infrasounds in the textbook by Gossared.[2]

Angular frequency
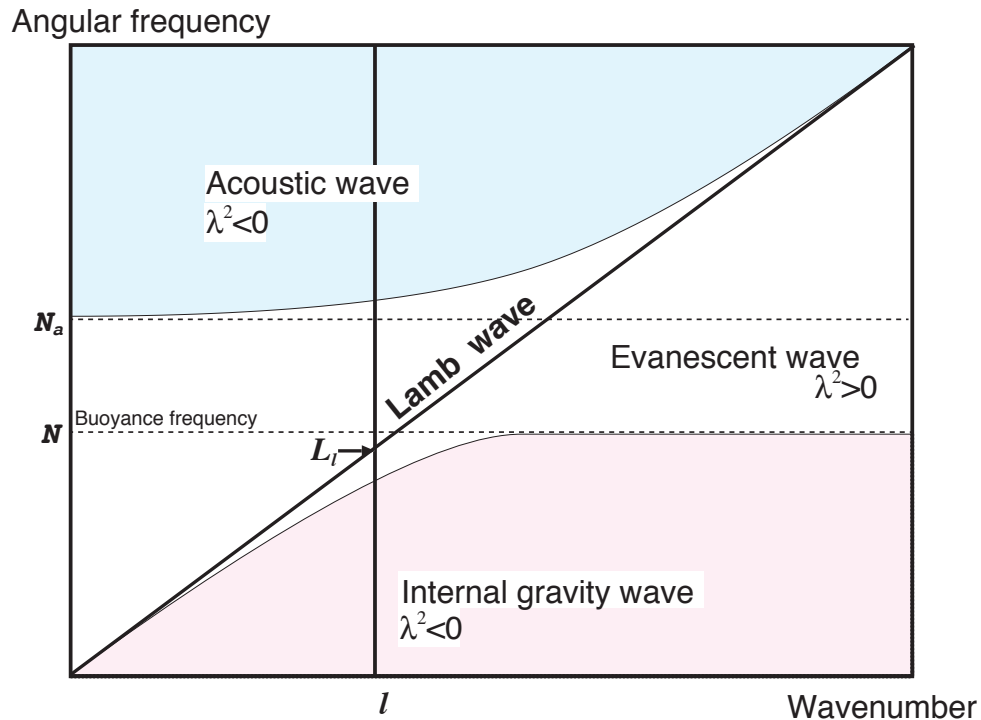
Fig. 7.1   Dispersion relation of atmospheric waves. The blue area shows a regime of an acoustic wave, and the red one shows a regime of an internal gravity wave. The white area shows an evanescent wave, which cannot propagate toward the vertical direction.

cannot sustain the acoustic wave below the frequency. N_a is higher than N. Although these frequencies depend on the height and the locations, typically N is about 2 mHz, and N_a is about 3 mHz.

   Figure 7.1 shows a diagram of the acoustic wave and internal gravity wave in frequency–wavenumber domain. The blue area shows a regime of an acoustic wave, and the red one shows a regime of an internal gravity wave. The white area shows an evanescent wave, which cannot propagate toward the vertical direction. A Lamb wave is a typical evanescent wave, which propagates horizontally with sound speed and equilibrates hydrostatically toward the vertical direction. The energy of Lamb wave is concentrated around the surface, and the energy decay exponentially with height as $\exp(-z/H_s)$[note 2]

--- Wavenumber-frequency spectrum ---

As depicted by Figure 7.1, the wavenumber-frequency spectrum plays a crucial role in understanding seismic wave propagations. Because, in particular, strong dispersion causes complexity in time domain, the wavenumber-frequency spectrum is effective for dispersive waves. Although from a mathematical point of view, treatments in the wavenumber-frequency domain are equivalent to those in spatial-time domain, they are complemental to each other.

[note 2] Lamb waves were observed when solar eclipses, nuclear bomb tests in the atmosphere, and volcanic eruptions. Because of the less attenuation, multi-orbit Lamb waves were reported.

§7.2 Bibliography

[1] Adrian E Gill. *Atmosphere-ocean dynamics*, Vol. 30. Academic press, 1982.

[2] E. E. Gossard and W.H. Hooke. *Waves in The Atmosphere*. Elsevier Amsterdam, 1975.

Ray theory

Chapter 8

The previous chapter explains SH wave propagations in a two-layer medium. Although it gives us insight into seismic wave propagations of realistic earth, the real Earth's structure is

Time [min]

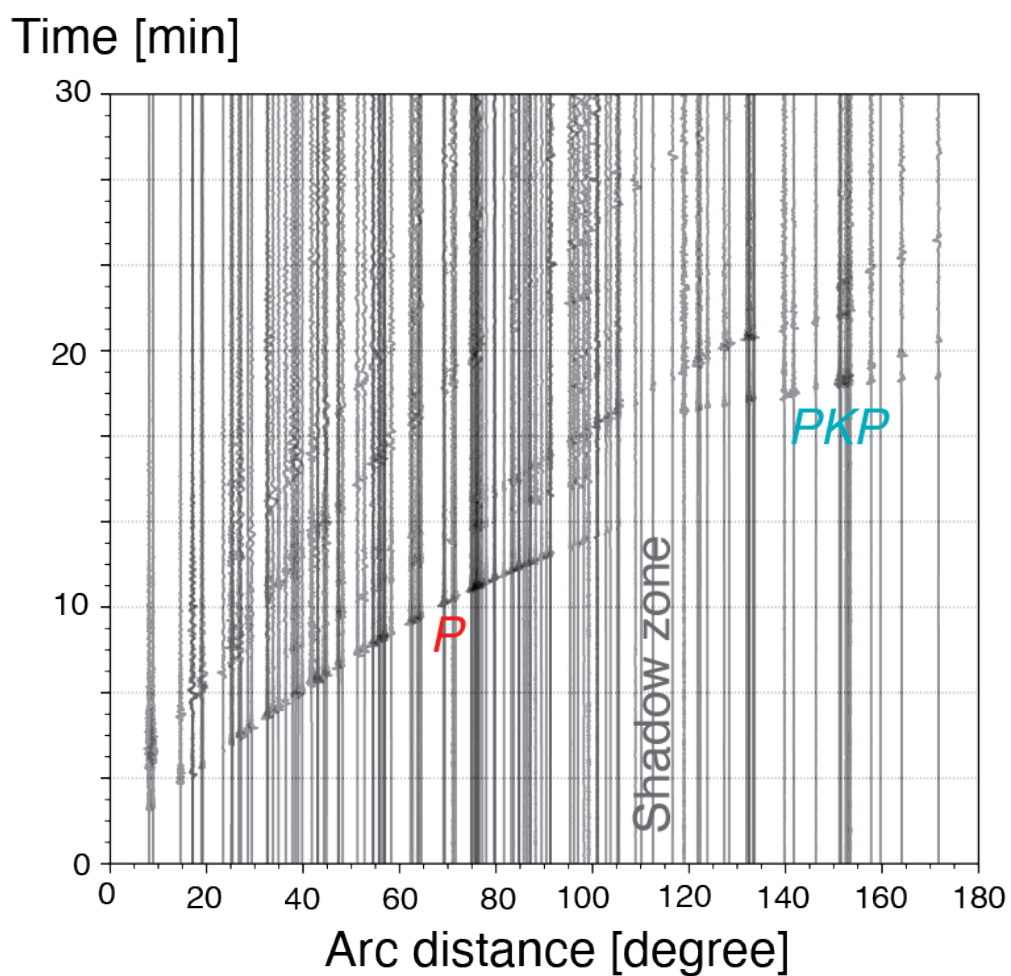Fig. 8.1 Observed records of the 2015 earthquake off the western coast of the Ogasawara Islands. The P-wave and S-wave are clear, but the waveforms are not so simple. The figure shows the shadow zone of the P-wave by the outer core, where the P-wave does not reach the surface (around the arc distance of 110 degrees).

more complex. To address seismic wave propagations for a more realistic Earth mode, the next is the multi-layer approximation of the Earth's structure.

A typical dominant frequency of teleseismic events recorded by seismometers is an order of 1 Hz. In this case, a spatial scale of the Earth's structure is approximated to be enough shorter than the wavelength of the seismic wave [note 1]. Figure 8.1 shows observed seismograms when the 2015 earthquake off the western coast of the Ogasawara Islands (the focal depth is deeper than 660 km) on the global scale. This figure exhibits many phases, which are classified in terms of the ray path and wave type. To interpret the seismic wave propagations, an approximation of geometrical optics is feasible. Exactly speaking, although this approximation is valid only for high-frequency limits, this approach is feasible for seismic exploration of Earth's structure in many cases practically.

Figure 8.2 shows the arrival times of the waves, which are visually picked by the onset time of observed seismograms, and plots them against the epicenter distance. Black represents the P-wave type, and red represents the S-wave type. The figure shows numerous phases (classified according to the ray path and the combination of wave types). Even if observed waveforms are so complicated (see figure 5.2, for example), it is easier to grasp the characteristics by the travel time plot. The pick of the arrival times is the operation of abstraction of observed data. This figure also shows that the Earth's internal structure can be approximated as a one-dimensional structure since the travel time is a function of only the epicentral distance. In addition, for P waves (angular distance of 100 degrees and a travel time of about 13 minutes), the travel times are highly scattered, which can be interpreted as large velocity heterogeneities at the core-mantle boundary.

This figure shows the arrival times of the seismic phase waves visually and plots them against the epicenter distance. Black represents the P-wave, and red represents the S-wave. Numerous phases (classified according to the path taken and the combination of wave types) can be seen. Since the whole waveforms are too complicated to model, it is easier to grasp the dominant features by simplified information: arrival times. This figure also shows that the Earth's internal structure can be approximated as one-dimensional because the measured travel time is a simple function of the epicentral distance. In addition, for P waves (angular distance of 100 degrees and travel time of about 13 minutes), the travel times are highly scattered, which can be interpreted as a large velocity inhomogeneity at the core-mantle boundary.

A theory of wave propagation based on geometrical optics is known as Ray theory. This theory has played an important role in seismology for a long time. In particular, the ray theory for a stratified medium (multi-layer medium) is a basic theory for seismic wave propagations. This chapter gives the outline of ray theory in a stratified medium for interpreting seismic wave propagations in a realistic Earth.

§8.1 High frequency approximation

[note 1] A wavenumber spectrum of Earth's heterogeneities shows that the long wavelength components are dominant (called as "red structure").
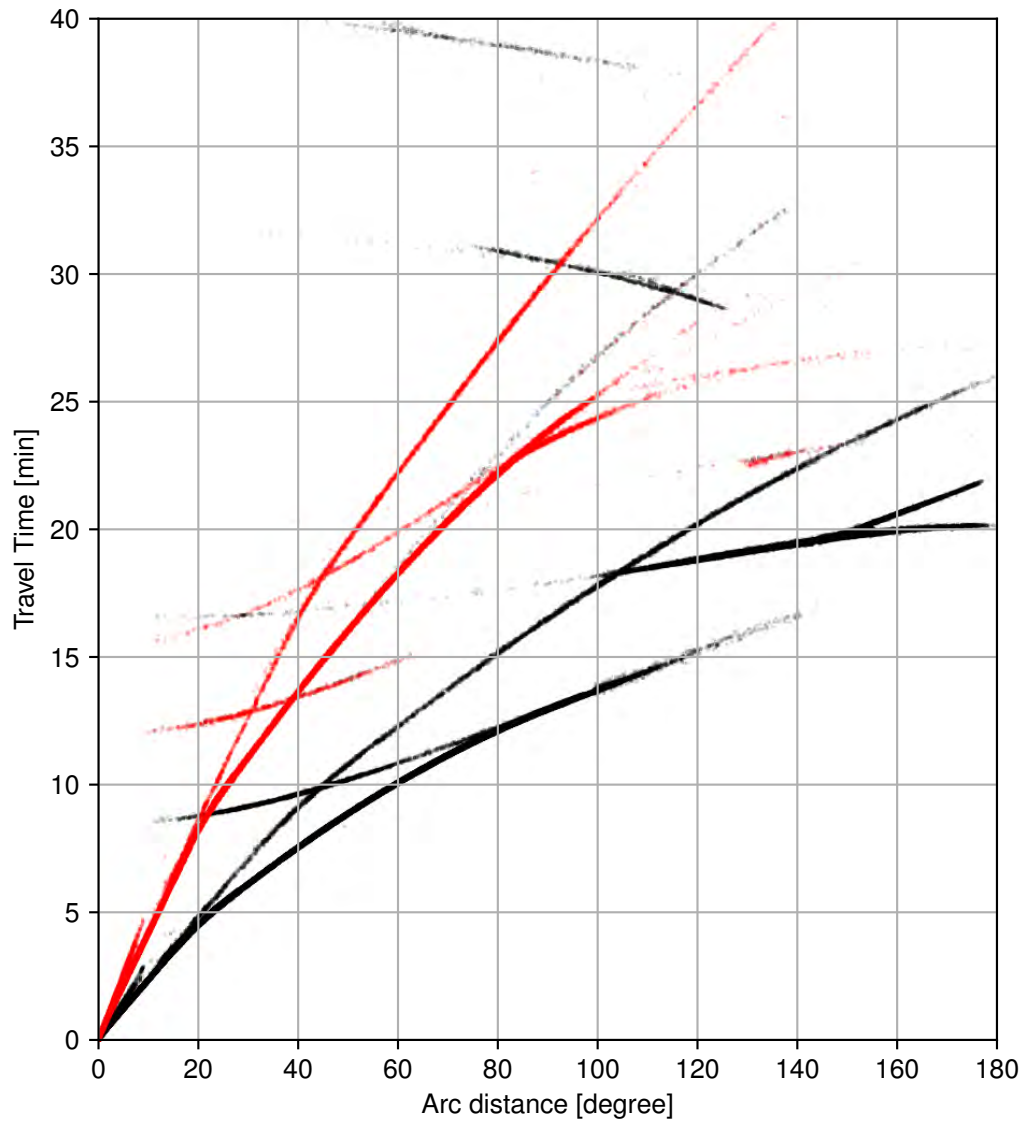
Fig. 8.2   Travel-time plots of various seismic phases. Black represents P-waves, and red represents S-waves. Events shallower than 20 km that occurred in 2018 were selected. Data are from International Seismological Centre (2021), On-line Bulletin, https://doi.org/10.31905/D808B830.

First, let us consider P-wave potential. With an assumption that typical spatial scales of physical properties (density and elastic constants) are enough longer than the wavelength of the P wave, the wave equation of P-wave can be simplified as

$$\ddot{\phi} = \alpha^2 \nabla^2 \phi. \tag{8.1}$$

Here we assume that a wave packet ϕ propagates with the shape as $\phi(x, t) = A(x)f(t - T(x))$. Because the potential is a function of a single variable, the spatial derivative is given by $\nabla f = \nabla T \dot{f}$. Insertion of the equation into the wave equation gives the following equation:

$$\frac{1}{\alpha^2}\ddot{\phi} = \nabla^2 A f(t - T) - 2\nabla A \cdot \nabla T \dot{f}(t - T) + A\ddot{f}(t - T)(\nabla T)^2 + A\dot{f}(t - T)\nabla^2 T. \tag{8.2}$$

Fourier transform of both sides is written by,

$$-\frac{\omega^2}{\alpha^2} = \nabla^2 A F(\omega) - 2i\omega\nabla A \cdot \nabla T F(\omega) - A^2\omega^2 F(\nabla T)^2 - A\omega i F \nabla^2 T. \tag{8.3}$$

With an assumption that angular frequency ω is enough large, the real part of the equation leads to the Eikonal equation as

$$|\nabla T|^2 = \frac{1}{\alpha^2}. \tag{8.4}$$

Here we define slowness vector p by ∇T.

On the other hand, the imaginary part in the high-frequency limit leads to the transport equation.

$$2\nabla A \cdot \nabla T + A\nabla^2 T = 0. \tag{8.5}$$

This equation can be rewritten as $\nabla \cdot (A^2 p) = 0$, which represents the conservation of energy. By solving the Eikonal equation, we get travel time T. Then we can estimate A from the transport equation with the estimated T.

§8.2 Ray tracing: Hamiltonian formalism

Based on ray theory, integration of the Eikonal equation gives travel time T. Ray tracing is one of the solving methods. Ray can be defined by successions of slowness vectors as already introduced. The wavefront expands with a speed of the seismic velocity in a direction of slowness vector. Below, I will explain the physical meanings of ray tracing: ray tracing can be interpreted as tracing of a particle motion under a potential. This physical system can be described in a simple manner by generating parameter σ instead of time, as explained later. Although the discussion is based on analytical mechanics, the formulation is helpful for interpretation.

Here we consider the problem of tracing a particle motion under a potential $-1/\alpha$. Instead of time, we define generating parameter σ [note 2)] for describing the location as

$$d\sigma = \alpha ds. \tag{8.6}$$

[note 2)] Although, for determining the locations in a mechanical system, we can use s or travel time T, we use generating parameter σ. This is simply because we can simplify the governing equation.

Here ds represents an infinitesimal path. The Hamiltonian H of this system is given by[note 3)]

$$H(x, p) = \frac{1}{2} \left[p \cdot p - \alpha^{-2}(x) \right] . \tag{8.7}$$

The eikonal equation can be interpreted as a condition of the constraint of this system. The eikonal equation can be rewritten as $H(x, p) = 0$ using Hamiltonian. Hamilton equations are written by

$$\frac{dx}{d\sigma} = \frac{\partial H}{\partial p} = p \tag{8.8}$$

$$\frac{dp}{d\sigma} = -\frac{\partial H}{\partial x} = \frac{1}{2} \nabla \alpha^{-2}. \tag{8.9}$$

These equations can be interpreted as

1. Let us consider a problem of tracing a particle motion under a potential $-\alpha^{-2}$.
2. The initial condition is given by p. Note that p is constrained by the equation $H(p,x) = 0$. (This condition is equivalent that the absolute value of p at the initial injection point is $1/\alpha$).
3. According to Hamilton equations, $dH = \partial_x H dx + \partial_p H dp = 0$. This means that at any point along the ray path, $H = 0$ if the initial value $H = 0$ at the injection point.
4. The particle motion can be traced by integrating the Hamilton equations. Physically, σ represents time.

The two first-order differential equations can be simplified as a single equation:

$$\frac{d^2 x}{d\sigma^2} - \frac{1}{2} \nabla \alpha^{-2} = 0. \tag{8.10}$$

This equation represents the equation of motion. The corresponding Lagrangian can be defined as,

$$L = \frac{1}{2} \left[\dot{x} \cdot \dot{x} + \alpha^{-2}(x) \right] , \tag{8.11}$$

which satisfy the relation of $p = \partial_{\dot{x}} L$ (definition of generalized momentum)[note 4)].

Here we consider a stratified medium. In this case, because α depends only on depth z[note 5)], p_x becomes a conserved quantity. p_x is also known as the ray parameter.

8.2.1 For spherical Earth

When we consider global seismic wave propagations, a spherical coordinate is more convenient. With an assumption that P-wave velocity $\alpha(r)$ depend only on radius r (spherical symmetry), the Lagrangian L is written by,

$$L = \frac{1}{2} (\dot{r}^2 + (r\dot{\theta})^2 + (r \sin \theta \dot{\phi})^2 - \alpha(r)^{-2}). \tag{8.12}$$

[note 3)] For details, read chapter 15 of Dahlen and Tromp [1998][(2)]

[note 4)] We often use symbol p for slowness vector, because the slowness vector can be interpreted as generalized momentum based on ray theory. When we use time as a variable for determining the location, the generalized momentum is not proportional to the particle velocity. On the other hand, generalized momentum using generating parameter is proportional to the particle velocity. Generating parameter gives us a more simple physical analogy.

[note 5)] In the context of analytical mechanics, such x is called a cyclic coordinate.

By the appropriate choice of the spherical coordinate, we can drop ϕ. Angular distance $Delta$ along θ direction can describe the propagations. For a spherical structure, the ray parameter p ray parameter $\boldsymbol{p} = (p_r, p_\theta, p_\phi)$ in the spherical coordinate is given by

$$
\begin{aligned}
p_r &= \frac{\partial L}{\partial \dot{r}} = \frac{dr}{d\sigma} \\
p_\theta &= \frac{\partial L}{\partial \dot{\theta}} = r^2 \frac{d\theta}{d\sigma} \\
p_\phi &= \frac{\partial L}{\partial \dot{\phi}} = (r \sin \theta)^2 \frac{d\phi}{d\sigma}.
\end{aligned}
\tag{8.13}
$$

Similarly, the Hamiltonian H is

$$
H = \frac{1}{2}(p_r^2 + r^{-2}p_\theta^2 + (r \sin \theta)^{-2}p_\phi^2 - \alpha(r)^{-2})
\tag{8.14}
$$

and the Hamilton equation can be written as

$$
\begin{aligned}
\frac{dr}{d\sigma} &= \frac{\partial H}{\partial p_r} = p_r, \\
\frac{d\theta}{d\sigma} &= \frac{\partial H}{\partial p_\theta} = \frac{p_\theta}{r^2}, \\
\frac{d\phi}{d\sigma} &= \frac{\partial H}{\partial p_\phi} = \frac{p_\phi}{(r \sin \theta)^2},
\end{aligned}
\tag{8.15}
$$

$$
\begin{aligned}
\frac{dp_r}{d\sigma} &= -\frac{\partial H}{\partial r} = \frac{1}{2}\frac{\partial \alpha^{-2}}{\partial r} + \frac{1}{r^3}\left[p_\theta^2 + \frac{p_\theta^2}{(\sin \theta)^2} \right], \\
\frac{dp_\theta}{d\sigma} &= -\frac{\partial H}{\partial \theta} = \frac{1}{2}\frac{\partial \alpha^{-2}}{\partial \theta} + \frac{1}{r^2}\frac{\cot \theta}{(\sin \theta)^2}p_\theta^2, \\
\frac{dp_\phi}{d\sigma} &= -\frac{\partial H}{\partial \phi} = \frac{1}{2}\frac{\partial \alpha^{-2}}{\partial \phi},
\end{aligned}
\tag{8.16}
$$

The result is as follows. In the case of a horizontally stratified structure, placing the emergence point at the pole does not lose generality. Also, since α does not depend on θ and ϕ, its partial derivative is 0. Therefore $P_\phi = 0$ and $\dot{P}_\theta = 0$. Therefore, as in the Cartesian coordinate case, p_θ is conserved along the wavy line, and In this case, it is also called the ray parameter.

8.2.2 Earth flattening transform

When considering ray theory, there is a simple correspondence between horizontally stratified structures ($\alpha(z)$ is a z-only function) and spherically symmetric structures. Once one problem is solved, the other can be solved by variable transformation (Earth flattening transform). Let us consider this variable transformation below.

Let us consider the problem in the θ direction for isotropic seismic wave radiation from a point. The Eikonal equation in spherical coordinates leads to the following equation.

$$
\left(\frac{\partial T}{\partial r}\right)^2 + \frac{1}{r^2}\left(\frac{\partial T}{\partial \theta}\right)^2 = \frac{1}{\alpha(r)^2}
\tag{8.17}
$$

Using the Earth radius R_e, we can rewrite the equation as

$$\frac{1}{R_e^2}\left(\frac{\partial T}{\partial \theta}\right)^2 + \frac{r^2}{R_e^2}\left(\frac{\partial T}{\partial r}\right)^2 = \frac{r^2}{R_e^2}\frac{1}{\alpha(r)^2}. \tag{8.18}$$

We can transform the equitation in spherical coordinates to an equation in Cartesian coordinates with the change of variable by $x = R_e\theta$, $r = R_e e^{-z/R_e}$, $\alpha(z) = R_e\alpha(r)/r$. The earth flattening transform is strictly valid within ray theory. It also holds for SH wave propagation, but only approximately for SV wave. Footnotesee Aki and Richards Box 9.9 for details[1].

Problem 8.0

Consider a sphere with uniform velocity and find the corresponding horizontal stratification structure using the Earth flattening transform. Also, consider a wavy line in the Cartesian coordinate system and consider its correspondence with the case of a uniform sphere.

▌ 8.2.3 Fermat's principle (principle of least action)

Ray path is the path which minimizes the integration of Lagrangian among the possible paths. This leads to the following relation:

$$\delta \int_{\sigma_1}^{\sigma_2} L(\boldsymbol{x}, \dot{\boldsymbol{x}}) d\sigma = \delta \int_{\sigma_1}^{\sigma_2} \left[\boldsymbol{p} \cdot \dot{\boldsymbol{x}} - H(\boldsymbol{x}, \boldsymbol{p}) \right] d\sigma. \tag{8.19}$$

This relation is equivalent to minimizing the corresponding travel time.

$$\delta \int_{\boldsymbol{x}_1}^{\boldsymbol{x}_2} \boldsymbol{p} \cdot d\boldsymbol{x} = \delta \int_{T_1}^{T_2} dT = 0 \tag{8.20}$$

leads to equivalence.

▌ 8.2.4 Direct solver of Eikonal equation

▌ §8.3 $\tau - p$ (Radon) transform

Travel time curves against epicentral distance become complex due to the multi-valued function. There exists a transform known as $\tau - p$ (Radon) transform into the single-valued function. Here we define intersection time τ by $\tau(p) = T - p_x X$ (this type of transform is known as Legendre transforms in physics). After the transformation from a pair of T and p_x to pair of τ and p_x, τ becomes the single-valued function even in a case with the positive jump as shown in 8.7.

Once we obtain τ against the ray parameter p_x, we can calculate the travel time T against the epicentral distance X by a relation of $d\tau/dp = -X$[note 6].

τ is also a useful observable for array analysis of seismic data (A slant stack method of array analysis is a technique of data processing that utilizes the information from densely distributed seismometers at around X). $\tau - p$ transform is a theoretical background of the array analysis[note 7]

We can extend $\tau - p$ into two dimensions. To define a new variable pair that has the same information to travel time T against the dependent variable X, we must consider Legendre transform[note 8].

$$\tau = T - \boldsymbol{p} \cdot \boldsymbol{X} \tag{8.22}$$

[note 6] From the definition, the derivative of τ with respect to the ray parameter p_x is given by

$$\frac{d\tau}{dp_x} = \frac{dT}{dp_x} - X - p_x \frac{dX}{dp_x} = \frac{dT}{dp_x} - X - \frac{dT}{dX}\frac{dX}{dp_x} = -X. \tag{8.21}$$

[note 7] For details on practical data analysis, read a textbook by Zhou (Practical Seismic Data Analysis[4]).

[note 8] Exactly speaking, Legendre requires the convexity to the dependent variable. Therefore we need to divide T into retrograde and prograde areas before the transform

For the transform from p to X,

$$\frac{d\tau}{dp_x} = -X, \tag{8.23}$$

$$\frac{d\tau}{dp_y} = -Y, \tag{8.24}$$

$$\tag{8.25}$$

is useful[note 9].

§8.4 Amplitude: geometrical spreading

As in a two-layer medium, the conservation of energy along a ray path leads to a theory for amplitudes of a ray theoretical Green's function for phases (e.g. P wave and S wave).

Here we consider seismic wave propagations in a stratified Earth model. When a seismic wave is radiated with the emergency angle of i_0 from the source, the infinitesimal solid angle $d\Omega_0 = \sin i_0 di_0 d\phi_0$ gives the conservation of energy. Here r_1 is the radius of the Earth, and ϕ is azimuth. When a radiated seismic wave with a solid angle reaches a surface point with angular distance Δ from the source,
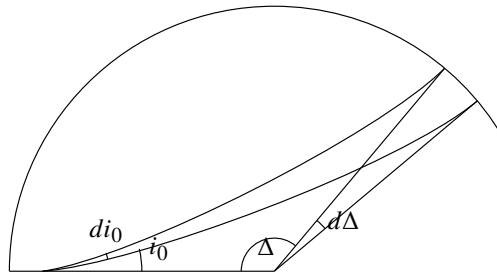
Fig. 8.3

The cross-section area on the surface S_1 is given by

$$dS_1 = r_1^2 \sin \Delta |d\Delta| d\phi_0 \cos i_1. \tag{8.26}$$

From the conservation of energy along the ray path, we obtain

$$E_0 d\Omega_0 = E_1 dS_1. \tag{8.27}$$

The energy at the surface point (the observed station) E_1 is represented by

$$E_1 = E_0 \frac{d\Omega_0}{dS_1} = E_0 \frac{\sin i_0 di_0}{r_1^2 \cos i_1 \sin \Delta |d\Delta|}. \tag{8.28}$$

Here

$$p = \frac{r_0}{\alpha_0} \sin i_0 = \frac{dT}{d\Delta} \tag{8.29}$$

$$\frac{dp}{d\Delta} = \frac{r_0}{\alpha_0} \frac{d \sin i_0}{d\Delta} = \frac{d^2 T}{d\Delta^2} \tag{8.30}$$

$$\frac{d \sin i_0}{d\Delta} = \frac{\alpha_0}{r_0} \frac{1}{\cos i_0} \frac{dp}{d\Delta}, \tag{8.31}$$

---

note 9) This relation can be proven as in a one-dimensional case.

where r_0 is the distance between the source and the center of the Earth. Then we obtain geometrical spreading $\mathcal{R}$, which gives information on the amplitudes as,

$$\frac{1}{\mathcal{R}^2} = \frac{E_1}{E_0} = \frac{1}{r_1^2} \frac{\alpha_0}{r_0} \frac{\tan i_0}{\cos i_1 \sin \Delta} \left| \frac{d^2T}{d\Delta^2} \right| \tag{8.32}$$

$$= \frac{1}{r_1^2} \frac{\alpha_0^2}{r_0^2} \frac{p}{\cos i_0 \cos i_1 \sin \Delta} \left| \frac{dp}{d\Delta} \right|. \tag{8.33}$$

$dp/d\Delta$ becomes larger with increasing ray density (see Figures in the previous section. This can be interpreted as (1) energy particles are radiated at the source toward every direction, (2) ray represents the trace of the particle (3) how many particles reach the observed station (4) by counting the energy particle, we can infer the amplitude of the phase.

If the heterogeneities of the medium near the source are weak, we can approximate Green's function by a Green's function in an infinite homogeneous medium. By connecting Green's function in an infinite homogeneous medium to ray theoretical Green's function, we can obtain a complete ray theoretical Green's function, including the absolute amplitude. When a station exists on the free surface, which doubles the amplitudes, the ray theoretical Green's function of a direct P wave is given by

$$G(\mathbf{x}_r, \mathbf{x}_s, f) = \frac{1}{4\pi\mathcal{R}} \left[\frac{\hat{\eta}_1 \hat{\eta}_2 e^{-2\pi f i T_p}}{\sqrt{\rho_1 \rho_2 \alpha_1^3 \alpha_2}} \right], \tag{8.34}$$

where $\hat{\eta}_1$ and $\hat{\eta}_2$ are polarization vectors at the source and the station, respectively, and T_p is P-wave travel time.

§8.5 Caustic

When

$$\left| \frac{d^2T}{d\Delta^2} \right| = \infty, \tag{8.35}$$

ray density diverges. This causes divergence of the amplitude in a framework of ray theory. For example, Figure 8.4 shows the concentration of ray paths at the center. This situation can be described by fire made by sunlight using glass. In this case, rays focus at the point known as "focus". In the case of caustic, the rays focus on a line (e.g. in the case of Figure 8.4, perpendicular to the page, patterns of the ray are homogeneous).

In a region where the spatial scale of amplitude variations is comparable to the wavelength, geometrical ray theory is not appropriate. At such singular points, we need to connect the analytic solution of the original wave equation. When a ray path passes a caustic, it causes a phase jump of 90°. For example, the phase of the PP wave (reflected P wave at the surface) actually is shifted 90°, because it passes caustic one. The wave packet of the PP wave can be represented by the Hilbert transform of the direct P wave mathematically.
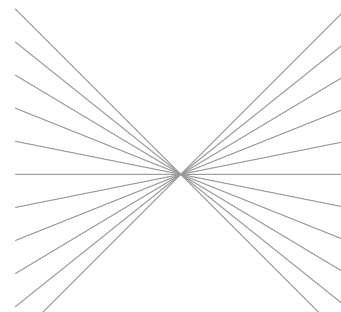

Fig. 8.4

Since the ray approximation is broken near caustic, let us consider the 2-D wave equation about a scalar quantity f in polar coordinate with the origin at the caustic:

$$\frac{1}{r}\frac{\partial f}{dr}\left(r\frac{d}{\partial r}\right) + \frac{1}{r^2}\frac{\partial^2 f}{\partial \phi^2} = -k_0^2 f. \tag{8.36}$$

With the ray approximation, we can assume that typical spatial scales are sufficiently larger than the wavelength, but there exist regions where r is shorter than the wavelength in realistic situations. For simplicity, let us consider the Fourier component $f \propto e^{in\phi}$ with respect to ϕ. Then we have

$$\frac{\partial^2 f}{\partial r^2} + \frac{1}{r}\frac{\partial f}{\partial r} = \left(-k_0^2 + \frac{n^2}{r^2}\right)f. \tag{8.37}$$

This is exactly the equation satisfied by the Bessel function. The Bessel function in far-field can be approximated as

$$J_n(kr) \propto \frac{1}{\sqrt{(kr)}}\cos\left(kr - n\frac{\pi}{2} - \frac{\pi}{4}\right). \tag{8.38}$$

We can see that $\pi/4$ is shifted by 2 times once it passes through the origin (caustic). This is because the change in curvature works better than the derivative with respect to r when viewed in polar coordinates. Here is a rough estimate. For example, in Cartesian coordinates $\cos\left(\sqrt{2}/2k_0 x\right)\cos\left(\sqrt{2}/2k_0 y\right)$ satisfies the wave equation. If the wavelength corresponding to k_0 is λ_0, the area of this positively inflated region can be written as $(\sqrt{2}\lambda_0/2)^2 = \lambda^2/2$. Considering that this is the same as the area of the circle centered at the origin, its radius is $\lambda/(\sqrt{2\pi})$. In other words, the first zero crossing point from the origin in polar coordinates is around 0.39 wavelengths away, which is more extended than $\lambda_0/4$ when considered in plane waves. This summation can be interpreted as giving the phase difference $\pi/4$ [note 10].

This phase shift can be interpreted from the conservation of energy with a natural extension of the negative cross section dS_2.

$$E_1 dS_1 = E_2 dS_2 \tag{8.39}$$

leads to $A_2 = A_1 i$. This originated from the flip of the ray coordinates before and after a passage at a caustic. In a case of a passage at a focus, the amplitude reverses because the phase flips twice ($i^2 = -1$) according to the two directions.

An example of the caustic is PP waves, whose phase is shifted to the direct P waves. This typical example is intuitively confusing, so I will explain it below. Since the ground reflection complicates the behavior, let us consider a mirror image of the hypocenter with respect to the surface (Figure 8.5). If we fold back the ray path of the PP wave radiated downward from the hypocenter at the surface, we can see that it intersects before the observed station. On the other hand, the pP wave radiated from the hypocenter does not intersect. Therefore, the waveforms of the pP and direct-directed waves have the same shape, but the PP wave has a distorted shape to the direct P wave (they are related by the Hilbert transform to each other).

Translated with www.DeepL.com/Translator (free version)

[note 10] For an accurate evaluation, we need to approximate the singularity by the Airy function using the WKBJ approximation (see Yomogida's textbook[5] for details). A more physical explanation (corresponding to diffraction) is given in Landau-Lifshitz's classical field theory §59
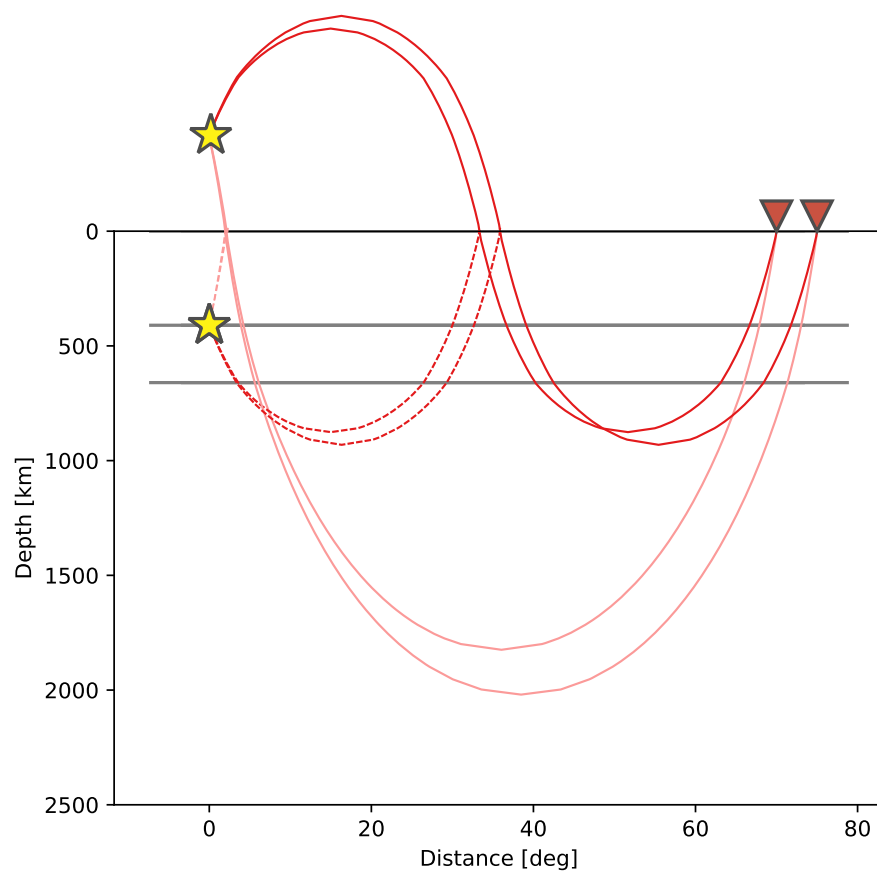
Fig. 8.5 Schematic diagram of PP waves passing through caustic. In this figure, we can see that the PP waves intersect, while the pP waves do not.

§8.6 Travel time analysis

Although generating parameter σ gives us an insight into this system, it is not related to observables directly. In this section, relations among observables: epicentral distance $X(p_x)$, travel time $T(p_x)$, and ray parameter p_x are presented for a stratified medium[note 11].

At the origin $\boldsymbol{p} = (p_x, \sqrt{\alpha(0)^{-2} - p_x^2})$. The deepest point of the ray z is given by $z = Z(p_x)$. In this case, the corresponding seismic velocity is represented by

$$\alpha(Z) = p_x. \tag{8.40}$$

z component of equation 8.8 leads to the following relation:

$$\frac{dz}{d\sigma} = p_z. \tag{8.41}$$

Let σ be the Σ it takes to reach the deepest point. Since the distance to the deepest point is half of $X(p_x)$, the x component of the equation 8.8 becomes

$$\frac{X(p_x)}{2} = \int_0^{\Sigma} p_x d\sigma = \int_0^{Z(p_x)} \frac{dz}{p_z}. \tag{8.42}$$

[note 12] To summarise this,

$$X(p_x) = 2p_x \int_0^{Z(p_x)} \frac{1}{(\alpha^{-2}(z) - p_x^2)^{1/2}} dz \tag{8.43}$$

Next, consider the travel time $T(p_x)$. Since we are now thinking in σ, let dt relate to generating parameter with the equation **??**,

$$dt = \frac{ds}{\alpha} = \frac{d\sigma}{\alpha^2}. \tag{8.44}$$

As in the case of X, by transforming $d\sigma$ into the integral of dz as well as X, T can be represented by

$$T(p_x) = \int_0^{s_d} \frac{ds}{\alpha} = 2 \int_0^{Z(p_x)} \frac{\alpha^{-2}}{(\alpha^{-2}(z) - p_x^2)^{1/2}} dz, \tag{8.45}$$

where s_d is the distance of the ray path from the source to the deepest point.

Finally, let us evaluate τ. Recall the definition:

$$\tau(p_x) = T(p_x) - p_x X(p_x). \tag{8.46}$$

Substituting the equation derived above, we obtain

$$\tau(p_x) = 2 \int_0^{Z(p_x)} \sqrt{\alpha(z)^{-2} - p_x^2} dz, \tag{8.47}$$

---

note 11) For details, read the textbook by Shearer[3]

note 12) Since p_x is a conserved quantity, it is often confusing to write $T(p_x) = \int p_x dX = p_x X(p_x)$. In this case. $T(p_x) = \int \boldsymbol{p} \cdot \boldsymbol{ds}$ must be evaluated. This is an example of how inconsistency can arise when considering the physical image of a moving particle if we do not take the generating parameter σ as the parameter instead of the time T.

τ has the advantage that the divergence to infinite disappears from the integral, making the actual evaluation easier.

For typical structures below, let us review the relationship between ray paths and travel time. [note 13]ß

8.6.1 In a case of monotonically increasing seismic velocity with depth

In the simplest case, let us consider travel time for monotonically increasing seismic velocity with depth. Figure 8.6 shows such an example. The ray parameter p_x conserves along the ray path. For this reason, the seismic velocity at the turning depth matches the corresponding apparent horizontal velocity $(1/p_x)$. The ray path dives to the turning depth, then it returns to the surface.

This figure shows that with decreasing parameter $p_x = \sin\theta/\alpha(z)$ (decreasing the emergency angle equivalently), the ray reaches farther (the epicentral distance $X(p)$ becomes longer). In this case, $dX/dp_x < 0$, as shown in the figure, is referred to as prograde. With increasing epicentral distance, the ray density decreases. (This means that ray density can be estimated by dp_x/dX as shown in this figure.) Therefore, the amplitude decreases with the epicentral distance.

[note 13] If you are interested in travel time calculations for real one-dimensional structures, please refer to [?, ?, Crotwell et al. 1999, Buland and Chapman, 1983]

Problem 8.1

1. Let us consider wave propagations in upper xz plane ($z > 0$). When the seismic velocity α is a linear function given by $a + bz$, show that the ray path becomes a circle given by

$$\left(x - \frac{\sqrt{1 - p_x^2 a^2}}{b p_x}\right)^2 + \left(z + \frac{a}{b}\right)^2 = \frac{1}{p_x^2 b^2}. \tag{8.48}$$

   Hint: The equation can be derived from Equation 8.8 and the Eikonal equation.
2. Derive equation 8.45.
3. Show that $T(p_x)$ is given by

$$T(p_x) = \frac{2}{b} \cosh^{-1}\left(\frac{1}{p_x a}\right). \tag{8.49}$$

4. We can calculate a ray path by numerically integrating the Hamilton equation with respect to σ. For example, ray paths in Figure 8.6 are calculated from the integration. Calculate the ray paths numerically in the same manner. Compare the analytic solution of the ray path and the numerical calculation.
   * **Note**: The first parameter of the Hamilton equation describes the change of the location, whereas the second one determines the slowness vector as conserved the total energy along the ray path (in other words, to satisfy the Eikonal equation).
   Hint:

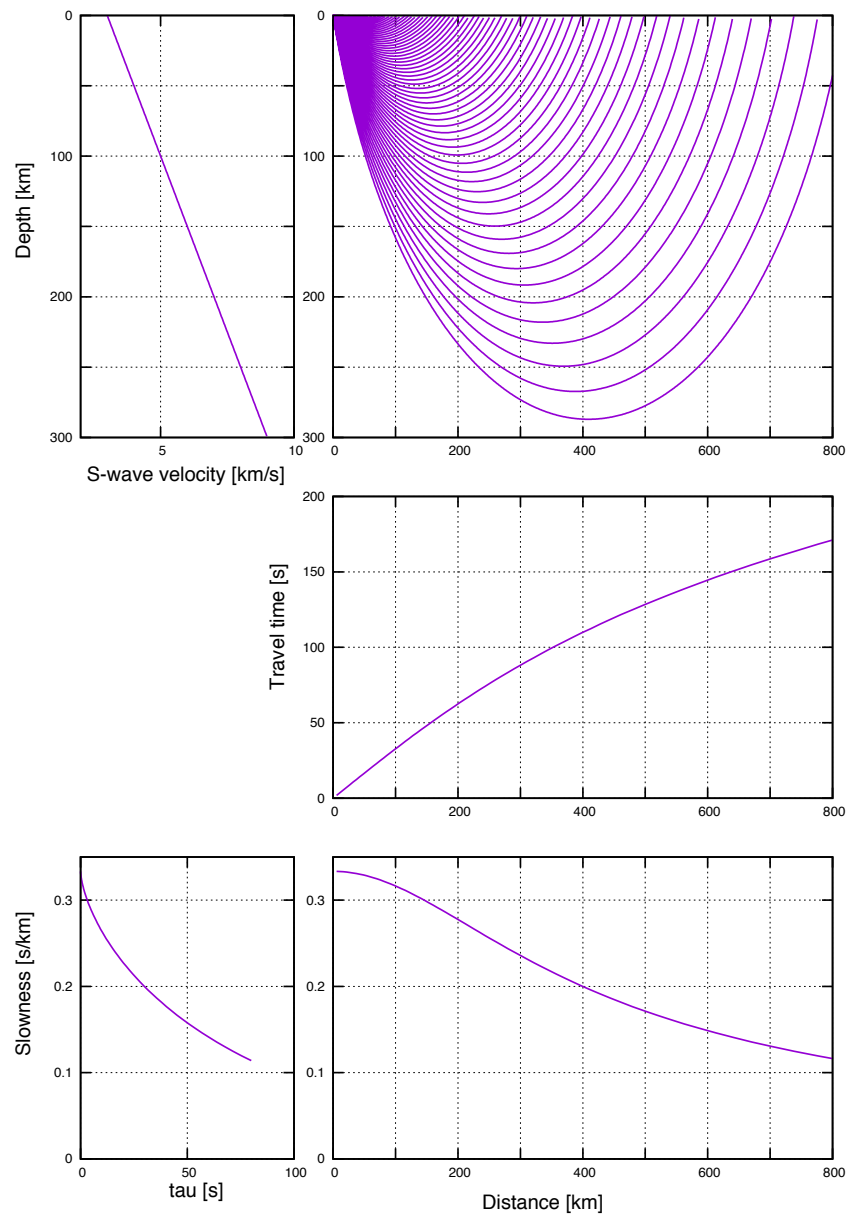$$\frac{d \cosh^{-1}(z)}{dz} = \frac{1}{\sqrt{z^2 - 1}} \tag{8.50}$$

Fig. 8.6 Ray paths for linearly increasing seismic structure with depth. We can see a relation of $p_x = dT/dx$.

8.6.2 In a case of a positive seismic jump at a depth

Next, let us consider a positive jump of seismic velocity at a depth.

When a ray path exists in the upper layer, it reaches further with the decreasing emergency angle (prograde $dX/dp<0$). When the ray enters the layer of steeply increasing seismic velocity, the ray path backs to the source side according to Snell's law. This feature characterized by $dX/dp > 0$ is referred to as a retrograde ray. When the emergency angle decreases furthermore, it dives into the deeper lower layer, and the ray path becomes prograde again. At the point for $dX/dp = 0$, known as caustic, because the ray path density diverges, the amplitudes diverge. Due to the singularity, ray theory cannot handle the wave field at around the point for $dX/dp = 0$[note 14].
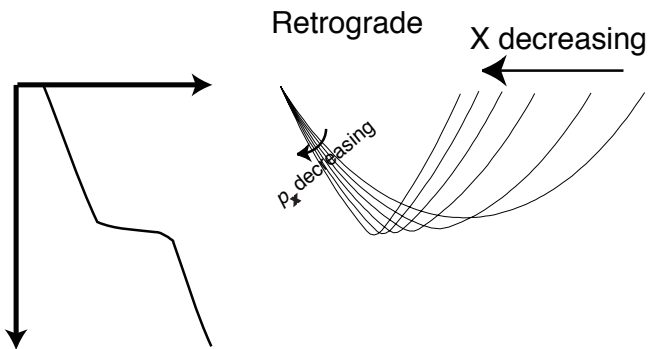
Retrograde X decreasing

p decreasing

Fig. 8.7   Schematic figure of a retrograde path.

Basic features, in this case, are common with those in a two-layer medium discussed in the previous chapter.

If you only look at the wavefront, you may find it difficult to see the triplication area because they overlap each other. Therefore, let's zoom in on the ray near the triplication area with the wavefront at the same time (Figure 8.9). The retrograde ray corresponds roughly to the green color. The caustic surface is formed at the point where the retrograde starts. When triplication occurs, the rays are folded. The wedge-shaped base of the folded wavefront corresponds to the wavefront that passes through the caustic surface, resulting in a 90-degree phase shift. You can also see that the positive velocity gradient just below the discontinuity bends the rays toward the surface, which increase the amplitude of the retrograde branch. Thus, when considering seismic waves, it is important to consider both the rays and the wavefront together. You can also see that in the $\tau - p$ region, triplication is unfolded and becomes a single-valued function.

Consider another example. It is known that a 410 km discontinuity and a 660 km discontinuity exist globally in the Earth's interior. These two discontinuities correspond to phase changes in minerals (corresponding to olivine $\longrightarrow$spinel and spinel$\longrightarrow$perovskite, respectively). Let's take a look at Figure 8.10. Here is a seismic waveform record in Alaska of an earthquake that occurred in the Aleutians at a depth of about 100 km. The waveforms are complicated, but we can see multiple P-wave packets arriving in $13° \sim 30°$. This is

---

note 14) Because the high-frequency approximation is broken down at the point close to the caustic, we must consider an appropriate solution of the wave equation which connects to the ray theoretical solution. Such a solution leads to jumping off the phase of 90° after the passage through the caustic. The phase jump is also discussed in the later section about amplitudes of a ray theoretical solution.
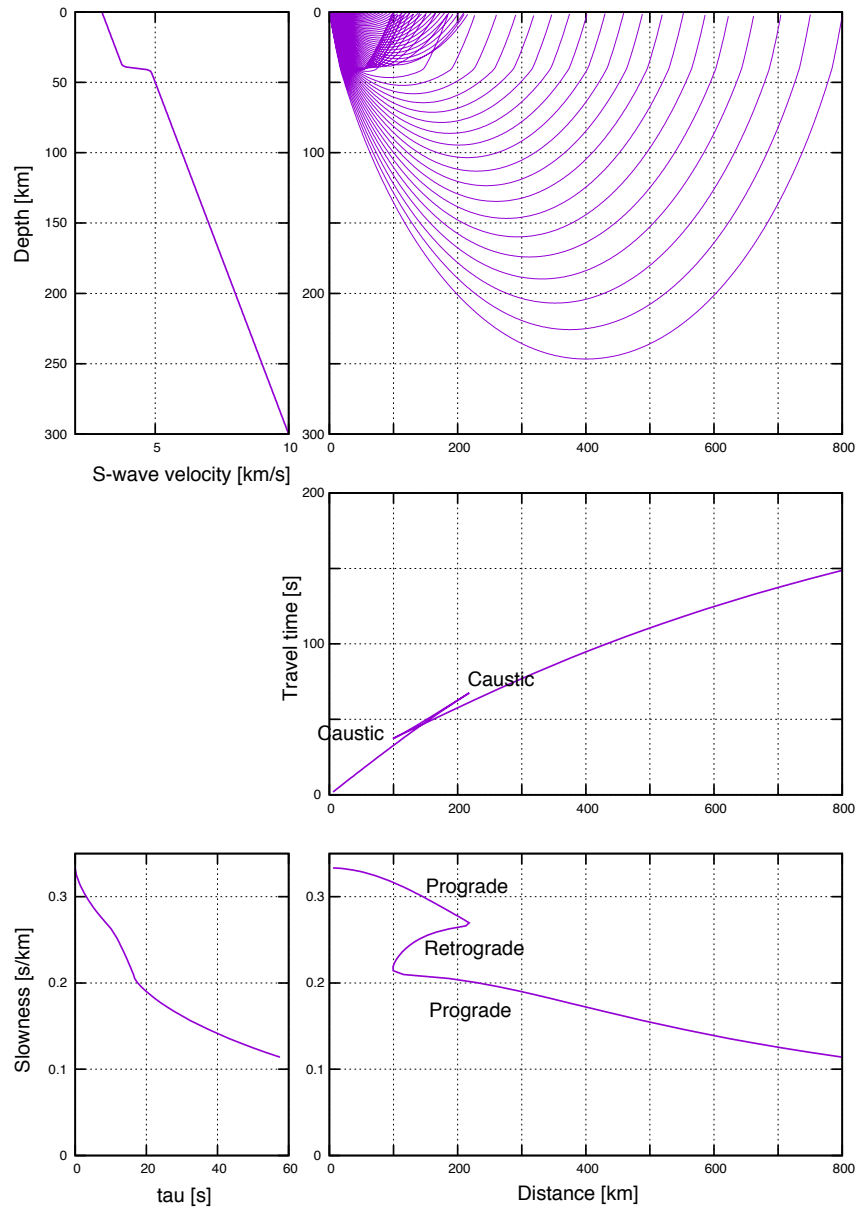
Fig. 8.8   Ray paths in a case of positive seismic jump at a depth.

the result of triplication at the 410 km and 660 km discontinuities. The lower figure shows the theoretical travel time. You can see that it roughly represents the characteristics of the observed waveforms.

Let us imagine that there is no information on the Earth's interior. From Figure 8.10, we can see that it is difficult to interpret the waveforms of the P wave except at the first arrival time when there are multiple arrivals. In the figure, this corresponds to the blue rising edge. The rise of the first arriving wave packet is easy to read (because the ground is quiet before

Fig. 8.9 Wavefront with positive seismic velocity jump. The emergence angle is shown
in color, and the wavefront (isochrones of travel time) is also shown

the arrival) and can be measured with good accuracy. If we only have information on the
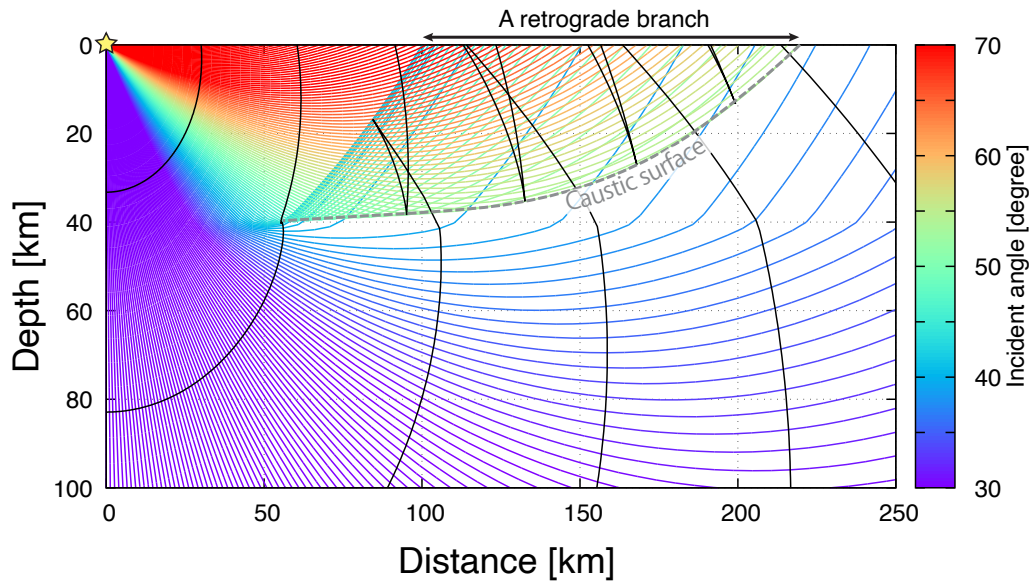first arrivals, it is difficult to distinguish it from the travel time curve for a structure without
the discontinuities (e.g, 8.6). In other words, when inferring the internal structure of the
earth from the travel time, without information on triplication, the information on the internal
discontinuity cannot be correctly estimated, and an over smooth structure will be inferred
(since the simple model can also explain the measured first arrivals).

Problem 8. 2

Let us consider wave propagation in xz plane ($z > 0$) for seismic speed α given by

$$\alpha(z) = 5 + (1 + \tanh(z - 40)) * 2 + \frac{z}{200}. \tag{8.51}$$

By numerical integration of Hamilton equations with respect to σ, calculate the ray
paths. And as in Fig 8.7, plot the relations between slowness and Travel time, that
between distance and τ, and that between τ and slowness. Then compare the results
with two layered mediums.
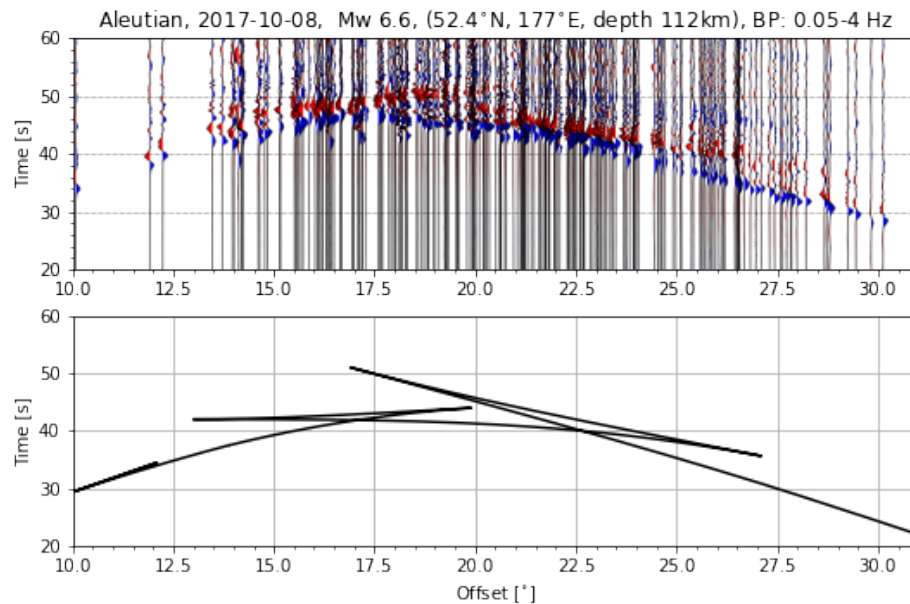
Fig. 8.10 A typical example with a positive seismic velocity jump. Velocity waveform (0.05-4 Hz) observed by USArray (Alaska) for an earthquake that occurred in the Aleutians. For a better display, the travel time of the waveform was reduced (specifically, $T(10 \text{ km/s})X$ is plotted against X). Positive amplitudes are shown in red and negative amplitudes are shown in blue. It can be seen that there are multiple arrivals of P-wave wave packets in this distance range. The lower figure also shows the corresponding theoretical travel times, where we can see the triplication corresponding to the positive jumps in the two seismic velocity jumps (410 km discontinuity and 660 km discontinuity).

8.6.3 In a case of a negative seismic jump at a depth

When a negative jump of seismic velocity with depth exists, rays cannot reach a certain area on the surface known as a shadow zone. Because rays tend to avoid the low-velocity zone, as shown in Figure 8.11, the seismic exploration of the seismic structure becomes difficult in general.

Fig. 8.11   Ray paths in a case of negative seismic jump at a depth.
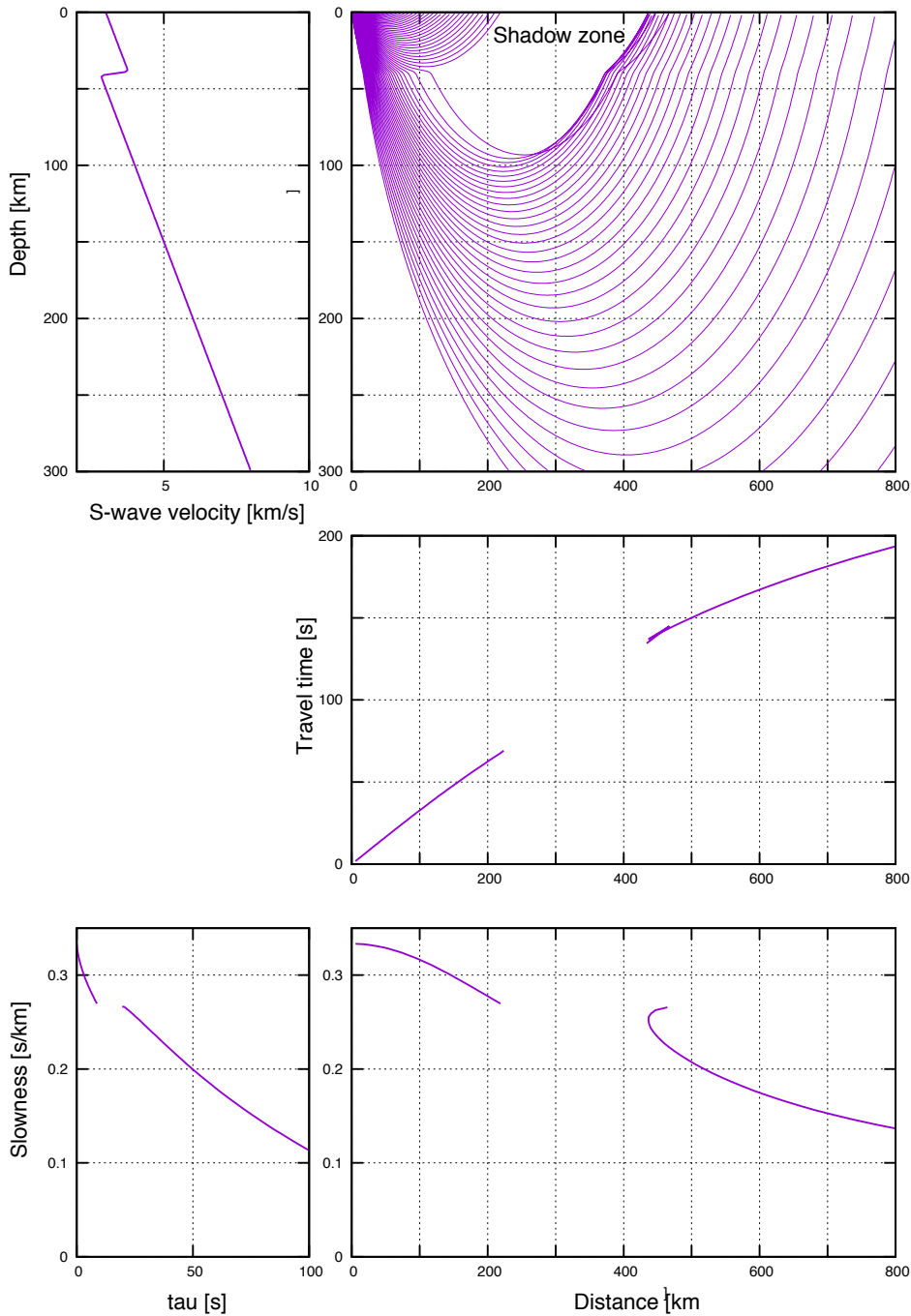
§8.7 1-D inversion

8.7.1 Herglotz-Wiechert inversion

$$T(p) = 2 \int_0^{z(p_x)} \frac{\alpha^{-2}(z)}{\sqrt{\alpha^{-2}(z) - p_x^2}} dz \tag{8.52}$$

$$X(p) = 2p \int_0^{z(p_x)} \frac{dz}{\sqrt{\alpha^{-2}(z) - p_x^2}} \tag{8.53}$$

Herglotz-Wiechert formulas

$$z(\alpha^{-1}) = \frac{1}{\pi} \int_0^{X(\alpha^{-1})} \cosh^{-1}(\alpha p_x) dX \tag{8.54}$$

8.7.2 τ-p inversion

Let us now consider the problem of inferring the structure of the Earth's interior from the travel time of seismic waves measured at the Earth's surface. Suppose we now have a perfectly measured travel time $T(X)$. In this case, the slowness p at location X is

$$p = \frac{dT}{dX}, \tag{8.55}$$

and can be obtained from its direction. The τ can be measured as the interception time (*y*-intercept) at which the tangent line is extended and intersects at $X = 0$.
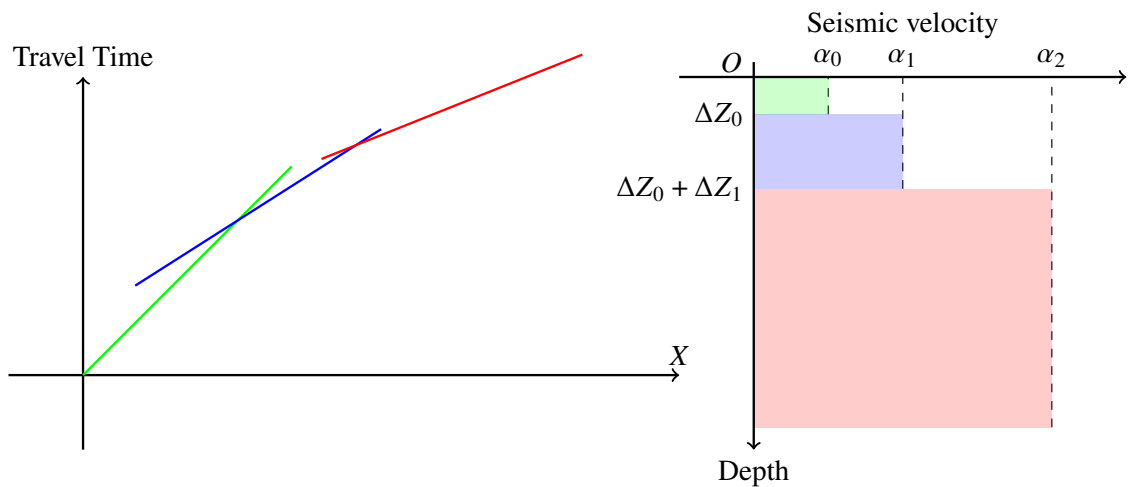

Fig. 8.12   Schematic figure of a segmented line approximation of the travel time curve.

Let us assume that the Earth's internal structure consists of n homogeneous layers. Let the thickness of the n layer be ΔZ_n and the seismic wave velocity be α_n (equation 8.12).

Discretising the equation for τ (equation 8.47), we obtain

$$\tau(p_x) = 2 \sum_{1}^{n} \sqrt{\alpha_n^{-2} - p_x^2} \Delta Z_n.$$ (8.56)

We can find here that if α_n is known, it is a linear equation. In fact, α_n can be measured from the graph. If each line is a direct wave (red), a head wave in the second layer, and a head wave in the third layer, each slowness corresponds to α_n^{-1}. The we can obtain the following relation:

$$
\begin{pmatrix} \tau_1 \\ \tau_2 \\ \vdots \\ \vdots \\ \tau_n \end{pmatrix} = 2 \begin{pmatrix} \sqrt{\alpha_0^{-2} - \alpha_1^{-2}} & 0 & 0 & \cdots & \\ \sqrt{\alpha_0^{-2} - \alpha_2^{-2}} & \sqrt{\alpha_1^{-2} - \alpha_2^{-2}} & 0 & \cdots & \\ \cdots & \vdots & & & \\ \sqrt{\alpha_0^{-2} - \alpha_n^{-2}} & \sqrt{\alpha_1^{-2} - \alpha_n^{-2}} & \cdots & & \sqrt{\alpha_{n-1}^{-2} - \alpha_n^{-2}} \end{pmatrix} \begin{pmatrix} \Delta Z_0 \\ \Delta Z_1 \\ \vdots \\ \vdots \\ \vdots \\ \Delta Z_n \end{pmatrix}.
$$ (8.57)

The linear form of the equation means that it is possible to solve the equation from the top layer.

Problem 8.3

Suppose that the travel time T [s] at a point X [km] can be measured at three locations. Assume each observation to be $(X_0, T_0) = (15, 3.00)$, $(X_1, T_1) = (80, 13.40)$ and $(X_2, T_2) = (120, 18.20)$, approximate the travel time T by a line connecting these points. Estimate the Earth's internal structure by calculating the $\tau - p$ plot.

§8.8 Tools for travel time analysis

When we calculate the travel time for a stratified Earth, taup (http://www.seis.sc.edu/taup/) is a common toolkit among seismologists. A direct Eikonal solver using fast marching algorithm is also common. This algorithm is applicable to a complex 3-D medium. Some different programs using fast marching algorithms are available at a website by Nick Rawlinson (http://rses.anu.edu.au/~nick/)。

§8.A IASPEI standard phase list

For details, see http://www.isc.ac.uk/standards/phases/.

8.A.1 CRUSTAL PHASES

Pg	At short distances, either an upgoing P wave from a source in the upper crust or a P wave bottoming in the upper crust. At larger distances also, arrivals are caused by multiple P-wave reverberations inside the whole crust with a group velocity of around 5.8 km/s.
Pb	(alt:P*) Either an upgoing P wave from a source in the lower crust or a P wave bottoming in, the lower crust
Pn	Any P wave bottoming in the uppermost mantle or an upgoing P wave from a source in the uppermost mantle
PnPn	Pn free-surface reflection
PgPg	Pg free-surface reflection
PmP	P reflection from the outer side of the Moho
PmPN	PmP multiple free surface reflection; N is a positive integer. For example, PmP2 is PmPPmP
PmS	P to S reflection/conversion from the outer side of the Moho
Sg	At short distances, either an upgoing S wave from a source in the upper crust or an S wave bottoming in the upper crust. At larger distances also arrivals caused by the superposition of multiple S-wave reverberations and SV to P and/or P to SV conversions inside the whole crust.
Sb	(alt:S*) Either an upgoing S wave from a source in the lower crust or an S wave bottoming in, the lower crust
Sn	Any S wave bottoming in the uppermost mantle or an upgoing S wave from a source in the uppermost mantle
SnSn	Sn free-surface reflection
SgSg	Sg free-surface reflection
SmS	S reflection from the outer side of the Moho
SmSN	SmS multiple free-surface reflections; N is a positive integer. For example, SmS2 is SmSSmS
SmP	S to P reflection/conversion from the outer side of the Moho
Lg	A wave group observed at larger regional distances and caused by the superposition of multiple S-wave reverberations and SV to P and/or P to SV conversions inside the whole crust. The maximum energy travels with a group velocity of approximately 3.5 km/s
Rg	Short-period crustal Rayleigh wave

8.A.2 MANTLE PHASES

P	A longitudinal wave, bottoming below the uppermost mantle; also an upgoing longitudinal wave from a sou below the uppermost mantle
PP	Free-surface reflection of P wave leaving a source downward
PS	P, leaving a source downward, reflected as an S at the free surface. At shorter distances, the first leg is represen by a crustal P wave.
PPP	analogous to PP
PPS	PP, which is converted to S at the second reflection point on the free surface; travel time matches that of PSI
PSS	PS reflected at the free surface
PcP	P reflection from the core-mantle boundary (CMB)
PcS	P converted to S when reflected from the CMB
PcPN	PcP are reflected from the free surface N-1 times; N is a positive integer. For example PcP2 is PcPPcP
Pz+P	(alt:PzP) P reflection from the outer side of a discontinuity at depth z; z may be a positive numerical valu km. For example, P660+P is a P reflection from the top of the 660 km discontinuity.
Pz-P	P reflection from the inner side of a discontinuity at depth z. For example, P660 − P is a P reflection fr below the 660 km discontinuity, which means it is precursory to PP.
Pz+S	(alt:PzS) P converted to S when reflected from the outer side of discontinuity at depth z
Pz-S	P converted to S when reflected from the inner side of discontinuity at depth z
PScS	P (leaving a source downward) to ScS reflection at the free surface
Pdif	(old:Pdiff) P diffracted along the CMB in the mantle
S	Shear wave, bottoming below the uppermost mantle; also an upgoing shear wave from a source below uppermost mantle
SS	Free surface-reflection of an S wave leaving a source downward
SP	S, leaving a source downward, reflected as P at the free surface. At shorter distances, the second leg is represen by a crustal P wave.
SSS	analogous to SS
SSP	SS converted to P when reflected from the free surface; travel time matches that of SPS.
SPP	SP reflected at the free surface
ScS	S reflection from the CMB
ScP	S converted to P when reflected from the CMB
ScSN	ScS multiple free-surface reflections; N is a positive integer. For example ScS2 is ScSScS
Sz+S	(alt:SzS) S reflection from the outer side of a discontinuity at depth z; z may be a positive numerical valu km. For example, S660+S is an S reflection from the top of the 660 km discontinuity.
Sz-S	S reflection from the inner side of discontinuity at depth z. For example, S660 − S is an S reflection from bel the 660 km discontinuity, which means it is precursory to SS.
Sz+P	(alt:SzP) S converted to P when reflected from the outer side of discontinuity at depth z
Sz-P	S converted to P when reflected from the inner side of discontinuity at depth z
ScSP	ScS to P reflection at the free surface
Sdif	(old:Sdiff) S diffracted along the CMB in the mantle

§8.B Stratified Earth models

You can find a reference stratified Earth model.

8.B.1 PREM

Preliminary Reference Earth Model http://ds.iris.edu/ds/products/emc-prem/

8.B.2 AK135

http://ds.iris.edu/ds/products/emc-ak135-f/
http://rses.anu.edu.au/seismology/ak135/intro.html

§8.3 Bibliography

[1] K. Aki and P.G. Richards. *Quantitative Seismology*. Univ Science Books, 2nd edition, 2009.

[2] F.A. Dahlen and J. Tromp. *Theoretical Global Seismology*. Princeton University Press, Princeton, 1998.

[3] P.M. Shearer. *Introduction to Seismology*. Cambridge University Press, 2009.

[4] H.W. Zhou. *Practical Seismic Data Analysis*. Cambridge University Press, 2014.

[5] 蓬田清. 演習形式で学ぶ特殊関数・積分変換入門. 共立出版, 2007.

Normal mode

Chapter 9

ここまで、実体波と表面波を概観してきました。地震学で取り扱う周期帯は $3 \times 10^{-4} \sim 100$ Hz の範囲です。おおよそ 0.005 Hz (5 mHz) より高周波数側では進行波 (実体波、表面波) として取り扱うことが多く，低周波数側では定在波 (地球自由振動) として取り扱う事が多くなります。地球自由振動帯域では、波長が 1000km を超え定在波の重ね合わせとして理解したほうが便利なためです。

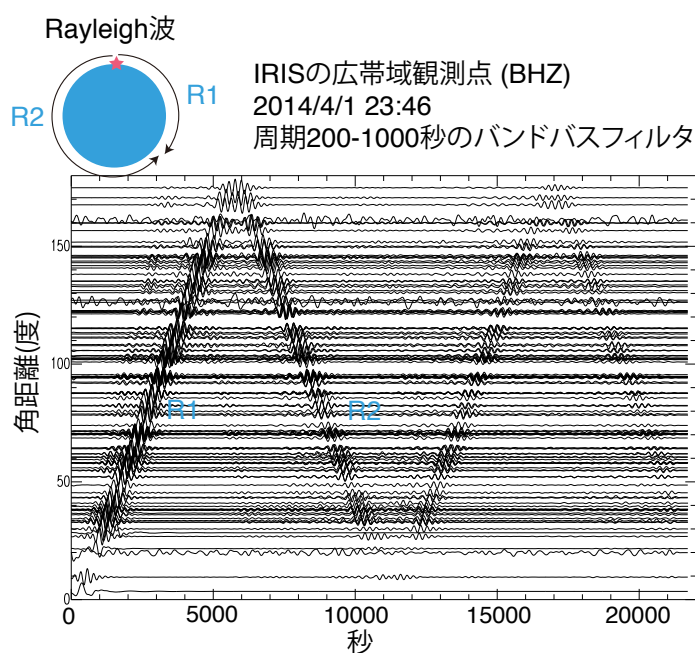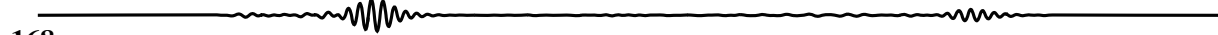## §9.1 Standing wave of the Earth: Earth's free oscillations

Fig. 9.1   Vertical components of broadband seismometers when the 2014 Chilean earthquake on April 1st.

When a huge earthquake occurs, a seismic wave with a period longer than 200 s propagates around the Earth, as shown in Figure 9.1. This figure shows global long-period surface wave propagations when the 2010 Chilean earthquake. They lasted for one day because the amplitudes attenuated with propagation distance. In this case, a modal approach is more feasible for interpreting them.

On December 26th, 2004, a huge earthquake in the Indian Ocean off Sumatra occurred. The moment magnitude is greater than 9, which is the largest one last 50 years. When the earthquake, a global network of seismometers recorded multi-orbit surface waves (more than 8). Although most of the modes (long-period surface wave equivalently) attenuated several days after the origin time, oscillations of the gravest modes lasted for several months. Only huge earthquakes (> 8.5) can excite the gravest mode on observable levels.

Figure 9.2 shows the vertical seismograms at Matsushiro, Japan. Although at a glance, this figure is similar to Figure 9.1, I note the difference of the horizontal scales. Figure 9.2 shows two-month records. The second panel shows seismogram bandpass filtered from 0.1 to 1mHz, which shows that the Earth was oscillating for more than one month. The standing wave is also known as Earth's free oscillation. Lower panels of Figure 9.2 show the spatial pattern of standing wave revealed by observed records (vertical components) at stations in Germany, the US, Australia, and Japan 1 month after the origin time. As already shown in previous figures, seismograms usually show seismic wave propagations. On the other hand Figure 9.2 shows a synchronized motion. This means that the Earth is expanding and shrinking alternatively (also known as breathing mode) with 1112 seconds. The amplitudes are about 0.03 mm. Although the amplitudes seem to be small, only a huge earthquake can excite the mode. Once the mode is excited, the mode oscillates for a long time. In the case of the Sumatra earthquake, the oscillation was lasting for 3 months on the observable level. There are many modes, such as football mode (see a box below) and pear mode, other than breathing mode.

A seismic wave field excited by an earthquake can be likened to playing the piano. Each key of a piano corresponds to a mode. The seismic wave field (sound of a piano) can be represented by a superposition of modes (striking keys of a piano). Seismologists imagine Earth's interior from Earth's sound.
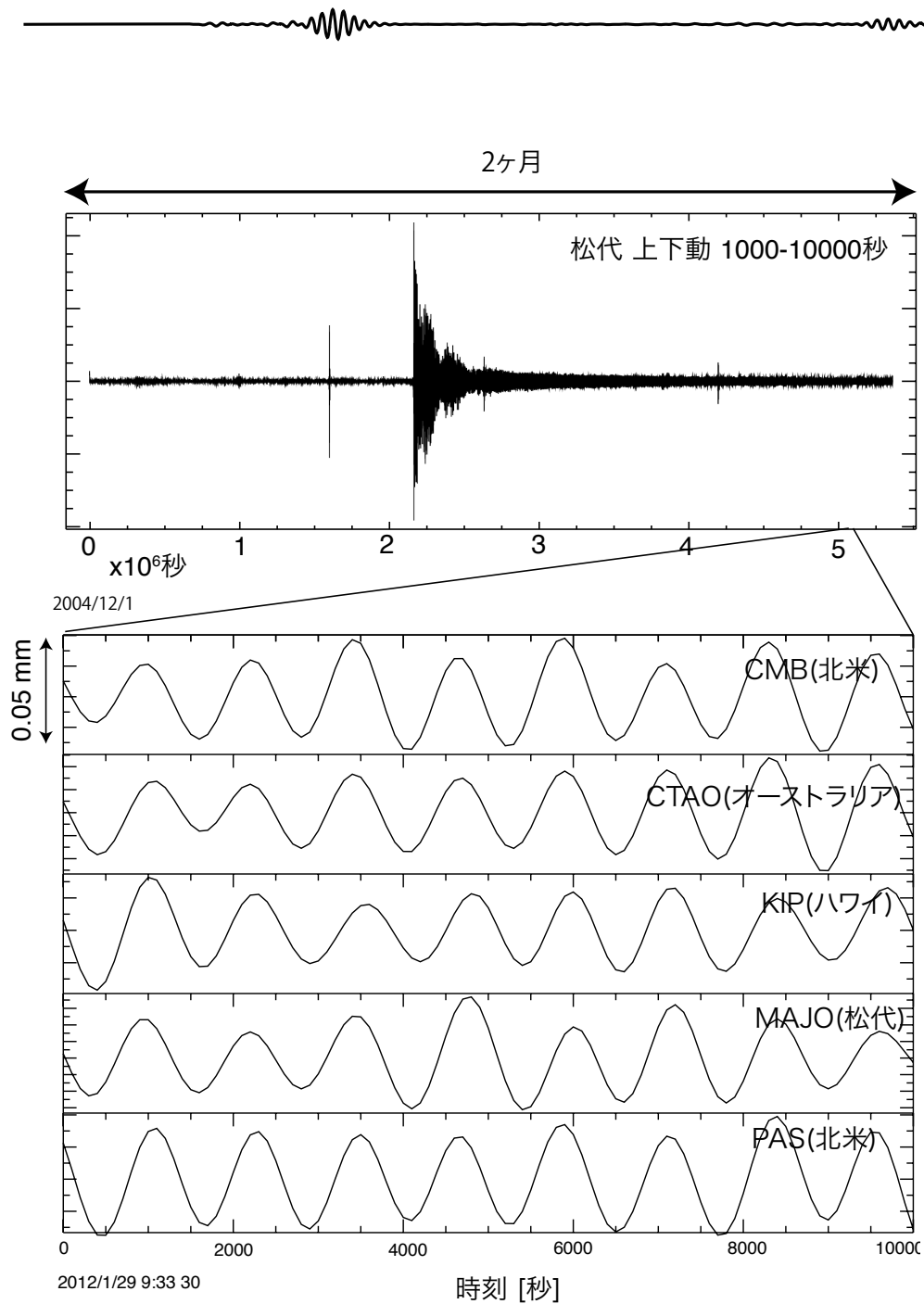
Fig. 9.2 Seismic records (vertical components) when the great Sumatra earthquake in 2004. This figure shows that the oscillation lasted for more than one month. Lowe panels is enlarged seismograms one month after the earthquake. They show synchronized vertical motions, which represent the breathing mode.

§9.2 Eigenfrequencies and eigenfunctions

(2)–(6)

§9.3 Oscillation of a string

長さ l の弦の振動を考えます。まず、波動方程式

$$\rho_0 \frac{\partial^2 u(x,t)}{\partial t^2} = \kappa_0 \frac{\partial^2 u(x,t)}{\partial x^2} \tag{9.1}$$

を満たす固有関数について考えてきます。境界条件として両端で固定端を考えます。固有周波数および対応する固有関数を、それぞれ次のようになります。

$$\omega_n = \frac{n\pi}{l} c_0, \qquad u_n(x) = A_n \sin \frac{n\pi x}{l} \tag{9.2}$$

正規化は $(\rho_0 u_i, u_j) = \delta_{ij}$ を満たすように係数 A_n を求めればよい。内積を計算すると、

$$(\rho u_i, u_j) = \int_0^l \rho_0 u_i^*(x) u_j(x) dx = \rho_0 A_i^* A_j \int_0^l \sin \frac{i\pi x}{l} \sin \frac{j\pi x}{l} dx = \rho_0 |A_i|^2 \frac{l}{2} \delta_{ij} \tag{9.3}$$

となるので、結局、

$$A_n = \sqrt{\frac{2}{\rho_0 l}} \qquad \text{i.e.} \qquad \underline{u_n(x) = \sqrt{\frac{2}{\rho_0 l}} \sin \frac{n\pi x}{l}} \tag{9.4}$$

が正規化された固有関数 (normalized eigenfunction) $u_n(x)$ です[note 1]。

次に撃力に対する応答を考えます。

$$\rho_0 \frac{\partial^2 u(x,t)}{\partial t^2} = \kappa_0 \frac{\partial^2 u(x,t)}{\partial x^2} + \delta(x - x_0)\delta(t) \tag{9.5}$$

この問題では、両端を固定された棒に対し 1 [Ns] の力積を与えたときに、どのような運動をするかを表しています[note 2]。両辺時間に対してフーリエ変換をとると

$$-\omega^2 \rho_0 \tilde{u}(x,\omega) = \kappa_0 \frac{\partial^2 \tilde{u}(x,\omega)}{\partial x^2} + \delta(x - x_0), \tag{9.6}$$

で表されます。ここで ˜ はフーリエ成分を表す。これと、波動解 $u(x,\omega)$ の固有関数展開

$$\tilde{u}(x,\omega) = \sum_{n=1}^{\infty} a_n(\omega) u_n(x) \tag{9.7}$$

[note 1] 固有関数の規格化から u_n^{-2} は重さの次元をもつことが分かります。この値は Modal mass と呼ばれます。

[note 2] 一見次元が分かりづらいが、$f(x) = -f_0 \delta(x - x_0)\delta(t)$ は [N/m] の次元を持つため、f_0 は [Ns] の次元をもちます。任意の力 $f(x,t)$ に対する振動は、以下で求める撃力応答 (Green 関数と呼ばれる) との畳み込み積分で表現出来ます。無限空間の場合、Green 関数は**??**参照。
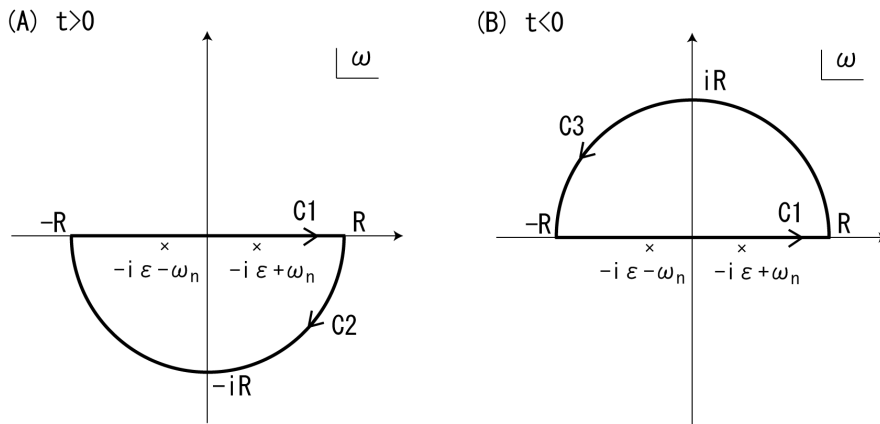
(A) t>0

(B) t<0

Fig. 9.3　積分経路

を式 (2) に代入して、両辺と固有関数 $u_n(x)$ の内積をとると、

$$\rho_0 \omega^2 a_n(\omega) - \rho_0 \omega_n^2 a_n(\omega) = -\rho_0 u_n(x_0) \qquad \text{i.e.} \qquad a_n(\omega) = -\frac{u_n(x_0)}{\omega^2 - \omega_n^2} \qquad (9.8)$$

を得ます。

最後に逆フーリエ変換で時間領域に戻す[note 3]。

$$a_n(t) = -\frac{1}{2\pi} \int_{-\infty}^{\infty} a_n(\omega) e^{-i\omega t} \, d\omega = -\frac{u_n(x_0)}{2\pi} \int_{-\infty}^{\infty} \frac{e^{-i\omega t}}{\omega^2 - \omega_n^2} \, d\omega \qquad (9.9)$$

ここで、積分値を求めるため、ω を複素数空間の変数だとみなして、図 9.3 のような経路で積分を実行し、$R \to \infty$ の極限をとります。ただし、積分経路上に極があると積分を実行できないため、極を実軸から $-i\epsilon$ ($\epsilon > 0$) だけずらした関数

$$g(\omega, t, \epsilon) = \frac{e^{-i\omega t}}{2\omega_n} \left(\frac{1}{\omega - \omega_n + i\epsilon} - \frac{1}{\omega + \omega_n + i\epsilon} \right) \qquad \left(\lim_{\epsilon \to 0} g(\omega, t, \epsilon) = \frac{e^{-i\omega t}}{\omega^2 - \omega_n^2} \right) (9.10)$$

の積分を実行してから $\epsilon \to 0$ の極限をとります。ここで、2 つの極を正にずらすか負にずらすかで 4 通り考えることができますが、いずれの場合も解は微分方程式を満たします。しかしながら、外力を受ける $t = 0$ 以前には変位がないという物理的な条件を満たすためには、2 つの極は負の方向にずらさなくてはいけません。

$t > 0$ の場合は極が積分経路内にあるので、

$$\int_{C1} g(\omega, t, \epsilon) \, d\omega + \int_{C2} g(\omega, t, \epsilon) \, d\omega \qquad (9.11)$$

$$= -2\pi i \{ \text{Res}_{\omega = -i\epsilon + \omega_n} g(\omega, t, \epsilon) + \text{Res}_{\omega = -i\epsilon - \omega_n} g(\omega, t, \epsilon) \} = -\frac{2\pi \sin \omega_n t \, e^{-\epsilon t}}{\omega_n}. \quad (9.12)$$

[note 3] 複素積分に関して詳しくは、Mathematical Methods for Physicists, Fifth Edition, Arfken, Weber, and Frank Harris[1] や演習形式で学ぶ特殊関数・積分変換入門、蓬田清[7] などを参照のこと。

この式が $t \to \infty$ で発散しないためにも、極は負にずらす必要があると言えます。正にずらした場合、$e^{\epsilon t}$ の項がかかってしまい、$t \to \infty$ で発散します。上式で $R \to \infty$ および $\epsilon \to 0$ の極限をとると、経路 $C2$ の積分が 0 になるので、

$$\int_{-\infty}^{\infty} \frac{e^{-i\omega t}}{\omega^2 - \omega_n^2} \, d\omega = -\frac{2\pi \sin \omega_n t}{\omega_n} \quad (t > 0). \tag{9.13}$$

一方、$t < 0$ の場合、積分経路内に極がないので、

$$\int_{C1} g(\omega, t, \epsilon) \, d\omega + \int_{C3} g(\omega, t, \epsilon) \, d\omega = 0. \tag{9.14}$$

上式において、$R \to \infty$ の極限をとると、経路 $C3$ の積分が 0 になるので、

$$\int_{-\infty}^{\infty} \frac{e^{-i\omega t}}{\omega^2 - \omega_n^2} \, d\omega = 0 \quad (t < 0). \tag{9.15}$$

以上より、求める $u(x,t)$ は $t > 0$ の場合、弦の振動の励起の式

$$u(x,t) = \begin{cases} \sum_n \frac{u_n^*(x_0) u_n(x)}{\omega_n} \sin \omega_n t & t \geq 0 \\ 0 & t < 0 \end{cases} \tag{9.16}$$

この式に規格化された固有関数を代入すると、求める $u(x,t)$ は $t > 0$ の場合、

$$u(x,t) = \sum_{n=1}^{\infty} a_n(t) u_n(x) = \sum_{n=1}^{\infty} \left[\frac{2 \sin \omega_n t}{\rho_0 l \omega_n} \sin k_n x_0 \sin k_n x \right] \tag{9.17}$$

となります[note 4]。ここで $k_n = n\pi/l$ と定義します。

見通しを良くするために、上記の式を積和の公式を用いて上式を書き直します[note 5]。

$$u(x,t) = -\frac{1}{2\rho l} \sum_{n=1}^{\infty} \frac{1}{\omega_n} \left[\sin(\omega_n t - k_n(x + x_0)) - \sin(\omega_n t + k_n(x + x_0)) \right.$$
$$\left. - \sin(\omega_n t - k_n(x - x_0)) + \sin(\omega_n t - k_n(x - x_0)) \right] \tag{9.18}$$

ここで $\sum_{n=1}^{\infty} \frac{\sin \omega_n t}{\omega_n}$ をじっとにらんでみると微分してみると δ 関数の形であることが分かります。つまり Heviside の階段関数 $H(t)$ [note 6] と関係していることが分かります。やや天下り的ですが、$0 \leq x < l$ の区間で $H(x) - x/l$ という式を考えフーリエ級数展開すると

$$H(x) - x/l = \frac{2}{\pi} \sum_{n=1}^{\infty} \frac{1}{n} \sin k_n x, \tag{9.19}$$

となります。この関係式を使って式を整理すると、

$$u(x,t) = \frac{1}{4\rho_0 c_0} \sum_{n=1}^{\infty} H_p(c_0 t + (x - x_0)) + H_p(c_0 t - (x - x_0)) - H_p(c_0 t - (x + x_0)) - H_p(c_0 t + (x + x_0)), \tag{9.20}$$

[note 4] 次元を考え式を眺めてみると、見通しが良くなります。1 [Ns] の力積を与えた場合の運動量変化分を求め、Modal mass で割って速度を計算します。そして、周波数で割って変位に直していると解釈できます

[note 5] 詳しくは、キーナー応用数学下巻

[note 6] Heviside の階段関数 $H(t)$ 以下のように定義される。

$$H(t) = \begin{cases} 1 & t > 0 \\ 0.5 & t = 0 \\ 0 & t < 0 \end{cases}$$

と書き下せます。ここで $H_p(x) = H(x) - H(-x), -l < x < l$ と定義し, 空間で $2l$ の周期性があるとします。$t = 0$ 直後の伝播の模式図を図 9.4 に示す。$t = 0$ では、最初の 2 項が完全に打ち消しあっています[note 7]。そこから伝播をはじめ、直後の $t = t_0$ では中心から変位が広がっていきます。これは力積を与えられて弦が上方に移動しようとしているとも解釈できます。左向きに伝搬している波 $H_p(c_0 t + (x - x_0))$ が左端 $x = 0$ に達すると、境界条件を満たすため位相が反転し反射 (固定端反射) します。反射はは $H_p(c_0 t - (x - x_0))$ で表現されます。$x = 0$ 付近では、$H_p(c_0 t - (x - x_0))$ と振幅を打ち消しあうので変位は 0 になります。
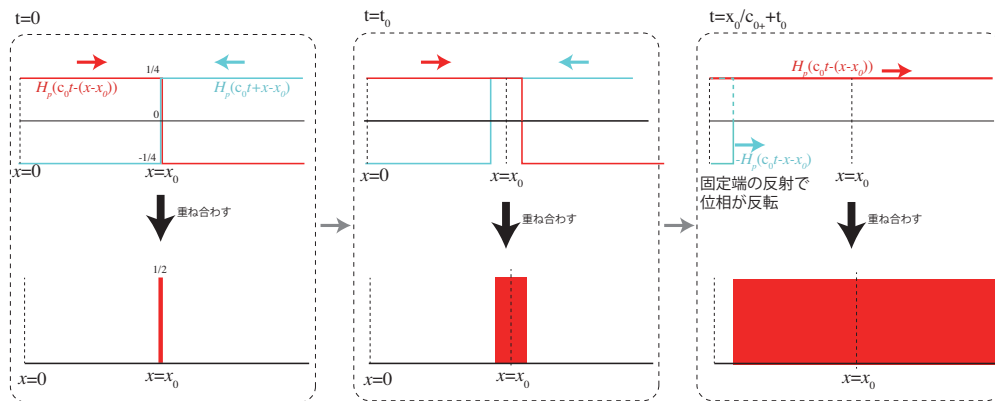

Fig. 9.4　模式図。

　実際に $n = 1, 2, \cdots, 40$ までを足してみた結果を図 9.5 左と図 9.6 に示します。パラメータは $\rho_0 = 1$[kg/m], $\kappa_0 = 1$ [N], $l = 1$ [m], $x_0 = 0.3$ [m] としました。このとき、情報は $c = 1$ [m/s] で伝播します。力を加えた場所から左右に常に正の振幅が伝播します。固定端で反射されると図 9.4 の一方の符号が反転するため、結果として、反射した波がもう一方の波の振幅と打ち消しあって 0 になる様子が見えます。

　また、$\sin(\omega_n t)/\omega_n$ を $\exp(-\omega_n^2 \tau_0^2) \cos(\omega_n t)$ で置き換え $\tau_0 = 0.01$ [s] とした場合の結果が図 9.5 の右図と 9.6 である[note 8]。パルスが波源から 2 方向に伝播し、両端で位相が逆になる様子が確認できます。また、伝播速度は 1 [m/s] であり、与えたパラメータから求まる速度 $c_0 = \sqrt{\kappa_0/\rho_0} = 1$ [m/s] と一致しています。

　以下補足です。次に弦の運動量変化を考えてみましょう。1 Ns の力積を与えたということは、棒が固定端を感じるまでは棒の持つ運動量は 1Ns となるはずです。そこで棒の持つ運動量を計算してみます。まず簡単のため $0 < x < l/2$ と仮定し $0 < t < x_0/c_0$ の時刻区間を考えます。運動量は
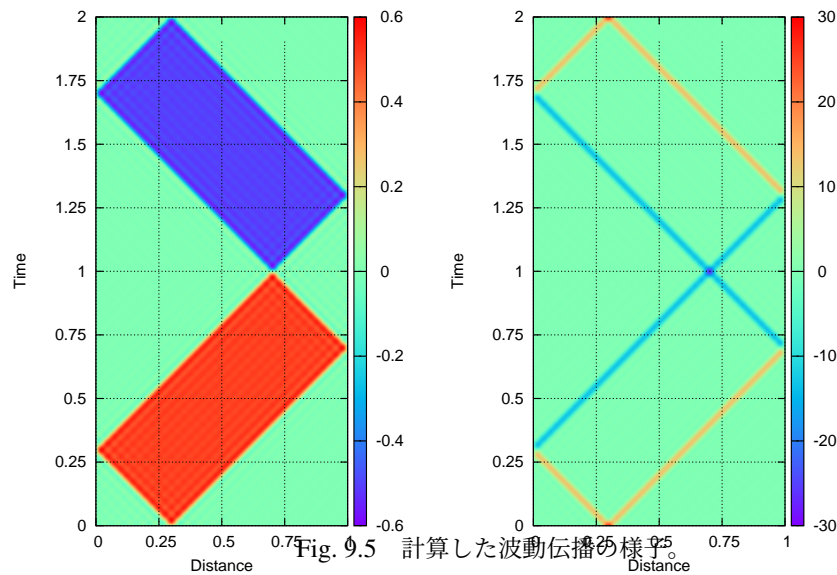
$$\rho \frac{du(x,t)}{dt} = \frac{\delta(c_0 t + (x - x_0)) + \delta(c_0 t - (x - x_0))}{2}, \tag{9.21}$$

と書けます。脚注でも述べたとおり図 9.5 右と図 9.6 のグラフは速度波形と対応するため、この速度波形の解析解とも対応しています。積分し棒全体での値を計算すると 1 [Ns] となる。$x_0/c_0 < t < (l - x_0)/c_0$ の時刻区間では

$$\rho \frac{du(x,t)}{dt} = \frac{-\delta(c_0 t + (l - x_0)) + \delta(c_0 t - (x - x_0))}{2}, \tag{9.22}$$

[note 7] 伝播方向が逆向きの $H_p(c_0 t + (x - x_0))$ と $H_p(c_0 t - (x - x_0)$ を考えている事に注意。ダランベールの解の形になっていて、直感的に理解しやすい。

[note 8] この置き換えは $\sin(\omega_n t)/\omega_n$ を時間微分して速度波形にし、周期 τ_0 でローパスフィルターをかけているとも解釈できます。
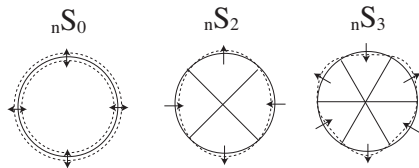
~~~~~~

Fig. 9.5 計算した波動伝播の様子。

となり、全空間で積分すると運動量は 0 [Ns] となります。つまり左端に波が到達すると、固定端のため端で下方に 1[Ns] の力積 (運動量変化分) をうけます。

9.3.1 ポイント

1. 規格化を忘れずに。$\kappa(x), \rho(x)$ が分布を持つ場合は、密度を含めた形で内積を定義しないと固有関数が直交しない。
2. 複素積分のさいに、t の符号により積分路を変える必要があることに注意。上記の議論で極が $z = 0$ より下にのみ存在する時は因果律を満たすことが分かる。主値積分を考える場合は、極限をとっても特異点周りの積分の寄与が消えないことに注意[note 9]。

§9.4 Spheroidal and toroidal modes

Earth's seismic mode of a stratified Earth can be categorized into (i) spheroidal modes and (ii) toroidal modes. seismic wave field can be represented by the superposition completely.

The reason why we can count up the number of modes is that the Earth has a finite spatial size. The scale of the Earth is closely related to the frequency spacing of the modes. From a mathematical point of view, this is an eigenvalue problem of ordinary differential equations.

- spheroidal modes $_nS_l$, where n represents the radial order, and l shows number of nodes in the horizontal direction. The superposition of spheroidal modes represents

---

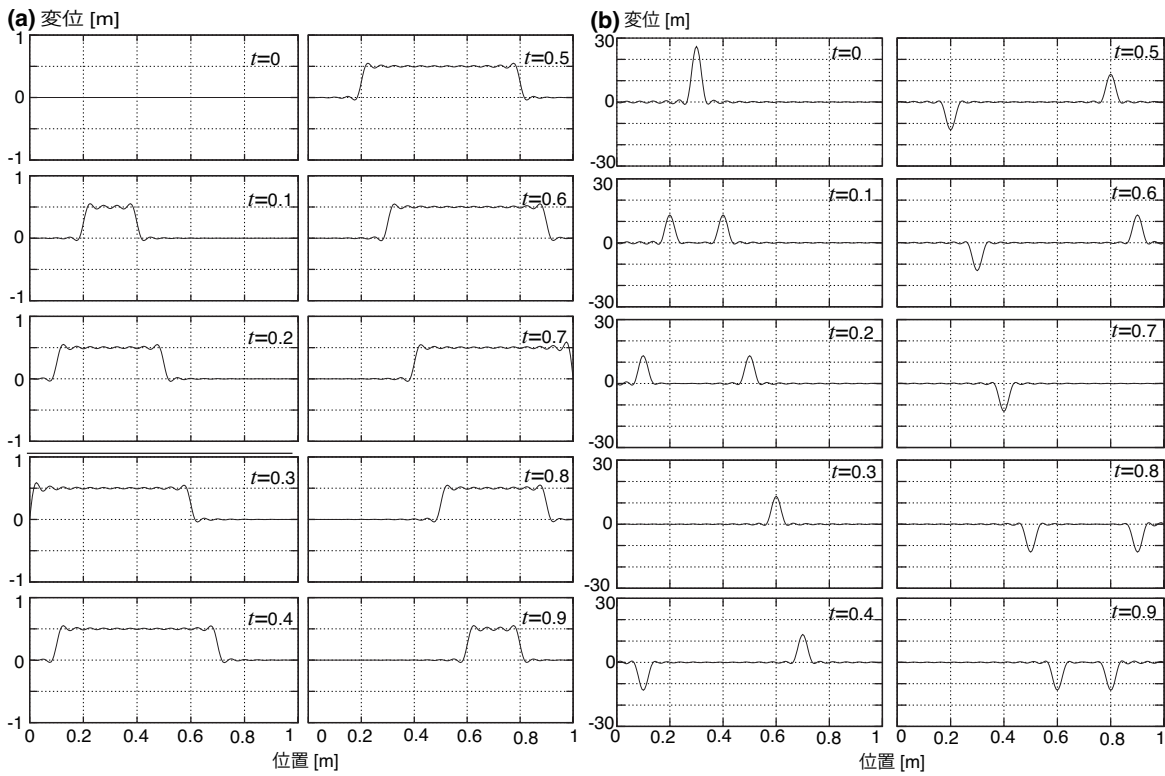[note 9] 複素積分をせずとも、$t = 0$ での解の接続を考えれば泥臭く解くことも出来る。

Fig. 9.6 (a) 撃力応答に対する、計算された波形のスナップショット。(b) 励起項を置き換えた場合の、波形のスナップショット。

the P-SV wave. In particular, spheroidal modes with $n = 0$ are called fundamental spheroidal modes, which correspond to the Rayleigh wave.

- Toroidal modes $_nT_l$, where n is the radial order, and l shows number of nodes in the horizontal direction. The superposition of toroidal modes represents the SH wave. In particular, toroidal modes with $n = 0$ are called fundamental toroidal modes, which correspond to Love wave.

§9.5 Normal mode of a homogeneous sphere

$$\nabla^2 P = -\frac{\omega^2}{c^2} P \tag{9.23}$$

$$\nabla^2 = \frac{1}{r^2}\left(\frac{\partial}{\partial r} r^2 \frac{\partial}{\partial r} + \nabla_1{}^2\right) \tag{9.24}$$

$$\nabla_1{}^2 = \frac{1}{\sin\theta}\frac{\partial}{\partial\theta}\sin\theta\frac{\partial}{\partial\theta} + \frac{1}{\sin\theta^2}\frac{\partial^2}{\partial\varphi^2} \tag{9.25}$$

Assuming that $P = R(r)\Theta(\theta)\Phi(\varphi)$.

$$\frac{1}{r^2}\left[\left(\frac{\partial_r r^2 \partial_r R}{R}\right) + \frac{\nabla_1^2(\Theta\Phi)}{\Theta\Phi}\right] = -\frac{\omega^2}{c^2}. \tag{9.26}$$

9.5.1 Horizontal direction

$\frac{\nabla_1^2(\Theta\Phi)}{\Theta\Phi}$ should be constant. Such a solution of $\Theta\Phi$ can be represented by a spherical harmonics Y_l^m with the angular oder l and azimuthal order m, because

$$\nabla_1^2 Y_l^m = -l(l+1)Y_l^m, \tag{9.27}$$

9.5.2 Radial direction

Search eigenvalues of the following ODE

$$\frac{1}{r^2 R}\left(\frac{d}{dr}r^2\frac{d}{dr}R\right) = \frac{l(l+1)}{r^2} - \frac{\omega^2}{c^2}. \tag{9.28}$$

with the boundary condition: $R = 0$ at $r = r_0$. The first term of the right-hand side represents the squared horizontal wavenumber, and the second one represents the squared total wavenumber.

§9.6 Vector spherical harmonics

$$\mathbf{R_{lm}} = Y_l^m \hat{\mathbf{r}} \qquad (9.29)$$

$$\mathbf{S_{lm}} = \nabla_1 Y_l^m \qquad (9.30)$$

$$\mathbf{T_{lm}} = -\hat{\mathbf{r}} \times \nabla_1 Y_l^m \qquad (9.31)$$

Vector spherical harmonics are more complicated than spherical harmonics, but they are also eigenfunctions for ∇_1^2 as e.g. $\nabla_1^2 \mathbf{T_{lm}} = -l(l+1)\mathbf{T_{lm}}$. See Dahlen and Tromp 1998 p. 872 for details (please be aware of the different normalization of spherical harmonics).

§9.7 Rayleigh wave and Love wave

§9.8 An example of an observed spectrum

Figure 9.7 shows an example of the Fourier spectrum of vertical ground motion at a Japanese station when the Chilean earthquake in 2010. We can identify many modal peaks of fundamental spheroidal modes. The dominance exhibits that the source depth is shallow. When a huge deep earthquake occurs, the Fourier spectrum shows large amplitudes of the overtones.
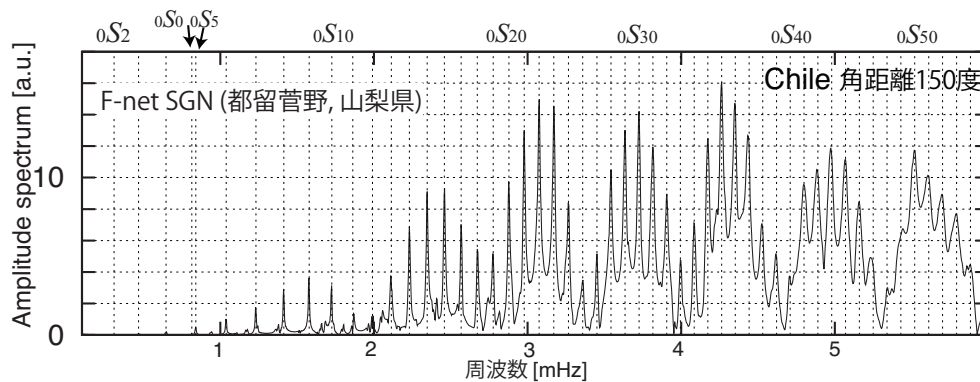

Fig. 9.7   Fourier spectrum of vertical ground motion at a Japanese station when the Chilean earthquake in 2010.

図 9.1 は Rayleigh 波の波群が地球をグルグルと巡っている様子が見てとれます。波群の現れる間隔は表面波が地球を一周する時間に対応しています。図 9.7 のスペクトルピークの間隔と、表面波が地球一周するのに要する時間を比較しみましょう。Jeans の関係式から波長 λ は地球半径を R_E とすると

$$\lambda_l = \frac{2\pi R_E}{l + 1/2} \tag{9.32}$$

と書くことができます。l に対応する固有周波数 f_l は位相速度を c_p とすると

$$f_l = \frac{c_p}{\lambda_l} = \frac{(l + 1/2)c_p}{2\pi R_E} \tag{9.33}$$

となります。大雑把に $c_p = 4.5$ km/s とすると、$f_{l+1} - f_l \sim 0.1$ mHz となり、おおよそ観測されたモードの間隔と一致します。

ピークの包絡線に注目すると周期的に山があるように見えます。この山について考察してみましょう。方位量子数 $l(m = 0$ を仮定$)$ のモードの振幅の絶対値は、震源と観測点の角距離を Θ とすると

$$|P_l^0(\cos\Theta)| \sim \sqrt{\frac{2}{l\pi\sin\Theta}}|\cos[(l + 1/2)\Theta - \pi/4]| \tag{9.34}$$

と書けます。いま Θ を固定して *l* を変化させると、おおよそ π/Θ ごとに山ができそれが繰り返されることが分かります。チリ地震の場合 SGN までの角距離は 154 度です。この場合対蹠点 (震源の真裏) に波が集まってくるので、対蹠点からの角度 (180-154) 度で見積もるとわかりやすい[note 10]。この場合山の幅は *l* が 7 個分と見積もられ観測と一致します。これらの現象は、単純にモードの節が繰り返し現れるために起こります。

§9.9 Bibliography

[1] G.B. Arfken and H.J. Weber. *Mathematical Methods for Physicists*. Elsevier Science, 2013.

[2] F. Gilbert. Excitation of normal modes of the earth by earthquake sources. *Geophys. J. R. Astron. Soc.*, Vol. 22, p. 223, 1971.

[3] G Laske and R Widmer-Schnidrig. 1.04 - theory and observations: Normal mode and surface wave observations. In Gerald Schubert, editor, *Treatise on Geophysics (Second Edition)*, pp. 117–167. Elsevier, Oxford, January 2015.

[4] Masanori Saito. *DISPER80; a subroutine package for calculation of seismic normal-mode solutions*, pp. 293–319. Acad. Press. San Diego, 1988.

[5] H. Takeuchi and M. Saito. Seismology: Surface waves and free oscillations. In B.A. Bolt, editor, *Methos in Computational Physics*, Vol. 11, pp. 217–295. Academic Press, New York, 1972.

[6] 斎藤正徳. 地震波動論. 東京大学出版会, 2009.

[7] 蓬田清. 演習形式で学ぶ特殊関数・積分変換入門. 共立出版, 2007.

[note 10] もちろん $\Theta = 150°$ でも見積もることができるが、その場合には *l* が整数であることに気をつけること。

Seismic Interferometry

Chapter 10

§10.1 Introduction

　地球内部の構造を知るには、地震波の伝わり方が重要な手がかりとなります。これまで、地震の引き起こした地面の震動を観測する事によって、地震波速度構造がイメージングされてきました。2000 年代に入り、地震以外の現象が引き起こすランダムな地面の揺れを調べる事で、地球の内部構造を調べる手法 (地震波干渉法) が一般的[note 1]となってきました。この章では、これまで学んだ知識を持とに、地震波干渉法の原理について解説していきます。

　本解説ではランダムな波動場として、海洋波浪が引き起こす脈動について取り上げます (4.7.1 章参照)。ランダムな波動場としては、地震のコーダ波 (多重散乱した地震波。詳しくは Sato Fehler and Maeda 2012[10] 参照) も重要です。コーダ波を使った地震波干渉法も広く研究されています (例えば Campillo and Paul, 2003)[2] が、今回は時間の都合上詳細は述べません。興味がある場合は、前に上げた review 論文や教科書を参照してください。

§10.2 A brief history of Seismic Interferometry

[note 1] 最近多くのレビュー論文 (例えば Snieder and Larose (2013)? や教科書 (例えば、Schuster, (2009)[19] Sato, Fehler and Maeda (2012),[10] Nakata et al (2019)[7] 等をを参照)。

　地震波干渉法は、地球だけではなく実験室スケール (e.g., Lobkis and Weaver, 2001)[6]、建築構造物 (e.g., Snieder and Wapenaar, 2010),[13] 日震学 (e.g., Gizon et al., 2010)[5]、海洋音響学 (e.g., Roux and Kuperman, 2004)[9] など色々な現象に適応されています。

　地震波干渉法のアイデアは 1950 年代までさかのぼります。Aki (1957)[1] による空間自己相関法 (SPAC 法) のアイデアは地震波干渉法の先駆けです。Ocean acoustics の分野では Cox (1973),[4] exploration seismology の分野では Claerbout (1968)[3] の先駆的が仕事があります。Aki のアイデアはしばらくの間注目されませんでした[note 2]。しかし発表から 26 年後の 1983 年に元北海道大学岡田広らを中心とする研究グループが Aki の手法に注目し (岡田・坂尻, 1983)[20]、主に表層付近の地盤特性を調べるための手法 (微動探査, microtremor survey) として盛んに研究されるようになりました。その後微動探査は地表付近のごく浅い構造を推定する際には、標準的と手法なりました。

　地震学の分野で地震波干渉法が注目されるようになったきっかけの論文は Campillo and Paul, [2003][2] です。この論文ではメキシコで発生した地震波を解析しました。地震波記録のなかでも、十分に散乱したコーダ波部分の相互相関を計算することによって、表面波の伝播を抽出できることを示しました。2005 年に Shapiro らは[12]、脈動が色々な方向から常に到来しているという事実を逆手に取り、その波の伝わり方からカリフォルニアの地殻構造を推定する事に成功しました。ambient noise tomography と呼ばれる手法です。この研究に続き、北米、日本、中国、ヨーロッパなど、数多くの地域で同種の研究が行われるようになりました。

Fig. 10.1　MAJO(松代) と他の観測点間の上下動記録の相互相関関数を観測点間の距離で並べた図。周期 20-200 秒のバンドパスフィルターをかけています。レーリー波の伝播を見て取れます。遅延時間が正の波束を causal part とよび，負の波束を acausal part とよびます。)

　地震波干渉法で基本になる観測量は、2 つの観測点を選び地震波形の相互相関関数である。相互相関関数の波形は、あたかも一方の観測点に震源 (a virtual source) があり、もう一方の観測点で波形を記録していると解釈できます。ここで図 10.1 を見て見ましょう。

[note 2] 安芸さんの仕事は博士論文としてまとめられています。自伝によると、ウィナーのサイバネティクス (筑摩文庫，岩波文庫) から着想を得たそうです。博士論文として、理論、観測機器の設計作成、観測、構造の推定まで独力で行いました。コンピュータが普及する前の時代なので、相互相関係数の計算もアナログ回路の設計からしたそうです。当時、東大理学部のグランドで観測を行ったそうで、最後自分でグラウンドを掘って、構造推定の結果を確かめたそうです。

松代にある観測点と他の観測点の相互相関関数を示しています。この手法には大きく分けてメリットが 2 つあります。

　1 つ目は地震が無い領域でも、仮想的にイベントを置くことが出来ることです。通常地震が無い領域では、地震波速度構造の詳しい地震波速度構造は分からないため、地震を必要としないのは大きなメリットである。図 10.1 も確かに、あたかも松代が震源であるかのような Rayleigh 波の伝播を見て取れます。

　2 つ目は地震を待つ必要がない点である。通常地震波トモグラフィ解析を行うためには、十分な地震データが蓄積されるのを待つ必要があります。地震波干渉法では、一定期間観測すれば十分な質のデータを確保することができます[note 3]。地震を待つ必要が無いという性質は、地震波速度構造の時間変化を調べる上で非常に有利です。地震を使って、微少な地震波速度構造の時間変化を調べるためには、繰り返し同じ場所で地震が起こる (繰り返し地震と呼ばれる) 事を待つ必要があります。しかし、そのような都合の良い地震が起こることは非常に希です。あるペアの相互相関関数を計算し、その時間変化を見ることは、繰り返し同じ場所で起こっている地震の記録を解析する事に相当します。実際、火山や地震に伴う構造の時間変化が盛んに研究されるようになってきたました (例えば Sens-Schönfelder Wegler, 2006[11])。

　ここでは、理論的背景を説明し、地震波干渉法の原理について解説していきます。ここの解析事例は、冒頭で挙げた review 論文を参考にしてください。

Rough Earth Club and Smooth Earth Club

SI brings a reunion of different research fields: ocean acoustic (Cox, 1973), seismic exploration (Claebout, 1968), and seismology (Aki 1957). Surprisingly the ideas were proposed independently and simultaneously.

Even in the seismological community, there were different cultures: one is the rough Earth club and smooth Earth club. Keiiti Aki defined them in his letter to V. I. Keilis-Borok, as

> . . . To a geodynamicist, the earth's property is smoothly varying within bodies bounded by large-scale interfaces. Most seismologists also belong to this "smooth earth club" because once you start with an initial model of smooth earth, your data usually do not require the addition of small-scale heterogeneity to your initial model. As summarized well in a recent book by Sato and Fehler (1998), the acceptance of coda waves in the data set is needed for the acceptance of small-scale seismic heterogeneity of the lithosphere. There is an increasing number of seismologists who accept it, forming the "rough earth club." I believe that you are also a member of the rough earth club, judging from the emphasis on the hierarchical heterogeneity of the lithosphere. . .

(''Seismology of Earthquake and Volcanic Prediction'', Lecture notes, Aki 2003). Seismic wavefield above 1 Hz was a territory of the "rough Earth club," whereas that below 0.1 Hz was a territory of the "smooth Earth club." The members of the rough Earth club are familiar with stochastic treatments of the seismic wavefield. The recent development of SI means a reunion between the "rough Earth club" and the "smooth Earth club."

The dominant frequency of microseisms at around 0.2 Hz corresponds to the gap between "*rough Earth club*" and "*smooth Earth club*". SI enables us to utilize coherent signals from random seismic wavefields with an assumption of stochastic stationary excitation. Although surface wave tomography was a tool of the "smooth Earth club," SI broke the gap. Scattering due to strong lateral heterogeneities in the crust and the sediment was a big barrier for "*smooth Earth club*." When we apply SI, the scatterer is important because it enhances the randomness.

[note 3] 周波数帯にもよりますが、大雑把な感覚でいうと、0.05-0.5 Hz であれば数ヶ月、それより高周波数だと数日で十分なことが多いです。もちろん、十分な精度を確保するためには長期間の観測の方が有利となります。

SI plays a complementary role in the "smooth Earth club." This role of SI is true of other communities, such as seismic exploration, acoustic, physical oceanography, and so on.

In this lecture, the next chapter explains the excitation mechanism of microseisms by ocean swell. The next chapter explains the basic principle of SI with a demonstration by a WEB application. Then the last chapter explains some applications, which are done by our group mainly.

§10.3 Theoretical background of Seismic Interferometry: a closed system

地震波干渉法の理論を理解するため単純な場合を考えてみましょう。[note 4]。

まず最初に、相互相関関数の定義をおさらいします。ウェブアプリを作ったので (`http://www.eri.u-tokyo.ac.jp/knishida/Seismology/wave2Drandom2.html`) 適宜実行しながら読むと分かりやすいと思います。

10.3.1 Cross-correlation analysis

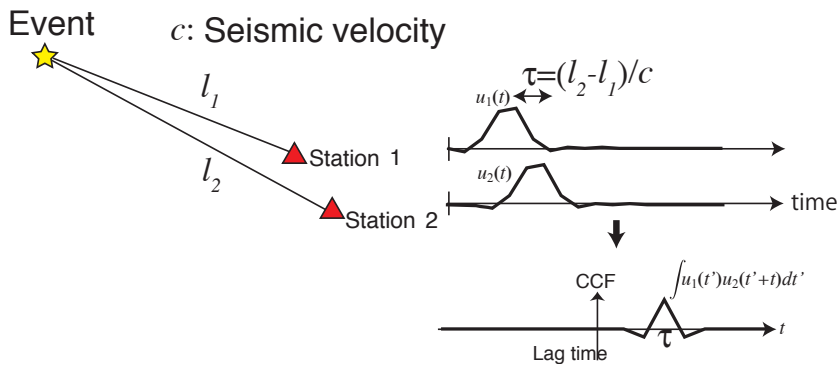Fig. 10.2 Schematic figure of cross-correlation analysis for a pair of seismograms when an earthquake ocurred.

First, we consider a transient phenomenon such as an earthquake or a volcanic explosion. 図 10.2 のようにある位置で地震が起きたことを考えます。観測点 1 と 2 の地震計記録に対して相互相関関数 ϕ_{12} を

$$\phi_{12}(t) = \lim_{T \to \infty} \frac{1}{T} \int_0^T u_1(\tau) u_2(t + \tau) d\tau. \tag{10.1}$$

のように定義します。相互相関関数は $|t|$ が大きくなると十分速く 0 に収束すると仮定するとそのフーリエ変換 $\Phi_{12}(\omega)$ を

$$\Phi_{12}(\omega) = \langle U_1^*(\omega) U_2(\omega) \rangle \tag{10.2}$$

と定義出来ます[note 5]。その場合、観測点 2 は観測点 1 より τ 秒だけ遅れて波が到達する

---

note 4) 理論的な取り扱いを大局的に理解するには、Snieder et al. (2010)[14] がお勧め。

note 5) 正確には、定常過程を考える場合には、長時間の積分をアンサンブル平均で近似しています。定常的に波動場が励起されていると仮定しているので、$u_i(t)$ は自乗可積分とはならないので、通常の意味でフーリエ変換は出来ません。より厳密に理解したい場合は時系列解析の参考書などを参照してください。

(図 10.2 右)。その場合相互相関関数は $t = \tau$ にピークをもつ。つまり、相互相関関数の
ピークの時刻を読むことによって、地震波到達時刻の差 (走時差) を読むことができます。
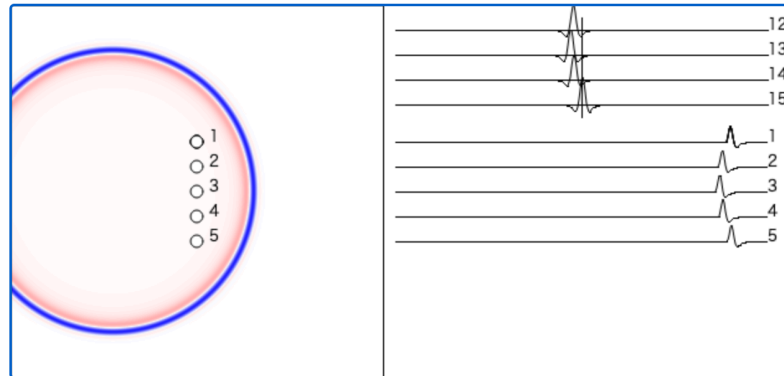実際精密に震源位置を決定するために、相互相関関数による精密な走時差の測定は良く利
用されます。

Fig. 10.3 点震源を置きシミュレーションした結果の例。右下の図は、観測点 1 から 5
で観測された波形を表し、右上はその相互相関関数を表す。

ウェブアプリでは、クリックすると震源を任意の場所に置くことが出来、s を押すとシ
ミュレーションが始まります。右下に観測点 1-5 での波形を、右上にその相互相関関数
(例えば 14 は 1 と 4 の相互相関関数) が表示されます。相互相関関数のピークの時刻を読
み取ることによって走時差を測定することが出来ます。色々試してみてください。

以後は過渡的な現象 (地震や火山の噴火) ではなく、微動や脈動など統計的にランダム
かつ定常と近似できる現象について考えていきます。

10.3.2 In a case of a closed system

地震波干渉法を理論的に考える上で、normal mode のアプローチは抽象的ですが本質
を捉えており、地震波干渉法のアイデアを理解しやすいという利点があります (例えば
Lobkis and Weaver, 2001[6])。そこで、まずは normal mode のアプローチで考えていき
ます。

弾性体が有限な大きさを持つ仮定は、地球が有限サイズを持つことを考えると、自然
な仮定である事が分かります。ここでは簡単のため 1 次元周期境界の問題を考えますが、
normal mode の議論をそのまま 2 次元、3 次元へと適応することができます。

Ensemble of repeating experiments

仮想的に、実験室で繰り返し実験している状況を考えます。$t = 0$ より前では弾性体は
静止しており、時刻 $t = 0$ で弦に対してランダムな力を $f^k(t, x)$ の力を加えます。力を加
えた後に、弦の振幅を測定するという実験を考えます。このような操作を k_0 回繰り返し
ます。[note 6]。

ランダムな力による励起の問題を normal mode のアプローチで考えていきます。$t = 0$

[note 6] 厳密に言うと、アンサンブル平均をとって期待値をとることと、最初に定義したような時間積分による相
互相関は一致するとは限りません (エルゴート性)。

に $\delta(t)f(x)$ という力がかかっている場合を考えます。この場合に運動方程式は

$$\rho\frac{\partial^2 u^k}{\partial t^2} = \kappa\frac{\partial^2 u^k}{\partial x^2} + f(x)\delta(t) \tag{10.3}$$

となります。

Green 関数を使って外力 f に対する変位の応答を考えていきましょう。9 章式 9.16 から、$t \geq 0$ での Green 関数は固有関数 u_n と固有周波数 ω_n を使って

$$G(x,x';t) = \sum_n \frac{u_n(x)u_n(x')}{\omega_n}\sin\omega t, \tag{10.4}$$

と書くことができます。k 回目の試行での外力 f^k に対する弦の励起振幅 $u^k(x,t)$ $(t \geq 0)$ を求めるためには、外力 f を Green 関数で畳み込むと

$$u^k(x,t) = \sum_n \frac{\sin(\omega_n t)}{\omega_n}u_n(x)\int u_n(x')f^k(x')dx', \tag{10.5}$$

となります。ここで $A_n^k \equiv \int u_n(x')f^k(x')dx'$ と定義すると

$$u^k(x,t) = \sum_n A_n^k u_n(x)\frac{\sin(\omega_n t)}{\omega_n}, \tag{10.6}$$

という形で変位応答を書くことができます。

White noise

ここではランダムに加えられた外力 f について考えていきます。今外力は、あらゆる波数成分を等しく含んでいる不規則変動だと定義しましょう。このような性質を持つことを白色雑音とよ呼びます[note 7]。そのために $\Phi(f) = const$ となります。

もう少し具体的に考えていきましょう。Figure 10.4 の左の図を見てください。いま空間間隔 Δt で離散化された外力 $f^k(i\Delta x)$ を考えます。各位置 $i\Delta x$ で、ランダムにサイコロを振り (平均 0 分散 1 の正規分布に従うとします)。ここで自己相関関数 $\phi(x,x')$ を考えてみましょう。

$$\phi(x,x') = \lim_{N\to\infty}\frac{1}{N}\sum_{k=0}^{N-1}f^k(x')f^k(x'+x) \tag{10.7}$$

と自己相関関数を定義します。いま 2 点間の位置が $\Delta x/2$ だけ離れたら、外力に相関では全く相関がないことを仮定します。そうすると ϕ は $x-x'$ だけの関数となり、$\xi \equiv x-x'$ とすると

$$\phi(\xi) = \begin{cases} 1 & |\xi| \leq \Delta x \\ 0 & else \end{cases} \tag{10.8}$$

となります。$\phi(\xi)$ フーリエ級数展開すると、$\Phi(k_n) = \Delta x$ となります。ここで k_n は波数 $2n\pi/L$ です。パワースペクトル (片側スペクトル) は $2\Delta x$ となります (図 10.4)。

理論的な事は計算できました。では実際に数値データを作り計算してみたらどうなるでしょうか？乱数を使い白色雑音を生成し、フーリエ解析してみましょう。

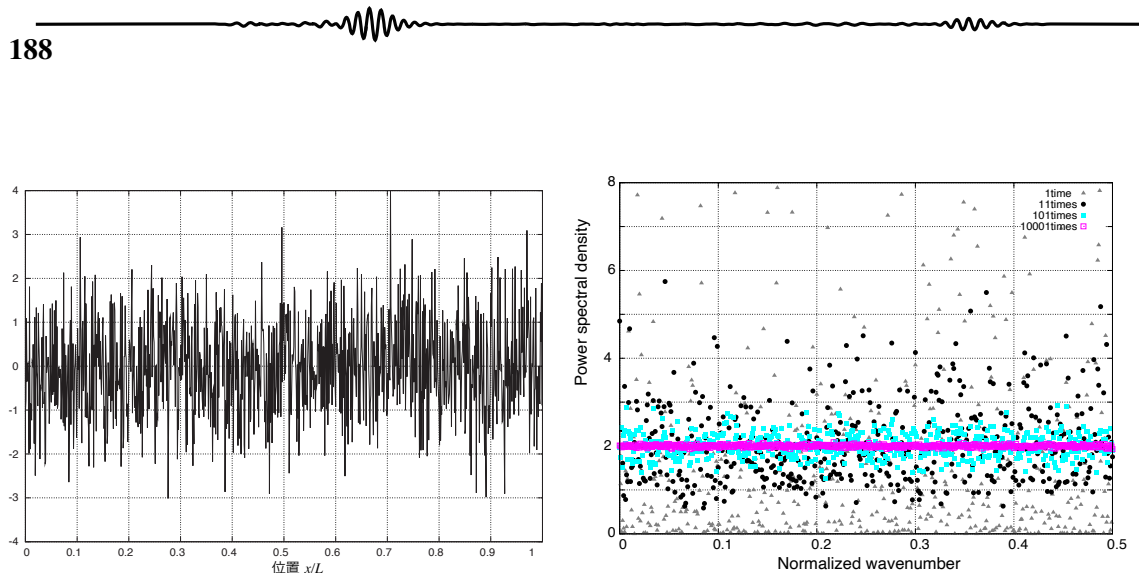[note 7] 太陽光のアナロジーです。一般に白色はあらゆる周波数成分を含む事を、赤色は低周波に富む事、青色は等は周に富むことを意味します。

Fig. 10.4　図左: 白色雑音の特徴を持つ外力 $f^k(x)$。図右: スペクトルをとりパワースペクトルを計算した結果。アンサンブル平均をとる数を増やす毎に、推定値は 1 に近づいていく。

　まずは切り出したウィンドウ 1 つを考えてみましょう。波数 k_n でのフーリエスペクトルを考えてみましょう[note 8]。$f(x_k)$ は乱数なので、そのフーリエ成分 $F(k)$ も乱数になります。パワースペクトルは $|U(k)|^2$ で計算出来るため、一定の値を足らずランダムな値を取ります[note 9]図 10.4 右のグレーの点が実際に計算した点です。これは少し奇妙です。$\Phi(f) = 1$ となるはずが 1 回離散フーリエ変換するだけでは、2 と同じ桁という程度のことしか分かりません。何故でしょうか？

　それは自己相関関数が統計的な量なためです。多くのアンサンブルに対して平均を (ここでは k がアンサンブルの要素に対応付けた番号です) 取らないと意味のある値になりません。より具体的に言うと推定誤差が 100% となってしまいます。一見とても奇妙ですが、この振る舞いは統計的に 1 サンプルのみを評価していることに起因します。

　そこで何度もフーリエ級数展開をしてアンサンブル平均をとってみましょう。段々と 2 に近づいていくことがわかると思います[note 10]。このようにパワースペクトルとるはあくまで統計的な量なため、十分な数だけ平均化しないと推定誤差が大きくなりすぎてしまいます。例えば N 回サンプリングして平均化した場合を考えてみましょう。時系列が正規分布に従う場合推定誤差は $1/\sqrt{N}$ となります。このように誤差が N にしたがって小さくなっていく様子も、図から見て取れます。

Equipartition of energy

　外力のした仕事がどのようにエネルギー分配されているか考えていきましょう。速度は

$$\frac{\partial u^k(x,t)}{\partial t} = \sum_n A_n^k u_n(x) \cos(\omega_n t), \tag{10.10}$$

[note 8] 実際に計算するには空間的に離散化する必要があり離散フーリエ変換する必要があります。離散フーリエ変換とフーリエ級数展開の整合性をとると

$$F(k_n) = \Delta x \sum_{j=0}^{N} f(x_j) e^{-i2\pi k_n x_j} = \delta F^{DFT}(k_n), \tag{10.9}$$

となります。

[note 9] 正確には χ^2 分布に従います。

[note 10] 確認ですが、今時間領域で分散 1 の時系列を考えています。Percival の公式からパワースペクトルの積分は 2×0.5 となり一致します。

モードあたりの運動エネルギー T_n は ρu_n をかけて空間積分すればよく

$$T_n = \frac{1}{2}(A_n^k)^2 \cos^2 \omega_n t) \tag{10.11}$$

となることが分かります。一方弾性エネルギー V_n は歪の固有関数 $\frac{\partial u_n}{\partial x}$ を両辺にかけて空間積分すると評価でき

$$T_n = \frac{1}{2}(A_n^k)^2 \sin^2 \omega_n t) \tag{10.12}$$

全エネルギー $T + V$ は

$$T + V = (A_n^k)^2 \tag{10.13}$$

で評価できることが分かります。つまり白色の特徴をもつ外力 f で叩くと、各モードにエネルギーの期待値 $\langle (A_n^k)^2 \rangle_k$ は一定となります。この条件が満たされるとき、エネルギーが当分配 (equipartition of energy) されていると呼ぶことにします。

Cross-correlation functions

ここで $u^k(x_1)$ と $u^k(x_2)$ の相互相関関数 $\phi^k(x_1, x_2; \tau)$ を考え、相互相関関数を

$$\phi^k(x_1, x_2; \tau) \equiv \lim_{T \to \infty} \frac{1}{T} \int_0^T u^k(x_1, t) u^k(x_2, t + \tau) dt, \tag{10.14}$$

と定義します。

k_0 回試行した後そのアンサンブル平均 $\phi(x_1, x_2; t)$ を

$$\phi(x_1, x_2; t) \equiv \left\langle \phi^k(x_1, x_2; t) \right\rangle_k = \lim_{k_0 \to \infty} \frac{1}{N} \sum_{k=0}^{N-1} \phi^k(x_1, x_2; t) \tag{10.15}$$

とします。ここで今後は簡単化のため $\langle \rangle_k$ は k に関するアンサンブル平均を表すことにします。

いま白色な特徴を持つランダムな力で叩いているため、各モードのエネルギー (弾性エネルギーと運動エネルギーの和 $T + V$) が等しく分配され、それぞれの変動 (振幅 A_n) が無相関です。A_n の相互相関の期待値は以下のように書くことが出来ます。

$$\langle A_m A_n \rangle \equiv \lim_{N \to \infty} \sum_k \sum_{k=0}^{N-1} A_m^k A_n^k = \delta_{mn} \frac{A_0^2}{\omega_n^2}. \tag{10.16}$$

となります。

簡単な計算の後

$$\phi(x_1, x_2; t) = -\frac{A_0^2}{2\omega_n^2} \frac{d}{dt} (G(x_1, x_2; t) - G(x_2, x_1; -t)) \tag{10.17}$$

と書ける。相互相関関数の微分とグリーン関数を結びつける式を導出した。また、この式を式変形し相互相関の微分の形、

$$\frac{d}{dt} \phi(x_1, x_2; t) = -\frac{A_0^2}{2} (G(x_1, x_2; t) - G(x_2, x_1; -t)), \tag{10.18}$$

に変形でき、オープンな系の場合と比較することが出来る[note 11]。

　現実の相互相関関数と比較する場合、一番大きな問題点は、エネルギー当分配の仮定です。球対称地球のを考える場合、地球内部を含め外力が白色の特徴を持つならば、水平方向 (angular order l と azimuthal order m) にはエネルギーの当分配を考えることができます。しかし、励起源が地表付近に集中している状況では、半径方向 (radial order n) にはエネルギーは等分配されません。特に $n = 0$ の基本モードが卓越することとなります

　また閉じた系で考えているため、減衰を考慮に入れないと、持続的な外力 (海洋波浪など) を考えた場合には振幅が発散してしまう[note 12]問題があります。この簡単な見積では、繰り返し実験するという (非現実的な) 状況設定なので定常状態を考えていないために発散の問題は起こりません。厳密な議論のためには減衰の効果を考慮する必要があります。

> **問題 9.1**
>
> 相互相関関数の具体的な表式を計算し、式 (10.18) を導け。

■ 10.3.3 In a case of an open system

　本節では 2 次元無限媒質中に 2 点観測点がある場合を想定します。単純ですが、表面波を考える上ではかなり良い近似です。また理想的な条件の元では、相互相関関数と Green 関数を結びつけることができます。[note 13]

　まずは閉じた系の問題設定を素直に拡張し、2 次元平面を考え、$t = 0$ のタイミングでランダムに叩く状況を考えます。表現定理を使って考察すると無数に励起源がある状況は、観測点を囲む閉曲線に沿って励起源を分布させることと等価である事が分かります。地震波干渉法を考えるときにいくつか違った仮定を用いるのですが、その等価性と違いを理解する事がこの節の目的です。

■ In a case of many random sources

　雨粒が水面を叩いている状況を思い浮かべてみましょう。雨粒のように、まずは 2 次元平面上に無数に励起源が分布している状況を考えてみましょう。ここでも $t = 0$ でランダムな外力が働く状況を、繰り返し観測している事を考えます。

　i 番目の励起源 ($i = 0, \cdots, N$) の力を $\delta(\boldsymbol{r}_i - \boldsymbol{r}_s)\delta(t) f_i^k$ とします。k 番目の試行での変位 $u^k(x, t)$ は

$$u^k(\boldsymbol{r}, t) = \sum_{i=0}^{\infty} g^{2D}(\boldsymbol{r} - \boldsymbol{r}_i; t) f_i^k, \tag{10.20}$$

と書けます。ここで $\boldsymbol{r}_i$ は i 番目の励起源の位置を表します。

[note 11] normal mode の章で述べたように Green 関数は

$$G(\boldsymbol{x}, \boldsymbol{x}', t) = \sum_k \frac{u_k(\boldsymbol{x})u_k(\boldsymbol{x}')}{\omega_k} \sin \omega_k t H(t), \tag{10.19}$$

と書ける。

[note 12] オープンな系であれば、境界から外向きのエネルギフラックスと、励起源による仕事の釣り合いを考えることができます。

[note 13] 相互相関関数を計算することにより観測点間の波動伝播が抽出されるデモを作成しました。実行しながら読むと理解が深まるかもしれません。http://www.eri.u-tokyo.ac.jp/knishida/Seismology/wave2Drandom2.html

ここで見通しをよくするために時間に関してフーリエ成分を考えます[note 14]。

$$U^k(\boldsymbol{r}, \omega) = \sum_{i=0}^{\infty} G^{2D}(\boldsymbol{r} - \boldsymbol{r}_i; \omega) f_i^k, \tag{10.21}$$
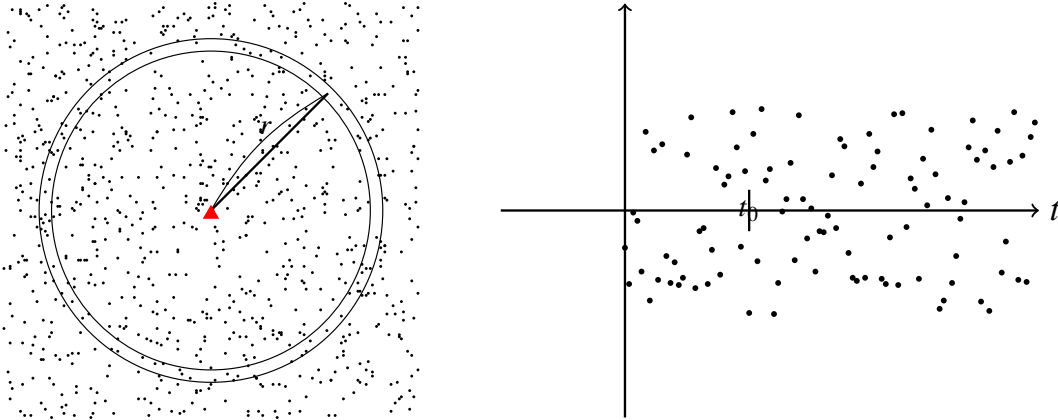

Fig. 10.5　平面内に一様にランダムな励起源が分布している場合の模式図。

　ここで $t = 0$ 以降に原点ではどのような振幅が観測されるかを考えていきましょう。時刻 t_0 での振幅を考えてみましょう。今 2 次元均質媒質の Green 関数を考えているために、原点から $r = ct_0$ だけ離れた点で励起された波が到着することになります。すなわち半径 r の同心円上に位置する外力が励起した波が一斉に原点に到達することになります。今外力の間隔は平均的に Δx だとします。そうすると半径方向に Δx の幅を考えると、おおよそ $2\pi r/\Delta x$ 個の外力が分布していることになります (図 10.5 左)。振幅の距離減衰はおおよそ $r^{1/2}$ ですので、原点での自乗振幅はおおよそ $2\pi r/\Delta x (r^{1/2})^2 = 2\pi/\Delta x$ となり距離に依存しなくなります。つまり原点には $t > 0$ ずっと同程度の振幅の波が到来し続けることとなります (図 10.5 右)。

　ここで、表現定理を思い出しましょう。今円内での変位を観測していることとします。この場合に、半径 r の円外に分布する外力によって励起された波は、円上の応力と変位が分かれば、円内の変位分布は完全に再現することができます。つまり、円外の外力の寄与は円上に分布させた外力で置き換えることができます。ただここで気をつけなくてはいけないのは、外力を加えたのは $t = 0$ のタイミングのみですが、円上に仮想的に考える励起源は時間的には $t > 0$ のあいだ励起が続くという点です。今 $t = 0$ で円内の外力も考えていますが、無限に長い時間を考えた場合にその寄与は無限に大きくなるために、円内の外力の効果は無視することができます。つまり、円上のみに外力が分布する場合 (ただし時間的には持続的) と等価であることが分かります。

　地震波干渉法の web 上のデモ `http://www.eri.u-tokyo.ac.jp/knishida/Seismology/wave2Drandom2.html` はこの条件でシミュレーションしています (図 10.6)。

　ここでは簡単のため、再び時間平均がアンサンブル平均と同じであると仮定します。つまり円周上に $F_i^k(\omega)$ の外力が分布しているとします。このような外力による地震波の励起を N 回行って、そのアンサンブル平均を考える状況を考えます。外力 F_i、他の励起源 F_j と互いに無相関であり、F が白色であると仮定すると

$$\langle F_i^{k*} F_j^k \rangle_k = \delta_{ij} F_0^2, \tag{10.22}$$

と書けます[note 15]。このことからクロス・スペクトル (相互相関関数のフーリエ変換)Φ_{12}

---

note 14) 大文字でフーリエ成分を表すことにします。

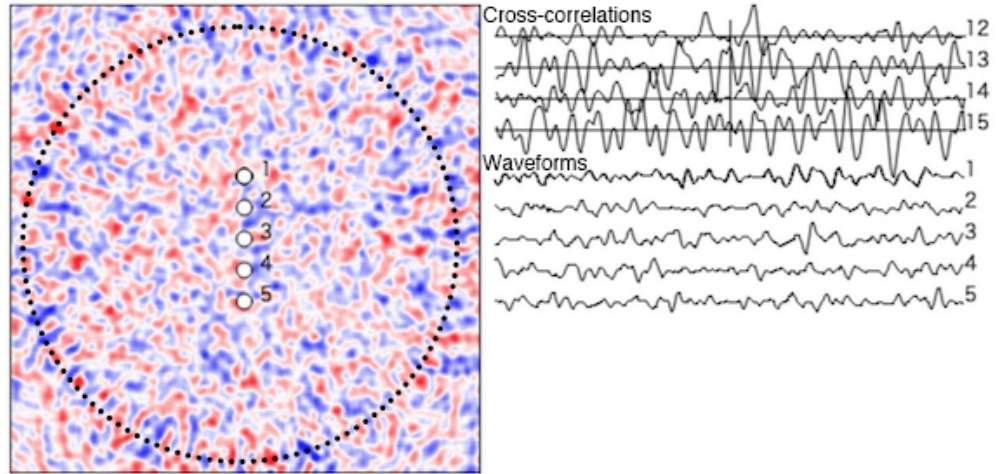note 15) $langle\rangle_k$ は k に関してアンサンブル平均を取った事を表すことにします

Fig. 10.6 円上にランダムな外力が分布している場合の波動場の例。励起は時間的に持続的である場合を考えています。

は

$$\Phi_{12}(\omega) \equiv \langle \Phi_{12}^k \rangle_k = \sum_{i,j} g^{2D*}(\boldsymbol{r}_1 - \boldsymbol{r}_i, \omega) G^{2D}(\boldsymbol{r}_2 - \boldsymbol{r}_j, \omega) \langle f_i^k(\omega) f_j^k(\omega) \rangle_k$$

$$= \sum_{i} G^{2D*}(\boldsymbol{r}_1 - \boldsymbol{r}_i, \omega) G^{2D}(\boldsymbol{r}_2 - \boldsymbol{r}_i, \omega) F_0^2 \tag{10.23}$$

と書くことが出来ます。

励起源の数が十分に大きいと、励起源が観測点を囲んでいる場合には上式の和は線積分で置き換えられ、

$$\Phi_{12} = f_0^2 \int_{l_s} G^{2D*}(\boldsymbol{r}_1 - \boldsymbol{r}_s, \omega) G^{2D}(\boldsymbol{r}_2 - \boldsymbol{r}_s, \omega) dl_s, \tag{10.24}$$

と書ける。グリーン関数の畳み込み積分を空間で積分している形になっています。この式が地震波干渉法における基本式です。

積分の評価: 相互相関関数と Green 関数の関係

この積分を評価するために、図 10.7 のような励起源の配置を考えます。励起源の位置は原点からの距離 r_s と角度 ϕ_s で表現します。

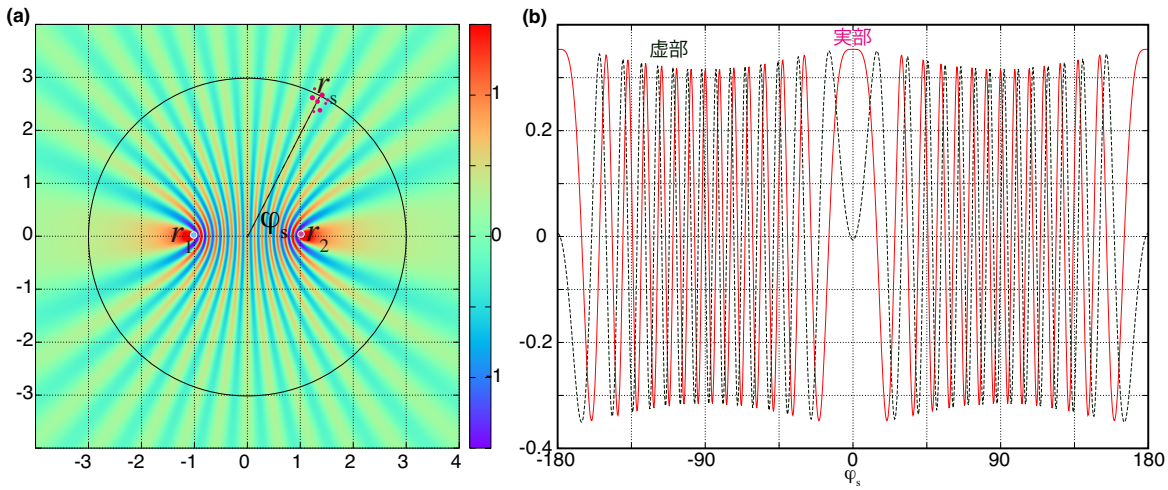単純化のため Green 関数が $e^{ikr-\pi/4}/\sqrt{kr}$ に比例すると近似します。この近似は距離 r

Fig. 10.7 (a) r_s を固定し ϕ_s に対し被積分関数をプロットした図。(b) は $r_s = 3$ の円 (図 10.7(a) 参照) に沿った値をプロットした図。

が波長に比べて長いときには妥当な近似です[note 16)]。そうすると

$$\Phi_{12} \propto \int_{l_s} \frac{e^{ik(r_{2s}-r_{1s})}}{k\sqrt{r_{1s}r_{2s}}} dl_s, \tag{10.25}$$

r_{1s}, r_{2s} は図 10.7 にあるように観測点 1r_1, 観測点 2r_2 と励起源 r_s の間の距離です。式にあるように、点震源 r_s から放射される波の観測点 1 と 2 とでの位相差は、距離の差を波長で割った値できまります。等位相差の曲線は観測点を焦点とする双曲線となります。そうすると、2 観測点を通るパスに沿っては位相の変化は緩やかとなり (停留点, stationary point)、その他の領域では激しく振動します (図 10.7)。ランダムな励起の問題を考える場合、二観測点間を通るパスに沿った励起源の寄与 (stationary zone と呼ばれる) が大きくなり、その他の領域の励起源の影響は打ち消されます (停留値法, 例えば蓬田 2007 参照)。また虚部は ϕ_s に対して反対称となっているため、励起源の分布が一様の場合には打ち消される[note 17)]。

　以下少し視点を変えて、もう少し直感的な説明を試みます。図 10.7 赤点で書いたようにランダムな励起源がある限られた領域に分布しているとき、十分に遠くで観測する場合多重極 (mono pole, dipole, quadrapole 等) の重ね合わせで表現できます (多重局展開と呼ばれる)。ψ_s が図にあるように 70° 程度の場合を考えます。この場合、2 観測点の間に節が入る確率はランダムです。そのために、r_s からでた波が 2 つの観測点で同位相である確率と逆位相である確率は等しくなります。一方 ϕ_s が 0 か π の時には (stationary zone の

[note 16)] Green 関数は具体的には

$$G^{2D}(\boldsymbol{r}, t) = -\frac{1}{2\pi} \frac{H\left(t - \frac{r}{c}\right)}{\sqrt{t^2 - \frac{r^2}{c^2}}},$$

周波数領域では、

$$G^{2D}(\boldsymbol{r}, \omega) = -\frac{i}{4} H_0^{(2)}(\omega r/c) \propto \frac{1}{\sqrt{kr}} e^{ikr - \pi/4},$$

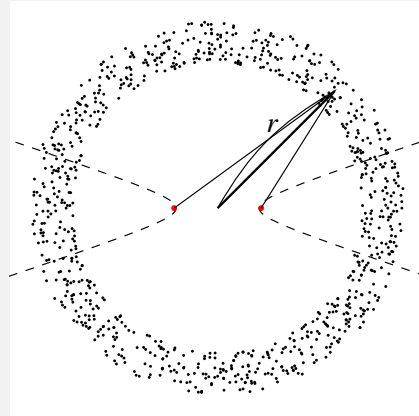と書けます。ここで波数 k は $k \equiv \omega/c$ と定義され、$H_0^{(2)}$ 第 2 種ハンケル関数である, $H()$ は Heviside の階段関数です。

[note 17)] 被積分関数が激しく振動する性質は重要です。なぜなら、一様に励起源が分布していない場合にも、stationary zone の寄与が卓越することが期待されるためです。励起源の分布に対して、相互相関関数の波形がロバストである性質は、データ解析上重要な点です。

場合)、励起源から見て 2 つの観測点の方向は同じため常に r_s から出る波は同位相となります。つまり stationary zone に励起源がある場合のみ、相互相関波形に寄与します。

問題 9.2

以上周波数領域で評価たが、相互相関波形の形を理解するために時間領域で考える。ここでは数のような状況をかんがえる。周波数領域で $G^{2D*}(r_1 - r_s, \omega) * G^{2D}(r_2 - r_s, \omega)$ と書いた項は時間領域 (フーリエ逆変換すると) グリーン関数の畳み込み積分で表現できる。

1. 図でしめした位置で外力を加えたとき、相互相関関数を計算せよ。
2. 図で示した円周上に体力が分布していることを考える。(1) で計算した相互相関関数を角度方向に平均し、相互相関関数を評価せよ。ここで、図中双曲線の内側にある外力の寄与が多きことに注意せよ。
3. 相互相関関数がピーク値を取る時刻と、観測手間の距離の関係を考察せよ。

以上大雑把に積分の寄与を見積もりました。ここで Wapenaar and Fokkema (2006)[17] に従い u が l_s 上で

$$\frac{\partial u}{\partial n} = -iku \tag{10.26}$$

という放射境界条件を満たすとして、もう少し考察していきます。。Rayleigh の相反定理と合わせて考えると

$$\Phi_{12} = f_0^2 \int_{l_s} G^{2D*}(r_1 - r_s, \omega) G^{2D}(r_2 - r_s, \omega) dl_s, \tag{10.27}$$

$$\sim f_0^2 \frac{\rho c}{2i\omega} \left(G^{2D*}(r_1 - r_1, \omega) - G^{2D}(r_1 - r_2, \omega) \right) \tag{10.28}$$

と、相互相関関数と Green 関数を結び付けられれます[note 18]。相互相関関数の微分が、Green 関数に比例する形式になっています[note 19]。

ここで重要なのは、ここでは減衰を考慮していないという点と、放射境界条件をとっているために地表反射等の自由境界表面を考慮できないという点です。現実の状況設定を考

---

note 18) 詳細は Wapenaar and Fokkema (2006)[17] 参照

note 19) Aki (1957) の spatial autocorrelation method (SPAC 法) では、遠方から平面波がランダムに入射している事を仮定して議論しています。大枠としては、この章の議論に近いが詳細は異なります。例えば 2 次元の場 SPAC 法に準拠すると (Nakahara 2006 参照)、相互相関関数の Hilbert 変換が Green 関数となります。これは遠方から入射する波が、Green 関数と平面波 $\exp\{i(\omega t - \mathbf{k}\dot{x})\}$ と違うことに起因すします。

えると、注目している領域を囲む形で地中にも励起源が分布していないと Green 関数とは解釈できません。そのため現実の相互相関関数は、Green 関数 (大雑把に言って地震記録) に比べ、実体波の振幅が小さくなります。実体波特に地表反射を上手く抽出できないという問題点は、コーダは (例えば Tonegawa et al., 2009)[15] ある程度回避することができます。

問題 9.3

地震波干渉法の web 上のデモ `http://www.eri.u-tokyo.ac.jp/knishida/Seismology/wave2Drandom2.html` を実行して、波が伝播するとこを確認し、理論との対応を考察すること。

10.3.4 In a case of an attenuating medium under a realistic situation

　系に対する入力 (励起源による仕事) と減衰によるエネルギーの散逸の釣り合いを考えることで、定常振幅を見積もってみましょう。ここでは単純化のために一次元の問題を考えます。運動方程式は、変位 u, 密度 ρ, 応力 σ, 外力 F を使って

$$-\rho\omega^2 U(x,\omega) = \frac{\partial\sigma(x,\omega)}{\partial x} + F(x,\omega) \tag{10.29}$$

とかけます。
　応力 $\sigma(x,\omega)$ は歪み $\epsilon = \partial U/\partial x$ を使って

$$\sigma(x,\omega) = \kappa(\omega)\epsilon(x,\omega) \tag{10.30}$$

と書けるとします。ここで κ は複素弾性定数とし、減衰を含めて考えます。式 10.30 を式 10.29 に代入すると、

$$\rho\omega^2 U(x,\omega) = \frac{\partial}{\partial x}\left(\kappa(\omega)\frac{\partial U(x,\omega)}{\partial x}\right) + F(x,\omega) \tag{10.31}$$

となります。
　周期境界条件の場合の問題を考えます。変位 $u(t,x)$ が周期境界条件、$u(t,x) = u(t,x+L)$ を満たすとします。

$$-\rho\omega^2 U(x,\omega) = \kappa(\omega)\frac{\partial^2 u(x,\omega)}{\partial x^2} + F(x,\omega) \tag{10.32}$$

ここで $F(x,\omega)$ は forcing term です。
　U と F を固有関数 $u_n(x)$ で展開すると

$$U(x,\omega) = \sum_n a_n(\omega)u_n(x)$$

$$F(x,\omega) = \sum_n f_n(\omega)u_n(x). \tag{10.33}$$

となります。そうすると複素固有値を $-k_n$ とすると

$$- \omega^2 a_n = -\kappa(\omega) k_n^2 a_n(\omega) + F_n(\omega) \tag{10.34}$$

とります。ここで簡単化のため複素固有周波数 $\omega_n^2 \equiv \kappa k_n / \rho$ を定義します。以上まとめると、

$$a_n(\omega) = -\frac{f_n(\omega)}{\omega^2 - \omega_n^2} \tag{10.35}$$

となります。

ここで、cross spectrum $\langle U^*(\omega, x_1), U(\omega, x_2) \rangle$ を考えます。

$$\langle U^*(\omega, x_1), U(\omega, x_2) \rangle = \sum_{n,n'} \langle a_n^* a_{n'} \rangle u_n^*(x_1) u_{n'}(x_2). \tag{10.36}$$

この式を評価するために $\langle a_n^* a_{n'} \rangle$ を評価します。ここで forcing がホワイトだと仮定すると、

$$\langle F_n^* F_{n'} \rangle = F_0^2 \delta_{n,n'} \tag{10.37}$$

と書けます。すなわち、

$$\langle U_n^* U_{n'} \rangle = \frac{F_0^2}{(\omega^2 - \omega_n^2)(\omega^2 - \omega_n^{*2})} \delta_{n,n'} \tag{10.38}$$

と書き直せ、クロススペクトル $\Phi(\omega, x_1, x_2) = \langle U^*(\omega, x_1), U(\omega, x_2) \rangle$ は

$$\Phi(x_1, x_2, \omega,) = \sum_{n=0}^{\infty} \frac{F_0^2}{(\omega^2 - \omega_n^2)(\omega^2 - \omega_n^{*2})} u_n(x_1) u_n^*(x_2) \tag{10.39}$$

$$= \sum_{n=0}^{\infty} \frac{F_0^2}{2 \, \text{Im}[\omega_n^2]} \left(\frac{1}{\omega^2 - \omega_n^2} - \frac{1}{\omega^2 - \omega_n^{*2}} \right) u_n(x_1) u_n^*(x_2) \tag{10.40}$$

$$= \sum_{n=0}^{\infty} \frac{F_0^2 Q_n}{2(\omega_n)^2} \left(\frac{1}{\omega^2 - \omega_n^2} - \frac{1}{\omega^2 - \omega_n^{*2}} \right) u_n(x_1) u_n^*(x_2) \tag{10.41}$$

と書き直せます。ここで $\omega_n \sim \text{Re}\{\omega_n\} + i \, \text{Re}\{\omega_n\}/(2Q_n)$ としました。ざっと式を見ると k_l に対して $\pm\omega_n$ の値で極大をとります。つまり x が正の方向に伝搬する波束 (causal part) と、負の方向に伝播する波束 (causal part) を表しています。

エネルギーがどのように分配しているか見ていきましょう。単位長さあたりの運動エネルギーは $\omega^2 \rho \Phi(x, x, \omega)$ となるため、全エネルギーは

$$\int \omega^2 \rho \Phi(x, x, \omega) dx \sim \sum_n \frac{F_0^2 Q_n}{\omega_n} \tag{10.42}$$

と見積もることが出来ます。つまり外力が白色雑音出会った場合にも、モードあたりのエネルギーは周波数に反比例し、Q_n に比例します。つまり $F_0^2 \sim \omega_n / Q_n$ となって初めてエネルギーは等分配されます。このため現実の地球はエネルギーは等分配されているわけではなく、その点を考慮する必要があります。

式 10.38 でモード間の相関が無いという点が本質的です。励起源の空間分布が不均質な場合にはモード間の相関が出てしまい、相互相関関数の評価は難しくなります。現象論的には、多くの場合モード間に相関が無いという仮定は第 0 次近似としては成り立っているように見えます。そこからの補正をどうするか、現在盛んに研究されています。

より 3 次元弾性体に対する見積もりは Nishida (2011) などを参照のこと。

まとめ: Green 関数と相互相関の比較

1. 地震波干渉法の理論は大きく分けて、オープンな系で外部を包むように内部を照らす状況設定と、閉じた系にたいし釣り合いを考える立場がある。色々なバックグラウンド (物理探査、グローバル地震学、強震動) の研究者がいるために、問題の取り扱い方が分野によって微妙に異なる。例えば equipartition という単語一つとっても文脈によって定義が統一されていないので注意が必要 (Snieder et al. 2010)。
2. 表面波のみ議論するときは Green 関数との比較が可能。ある程度励起にむらがあっても、観測点間の情報を抽出することが可能。
3. 実体波の相対振幅は、Green 関数より相互相関関数の方が小さいと期待される。
4. とくに相互相関により地表反射波を抽出することは難しい。

Summary: pros and cons

1. ∘伝搬距離が短いパスの情報を使える。
2. ∘0.05 Hz よりも短周期でも、散乱や 減衰の効果を受けづらい。
3. ×励起源の分布に偏りがあると、見かけの走時異常が生じる可能性がある。

まとめ: Ambient noise tomography の強みと弱み

1. ∘パスが震源分布に依存せず、 パス密度に偏りが少ない。
2. ∘アレー観測の場合には、良い初期モデル (局所的 1 次元構造) を推定することが可能。
3. ×励起源の分布に偏りがあると、見かけの走時異常が生じる可能性がある。特に方位異方性の推定や、減衰構造の推定に際して深刻。

ToDO: バネおもりモデルを使った地震は干渉法とブラウン運動の関係

§10.4 An application for seismic monitoring

　地球内部で起こる現象のダイナミクスを考える上で、速度構造の時間変化を捉える事は非常に重要です。火山噴火や地震に伴い応力やひずみの状態が変化し、それに伴って速度構造や異方性の変化することが期待されるためです。

　実際に地下構造の時間変化を求めようとする場合、コントロールソースを用いて繰り返し地震波トモグラフィを繰り返す事が想的です。しかし多くの場合現実的ではありません。一方自然地震を使う場合、震源の不確定性や震源分布の偏りなどに起因する不確定性が速度構造の不確定性を引き起こします。そのため、たとえ時間変化が見かけ上見えたとしても、それはただのノイズなのか本当の速度変化なのかはっきりとしません。

　それに対し、地下構造の時間変化を検出する場合に地震波干渉法は非常に有効な方法です。なぜなら、期間を区切って相互相関関数を計算することによって、仮想的に繰り返し地震を観測出来るためです。最も単純な例を考えてみましょう。地表宇野 2 点で地震観測をし、その記録の相互相関関数の変化を見続けます。この場合には、その 2 点間の局在化された構造変化を時々刻々モニターすることができます。ここでは詳細については述べませんが、先駆的な研究として、 Sens-Schönfelder Wegler (2006) (インドネシアの Merapi 火山) や Wegler and Sens-Schönfelder (2007) (中越地震の解析) がある。

§10.5 Practical problems when applying actual data

10.5.1 Azimuthal dependence of incident waves

入射波振幅の方位依存性を考えるために、Cox の式 [4]

$$\sum_{m=0}^{\infty} i^m J_m\left(\frac{\omega r}{c(\omega)}\right) [a_m(\omega)\cos(m\zeta) + b_m(\omega)\sin(m\zeta)] \qquad (10.43)$$

を考えます。
　この場合に走時異常は

$$\delta t = \frac{B''(0)}{2t\omega^2 B(0)} \text{for the causal part}$$

$$= \frac{B''(180)}{2t\omega^2 B(180)} \text{for the acausal part} \qquad (10.44)$$

と書くことが出来ます (Weaver et al., 2009)[18]。この式を使って、入射波の非等方性を補正する事が可能です。

10.5.2 Finite frequency effects

　地震波干渉法を適応する場合には、通常の地震と同じ sensitivity kernel を考慮すれば良いのか自明ではありません [16]。励起源が等方均質の場合に、表面波の sensitivity kernel は地震と同じである事は分かっていますが [8]、励起源にむらがある場合には厳密には補正が必要です。

§10.6 Bibliography

[1] Keiiti Aki. Space and time spectra of stationary stochastic waves, with special reference to microseisms. *Bull. Earthq. Res. Inst.*, Vol. 35, pp. 415–457, 1957.

[2] Michel Campillo and Anne Paul. Long-range correlations in the diffuse seismic coda. *Science*, Vol. 299, No. 5606, pp. 547–549, January 2003.

[3] Jon F Claerbout. SYNTHESIS OF a LAYERED MEDIUM FROM ITS ACOUSTIC TRANSMISSION RESPONSE. *Geophysics*, Vol. 33, No. 2, pp. 264–269, April 1968.

[4] Henry Cox. Spatial correlation in arbitrary noise fields with application to ambient sea noise. *J. Acoust. Soc. Am.*, Vol. 54, No. 5, pp. 1289–1301, 1973.

[5] Laurent Gizon, Aaron C Birch, and Henk C Spruit. Local helioseismology: Three-Dimensional imaging of the solar interior. *Annu. Rev. Astron. Astrophys.*, Vol. 48, No. 1, pp. 289–338, August 2010.

[6] Oleg I Lobkis and Richard L Weaver. On the emergence of the green's function in the correlations of a diffuse field. *J. Acoust. Soc. Am.*, Vol. 110, No. 6, p. 3011, 2001.

[7] Nori Nakata, Lucia Gualtieri, and Andreas Fichtner. *Seismic Ambient Noise*. Cambridge University Press, March 2019.

[8] Kiwamu Nishida. Two-dimensional sensitivity kernels for cross-correlation functions of background surface waves. *C. R. Geosci.*, Vol. 343, No. 8-9, pp. 584–590, September 2011.

[9] Philippe Roux and W A Kuperman. Extracting coherent wave fronts from acoustic ambient noise in the ocean. *J. Acoust. Soc. Am.*, Vol. 116, No. 4, pp. 1995–2003, October 2004.

[10] H Sato, M C Fehler, and T Maeda. *Seismic wave propagation and scattering in the heterogeneous earth*. Springer, 2012.

[11] C Sens-Schönfelder and U Wegler. Passive image interferometry and seasonal variations of seismic velocities at merapi volcano, indonesia. *Geophys. Res. Lett.*, Vol. 33, No. 21, p. L21302, November 2006.

[12] Nikolai M Shapiro, Michel Campillo, Laurent Stehly, and Michael H Ritzwoller. High-resolution surface-wave tomography from ambient seismic noise. *Science*, Vol. 307, No. 5715, pp. 1615–1618, March 2005.

[13] R Snieder. Extracting the building response using seismic interferometry: Theory and application to the millikan library in pasadena, california. *Bull. Seismol. Soc. Am.*, Vol. 96, No. 2, pp. 586–598, April 2006.

[14] Roel Snieder and Kees Wapenaar. Imaging with ambient noise. *Phys. Today*, Vol. 63, No. 9, pp. 44–49, September 2010.

[15] Takashi Tonegawa, Kiwamu Nishida, Toshiki Watanabe, and Katsuhiko Shiomi. Seismic interferometry of teleseicmic S -wave coda for retrieval of body waves: an application to the philippine sea slab underneath the japanese islands. *Geophys. J. Int.*, Vol. 178, No. 3, pp. 1574–1586, September 2009.

[16] Jeroen Tromp, Yang Luo, Shravan Hanasoge, and Daniel Peter. Noise cross-correlation sensitivity kernels. *Geophys. J. Int.*, Vol. 183, No. 2, pp. 791–819, November 2010.

[17] Kees Wapenaar and Jacob Fokkema. Green's function representations for seismic inter-ferometry. *Geophysics*, Vol. 71, No. 4, p. SI33, 2006.

[18] Richard Weaver, Berenice Froment, and Michel Campillo. On the correlation of non-isotropically distributed ballistic scalar diffuse waves. *J. Acoust. Soc. Am.*, Vol. 126, No. 4, p. 1817, October 2009.

[19] B.F. シュッツ. 物理学における幾何学的方法. 物理学叢書. 吉岡書店, 1987.

[20] 広岡田, 直巳坂尻. やや長周期微動による地下構造の推定. 北海道大学地球物理学研究報告, Vol. 42, pp. 119–143, October 1983.